PONTIFÍCIA UNIVERSIDADE CATÓLICA
DO RIO DE JANEIRO

Letícia Oliveira de Souza

The effect of micro and nano cellulose fibers on the chemical, physical and mechanical properties of cement pastes

Tese de Doutorado

Thesis presented to the Programa de Pós-Graduação em Engenharia Civil of PUC-Rio in partial fullfilment of the requirements for the degree of Doutor em Ciência – Engenharia Civil.

Advisor: Prof. Flávio de Andrade Silva

Coadvisor: Prof. Lourdes Maria Silva de Souza

Rio de Janeiro
September 2022

PONTIFÍCIA UNIVERSIDADE CATÓLICA
DO RIO DE JANEIRO

Letícia Oliveira de Souza

The effect of micro and nano cellulose fibers on the chemical, physical and mechanical properties of cement pastes

Thesis presented to the Programa de Pós-Graduação em Engenharia Civil of PUC-Rio in partial fullfilment of the requirements for the degree of Doutor em Ciência – Engenharia Civil. Approved by the Examination Committee.

Prof. Flávio de Andrade Silva
Advisor
Department of Civil and Environmental Engineering – PUC-Rio

Prof. Lourdes Maria Silva de Souza
Co-advisor
Department of Civil and Environmental Engineering – PUC-Rio

Prof. Daniel Carlos Taissum Cardoso
Department of Civil and Environmental Engineering – PUC-Rio

Prof. Luiz Fernando Martha
Department of Civil and Environmental Engineering – PUC-Rio

Prof. Conrado de Souza Rodrigues
CEFET-MG

Prof. Holmer Savastano Júnior
USP

Rio de Janeiro, September 23rd, 2022

Letícia Oliveira de Souza

Graduated in Civil Engineering at Universidade Federal Fluminense in 2015 and obtained her M.Sc. Degree in Civil Engineering from the Pontifícia Universidade Católica do Rio de Janeiro in 2017.

Bibliographic data

Souza, Letícia Oliveira de

The effect of micro and nano cellulose fibers on the chemical, physical and mechanical properties of cement pastes / Letícia Oliveira de Souza ; advisor: Flávio de Andrade Silva ; co-advisor: Lourdes Maria Silva de Souza. – 2022.

205 f. : il. color. ; 30 cm

1. Engenharia Civil e Ambiental - Teses. 2. Pasta de cimento. 3. Nanocelulose. 4. Retração. 5. Reologia. 6. Tração direta. I. Silva, Flávio de Andrade. II. Souza, Lourdes Maria Silva de. III. Pontifícia Universidade Católica do Rio de Janeiro. Departamento de Engenharia Civil e Ambiental. IV. Título

CDD: 624

Acknowledgements

This study was financed in part by the Coordenação de Aperfeiçoamento de Pessoal de Nível Superior - Brasil (CAPES) - Finance Code 001, and also with the financial support of the PROBRAL program.

No research, especially the experimental ones, is carried by a single person and his advisors. Fortunately, I have lot of people to thank to.

I would like to thank Prof. Flávio de Andrade Silva for his guidance through these past six years. When we started to work together, I had recently graduated and now I can consider myself a professional researcher. So, thank you to contribute to it. I also want to thank Prof. Lourdes Maria Silva de Souza to join as co-advisor and take part to the improvement of this work. I appreciate the advises, the presential meetings (that would become virtual ones) that led to the present study. I appreciate the respect that you both demonstrated so I could pursuit and develop my personal vision. The opportunities to participate of national and international conferences and to work in other laboratories were also responsible for my professional growing.

I also like to thank Prof. Gustavo Tonoli and Matheus Cordazzo for supplying the nanocellulose used in this work. Thank you both for helping me to work with this material, especially in the beginning when it was a bit challenging. The characterization you provided was essential to the development of this work and I am happy that we could together bring up a nice publication from it.

I here express my gratitude to all technicians and lab staff to whom I had contact with and helped me with the experiments, analyses, tests, specimen productions and all sort of demands. The first two years of this research was conducted at the Laboratory of Structures and Materials (LEM-DEC) at PUC-Rio, and the assistance of Euclides, Bruno, Rogério, Marques, José Nilson, Jhansen and Anderson to varied phases was crucial for me. It was at PUC-Rio that I met the people that latter would become my support network to the most varied issues: Ana, Daiana, Raylane, Rebecca and Tathiana (and Luna). I honestly have no words to describe how grateful I am to have you in my life. I would not make it without you.

The second part of the experimental studies were conducted at TU Dresden (Germany), under supervision of Prof. Viktor Mechtcherine. There, the

experiments were carried in the *Labor Für Gefügemorphologie* and *Alfred-Hütter-Laboratorium*. I want to thank Dr. Marco Liebscher for the shared insights that enabled great part of this work. I also want to thank Mrs. Willomitzer, Mrs. Hempel and Mrs. Noack for the analyses patiently performed. I also appreciate the lab support provided by Christian Stahn, Tilo Günzel and Fabian Israel. A special thanks to Mr. Mehlisch for the tensile test arrangement development, the companion and for teaching me how to proper open a bottle in German style. I believe that abroad experiences foster not only our professional knowledge but also develop our personal growing. So, here I express my sincere gratitude to Philipp, Steffen, Irina, Ting and Shirin to include me as "part of the group" – I did not feel alone even considering we were in a pandemic situation. Lulu, Tales, Dwight and Anuj: thank you for being my family while I was in Dresden.

I would also like to thank the Professors members of this thesis committee, for their availability and careful reading of this study.

Finally, I want to thank my family, especially Bruno, for your unconditionally support, patience and understanding. I am extremely grateful to have you in my life. This thesis belongs partially to you.

Abstract

Oliveira de Souza, Letícia; de Andrade Silva, Flávio (Advisor). **The effect of micro and nano cellulose fibers on the chemical, physical and mechanical properties of cement pastes**. Rio de Janeiro, 2022. 205 p. Tese de Doutorado – Departamento de Engenharia Civil e Ambiental, Pontifícia Universidade Católica do Rio de Janeiro.

The seek for low environmental impact materials has become one of the priorities of construction building materials engineers. One of the reasons is the massive growing contribution of cement production industry in worldwide CO_2 emissions. In this scenario, the dissemination of nanotechnology into varied areas is drawing attention for enabling new possibilities. The idea of the present thesis is to associate a material provided from a natural source with the potential benefits of nanotechnology to modify conventional cement pastes regarding their chemical, physical and mechanical aspects. Nanocellulose arises as an alternative that meets an eco-friendly source with remarkably properties expected from nanomaterials. There are different types of nano cellulosic materials that may be tailored to achieve desired compatibilities with varied cementitious materials. In this work, nanofibrillated cellulose (NFC) in the form of gel, and microcrystalline cellulose (MCC) particles were investigated, so a comparison could be traced between them. The use of both NFC and MCC in cementitious materials is recent and there are important gaps regarding their effect. For that reason, the feasibility of MCC and NFC to act as reinforcement on cement pastes was evaluated through compressive and flexural tests. Then, the possible mechanisms behind the effect of MCC and NFC on the microstructure of cement pastes were investigated through distinct chemical and physical analyses. Moreover, the total and autogenous shrinkage were characterized, as well as the dynamic and static rheological behaviors. Due to rheological modifications, the mixture of cement pastes with NFC was facilitated by a superplasticizer,

especially for percentages higher than 0.050% wt. The MCC and NFC promoted the reinforcement of the cement pastes, regarding flexural and tensile stresses, increasing the composite strength and modulus. It was observed that he water present in the NFC gel is not totally available as mixing water due to the morphology and hydrophilicity of the fibrils. If associating certain levels of inclusions and water ratio, the NFC inclusion led to a decrease in autogenous shrinkage. The addition of 0.040% of NFC resulted in similar outcomes to 1.000% of MCC regarding their ability to increase yield stress and viscosity.

Keywords

Nanofibrillated cellulose; microcrystalline cellulose; cement paste; mechanical properties; shrinkage; rheology.

Resumo

Oliveira de Souza, Letícia; de Andrade Silva, Flávio (Orientador). **A influência de micro e nanofibras de celulose em propriedades químicas, físicas e mecânicas de pastas de cimento.** Rio de Janeiro, 2022. 205 p. Tese de Doutorado - Departamento de Engenharia Civil, Pontifícia Universidade Católica do Rio de Janeiro.

A busca por materiais que não impactem negativamente o meio ambiente tem sido uma das prioridades de engenheiros que trabalham com materiais de construção. A emissão expressiva de CO_2 na produção de cimento contribui para tal preocupação. Dentro deste cenário, soluções com emprego de nanotecnologia vêm chamando a atenção em diversas áreas por proporcionar novas soluções. O principal objetivo da presente tese é associar um material proveniente de uma fonte natural com benefícios provenientes da nanotecnologia a fim de modificar propriedades de pastas de cimento considerando seus aspectos químicos, físicos e mecânicos. A nanocelulose se apresenta como material proveniente de fonte renovável que apresenta propriedades atraentes aos materiais cimentícios, sendo assim uma opção a ser utilizada em conjunto com o cimento. Dentre os diversos tipos disponíveis, a celulose nanofibrilada (CNF) foi elencada para ser investigada neste trabalho. A celulose microcristalina (CMM) foi incluída nas investigações para possibilitar uma comparação direta entre as fibrilas da CNF e as partículas de CMM. O uso desses materiais celulósicos pode ser considerado recente e, com isso, existem ainda lacunas no que tange o entendimento dos seus efeitos em materiais cimentícios. Assim, a viabilidade da CNF e da CMM enquanto reforços em pastas de cimento foi avaliada por meio de ensaios de compressão e flexão. Os possíveis mecanismos responsáveis pelo efeito de ambas CMM e CNF foram estudados por meio de análises químicas e físicas. Por fim, foi realizada a caracterização das pastas reforçadas quanto à retração, total e autógena, e à reologia, nos regimes estático e dinâmico. Por conta dos impactos na

trabalhabilidade promovidos pela inclusão de CNF, a mistura delas nas pastas de cimento foi facilitada com a adição de superplastificante, especialmente em porcentagens maiores que 0.050%, em peso. A CMM e a CNF se mostraram eficazes em reforçar as pastas de cimento quanto a esforços de flexão e tração, levando ao aumento das respectivas resistências e módulos. Os resultados obtidos mostraram que a água presente no gel da CNF não está totalmente disponível como água de mistura por conta da morfologia e hidroficilidade das fibrilas. Observada uma certa combinação de porcentagem e fator água-cimento, a inclusão de CNF diminuiu a retração autógena das pastas. A inclusão de 0,040% de NFC levou a resultados semelhantes aos da adição de CMM referente ao aumento da tensão de escoamento e da viscosidade.

Palavras – chave

Celulose nanofibrilada; celulose microcristalina; pasta de cimento; propriedades mecânicas; retração; reologia de pastas.

Table of contents

List of figures

List of tables

Dalva poderia tantas coisas se pudesse. Mas só pôde o que fez. Quem vê de fora faz arranjos melhores, mas é dentro, bem no lugar que a gente não vê, que o não dar conta ocupa tudo.

Carla Madeira, *Tudo é rio*

1. Introduction

1.1. Motivation

The search for innovative materials has always been an important aspect of the evolution of our society. Cellulose is the main component responsible for the strength of plants. If one removes the defects and the parts that are not as strong as cellulose from natural fibers, the resulting material, i.e., micro or nanocellulose, is expected to possess superior properties than its source. Thus, the objective of using nanocellulose is to explore all the benefits of cellulose. With impressive mechanical properties, around 100 GPa of strength and 130 GPa for elastic modulus, nanocellulose fibers are able to reinforce different types of matrices while allowing flexibility. Additionally, they present a high specific area, high water absorption capacity and, are expected to be more stable towards durability than their source plant. These materials are also desirable due to their environmentally friendly characteristic and their availability since they are the most abundant polymer on Earth [1–5]

Due to the aforementioned reasons, nanocellulose is a material with extraordinary properties and its impact on cementitious materials' properties should be studied. The use of nanocellulose in cementitious materials is quite recent and dates from 2009 [6]. There are some research papers about nanocellulose inclusions in cementitious materials and they had evidenced their effect on both fresh and hardened properties. The most affected properties seem to be the workability, hydration reactions, and mechanical response. The main reasons for the changes in the properties reported by the authors are the presence of hydroxyls free groups and the nanocellulose's porous and hydrophilic microstructure. In addition, two mechanisms, steric stabilization, and short-circuit diffusion, also seem to be responsible for nanocellulose interactions with cement particles and hydration products.

Despite the seeming benefits, the dispersion of nanomaterials is one of the primary issues in the successful use of this type of material. In fact, the dispersion

of nanocellulose is the limiting factor of the amount of inclusion in cementitious materials. A full understanding of how micro and nanocellulose act in a cementitious environment allows the comprehension of the multiple properties modified by the presence of those materials.

1.2. Goals

This work aims to investigate how the mechanical and physical properties of cement pastes are modified by the presence of microcrystalline cellulose (MCC) and nanofibrillated cellulose (NFC). But first, a proper dispersion method that considered the particularities of each cellulosic inclusion was developed. How the modifications can be related to the microstructure of the cement pastes was assessed by chemical analysis. The present work also intends to characterize the reinforced cement pastes according to shrinkage and rheological behaviors. The unique morphology of MCC and NFC and how each type convey the water present in the system were discussed through the thesis in order to improve the discussion.

1.3. Thesis organization

The present thesis includes this introduction as part of the Chapter 1, a literature review on Chapter 2 and four chapters, 3-6, besides a conclusion Chapter 7. The introduction chapter brings the motivation and the goals of this work. The literature review chapter presents an introduction with the main aspects of cellulose-based materials, their influence on cementitious matrices' properties, and current dispersion methodologies used. By the end of the literature review, the gaps and challenges about the use of micro and nanocellulose in cementitious matrices are addressed. The following four chapters were developed to meet the needs aforementioned.

(i) Chapter 3: "*Investigation of dispersion methodologies of microcrystalline and nanofibrillated cellulose on cement pastes*", published in Cement and Concrete Composites (https://doi.org/10.1016/j.cemconcomp.2021.104351). The first chapter brings the characterization of the cellulosic inclusions. The feasibility of using NFC and MCC as reinforcements of elements on

a mesoscale was checked. This study was performed along with the development of dispersion and mixture methods. The objective of this chapter was to validate the use of the MCC and NFC as reinforcement on subsequent structural elements and to develop mixture methodologies for them.

(ii) Chapter 4: "*Effect of microcrystalline and nano-fibrillated cellulose on the hydration and mechanical behavior of cement pastes*". After the verifications made in Chapter 3, the possible hydration mechanisms were investigated, at mechanical reinforcement and microstructure levels.

(iii) Chapter 5: "*Effect of nanofibrillated cellulose on shrinkage of cement paste*". The use of the nanofibrillated fibrils as shrinkage-decreasing agents, both total and autogenous, was verified by means of a series of tests. A brief discussion on the relation of the water and the NFC gel was initiated.

(iv) Chapter 6: "*Nanofibrillated and microcrystalline cellulose effect on rheological properties of cement pastes*". The rheological characterization of the reinforced cement paste was made by means of two-point tests, under the dynamic and static regimes. In this Chapter, the discussion of the role of the water present in the NFC gel was improved due to investigations made on cement pastes with different water-to-cement ratios.

The investigations made on Chapters 3 and 4 were driven with the aim of verify the usage potential of the materials on further structural elements and to understand how the inclusions work on the cement pastes. The Chapters 5 and 6 bring the discussions of important aspects for possible applications of cement pastes reinforced with NFC or MCC. The last Chapter, the seventh, brings the conclusions made based on the Chapters 3-6, and suggestions for future works. The outline of the thesis is presented in Figure 1-1.

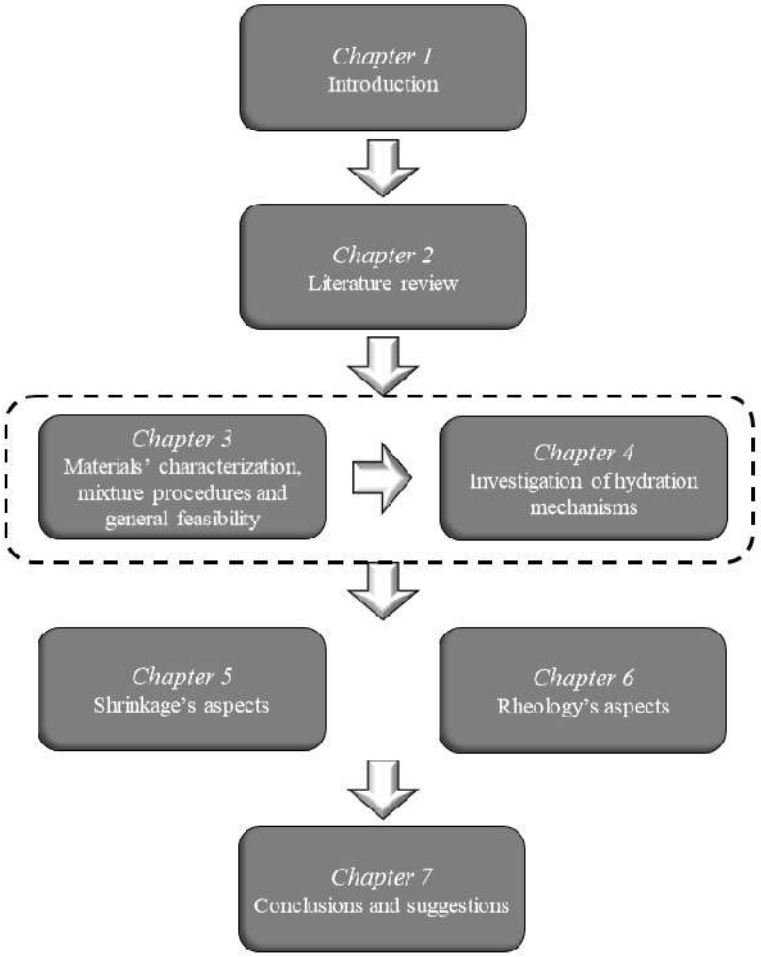

Figure 1-1 Outline of the thesis organization.

It is important to mention that while Chapter 3 was almost fully developed at PUC-Rio, in Brazil, the experiments that belong to Chapters 4-6 were carried at TU-Dresden, in Germany. This two-part collaboration was possible due to the Probral program and lasted 13 months. The work carried at TU-Dresden was developed under supervision of Prof. Viktor Mechtcherine on the Faculty of Civil Engineering (Labor Für Gefügemorphologie and Alfred-Hütter-Laboratorium).

1.4. References

[1] Cellulose and potential reinforcement. In: **Nanocellulose: From Nature to High Performance Tailored Materials.** Berlin: De Gruyter, 2012. p. 1–42.

[2] ABDUL KHALIL, H. P. S. *et al*. Production and modification of nanofibrillated cellulose using various mechanical processes: A review. **Carbohydrate Polymers**, v. 99, p. 649–665, 2014.

[3] MONDAL, S. Preparation, properties and applications of nanocellulosic

materials. **Carbohydrate Polymers**, v. 163, p. 301–316, 2017.

[4] DUFRESNE, A. Nanocellulose: A new ageless bionanomaterial. **Materials Today**, v. 16, n. 6, p. 220–227, 2013.

[5] EICHHORN, S. J. *et al*. Review: Current international research into cellulose nanofibres and nanocomposites. **Journal of Materials Science**, v. 45, n. 1, p. 1–33, 2010.

[6] STEPHENSON, K. M. **Characterizing the behavior and properties of nanocellulose reinforced ultra high performance concrete**. 2011. 152 f. Maine. 2011.

2. Literature review

2.1. Overview of the cellulose-based materials

Cellulose is the natural polymer most found in nature with the formula $(C_6O_{10}H_5)n$. This organic compound consists of linked monosaccharides (glucose) arranged in linear chains, where carbon 1 (C-1) of every glucose molecule is bonded to C-4 of the next unit [1,2]. The cellulose chains have hydroxyls intramolecularly disposed, forming fibrous structures called nanofibrils [3,4]. Cellulose is the main component of plant cell walls that, associated with lignin and hemicellulose, confers to them strength and sustenance. Their characteristics such as fibrils length and crystallinity depend on the source, in other words, the type of the source plant [2,5,6].

There are different types of cellulose-based materials. The dominate size distribution leads their classification on the micro or nanoscale. The nanocellulose term covers the range of materials derived from cellulose with at least one dimension in the nanometer scale [6,7]. One can divide them into two groups: the fibrils, such as cellulose nanofibrils, nanofibrillated cellulose, cellulose nanofibers, and the crystals, such as, cellulose nanowhiskers, cellulose whiskers, cellulose nanocrystals.

Owing to natural fibers hierarchical structure and semi-crystalline nature, nanoparticles can be extracted from them using a top-down mechanically or chemically induced deconstructing strategy [4,6,8,9]. The production methods are different for each nanomaterial desired. In general, nanocellulose can be extracted from various lignocellulosic plant sources by using mechanical, chemical, enzymatic methods or even a combination of them [7]. The mechanical methods involve considerable consumption of energy, while the chemical processes usually use acids that may be considered as not a sustainable option. Thus, research has been focused on finding environmental conservation, high efficiency, and low costs methods to isolate nanocellulose [5].

Two types of cellulose-based material were select as materials of investigation on the present research. According to the aforementioned nomenclature, the microcrystalline cellulose (MCC) is not on the nanoscale but on the microscale and it is part of the crystal group. The nanofibrillated cellulose (NFC) is on the nanoscale and within the fibrils group. MCC and NFC used in this present work are presented in **Figure 2-1**a and b, respectively. Their particularities and extraction approaches are discussed on the following items, although the main difference between them is the presence of a hydrolysis step on the MCC's production. The characterization of the ones used in this study is detailed in Chapter 3.

(a)

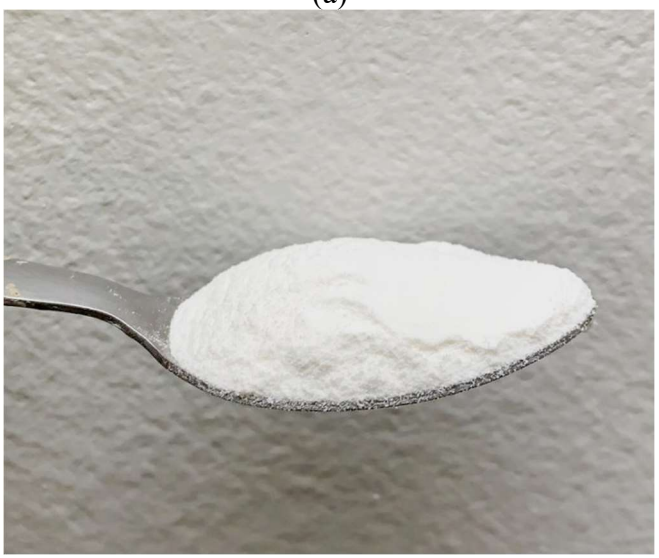

(b)

Figure 2-1 Macro aspects of (a) MCC powder and (b) NFC gel.

2.1.1. Microcrystalline cellulose (MCC)

MCC consists almost exclusively of cellulose crystals with variable length within the microscale range [6,9]. The shape of the particles varies since larger fibrous rod-like to smaller irregular cubes. The top-down approach is utilized to produce microcrystalline cellulose. MCC is usually presented in powder form and may be derived from cellulose by acid hydrolysis followed by homogenization [6,9,10]. One benefit of MCC is that they are currently commercially available, which facilitates their applications [2,11–13].

Parveen *et al*. [14] observed by atomic force microscopy (AFM) images the presence of pure crystalline structures. Such structures may be extracted through chemical and/or mechanical means from the MCC particles resulting in cellulose nanocrystals (CNC) [15,16]. MCC may also be produced from α-cellulose found in, for example, agro-wastes, if submitted to purification process. This purification occurs usually by reactions in boiling acids, as hydrochloric acid (HCl) [17] and sulfuric acid (H_2SO_4) [18].

2.1.2. Nanofibrillated cellulose (NFC)

NFC is composed of fibrillar units with both cellulose crystals and amorphous parts. It presents a high aspect ratio and usually forms agglomerated networks [10,19,20]. The top-down mechanical approach is usually combined with pre-treatments in order to extract fibrils. Mechanical shearing actions applied to cellulosic fibers release individual micro-fibrils. This material is usually called microfibrillated cellulose (MFC). The chosen method and the plant source will determine the morphology and properties of the fibrils. The mechanical processes include high-pressure homogenization and grinding [5,21–23]. Applying only mechanical procedures to achieve MFC may consume a high amount of energy. Thus, different pre-treatments have been proposed to facilitate the process and to enable the production of thinner and higher crystallinity fibers.

Among the pre-treatments, there are mechanical cutting, acid hydrolysis, enzymatic treatment, bleaching and the introduction of charged groups through carboxymethylation or 2,2,6,6-tetramethylpiperidine-1-oxyl (TEMPO)-mediated oxidation [4,6,24–26]. These pre-treatments usually generate finer fibrillated cellulose, called nanofibrillated cellulose (NFC) [6,24]. The diameter of MFC is

in the range of 10 to 100 nm and NFC is about 4 to 20 nm [24]. The length depends on the source of cellulose, defibrillation process and pre-treatment applied [2,6]. Although it is difficult to measure the length due to entanglements, this physical property is usually considered higher than 1 μm [6,27]. By the end of the processes, MFC and NFC are obtained as a suspension in a liquid, usually water.

The NFC here used was obtained by the mechanical defibrillation on pulp and the process will be detailed in Chapter 3. This procedure is rather usual and applied elsewhere before [8,28–31]. The refinement of the fibrils is promoted by the number of defibrillation steps and the morphology of the resulting fibrils can be followed by image analysis [29,30]. In general, the more time processing, the thinner is the NFC [8,9,28].

2.2. The influence of cellulose-based inclusions on the properties of cementitious materials

The terminology of microfibrillated cellulose was first coined in the 1980s [32]. The majority of the current research and applications of nanocellulose is on polymeric matrices [7,33,34]. When it comes to cementitious matrices, the first paper, to the best of the author's knowledge, is from 2009 [35]. Ever since, there is a growing interest in exploring the changes in cementitious materials upon the presence of micro and nanocellulose.

The use of cellulose-based materials in cementitious composites may have different approaches as they can be used as reinforcement or as additions. For their small size, the particles may fill gaps in the microstructure of the matrix, altering hydration reactions [25,28,36,37]. The concept of using nanocellulose as reinforcement comes from the attempt to explore the high stiffness, strength and the high aspect ratio they present [6,38–40]. These characteristics could be responsible for arresting microcracks and favor a more ductile behavior [26,41–45]. Furthermore, nanocellulose owns a high specific surface area that may provide good fiber-matrix bonding. The hydroxyl groups available on cellulose chains could enable the formation of hydrogen bonds between nanocellulose and cementitious matrix, leading to an increase in the interface bonding [28,46,47]. These interactions affect mostly hydration reactions [25,36,37,47–49] and fresh

properties [24,28,37,48,50–54] resulting in an impact on the mechanical response [18,25,26,28,35,36,49,50,52,55].

The following Sections are devoted to summarizing the main findings regarding the effects of micro and nanocellulose on diverse properties of cementitious matrices. The examples are focused on the effects of the inclusion of MCC and NFC. Those properties include rheology, hydration, porosity, mechanical performance, and shrinkage.

2.2.1. Influence on rheology

2.2.1.1. Concepts of rheology

Rheology can be understood as the study of the flow behavior of a material submitted to stresses, under specific thermodynamic conditions, during a time interval [56]. In the case of cementitious materials, the comprehension of flow behavior refers mainly to the fresh state of the cement-based materials. The flow characteristics of concrete can limit its utilization and interferes on the way of processing it. The cement particles react with water and the hydrates form a plastic paste that develop rigidity within a few hours. The following hard state is when it develops compressive strength over several months [57].

The cement paste can be considered a non-homogenous viscous liquid, or a flocculated suspension, that needs an initial stress different from zero to start to flow. In short, from the first contact with water, the hydration process starts and until the end of the dormant period, the cement paste presents itself on the fresh state until it sets. The first hydrates formed on the cement particles edges bridge to each other, big capillary pores are formed and with the evolution of the hydration reactions, the pore network becomes more refined. Those processes lead to the formation of a mineral skeleton that brings the cement paste to a solid state. Thus, the cement paste is a material which flow characteristics are highly time dependent [57–59].

According to Ramachandran and Beaudoin [58], the volume fraction of solid particles and the rate of agglomeration, or flocculation, affect the flow behavior of suspensions. In the case of cement paste, the fraction of solid particles is related to the water-to-cement ratio. Theoretically, the interparticle forces due to electrostatic are weak, so they can be broken by shear stresses. In the case of

cement pastes, in addition to the colloidal forces, the hydration products also act bridging the particles. For the suspension to start to flow, some of the links between the particles must be broken. The shear stress that triggers the flow is called yield stress. The interparticle forces, closely related to the yield stress, depend on the shape and size distribution of the solid particles. The size and shape of the created flocs also affect the rheology of the cement pastes [60]. With enough shear stress, the flocs are reduced to the original particles, decreasing the resistance to flow. When the paste come to rest, it is possible to occur a re-flocculation and thickening of the paste. For most of cementitious materials, the changes provoked by the shear rate and hydration evolution are not completely reversible, so the terms structural breakdown and build-up are preferable [57,59].

In order to measure the flow behavior of cementitious materials, there are mainly two types of tests: the static and the dynamic methods. For each test, the shear stress is measured for a given shear rate applied, and when the experiment is performed for a certain number of shear rate (or stress) values, a flow curve can be created. With the purpose of investigating and comparing the flow behavior among different materials, constitutive models are often used. The models basically describe the constitutive behavior of the materials, reducing the existing complexities into rheological parameters that are easier to be defined. Those parameters establish general relations and aspects enabling comparisons. Another important concept is the hysteresis curve, which is generated by the loading and unloading a suspension. There is a lack of equilibrium between the microstructure and the shear rate when a stress range difference between loading and unloading is noticed. Usually, the aim is to perform the measurements at steady state. So, it is a custom to consider only the unloading portion of the curve for the tests [58].

It is possible to find in the state-of-art that all flow curves show the existence of the yield stress, although with a considerable value range of this parameter. Even for a same water to cement ratio, the values can be discrepant. The differences are usually attributed to experimental techniques, apparatus, mixture handling and test parameters [61]. It is also frequently noticed on the literature the non-linearity of the cement paste flow, with a decreasing yield stress as the shear rate or the total shear energy increases [60,62].

2.2.1.2 Effect of cellulose-based inclusions on the rheology of cementitious materials

Previous researches have shown that the addition of cellulose nanocrystals (CNC) changes the rheological behavior of cement pastes depending on their inclusion percentage [37,54,63]. At low additions, the CNC act by dispersing the cement particles and consequently increasing the flowability of the fresh material. This effect is called steric stabilization, and it is comparable to the water-reducing admixture's effect [37]. When the dosage is superior to a specific value, the yield stress increases. Montes *et al*. [54] showed that different types of CNC lead to distinct influences on the yield stress of cement pastes. Moreover, how the CNCs act on the rheological behavior is also dependent on the type of cement and the water-to-cement (w/c) value.

MCC was proved to be an interesting material in the 3D-printing field. Long *et al*. [64] investigated the possibilities of improving the rheological properties of 3D-printing mortar with the inclusion of MCC. One percent of MCC increased the plastic viscosity by around 21% and the yield stress by 190%, as well as the thixotropy value. In addition, the presence of MCC also improved the shape retention capacity of the extruded layers and their heights, indicating an enhanced buildability. Those improvements were attributed to the micro-size MCC presents, its water-retention ability, and the interactions promoted by the hydroxyl groups. Although the decrease of workability is usually observed in matrices with MCC [14,65,66], there are exceptions [67,68]. This subject will be discussed in Chapters 3 and 6

In opposition to cellulose nano and microcrystals, cellulose nanofibers (CNF) increase the yield stress even at low inclusions [63,69]. Sun *et al*. [70] showed that the more CNF the slurry contained, the more the shear-thinning behavior became evident. A similar trend was found by Kolour *et al*. [53] and Hisseine *et al*. [43] where the CNF inclusion increased the yield stress and viscosity, in both concrete and cement pastes. In fact, Kolour *et al*. [53] observed that for each 0.1% of CNF, it is needed around 8% of extra mixing water so concretes can present comparable workability. The cellulose nanofibrils retain part of the mixing water [43] in the fresh state, and it seems that this water is not fully available for workability purposes, at least initially. This effect was more noticeable in mixtures with a lower water-to-cement ratio [53]. Furthermore, the degree of

defibrillation of the CNF also affects the rheological behavior of oil-well cement slurries, as observed by Tang *et al*. [63]. The effect of passing the CNF through the grinder, i.e., improving refining, led to higher rheological parameters values, namely yield stress, viscosity and gel strength, similar to an increase in the CNF percentage [63]. Even with an increasing dosage of superplasticizer, the CNF is still able to increase both yield stress and plastic viscosity of cement pastes and concretes [71,72].

Similar to cellulose nanofibers, the cellulose filaments (CF) can be used as viscosity modifier agents in cement pastes and concretes [43,72]. The CF addition enhanced the stability of the fresh cementitious materials and contributed to their shear-thinning behavior. Although the effect of increasing the rheological parameters was observed for both yield stress and viscosity, this impact was more severe on the yield stress values [43,71,72]. This has been observed on cementitious materials with MCC [64].

Besides the impact of the morphological aspects and the hydrophilicity on the rheological properties of cementitious materials, the characteristics of the gel itself also play a role in those properties. Ez-zaki *et al*. [73] observed that the degree of dispersion of cellulose fibrils suspensions and the degree of oxidation resulting from the producing stage alter the rheological behavior of cementitious materials. Those characteristics influence how strong the fibrils interactions are and the water retention capacity of the CNFs, which consequently affects the cement's rheology.

2.2.2. Influence on hydration

The study of hydration can be divided into degree of hydration and hydration kinetics. The degree of hydration is often based on the non-evaporable water content, often analyzed by thermogravimetric (TG) methods. In order to quantify and classify the hydration products, mineralogical analysis, as X-Ray diffraction (XDR), and Fourier transform infrared spectroscopy (FTIR) can be performed. The hydration kinetics is evaluated by means of the heat flow evolution, including the cumulative heat and the peak hydration time and value. Initial and final setting times can also be used to investigate the hydration changes face the nanocellulose inclusions.

Most of the research papers show that the addition of micro and nanocellulose into cementitious materials positively affects the degree of hydration [25,28,74,36,37,44,47,65,67,69,70]. Generally, the presence of cellulose-based materials increases the heat peak of hydration [25,36,37,40,43,47–49,72,73]. A delay in reaching this peak can be observed [25,37,73,75] or not [47,48].

Between the reasons for the hydration alterations, the alkaline hydrolysis is mentioned due to their exothermal reactions that can contribute to increase the heat peak [49]. A possible induced internal curing due to hydrophilic characteristic of nanocellulose is also mentioned as one of the causes for hydration enhancing [44,48,49,65]. In addition, due to its size, the nanocellulose may not only behave as a hydration activator but also as a filler, with a physical effect [25,35,48]. Another possibility is that nanocellulose acts as a nuclei to facilitate the hydration reactions, increasing the degree of hydration [14,25,47]. Cao *et al*. [36,37] explained nuclei effect as "short-circuit diffusion". According to them, the cellulose nanocrystals could act as a path for the water to achieve the inner grain.

The delay in hydration reactions may be related to the decrease of the cement particles' surface area if the nanocellulose adhere on them [47]. This effect is similar to the aforementioned steric stabilization [36,37]. The hydration delay is also compared to the effect that superplasticizer addition presents when they are incorporated on cementitious materials [49]. The –OH presence and their interactions between cellulose molecules, cement particles and cement hydration products may also delay the hydration reactions [48]. Even a small reduction in the temperature released in the first hours of hydration may signify less thermal cracks and shrinkage on large masses of concrete [48].

The presence of micro and nanocellulose on cementitious matrices usually increase the degree of hydration in around 10%, in comparison to the plain matrix [37,40,47,72,75]. Although an impressive improvement of more than 100% had already been reported [25]. It is important to point out that not every cellulose-based inclusion led to hydration improvement at all ages and percentages of inclusion. And it is also important to highlight that those hydration analyses are usually performed on early age (younger than 28 days) samples.

Regarding the MCC effect, Parveen *et al*. [14] studied the hydration effect of cement pastes reinforced with it. From differential thermogravimetric analysis

(DTG) curves, it was possible to observe a sharper peak related to calcium hydroxide (CH), indicating the formation of larger CH crystals with MCC addition. The peak related to calcium carbonate ($CaCO_3$) was considerably lower for samples with MCC. This was associated with the denser microstructure that would have obstructed the carbon dioxide (CO_2) diffusion into the cementitious matrix to form $CaCO_3$. Similar findings were reported by Silva *et al*. [66] and Parveen *et al*. [65]. A decrease in the peak temperature of 5°C was observed by Hoyos *et al*. [48], which behavior was attributed to polysaccharide effects. Even resulting in a decrease in the heat peak, an enhancement in the hydration degree was evidenced by TGA results.

2.2.3. The microstructure of cementitious materials with cellulose-based materials

Modifications on the microstructure of the composites reinforced with cellulose-based materials are partially responsible for changes in their macro properties. Some improvements are attributed to a stiffer microstructure promoted by micro and nanocellulose inclusions. Depending on the cementitious matrix and the cellulose-based material combination, the total porosity can increase [47,73,74,76] or a decrease [25,36,47,55,77,78]. In the latter case, the decrease of porosity is usually related to changes in hydration: the hydration of unhydrated cement particles can form more products of hydration, filling the pores and thus, reducing their size.

Even in the cases where an increase of the total porosity was observed, there were modifications on the pore size distribution profile. For instance, it was reported an increase in the number of small pores [74,76,77] and a decrease in the dominant pore diameter [47,74,77]. Those outcomes can also be considered as a densification of the matrix, depending on what is in consideration. Some specific examples are following.

Jiao *et al*. [47] through a mercury intrusion porosimeter (MIP) technique, investigated the effect of the TEMPO modified NFC inclusions on the porosity of cement pastes. The mean pore size decreased in 1 nm and the total porosity decreased 0.5% with 0.15% of CNFs. It was observed that the range of the pore size distribution changed from 15 - 40 nm to 10 – 22 nm with 0.4% of NFC. Mejdoub el at. [25] also investigated the effect of the addition of NFC on the

porosity of cement pastes. The percentage with relation to cement weight varied between 0 and 0.5% in the samples. Results showed, at an optimum inclusion of 0.3% of NFC, an increase of 2% in bulk density and 36% less porosity. However, beyond 0.3% of NFC, negative effects in density and thermal conductivity were observed. This was attributed to a poor dispersion.

Fonseca *et al*. [26] compared the microstructure of extruded cement-based composites reinforced with macro fibers and NFC by means of water absorption (WA) and apparent void volume (AVV) tests. When compared with macro fibers, the nanofibrillated cellulose reinforced composite presented lower WA and AVV values for contents of 0.5% and 1.0%. Regarding the non-reinforced specimens, the WA and AVV values were the same than the NFC specimens.

Regarding the use of MCC particles on cementitious matrices, their effect seems to be more constant. The inclusion of MCC led to an increase in the small pore volume and a decrease in the average pore diameter. Interestingly, it was also reported the appearance of new peaks on the intrusion volume [14,65,66]. Parveen *et al*. [14] used SEM analysis and MIP technique to study the microstructure of cement pastes reinforced with MCC. Results showed that the total porosity increased with MCC addition although the mean pore size changed from 95 nm to 50 nm. That is, with MCC addition, there are more pores of smaller diameters. Silva *et al*. [66] also investigated the effect of MCC in the microstructure of mortars and had similar results: the mean pore diameter measured with MIP decreased from 47 nm to 30 nm for specimens with 0.6% of MCC, although the porosity increased around 2% for these specimens. The dry bulk density increased until the optimal amount of 0.2% of MCC. This behavior was attributed to MCC's size and internal curing capacity.

2.2.4. The impact on the mechanical properties

Improvements in mechanical performance upon nanocellulose addition even with low fiber content had been widely shown [18,25,28,35,36,47,49,50,52,55]. Most of the studies indicate the existence of an optimal percentage of fibers that lead to the best mechanical response; beyond this value, agglomerations are formed and the performance decreases [25,28,35,37,49,50,52,55,79]. The advances in mechanical behavior are usually attributed to a greater degree of hydration and its effects, as already discussed in Sections 2.2.2 and 2.2.3.

However, the assumption that the fibrils-like cellulosic materials could act as load-bearing agents or bridges for cracked faces is becoming frequent [26,41–45].

In general, there is in Literature a higher frequency of positive effects in flexural properties than in compressive ones when micro and nanofibrillated cellulose are added to the matrices [41,43–45,72], especially when nanofibrils and nanocrystals are directly compared [77]. In fact, some adverse effects in compressive strength of specimens reinforced with NFC were already reported [43,45,53,73]. However, there is still no agreement whether the NFC fibrils influence more the early ages [25,40,41,80] or the long term [39,43,47,72] mechanical properties.

Fonseca *et al*. [26], with an extrusion technique to produce nanofibrillated cellulose cement composites, compared the mechanical performance between NFC and macro natural fibers, maintaining the amount of fiber content: 0.5%, 1% and 2%. The nanocellulose specimens presented generally the best results, regarding the bending properties, and this was attributed to the greater surface area of the nanocellulose and to its intrinsic properties. The pullout of the nanofibrils is possibly responsible for the toughening and energy absorption mechanisms.

Another example of the difference between the reinforcement promoted by micro and nanofibers, is the work of Ardanuy *et al*. [28]. While microfibers provided higher fracture energy and ultimate displacement, nanofibers elevated both flexural modulus and strength. Nanofiber's characteristics such as intrinsic strength and stiffness, length and superficial area were cited as main causes of the brittle versus pseudo-ductile behavior. The presence of hydroxyl groups on nanocellulose enables the formation of hydrogen bond with the cementitious matrix, enhancing their bonding and thus, favoring the brittle response. Based on these results, Ardanuy *et al*. [28] suggested that the hybridization of the two types of fibers could lead to an optimal response. One example of hybridization was carried by Correia *et al*. [46], with pulp and nanofibrillated cellulose. The four-point bending tests parameters did not significantly change, although the mean value of modulus of elasticity was higher for the hybrid specimens (8% pulp + 1% NFC).

Despite the brittle failure mode found by Ardanuy *et al*. [28], advances in tailoring the matrix regarding ductility upon NFC inclusions have been made. In

fact, Supit *et al*. [42] observed a well-post crack behavior of mortars promoted by NFC with a fracture mechanics test. They noticed an increase of 36% and 20% in the peak load and the toughness, respectively. Furthermore, Hisseine *et al*. [44] showed that in more fine-grained concrete formulations, NFC is capable of increasing by 74% the flexural toughness. Those results indicate that nanofibrils may have a reinforcement potential.

Onuaguluchi *et al*. [49] evaluated flexural mechanical properties of different proportions of NFC inclusions: 0.05, 0.1, 0.2 and 0.4% of cement weight. It was observed that the addition of 0.1% of NFC was the optimal percentage with improvement of 106% and 184% in flexural strength and energy absorption, respectively. Mejdoub *et at*. [25] evaluated the addition of 2,2,6,6-Tetramethylpiperidinyloxy (TEMPO) pre-treated NFC on the compressive strength of cementitious composites. Compressive strength increased with the NFC addition, presenting the highest increase of 43% for 0.3% of fiber inclusion. Negative effects were observed for specimens with 0.5% of fiber addition due to poor dispersion. The degree of hydration presented an almost linear relation with compressive strength.

Regarding the effect of MCC on cementitious materials, improvements in compressive strength of around 20% were reported [64,66,67] as well as adverse effects [18,48]. With respect to flexural parameters, the enhancement in flexural modulus is usually greater than in flexural strength [14,65,66]. The improvements in the mechanical performance of specimens with MCC, if any, are often attributed to modifications on the hydration products and to the denser matrix.

It is worth to mention that the mechanical properties of specimens containing MCC are susceptible to treatments performed on its particles. Anju *et al*. [18] prepared MCC from cotton and treated with tetraethyl orthosilicate (TMCC). The specimens with treated microfibers presented higher values of the properties assessed in comparison with MCC without the treatment. The most affect parameter was the flexural strength with 94% of improvement with TMCC, against the 50% reached by MCC.

The dimensions of the specimens discussed in this Section are mainly in the millimeter scale (see Table 2-1). Regarding further applications, one may considerer scale effects, that is, the size of the specimen may have an influence on the mechanical response of the composite.

Table 2-1 - Specimen small dimensions for different tests performed.

Test	Specimen dimension (mm)	References
Compression	40²; 8 x 16; 50³	[35,48,50,52,55]
Bending	40² x 160; 40 x 20 x 160; 30 x 50 x 220; 23 x 37 x 170; 28 x 18 x 200;	[26,28,35,37,48–50,52,79]

2.2.5. The shrinkage of cementitious matrices with cellulose-based materials

In cementitious materials, shrinkage takes place in the cement paste, and it can be subdivided according to the different sources of the trigger mechanisms. For instance, drying shrinkage is trigged by physical water loss. In order to keep the humidity equilibrium, the moisture present in the porous structure evaporates leading to a decrease in volume [81]. Its magnitude is considerable and, while for concrete the recommendation is not to exceed 400 με [82], cement pastes values range from 1000 to 3500 με, including total shrinkage values [53,83–85]. Autogenous shrinkage deals with the internal humidity movement, in a combination of chemical and physical mechanisms induced mainly by self-desiccation [86]. It is most significant for water-to-cement ratios lower than 0.40 [87], and its order of magnitude in cement pastes considerably varies, reaching more than 1000με in 14 days [88].

Since shrinkage is related to water movement on the cementitious microstructure, a material that works like an internal reservoir may facilitate ongoing hydration and mitigate autogenous shrinkage cracking, such as lightweight aggregates, can be used [89–91]. The use of nanocellulose inclusions may lead to similar behavior. This ability is attributed to their porous structure, hydrophilic character and water retention capability, enabling the formation of "moisture paths" inside the matrices [92]. Different shrinkage tests were performed to validate this hypothesis [35,39,40,50,53,92]. In a general manner, nanocellulose inclusions are able to promote a reduction in shrinkage, especially in early-age samples [35,39,50,92].

Hisseine *et al*. [39] showed that cellulose fibrils are able to decrease the autogenous shrinkage due to an internal curing effect and due to a reinforcement effect at the nanoscale. In fact, the presence of cellulose fibrils led to a volumetric expansion in the first hours of test. When compared to the non-reinforced matrix,

the deformation reduction was 75% in the first hours and then stabilized at around 50% beyond 7 days. They correlated the deformation increase, i.e. the expansion, to the ability of the fibrils of releasing the water that was first retained by them.

Different scales of natural fibers were investigated on autogenous and drying shrinkage, including macro sisal fibers (volume of 1.28%), micro eucalypt fibers (volume of 1.28%) and nanofibrillated cellulose (volume of 0.2%) by Ferrara *et al*. [92]. The NFC addition showed to be able to decrease autogenous shrinkage, although its presence led to an increase in the total shrinkage. The shrinkage of ultra-high performance concrete reinforced with 0.5% of nanocellulose was investigated by Stephenson [35]. The results indicated that the nanofibers addition had more influence on the shrinkage behavior on the first two days. By the end of 13 days, the specimens with 0.5% of nanocellulose decreased the strain by 72% when compared with unreinforced ones. Despite this positive effect, it is worth commenting that the water/cement ratio was higher for specimens with nanocellulose. Cellulose nanocrystals had already been used as reducing draying shrinkage agents, with a decrease in 55% of the deformation in comparison to plain matrix [93].

The effectiveness of the cellulose fibrils in decreasing shrinkage deformation is not a total consensus. Kolour *et al*. [53] showed that the free shrinkage may increase or decrease face the inclusion of nanocellulose. It takes a certain combination of water-to-cement ratio and nanocellulose percentage to obtain positive results. They further found that the increase in shrinkage deformation may be related to the water retained by the fibrils [40]. This negative effect may be reduced if the water present within the fibrils is not discounted from the mixing water [40].

2.3. Dispersion of cellulose-based inclusions on cementitious materials

When micro and nanocellulose are added into cementitious matrices they tend to form agglomerates that may act as defects or stress concentrators, as shown in Figure 2-2, due to the existence of interaction forces between the particles [6,7,79]. These inter-particle interactions may limit the potential of mechanical reinforcement [25,28,35,37,49,50,52,55,79]. This phenomenon is magnified when the size of the particle decreases [2,6].

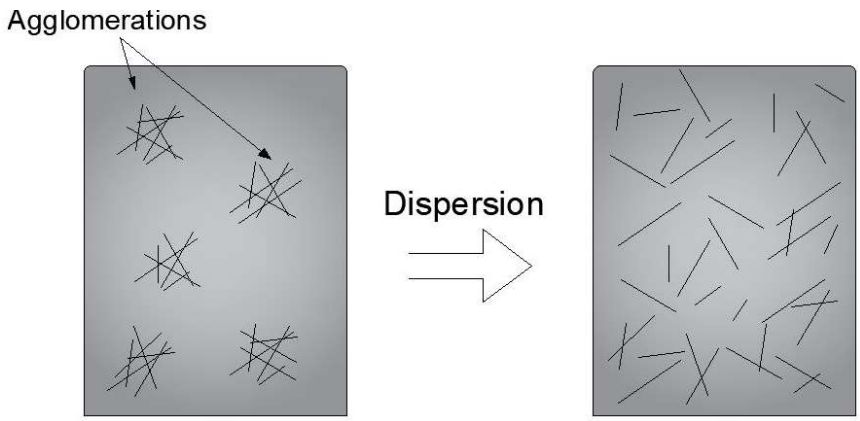

Figure 2-2 – Schematic representation of agglomerate and the result of a properly dispersion processing. Adapted from [79].

Proper dispersion agents or procedures may be employed to ensure the total benefit that can be explored from nanocellulose reinforcement ability. One can dispose nanocellulose within cementitious matrix by using chemical methods, such as superplasticizer, surfactants and stabilizing agent, or mechanical methods, such as ultra-sonication, ultrasonic bath, and magnetic or mechanical stirring, or even a combination of both methods. Dispersion in cementitious materials is usually carried as a step in the mixing process [18,38,39,41,25] or as a pre-treatment in case of TEMPO-mediated oxidation [25,47] and tetraethyl orthosilicate [18]. 2,2,6,6-Tetramethylpiperidine-1-oxyl (TEMPO) oxidation is a pretreatment that facilitates the isolation of nanofibers by introducing carboxyl groups at the carbon 6 (C6) of the glucose unit.

Some procedures adopted for dispersion in cement-based materials are following listed:

- Superplasticizer addition into water and nanocellulose mixture [35,49,50,52];
- Ultrasonication [36,47,79];
- Chemical modifications, as TEMPO modification [25,47] , as well as tetraethyl orthosilicate (TEOS) modification [18];
- Ultrasonic bath [14,25,49,65];
- Surfactant [65];
- Stabilizing agent carboxymethyl cellulose (CMC) [65];
- Magnetic stirring [47,66].

The methods above listed were divided according to the type of nanocellulose (NFC and MCC) in order to enlighten the possibilities for the present work. Table 2-2 presents the methods used for each type of nanocellulose.

Table 2-2 – Different methods of dispersion of NFC and MCC into cementitious matrix. UB = ultrasonic bath; MagS = magnetic stirring; Super = superplasticizer; MecS = mechanical stirring.

NFC		MCC	
Method	*Ref*	*Method*	*Ref*
TEMPO + UB	[25]	Super	[18]
TEMPO + MagS + Ultrasonication	[47]	Surfac + Super + UB	[65]
Super	[35,50,52]	CMC + Super + UB	[65]
Super + MecS	[49]	MagS	[66]
		UB + Super	[14]

Onuaguluchi *et al*. [49] investigated the dispersion of NFC in cement pastes using a scanning electron microscope (SEM) and mechanical tests. The dispersion method used consisted of 5 minutes of mixture (NFC gel and water), addition of 1.6% of superplasticizer and 10 minutes of ultrasonic bath. No comparison with mixtures without dispersion was made. The specimens with 0.1% of fibers presented less small pores than the ones with 0.4% and the latter presented some large-sized clumps. Mechanical tests indicated dispersion issues in specimens with more than 0.2% of nanofibers. Jiao *et al*. [47] performed 15 minutes of magnetic stirring and subsequently 15 minutes of sonication on NFCs modified by TEMPO oxidation. The optimal content based on mechanical response was of 0.15%. No comparison with mixtures without dispersion was made.

Cao *et al*. [79] carried a direct study on how the nanofibers dispersion affects the flexural strength. Results from rheological tests showed that agglomeration starts for CNC concentration higher than 1.35% in volume in deionized water. If the solution is the one that simulates the pore solution, the one found in the matrix in fresh state, the CNC began to agglomerate on a lower concentration, about 0.18% in volume. This result agrees with flexural tests, which indicated the higher value of strength for specimens with 0.2% of CNC. As dispersion methods, two approaches were used: the use of ultra-sonication and water reducing agent addition (WRA). It was found that the longer the nanocellulose suspension went under sonicating (up to 30 minutes), the more transparent it got and less shear

stress it presented. Flexural tests indicated an increase of 50% in strength on specimens with CNC sonicated for 30 minutes, and the strength continued increasing even for concentrations above 0.2%. Thus, based on experimental observations, the key to improve flexural strength of cement paste with high concentration of CNC is good dispersion. The addition of WRA did not show any significant improvement.

Parveen *et al*. [65] compared surfactant and stabilizing agent (CMC) efficiency on MCC dispersion. By visual inspection of sedimentations, CMC was not able to disperse any percentage of MCC in water. On the other hand, surfactant addition was able to disperse up to 0.6% of MCC on 1:5 (surfactant:MCC) ratio and 1% of MCC on 1:1 ratio. This tendency was confirmed by UV-Vis spectra results: the highest concentration of MCC in aqueous suspension was achieved at 0.6% of MCC. Contradictorily, CMC resulted in greater concentration according to UV-Vis analysis. Higher values of flexural strength were obtained for 0.5% of MCC when surfactant (1:5 ratio) was added and 30 minutes of magnetic stirring was employed. Silva *et al*. [66] found, after optical microscopy analysis, that magnetic stirring for 45 minutes was able to disperse up to 0.8% of MCC. Despite that, compression and bending tests showed best results for 0.2% of MCC inclusions. For the same material, Parveen *et al*. [14] submitted MCC suspensions to ultrasonic bath for different periods, 15, 30, 45 and 60 minutes. They also used UV-Vis spectra in order to calculate the extractability of the suspensions (a measure of dispersion degree), and then selected the best duration of the dispersion method which was 30 minutes. In the last three discussed papers [14,65,66] no comparison with mixtures without dispersion was made.

The range of the percentage of nanocellulose used in the present work was based in Table 2-3 that lists the optimal percentage of different types of nanocellulose into cement-based matrixes. The references with asterisk are the ones with no variation of the percentage, that is, the percentage is not the optimal, is the only one used.

Table 2-3 – Optimal percentage for nanocellulose inclusions in cementitious matrices in literature. Percentage referenced to cement weight.

MCC		NFC		Other	
%	Reference	%	Reference	%	Reference
10	[18]*[a]	0.15	[47]	0.2	[94]
0.5	[65]	3.0	[95]*	0.2	[17]
0.5	[14]	1.0	[35]	0.4	[50]
0.2	[66]	0.2	[92]*[b]	3.0	[52]
3.0	[48]*	3.3	[28]*	0.2	[36,37,96][b]
		0.3	[25]	0.5	[79]
		0.1	[49]	0.04	[69]*

[a] = surface modified
[b] = % in cement volume

2.4. Conclusions

From the Literature review carried in Chapter 2, it was clear the potential of the cellulose-based materials demonstrates as inclusions in cementitious matrices. The presence of those micro- and nanoscale materials alters the behavior of cementitious materials under several aspects, including macro properties in both fresh and hardened states. Although there are similarities in the outcomes provided by those cellulose-based materials, the way they act in cementitious matrices seem to be different. The reason for that may be relied on their distinct morphology and physical characteristics. Another possible key factor for this discussion is the relation between the cellulose-based materials, especially the fibrils, and the water ratio.

It was also possible to notice that although MCC and NFC have a significant influence on the workability of cementitious materials, there is still a lack of a more complete rheological characterization of them. Moreover, there is a divergence in respect to their involvement regarding shrinkage behavior.

Most of the reviewed works were conducted with rather small specimens, so the ability of MCC and NFC to reinforce specimens considered on the mesoscale should be tested. In addition, due to the structure of MCC and NFC and the form they present i.e., powder or gel, there is a necessity for a specific mixing method to each inclusion. Thus, a proper way to mixture each inclusion targets a better exploitation of their intrinsic properties.

Based on the aforementioned gaps found in the Literature, the present thesis was designed to improve the discussion of the role of MCC and NFC on cement paste regarding chemical, mechanical and physical aspects.

2.5. References

[1] Cellulose and potential reinforcement. In: **Nanocellulose: From Nature to High Performance Tailored Materials.** Berlin: De Gruyter, 2012. p. 1–42.

[2] EICHHORN, S. J. *et al*. Review: Current international research into cellulose nanofibres and nanocomposites. **Journal of Materials Science**, v. 45, n. 1, p. 1–33, 2010.

[3] ABITBOL, T. *et al*. Nanocellulose, a tiny fiber with huge applications. **Current Opinion in Biotechnology**, v. 39, n. I, p. 76–88, 2016.

[4] PARVEEN, S.; RANA, S.; FANGUEIRO, R. **Macro- and nanodimensional plant fiber reinforcements for cementitious composites**. [s.l: s.n.].

[5] ABDUL KHALIL, H. P. S. *et al*. Production and modification of nanofibrillated cellulose using various mechanical processes: A review. **Carbohydrate Polymers**, v. 99, p. 649–665, 2014.

[6] DUFRESNE, A. Nanocellulose: A new ageless bionanomaterial. **Materials Today**, v. 16, n. 6, p. 220–227, 2013.

[7] MONDAL, S. Preparation, properties and applications of nanocellulosic materials. **Carbohydrate Polymers**, v. 163, p. 301–316, 2017.

[8] GUIMARÃES JUNIOR, M.; TEIXEIRA, F. G.; TONOLI, G. H. D. Effect of the nano-fibrillation of bamboo pulp on the thermal, structural, mechanical and physical properties of nanocomposites based on starch/poly(vinyl alcohol) blend. **Cellulose**, v. 25, n. 3, p. 1823–1849, 2018.

[9] XU, X. *et al*. Cellulose Nanocrystals vs. Cellulose Nano fi brils: A Comparative Study on Their Microstructures and E ff ects as Polymer Reinforcing Agents. **ACS applied materials & interfaces**, v. 5, p. 2999–3009, 2013.

[10] NETRAVALI, A. N.; CHABBA, S. Composites get greener. **Materials Today**, n. April, p. 22–29, 2003.

[11] LAVOINE, N. Microfibrillated cellulose – Its barrier properties and applications in cellulosic materials: A review. . **Carbohydrate Polymers, 90, pp.735– 764.**, v. 90, p. 735–764, 2012.

[12] POSTEK, M. T. *et al*. Production and Applications of Cellulose

Nanomaterials. p. 3–317, 2013.

[13] PHANTHONG, P. *et al*. Nanocellulose: Extraction and application. **Carbon Resources Conversion**, v. 1, n. 1, p. 32–43, 2018.

[14] PARVEEN, S. *et al*. Ultrasonic dispersion of micro crystalline cellulose for developing cementitious composites with excellent strength and stiffness. **Industrial Crops and Products**, v. 122, n. May, p. 156–165, 2018.

[15] ÇETIN, N. S. *et al*. Acetylation of cellulose nanowhiskers with vinyl acetate under moderate conditions. **Macromolecular Bioscience**, v. 9, n. 10, p. 997–1003, 2009.

[16] BONDESON, D.; MATHEW, A.; OKSMAN, K. Optimization of the isolation of nanocrystals from microcrystalline cellulose by acid hydrolysis. **Cellulose**, v. 13, n. 2, p. 171–180, 2006.

[17] MAZLAN, D. *et al*. Cellulose Nanocrystals Addition Effects on Cement Mortar Matrix Properties. **International Journal of Advances in Mechanical and Civil Engineering**, v. 3, n. 1, p. 44–48, 2016.

[18] ANJU, T. R.; RAMAMURTHY, K.; DHAMODHARAN, R. Surface modified microcrystalline cellulose from cotton as a potential mineral admixture in cement mortar composite. **Cement and Concrete Composites**, v. 74, p. 147–153, 2016.

[19] TONOLI, G. H. D. *et al*. Properties of cellulose micro/nanofibers obtained from eucalyptus pulp fiber treated with anaerobic digestate and high shear mixing. **Cellulose**, v. 23, n. 2, p. 1239–1256, 2016.

[20] BUFALINO, L. *et al*. How the chemical nature of Brazilian hardwoods affects nanofibrillation of cellulose fibers and film optical quality. **Cellulose**, v. 22, n. 6, p. 3657–3672, 2015.

[21] JAWAID, M.; KHALIL, H. P. S. A. Cellulosic / synthetic fibre reinforced polymer hybrid composites : A review. **Carbohydrate Polymers**, v. 86, p. 1–18, 2011.

[22] KHALIL, H.P.S.; A.H. BHAT; A.F. IREANA YUSRA. Green composites from sustainable cellulose nanofibrils: A review. **Carbohydrate Polymers**, v. 87, p. 963–979, 2012.

[23] WANG, Y. *et al*. Homogeneous isolation of nanocellulose from cotton cellulose by high pressure homogenization. **Journal of Materials Science and Chemical Engineering**, v. 1, n. October, p. 49–52, 2013.

[24] FU, T. *et al*. **Cellulose nanomaterials as additives for cementitious materials**. [s.l.] Elsevier Ltd, 2017. v. C

[25] MEJDOUB, R. *et al*. Nanofibrillated cellulose as nanoreinforcement in Portland cement: Thermal, mechanical and microstructural properties. **Journal of Composite Materials**, v. 51, n. 17, p. 2491–2503, 2017.

[26] FONSECA, C. S. *et al*. Jute fibers and micro/nanofibrils as reinforcement in extruded fiber-cement composites. **Construction and Building Materials**, v. 211, p. 517–527, 2019.

[27] PENG, B. L. *et al*. Chemistry and applications of nanocrystalline cellulose and its derivatives: A nanotechnology perspective. **Canadian Journal of Chemical Engineering**, v. 89, n. 5, p. 1191–1206, 2011.

[28] ARDANUY, M. *et al*. Nanofibrillated Cellulose (Nfc) As A Potential Reinforcement For High Performance Cement Mortar Composites. **BioResources**, v. 7(3), p. 3883–3894, 2012.

[29] DEEPA, B. *et al*. Utilization of various lignocellulosic biomass for the production of nanocellulose: a comparative study. **Cellulose**, v. 22, n. 2, p. 1075–1090, 2015.

[30] ABRAHAM, E. *et al*. Extraction of nanocellulose fibrils from lignocellulosic fibres: A novel approach. **Carbohydrate Polymers**, v. 86, n. 4, p. 1468–1475, 2011.

[31] XU, X. *et al*. A Comparative Study on Their Microstructures and Effects as Polymer Reinforcing Agents. **ACS Applied Material Interfaces**, n. 5, p. 2999–3009, 2013.

[32] TURBAK, A. F.; SNYDER, F. W.; SANDBERG, K. R. **Microfibrillated cellulose, a new cellulose product: properties, uses, and commercial potential**. Journal of Applied Polymer Science: Applied Polymer Symposia. **Anais**...1982

[33] FERRO, G. *et al*. New Concepts for Next Generation of High Performance Concretes. **Procedia Materials Science**, v. 3, p. 1760–1766, 2014.

[34] MOON, R. J.; SCHUENEMAN, G. T.; SIMONSEN, J. Overview of Cellulose Nanomaterials, Their Capabilities and Applications. **Jom**, v. 68, n. 9, p. 2383–2394, 2016.

[35] STEPHENSON, K. M. **Characterizing the behavior and properties of nanocellulose reinforced ultra high performance concrete**. 2011. 152 f. Maine. 2011.

[36] CAO, Y. *et al*. The influence of cellulose nanocrystals on the microstructure of cement paste. **Cement and Concrete Composites**, v. 74, p. 164–173, 2016.

[37] CAO, Y. *et al*. The influence of cellulose nanocrystal additions on the performance of cement paste. **Cement and Concrete Composites**, v. 56, p. 73–83, 2015.

[38] LEE, K. Y. *et al*. On the use of nanocellulose as reinforcement in polymer matrix composites. **Composites Science and Technology**, v. 105, p. 15–27, 2014.

[39] HISSEINE, O. A. *et al*. Nano-engineered ultra-high performance concrete for controlled autogenous shrinkage using nanocellulose. **Cement and Concrete Research**, v. 137, n. September, p. 106217, 2020.

[40] KOLOUR, H.; ASHRAF, W.; LANDIS, E. N. Hydration and Early Age Properties of Cement Pastes Modified with Cellulose Nanofibrils. **Transportation Research Record: Journal of the Transportation Research Board**, p. 036119812094599, 2020.

[41] FU, C. *et al*. A comparative study on the effects of three nano-materials on the properties of cement-based composites. **Materials**, v. 13, n. 857, 2020.

[42] SUPIT, S. W. M.; NISHIWAKI, T. Compressive and flexural strength behavior of ultra-high performance mortar reinforced with cellulose nano-fibers. **International Journal on Advanced Science, Engineering and Information Technology**, v. 9, n. 1, p. 365–372, 2019.

[43] HISSEINE, O. A.; OMRAN, A. F.; TAGNIT-HAMOU, A. Influence of cellulose filaments on cement paste and concrete. **Journal of Materials in Civil Engineering**, v. 30, n. 6, p. 1–14, 2018.

[44] HISSEINE, O. A. *et al*. Nanocellulose for improved concrete performance: A macro-to-micro investigation for disclosing the effects of cellulose filaments on strength of cement systems. **Construction and Building Materials**, v. 206, n. February, p. 84–96, 2019.

[45] EL-FEKY, M. S. *et al*. Nano-fibrillated cellulose as a green alternative to carbon nanotubes in nano reinforced cement composites. **International Journal of Innovative Technology and Exploring Engineering**, v. 8, n. 12, p. 484–491, 2019.

[46] COSTA CORREIA, V. DA *et al*. Nanofibrillated cellulose and cellulosic pulp for reinforcement of the extruded cement based materials. **Construction and Building Materials**, v. 160, p. 376–384, 2018.

[47] JIAO, L. *et al*. Natural cellulose nanofibers as sustainable enhancers in construction cement. **PLoS ONE**, v. 11, n. 12, p. 1–13, 2016.

[48] GÓMEZ HOYOS, C.; CRISTIA, E.; VÁZQUEZ, A. Effect of cellulose microcrystalline particles on properties of cement based composites. **Materials and Design**, v. 51, p. 810–818, 2013.

[49] ONUAGULUCHI, O.; PANESAR, D. K.; SAIN, M. Properties of nanofibre reinforced cement composites. **Construction and Building Materials**, v. 63, p. 119–124, 2014.

[50] NILSSON, J.; SARGENIUS, P. Effect of microfibrillar cellulose on concrete equivalent mortar fresh and hardened properties. p. 89, 2011.

[51] BENTCHIKOU, M. *et al*. Effect of recycled cellulose fibres on the properties of lightweight cement composite matrix. **Construction and Building Materials**, v. 34, p. 451–456, 2012.

[52] PETERS, S. *et al*. Nanocellulose and Microcellulose Fibers for Concrete. **Transportation Research Record: Journal of the Transportation Research Board**, v. 2142, p. 25–28, 2010.

[53] KOLOUR, H. H. *et al*. An investigation on the effects of cellulose nanofibrils on the performance of cement paste and concrete. **Advances in Civil Engineering Materials**, v. 7, n. 1, p. 463–478, 2018.

[54] MONTES, F. *et al*. Rheological impact of using cellulose nanocrystals (CNC) in cement pastes. **Construction and Building Materials**, v. 235, p. 117497, 2020.

[55] MOHAMED, M. A. S.; GHORBEL, E.; WARDEH, G. Valorization of micro-cellulose fibers in self-compacting concrete. **Construction and Building Materials**, v. 24, n. 12, p. 2473–2480, 2010.

[56] BIRD, R. B.; STEWART, W. E.; LIGHTFOOT, E. N. **Transport phenomena**. New York: John Wiley and Sons, 1960.

[57] BANFILL, P. Rheology of Fresh Cement and Concrete. **Rheology Reviews**, p. 61–130, 2006.

[58] RAMACHANDRAN, V.S.; BEAUDOIN, J. J. **Handbook of Analytical Techniques in Concrete Science and Technology**. [s.l: s.n.].

[59] BANFILL, P. F. G. **The rheology of fresh cement and concrete - a review**. Proceedings of the 11th international cement chemistry congress. **Anais**...2003Disponível em: <http://www.bsr.org.uk>

[60] DILS, J.; SCHUTTER, G. DE; BOEL, V. Influence of mixing procedure and mixer type on fresh and hardened properties of concrete: A review. **Materials and Structures/Materiaux et Constructions**, v. 45, n. 11, p. 1673–1683, 2012.

[61] HEWLETT, P.; LISKA, M. **Lea's Chemistry of Cement and Concrete**. Fourth ed. [s.l.] Elsevier Science & Technilogy Books, 2004. v. 58

[62] FLATT, R.; SCHOBER, I. **Superplasticizers and the rheology of concrete**. [s.l.] Woodhead Publishing Limited, 2012.

[63] TANG, Z. *et al*. Influence of cellulose nanoparticles on rheological behavior of oilwell cement-water slurries. **Materials**, v. 12, n. 2, p. 1–14, 2019.

[64] LONG, W. J. *et al*. Rheology and buildability of sustainable cement-based composites containing micro-crystalline cellulose for 3D-printing. **Journal of Cleaner Production**, v. 239, p. 118054, 2019.

[65] PARVEEN, S. *et al*. A novel approach of developing micro crystalline cellulose reinforced cementitious composites with enhanced microstructure and mechanical performance. **Cement and Concrete Composites**, v. 78, p. 146–161, 2017.

[66] SILVA, L. *et al*. A facile approach of developing micro crystalline cellulose reinforced cementitious composites with improved microstructure and mechanical performance. **Powder Technology**, v. 338, p. 654–663, 2018.

[67] FILHO, A. *et al*. Mechanical and micro-structural investigation of multi-scale cementitious composites developed using sisal fibres and microcrystalline cellulose. **Industrial Crops and Products**, v. 158, n. April, p. 112912, 2020.

[68] OLIVEIRA DE SOUZA, L. *et al*. Investigation of dispersion methodologies of microcrystalline and nano-fibrillated cellulose on cement pastes. **Cement and Concrete Composites**, v. 126, n. February 2022, 2022.

[69] SUN, X. *et al*. Rheology, curing temperature and mechanical performance of oil well cement: Combined effect of cellulose nanofibers and graphene nano-platelets. **Materials and Design**, v. 114, n. August, p. 92–101, 2017.

[70] SUN, X. *et al*. Cellulose Nanofibers as a Modifier for Rheology, Curing and Mechanical Performance of Oil Well Cement. **Scientific Reports**, v. 6, p. 1–9, 2016.

[71] BAKKARI, M. EL *et al*. Preparation of cellulose nanofibers by TEMPO-oxidation of bleached chemi-thermomechanical pulp for cement applications. **Carbohydrate Polymers**, v. 203, n. September 2018, p. 238–245, 2019.

[72] HISSEINE, O. A. *et al*. Feasibility of using cellulose filaments as a viscosity modifying agent in self-consolidating concrete. **Cement and Concrete Composites**, v. 94, n. September, p. 327–340, 2018.

[73] EZ-ZAKI, H. *et al*. Influence of cellulose nanofibrils on the rheology, microstructure and strength of alkali activated ground granulated blast-furnace slag: a comparison with ordinary Portland cement. **Materials and Structures**, v. 54, n. 1, p. 1–18, 2021.

[74] CUENCA, E.; MEZZENA, A.; FERRARA, L. Synergy between crystalline admixtures and nano-constituents in enhancing autogenous healing capacity of cementitious composites under cracking and healing cycles in aggressive waters. **Construction and Building Materials**, v. 266, p. 121447, 2021.

[75] ONUAGULUCHI, O.; PANESAR, D. K.; SAIN, M. Properties of nanofibre reinforced cement composites. **Construction and Building Materials**, v. 63, p. 119–124, 2014.

[76] GONCALVES, J. *et al*. Cellulose nanofibres (CNF) for sulphate resistance in cement based systems. **Cement and Concrete Composites**, v. 99, n. March, p. 100–111, 2019.

[77] BARNAT-HUNEK, D. *et al*. Effect of cellulose nanofibrils and nanocrystals on physical properties of concrete. **Construction and Building Materials**, v. 223, p. 1–11, 2019.

[78] ALOULOU, F.; SABRINE, A.; SAMMOUDA, H. Influence and dispersion of nanofiber of wood modified on properties of cement based mortars. **Journal of Renewable Materials**, v. 7, n. 7, p. 631–641, 2019.

[79] CAO, Y. *et al*. The relationship between cellulose nanocrystal dispersion and strength. **Construction and Building Materials**, v. 119, p. 71–79, 2016.

[80] EL-FEKY, M. S. *et al*. Effect of nano silica addition on enhancing the performance of cement composites reinforced with nano cellulose fibers. **AIMS Materials Science**, v. 6, n. 6, p. 864–883, 2019.

[81] NAGATAKI, S.; YONEKURA, A. Thw mechanisms of drying shrinkage and creep of concrete. **Concrete Journal**, v. 20, n. 12, p. 177–191, 1982.

[82] MEHTA, K.; MONTEIRO, P. **Concrete: microstructure, properties and materials**. Third ed. [s.l.] McGraw-Hill, 2014.

[83] SANTOS MOTTA, M. DOS; SOUZA, L. M. S.; ANDRADE SILVA, F. DE. Early-age shrinkage of cement pastes with polypropylene and curaua fibres.

Advances in Cement Research, v. 33, n. 4, p. 156–167, 2021.

[84] LU, Z. *et al*. Early-age interaction mechanism between the graphene oxide and cement hydrates. **Construction and Building Materials**, v. 152, p. 232–239, 2017.

[85] ALMUDAIHEEM, J. A. Prediction of Drying Shrinkage of Portland Cement Paste: Influence of Shrinkage Mechanisms. **Journal of King Saud University - Engineering Sciences**, v. 3, n. 1, p. 69–86, 1991.

[86] AITCIN, P. **Demystifying Autogenous ShrinkageConcrete International**, 1999.

[87] LURA, P. **Autogenous Deformation and Internal Curing of Concrete**, 2003.

[88] JENSEN, O. M.; HANSEN, P. F. Autogenous deformation and RH-change in perspective. **Cement and Concrete Research**, v. 31, n. 12, p. 1859–1865, 2001.

[89] AKCAY, B.; TASDEMIR, M. A. Effects of distribution of lightweight aggregates on internal curing of concrete. **Cement and Concrete Composites**, v. 32, n. 8, p. 611–616, 2010.

[90] CHENG, S. *et al*. Multiple influences of internal curing and supplementary cementitious materials on the shrinkage and microstructure development of reefs aggregate concrete. **Construction and Building Materials**, v. 155, p. 522–530, 2017.

[91] LONG, G.; YANG, J.; XIE, Y. The mechanical characteristics of steam-cured high strength concrete incorporating with lightweight aggregate. **Construction and Building Materials**, v. 136, p. 456–464, 2017.

[92] FERRARA, L. *et al*. **Effect of Cellulose Nanopulp on Autogenous and Drying Shrinkage of Cement Based CompositesNanotechnology in Construction**, 2015.

[93] LEE, H. J. *et al*. A Study on the Drying Shrinkage and Mechanical Properties of Fiber Reinforced Cement Composites Using Cellulose Nanocrystals. **International Journal of Concrete Structures and Materials**, v. 13, n. 1, p. 1–11, 2019.

[94] FU, T. *et al*. The influence of cellulose nanocrystals on the hydration and flexural strength of Portland cement pastes. **Polymers**, v. 9, n. 9, 2017.

[95] CLARAMUNT, J. *et al*. **Mechanical performance of ductile cement**

mortar composites reinforced with nanofibrillated cellulose. 2nd International RILEM Conference on Strain Hardening Cementitious Composites. **Anais**...2011

[96] CAO, Y. Z.; VERIAN, K. P. A VEDA simulation on cement paste: using dynamic atomic force microscopy to characterize cellulose nanocrystal distribution. **Mrs Communications**, v. 7, n. 3, p. 672–676, 2017.

3. Investigation of dispersion methodologies of microcrystalline and nanofibrillated cellulose on cement pastes[1]

3.1. Introduction

Cementitious materials are present in most construction applications, including buildings, transportation infrastructure, water- and waste-management, and many nonstructural uses such as in claddings and in oil well cement applications. Natural fibers have been reinforcing cementitious materials in diverse scales, such as macro fibers, textile, micro single fibers, and pulp [1–3]. Most recently, the use of natural fibers in their lesser extension, known as nanofibrils and nanocrystals, is gaining attention [4–6]. Those types of cellulose-based materials are supposed to contribute to the development of new cementitious materials that exhibit improved mechanical properties and, as a bonus, are made of renewable raw materials.

In this context, two types of cellulose-based materials, namely, microcrystalline cellulose (MCC) and nanofibrillated cellulose (NFC), have arisen as a purposeful option to modify the properties of cementitious products. Their morphology, crystallinity, form, and physical and mechanical properties depend on the source and production by either mechanical and/or chemical means [7–9]. The addition of such cellulose products in cement-based mixtures alters the properties of the matrices in both their fresh and hardened states [10–16]. Comparing the effect of macro-fiber and nanocellulose derived from the same plant-source, the composites containing nanocellulose can yield higher values of strength and modulus of elasticity [10,17,18] and even improve fracture toughness in the matrix [10,18]. The hybridization process between nano- and macro-fibers is possible and facilitates the improvement of the modulus of elasticity [19,20].

[1] This Chapter was published in Souza *et al*, Investigation of dispersion methodologies of microcrystalline and nano-fibrillated cellulose on cement pastes, Cement and Concrete Composites, 2022 [68].

More about the influence of MCC and NFC in cementitious matrices is found in Chapter 2.

Due to the existence of interacting forces among the particles, micro- and nanocellulose added into the matrix tend to form agglomerates that may act as defects or stress concentrators [8,21,22]. These interparticle interactions may limit the potential for mechanical reinforcement, indicating that the optimal content of inclusion is associated to the agglomeration effect [10–12,22–27]. This phenomenon is magnified with decreasing particle size [8,9]. Poor dispersion of such cellulose-based materials into cementitious matrices is usually the bottleneck of its utilization as reinforcement.

One may promote the dispersion of micro and nanocellulose by using chemical or mechanical methods, or even a combination of both. Among the chemical methods used for cementitious matrices, there is the use of surfactants and stabilizing agents [11,16,24,28,29]. The mechanical approaches include ultrasonication, ultrasonic bath, and magnetic or mechanical stirring [11,12,14,16,22,28,30,31]. The dispersion of micro- and nanocellulose is usually a step in the mixing process. Usually, the fiber is first dispersed in water, and then the suspension is mixed with other matrix's constituents. The dispersion step may even be improved with a pre-treatment of the fiber during its production, for instance, by the TEMPO-mediated oxidation of NFC [12,14,32] or tetraethyl orthosilicate treatment of MCC [13]. In the case of the nanocellulose already dispersed as a gel, the dispersion agents or procedures may act as mixing facilitators. One example is the use of superplasticizer in order to ease the intermixing of nanocellulose and also to mitigate issues related to fresh mixture rheology [11,24–26].

The objective of this work is to carry on a comparison of the inclusion of two types of cellulose-based materials in cement paste: commercially available microcrystalline cellulose (MCC) and nano-fibrillated cellulose (NFC) obtained from eucalyptus pulp. The MCC and NFC were first characterized according to their morphology by means of light microscopy (LM), transmission electron microscopy (TEM) and scanning electron microscopy (SEM) images. The water retention value was also assessed. This Chapter explores a range of dispersing and mixing protocols for the two distinct types of cellulose: MCC, in the form of "powder", and NFC, in the form of gel. The strategies were explored to provide a

well-dispersed solution of MCC and water. The same strategies were applied to NFC solutions to ease their intermixing with the cement. The methodologies include mechanical means, i.e., mechanical stirring, magnetic stirring, and ultrasonication; and chemical means such as superplasticizer and a nonionic surfactant. Besides that, pretreatment by 2,2,6,6-Tetramethylpiperidine-1-oxyl (TEMPO) oxidation was applied during the production of the NFC as another approach aiming at better dispersion of the fiber material. Workability using flow table tests was investigated in every case. The effectiveness of the dispersion methods was evaluated by means of compression tests on MCC- and NFC-reinforced cement paste specimens. Subsequently, the more compatible methods for each cellulose-based material were employed, and the optimal contents of MCC and NFC were assessed by means of four-point bending tests. In addition, thermo-gravimetric analysis (TGA) and mercury intrusion porosimetry (MIP) allowed a pre investigation of the hydration and microstructure modifications of the cellulosic inclusions.

3.2. Experimental program

3.2.1. Materials

Portland cement (PC) paste was used as the matrix to investigate the addition of micro- and nanocellulose. The cement was the Brazilian Type V, with specifications according to NBR 16697. Its chemical composition is presented in Table 3-1. The water-to-cement ratio was 0.45, and tap water was used. The poloxamer Pluronic F-127 was obtained from Sigma-Aldrich. The polycarboxylic ether-based superplasticizer (Glenium 51 MS) with a solid content of 32% was obtained from BASF. The microcrystalline cellulose (MCC Avicel PH-101) was obtained from Sigma-Aldrich.

Table 3-1 Chemical composition of the Brazilian Portland cement Type V (provided by the manufacture).

Oxides	%
Silicon dioxide (SiO_2)	19.1
Aluminium oxide (Al_2O_3)	5.0
Ferric oxide (Fe_2O_3)	2.7
Calcium oxide (CaO)	62.3
Magnesium oxide (MgO)	1.0
Sulfur trioxide (SO_3)	3.0
Insoluble residue	1.6

Nano-fibrillated cellulose was produced from bleached *Eucalyptus* pulp. The pulp was dispersed in water at a fiber content of around 2.0 wt.% for 48 h. Subsequently, the mixture was submitted to mechanical stirring in order to facilitate the defibrillation process. The solution was then processed for 30 cycles through the mechanical fibrillator (SuperMasscolloider grinder, Massuko-Sangyo, model MKCA6-2), using 1,500 rpm grindstone rotation, with a gap of 0.01 mm between the rotating grindstones. The electric current consumed energy during the nano-fibrillation was measured and kept around 4 ampère (A). The resulting NFC consisted of a gel with around 2% of nanofibers.

To enable the intermixing of matrices with a high amount of NFC, i.e., higher than 0.5%, the content of water in the gel should be reduced. Thus, the NFC gel went through a filtering process, where two 6-µm filter papers were used with a vacuum pump of 0.9 bar. This process resulted in a solid phase of nanofibers of around 10% by mass.

The fabrication of the TEMPO-mediated oxidation was carried on based on the methodology of Fukuzumi *et al*. [33]. The same cellulosic fibers of *Eucalyptus* were suspended in distilled water, obtaining a suspension with a concentration of 2.5%, in weight to volume (w/v). Then 1.12 g of TEMPO reagent was dissolved in distilled water, in which it was stirred uninterrupted for 1 hour. Seven grams of NaBr were also dissolved in water under constant stirring for 1 hour. After, the two reagents were added to the cellulosic fiber suspension, and the system was constantly agitated for 20 minutes. After this period, 437.8850 ml of 10% NaClO was gradually added, establishing in the system a pH of approximately 10. The pH was maintained around 10 by adding drops of 0.5 M sodium hydroxide (NaOH) solution. The reaction was set forth for 3 hours under constant stirring at

room temperature. After that 100 ml of ethanol was added to stop the reaction, and the system pH was adjusted to 7 by adding drops of 0.5 M hydrochloric acid (HCl). Finally, the fibers were washed in running water.

3.2.2. Dispersion and mixing protocols

Six different dispersion strategies have been explored in the present paper, including mechanical and chemical methods. The techniques were applied to the suspension of MCC or NFC in water to promote their dispersion. The strategies were all, except for the TEMPO oxidation, employed as a pre-step in the mixture process with cement paste. The TEMPO-mediated oxidation is a pre-treatment in the production of NFC, and it does not apply to MCC in this case.

The mechanical approaches consisted of mechanical stirring (*MecS*), magnetic stirring (*MagS*) and ultrasonication (*US*). The mechanical dispersion methods were applied to suspensions constituted of the cellulosic inclusion and part of the mixing water. The mixing water amount varied for each method and is further specified. These strategies aimed to use the mechanical energy to create shear stress on the suspension to overcome the energy that binds the cellulose particles into agglomerates. In the case of mechanical stirring, the dispersion is promoted by the rotation of the mixer blades and depends on the rotational speed and the geometry of the blades and container [34]. The mechanisms of dispersion using the magnetic stirring are similar to mechanical stirring although the amount of transmitted energy and the geometry of the device are different. Regarding ultrasonication, the dispersion is promoted by the formation of bubbles, otherwise known as cavitation. The bubbles are formed in the low-pressure region of the waves, and the collapsing bubbles cause high shear rates in the suspension [34,35]. In this case, the transmitted energy depends on the properties of the operational parameters of the ultrasonic device [36]. Ultrasonication and ultrasonic bath have been used as successful means for dispersion of nanocellulose into cementitious matrices, especially in the case of micro and nanocrystals [14,22,28,30,31].

The chemical approaches consist of the use of two types of surfactants: a polaxamer and a superplasticizer. Surfactants are amphiphilic polymers with one part of their structure polar or hydrophilic, and the other apolar or hydrophobic. Due to their chemical duality, they are commonly used to promote interfaces

between phases, in this case between water and cellulosic particles. The bonding mechanisms are based on a strong hydrophilic attraction between the surface of the solid phase and the hydrophilic part of the surfactant [37]. The micelles formed by the arrangement of the Pluronics are intended to separate one cellulosic particle from the other, thus accomplishing the desired dispersion. The aim behind the use of superplasticizer is similar to that of a Pluronic. Polycarboxylate-based superplasticizers are used in cementitious materials since the 1980's [38] and are frequently applied as water-reducing agents. Essentially the superplasticizer's molecules adsorb onto cement particles, working as obstacles to the attractive forces that cause agglomeration. When used as a dispersion agent for micro- and nanocellulose, the intention is that the superplasticizer works also as an obstacle, leading to a steric effect between the cellulosic inclusions and water.

The methodology of the dispersion/mixture techniques is described as follows. In brackets, the corresponding abbreviations are given as used in the article.

i. Mechanical stirring (*MecS*): The MCC and NFC were added to the mixing water and then loaded into a mixer revolving at around 900 rpm for 30 min;

ii. Magnetic stirring (*MagS*): The MCC and NFC were added to half of the mixing water and loaded into a magnetic stirrer for 1 h; Then the suspension was mixed with the cement and the remaining water.

iii. Ultrasonication (*US*): 20 ml of water and the MCC and NFC were subjected to ultrasonication in a SONICS Vibra-Cell for 30 min at maximum amplitude (100%) with a half-inch probe. Every 10 min, the process was interrupted to cool the container down. After the process, it took around 1 h for the suspension to reach room temperature so that its temperature would not influence the hydration reactions. Then, the suspension was mixed with the cement and the remaining water.

iv. Surfactant (*Surf*): The surfactant Pluronic F-127 was added to the mixing water together with the micro- or nanocellulose. The proportion of MCC or NFC to surfactant in weight was of 5:1. In this case the mechanical stirrer (item i) was used for 30 min to enable a more homogeneous particle distribution.

v. Superplasticizer (*Super*): The superplasticizer was added to the mixing water with the cellulosic inclusions in a proportion of 1% by wt.

relative to the cement mass. As in the surfactant case, the prepared suspension was mixed for 30 min under mechanical stirring (item i) to promote homogeneity.

vi. TEMPO-mediate oxidation (*TEMPO*): Unlike the other strategies, where dispersion takes place as a mixture process pre-step, the modification in this case occurred in the production stage as detailed in Section 3.2.1. Mixing was carried out without chemical or mechanical means.

From the descriptions above, it can be remarked that the chemical dispersion methods, items iv and v, were combined with mechanical stirring to homogenize the chemical additions with the suspension of cellulose in water. For comparison purposes, MCC and NFC were added into the cement paste without dispersion techniques (*WD*). Reference specimens with no inclusion were also produced (*0%*).

3.2.3. Testing methodology

3.2.3.1. Morphology of the MCC and NFC

The MCC and NFC suspensions were characterized using a light microscope (Zeiss Axio AX10, Germany). The suspensions were previously diluted to 0.1 % by wt., stirred for 10 min with Ultra Turrax (IKA T-25) at 10000 RPM, and plunged for five minutes into an ultrasonic bath to obtain better dispersion. Pictures were taken at 10× magnification in a window of 2584 × 1936 pixels and analyzed using Fiji software [39]. To perform the analysis, the images were transformed to 8-byte format and segmented by threshold.

The morphology of the NFC was also investigated using a transmission electron microscope, specifically a model Tecnai G2-12 (FEI, Hillsboro, OR, USA) instrument with an accelerated voltage of 80 kV. Sample preparation and TEM configurations followed recommendations described elsewhere [40]. Diameter measurements of nanofibrils were performed for at least 100 individual particles per image using the ImageJ software [39].

A scanning electron microscope (Quanta 250 FEG, FEI Eindhoven/The Netherlands) was used to investigate the morphology of the MCC as received at an accelerating voltage of 5 kV.

3.2.3.2. Determination of Water Retention Value (WRV)

The NFC water retention value (WRV) was determined based on the Scandinavian test method SCAN – C 62:00 (2000). The NFC suspensions were first concentrated to a suspension of concentration 10%, and then the suspensions were centrifuged by a Heraeus Megafuge 16R Centrifuge (Thermo Fisher Scientific, Waltham, MA, USA), using a centrifugal force of 3000 G for 15 min for dewatering, after which the wet filtered NFC fibrils were weighed. After oven-drying at 105 ± 2 °C for 24 h the weight was measured again. The WRV was determined according to Eq. (3.1) as follows:

$$WRV = \frac{W_0 - W_1}{W_1} \qquad \text{Eq. (3.1)}$$

where W_0 and W_1 are the weights of wet and oven-dried pulps, respectively.

3.2.3.3. Flow table test

The flowability of the cement pastes was assessed by means of the flow table test according to ASTM C1437-15, although applying 30 strokes. Cement pastes containing 0.5% by wt. of MCC or NFC relative to the mass of cement, were compared to the cement paste without cellulosic fibers. Regarding NFC, the percentage of inclusion is the solid phase present in the gel, in mass. Information on matrix composition for each percentage and type of fiber is given in Table 3-2. All the dispersion/mixture methods were applied for 0.5% by wt. of MCC and NFC additions. Figure 3-1 shows a schematic illustration of the methodology applied. The selection step was based on strength improvement.

Table 3-2 Matrix composition of the mixtures in weight (g).

Mixture	Cement	Water	MCC	NFC		Chemical dispersant
				Gel	*Solid*	
Ref (0%)	100	45	-	-	-	-
0.05% MCC	100	45	0.05	-	-	-
0.50% MCC	100	45	0.5	-	-	-
0.50% MCC Super	100	45	0.5	-	-	1
0.50% MCC Surfac	100	45	0.5	-	-	0.2
0.75% MCC	100	45	0.75			
1.00% MCC	100	45	1	-	-	-
0.05% NFC	100	44.5	-	0.5	0.05	-
0.05% NFC TEMPO	100	44.5	-	0.5	0.05	-
0.50% NFC	100	40.5	-	5*	0.50	-
0.50% NFC Super	100	40.5	-	5*	0.50	1
0.50% NFC Surfac	100	40.5	-	5*	0.50	0.2
0.50% NFC TEMPO	100	40.5	-	5*	0.50	0.2
1.00% NFC	100	36	-	10*	1.00	-
1.00% NFC Super	100	36	-	10*	1.00	1
1.00% NFC Surfac	100	36	-	10*	1.00	0.2

*Gel of nano-fibrillated cellulose (NFC) with 10% of solids.

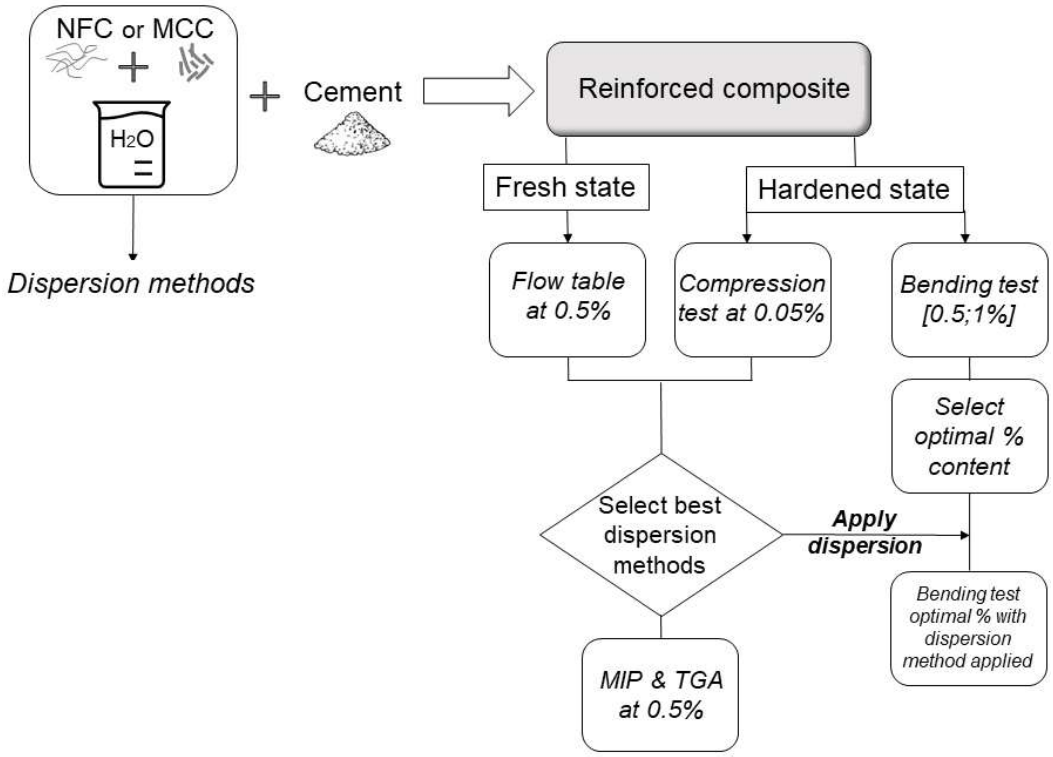

Figure 3-1 Flowchart of the methodology adopted.

3.2.3.4. Compression test

One of the tests used to determine the effectiveness of the dispersion was the compression test. The specimens consisted of cylinders of 50 mm x 100 mm (diameter x height). At least three specimens of each parameter combination were tested at an age of 28 days. To measure axial displacement, two 7-mm linear variable displacement transducers (LVDTs) were coupled to the specimen. The mean of the readings of both LVDTs was used to calculate the compressive strain. The compression tests were performed using a universal MTS machine, model 810, with 500 kN of load capacity. The rate of the crosshead displacement was set to 0.4 mm/min.

In order to explore the distinct dispersion techniques, the specimens of cement pastes were produced with addition of MCC or NFC subject to the five abovementioned processes (*MecS*, *MagS*, *US*, *Surf* and *Super*). In addition, specimens containing NFC with TEMPO oxidation (*TEMPO*) were produced and tested; see Figure 3-1 for the details of the adopted methodology. The proportion was of 0.05% of micro- and nanocellulose, by weight of cement. In the case of the specimens with NFC, the water present in the gel was subtracted from the amount of mixing water to keep the water-to-cement ratio of 0.45; see Table 3-2.

3.2.3.5. Four-point bending test

Four-point bending tests were performed on specimens with dimensions of 250 mm x 60 mm x 10 mm (length x width x height), based on ASTM C1161 with modifications on the geometry. At least three specimens were tested for each parameter combination at an age of 28 days. The total span tested was 210 mm, the distance between the blades and the supports were uniformly 70 mm. To measure the displacement two displacement transducers of 10 mm were mounted on the mid-center of the specimens. The mean of the readings of the two transducers was used to calculate the mid-span displacement. The bending tests were performed using an MTS system with a capacity of 100 kN. To ensure accurate force acquisition, a load cell of 2.5 kN was used. The actuator displacement rate was 0.05 mm/min.

The content of MCC and NFC was 0%, 0.5%, and 1%. Firstly, they were all introduced without any dispersion method applied. The optimal content was

selected according to the strength values obtained. Then the dispersion methods that showed positive results on the compressive tests were applied to the optimal percentage for further bending tests. Information about the composition for each variation under investigation and the corresponding percentages of MCC and NFC used is given in Table 3-2.

The relation between the mechanical properties of a given specimen with NFC or MCC reinforcement and the reference specimen is presented by the strength ratio (SR), modulus ratio (MR), and deflection ratio (DR). Therefore, each mechanical parameter ratio, namely strength, modulus, and deflection, is calculated by dividing the mean value obtained for specimens containing fibers by the corresponding value obtained for the reference mixture.

3.2.3.6. Thermogravimetric analysis (TGA)

To investigate the possible changes in cement hydration on addition of MCC and NFC, and the effect of selected dispersion methods if any, thermogravimetric analysis (TGA) was performed. Samples without and with 0.5% of MCC or NFC were analyzed at an age of 28 days with a thermo-gravimetric analyzer (NETZSCH STA 409C/CD). The measurements were performed at a uniform heating rate of 10 C°/min under an oxygen atmosphere.

3.2.3.7. Porosimetry

The microstructures of the hardened cement pastes reinforced with MCC and NFC were analyzed according to their pore size distribution as obtained through mercury intrusion porosity (MIP). A Porotec Porosimeter PASCAL 140/440 equipment was used, and measurements were carried in a pressure range from 0 to 400 MPa. The procedure was applied to the samples of approximately 1 cm^3 with 0.0 and 0.5% of MCC and NFC at 28 days of age. Samples subjected to the selected dispersion methods were also analyzed.

3.3. Results and discussion

3.3.1. Characterization of MCC and NFC

3.3.1.1. Morphological properties

Microcrystalline cellulose (MCC) is a cellulose form resulting from acid hydrolysis followed by homogenization and is currently commercially available [41]. Figure 3-2 shows a scanning electron microscope (SEM) image of dry MCC as received. From the image one can observe its non-uniform morphology, ranging from long fibrous rods to various short, irregular shapes.

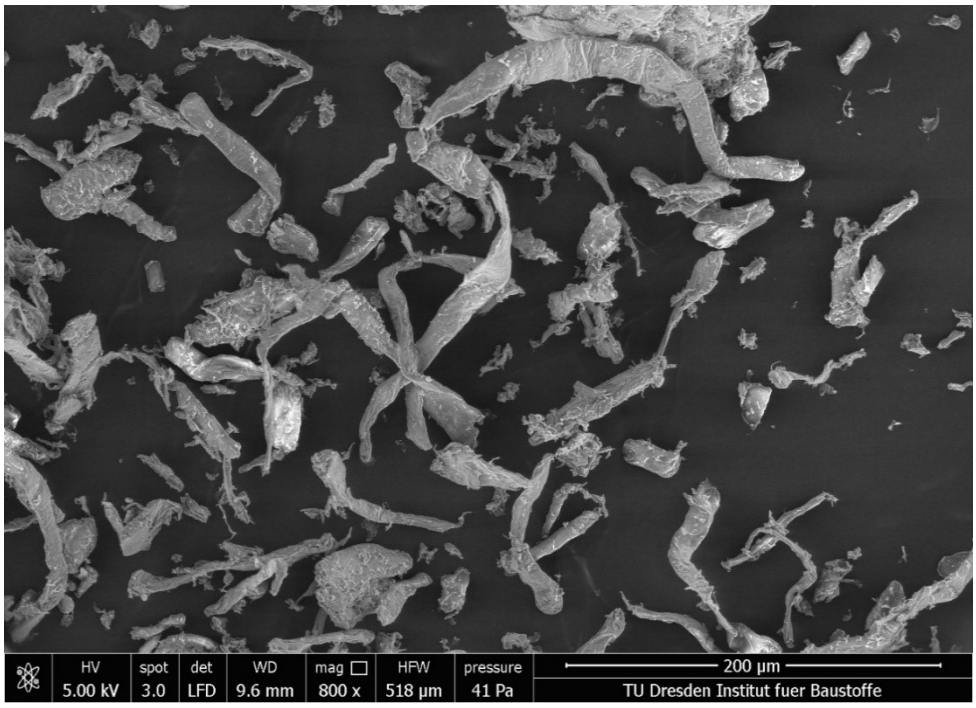

Figure 3-2 SEM image of the pristine MCC particles.

The Avicel PH-101 MCC presents a particle size ranging from 2 to 260 µm with a mean diameter of around 50 µm, as reported by Zhang *et al*. [42]. The results of the light microscopy showed an average size of 115 µm of the particles, as shown in Table 3-3.

Table 3-3 Results of analysis by light microscopy, including the average size of the MCC and NFC, pristine and with addition of superplasticizer (NFC *Super*).

Sample	Particles per image	Total area (μm²)	Average size (μm)
MCC	1047 ± 52	119790 ± 33184	115 ± 34
NFC	3581 ± 380	128146 ± 17360	36 ± 4.0
NFC *Super*	2561 ± 475	94925 ± 16851	37 ± 3.5

The morphological structure and diameter distribution of NFC are shown in Figure 3-3a (NFC Control) and Figure 3-3b (TEMPO oxidized NFC). Note that the fibrillation process produced nanofibrils with high aspect ratios and a considerable range of different diameters, with the diameter distribution concentrating itself at 15 to 30 nm. This range represented 33% of the measured entities, while the average diameter was 48 nm for NFC Control. As for NFC TEMPO, the diameter distribution also concentrated in the range from 15 to 30 nm (40% of the measured entities), and the average diameter was 29 nm. Due to the fibrils' mutual electrostatic repulsions, caused by the replacement of C6 by a carboxyl group in the cellulose structure, NFC obtained from TEMPO-modified fibers have smaller diameters than those that were not subjected to any treatment [43].

(a)

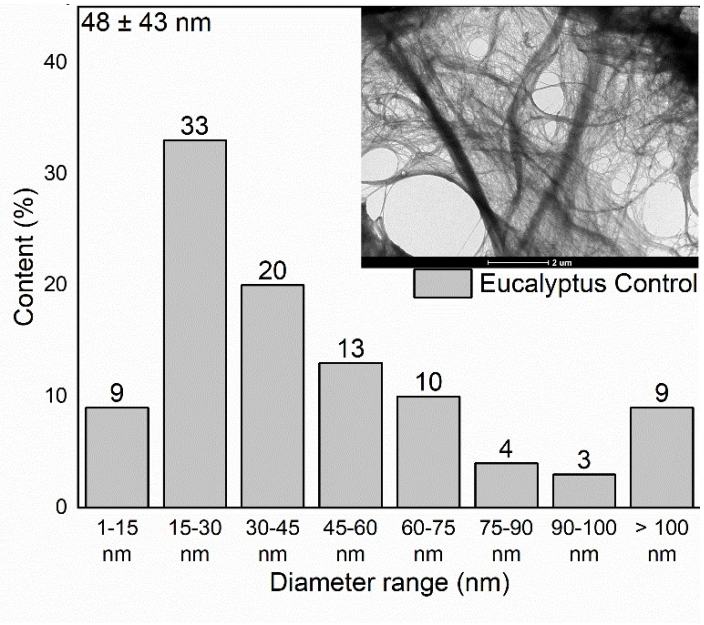

(b)

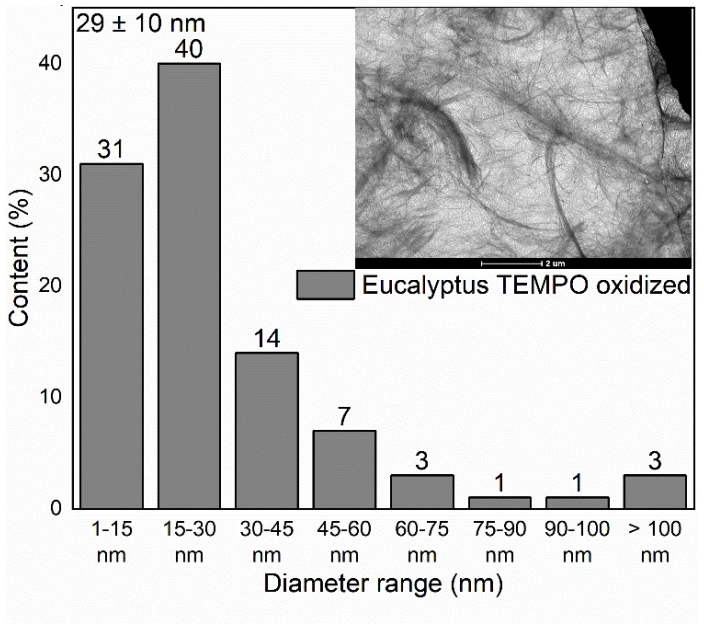

Figure 3-3 Diameter size distribution and TEM images of (a) NFC and (b) NFC modified by TEMPO oxidation.

Table 3-3 summarizes the main information obtained by light microscopy. The number of MCC particles per image was the lowest (1,047), while NFC presented 3,581 particles per image. This can be traced back to the MCC's having larger dimensions (115 μm) than the NFC (around 36 μm) forcing each particle to occupy a larger area in the image window. Since MCC contains mainly a

crystalline fraction, which is less reactive than amorphous cellulose, there is a decrease regarding interactions between the particles [44].

It can be seen in Figure 3-2 that the MCC presents larger and more individualized fragments in relation to NFC, which are formed by an interlaced network of fibrils that interact with each other. The NFC exhibits an entangled network with some agglomeration spots, and cell wall structures not so deconstructed. This appearance was expected since the hydroxyl groups on the surfaces of the fibrils enable them to interact.

3.3.1.2. Water retention value

WRV is a measure of the amount of water retained by the fiber or fibrils after controlled centrifugation, and it includes the amount of water in pores as well as in the thin layer on fiber or fibril external surfaces, especially those in the inter-fiber or inter-fibril meniscus [45,46]. The water retention value changed from 1.4 g/g for untreated cellulose fibers to 2.13 g/g for TEMPO oxidized cellulose fibers. Similar results were reported by Dias *et al*. [47], and by Qian *et al*. [48]. For NFC the values changed from 5.59 g/g to 9.24 g/g after the TEMPO oxidation process, indicating finer fibrils with possibly higher intrinsic strength [10,32].

The elevated water retention capacity comes from the hierarchical structure of the nanocellulose because the presence of hydroxyl groups makes it highly hydrophilic. The more the material is on a nanoscale, the higher the viscosity of the suspension and the more pronounced its appearance as a gel. This is due to a greater capacity of the material to bind water molecules, as can be seen with the increase in WRV values after treatment with TEMPO. Besides that, the higher WRV presented by the NFC-TEMPO is also due to the fact that the oxidation process loads the surface of the fibrils with negative charges, which ultimately generates electrostatic repulsions between the NFCs, causing them to disperse further from each other.

Essentially, the WRV can be used as an indicator of the degree of nanofibrillation of the NFC gel. It also reflects the level of fiber deconstruction: refining aims at separating, individualizing, or fibrillating the fibers. The defibrillation process causes the individualization of the micro/nanofibrils in the fiber cell wall structure into defibrillated micro/nanofibrils. Thus, this process increases the specific surface of the material, also increasing its reactivity with the

water molecules, implicating a higher WRV. With this principle in mind, a lower WRV indicates a less deconstructed fiber, i.e., the micro/nanofibrils (NFC) in the fiber cell wall are still bonded together with fewer free sites available for water molecules to bind to the NFC in this condition. A higher WRV value indicates a more effective individualization of the nanofibrils (deconstruction of the fiber cell wall), allowing more interactions of them with water molecules, and better-dispersed suspensions.

3.3.2. Flow behavior of cement paster upon addition of MCC and NFC

Although a more complete characterization of the flow of the cement pastes with MCC and NFC will be brought in Chapter 6, the flow table test gives an idea of the order of magnitude of this important parameter. The flow table test was performed to investigate the influence of each type of cellulose-based material inclusion on the workability of the fresh cement paste and as a first indicator for the quality of dispersion. The spread diameters of the several fresh cement pastes are shown in Table 3-4.

Table 3-4 Flow table results of cement pastes with 0.5% by wt. of MCC or NFC. Standard deviation of 4% according to ASTM C1437-15.

Dispersion/mixture method	Flow values (mm)	
	MCC	*NFC*
Reference – 0%	195	195
WD	214	102
MecS	212	110
MagS	197	103
US	180	-
Super	260	175
Surf	209	109
TEMPO	-	158

Firstly, by analyzing the matrices with the cellulose added without using any dispersion method (*WD*) in comparison with the reference, it is possible to notice the different effects of MCC and NFC on the flowability of the samples. While the NFC led to a significant decrease in workability, the MCC had almost no influence on this parameter. In fact, the presence of 0.5% by wt. of MCC slightly

increased the fluidity of the paste. This difference is most probably related to the distinct morphology of the cellulosic inclusions that affect their capacity to absorb water. As shown in Figure 3-2, MCC presents a rod-like shape that may ease the flow behavior between this material and cement particles. Although this trend contradicts most other reports [16,20,28,30,49,50], the increase in workability had been already observed in cement pastes with cellulose nanocrystals (CNC) by Cao *et al*. [27]. The authors attribute the reported decrease in yield stress to the steric stabilization mechanism, where the particles behave as water-reducing agents, dispersing cement particles.

The addition of NFC halved the flow value in comparison to the reference. The reduced workability observed in the samples with NFC may be associated with their morphology and physical properties. The hydrophilicity presented by nanocellulose provides a high capacity for water retention, observed at 5.59 g/g, that may decrease the water-to-cement ratio locally, leading to denser fresh material. In addition, the long fibrils with high aspect ratios, ranging from 25 to 500 [51], facilitate the formation of networks that may arrest cement particles, thus decreasing the flowability of fresh material. The strong bond facilitated by secondary interactions, mainly due to the presence of hydroxyl groups, is also mentioned as a possible reason behind the changes in flow behavior upon the addition of NFC [9,52].

Regarding the effects of the dispersion methods applied to the MCC specimens, one may highlight the use of superplasticizer and ultrasonication since they had a meaningful impact on the flow behavior of the cement pastes. The use of superplasticizer promoted segregation followed by exudation, leading to an increase of the flow value by 30% when compared to the reference. Thus, this amount of superplasticizer was unsuitable for purposes of promoting the dispersion of MCC in water while avoiding undesirable effects on the cement paste. The ultrasonication process resulted in the opposite effect, reducing the flow value. This may indicate that this method is efficient in dispersing the MCC particles in water and is able to maintain the dispersion after the mixture with cement [16]. The mechanical tests results discussed in the following sections support this assumption. The other methods (*MecS*, *MagS* and *Surf*) of dispersion did not have a significant impact on the flow behavior of the specimens with MCC.

Among the mixing methods employed on the specimens containing NFC, the flow values for *Super* and *TEMPO* were superior to the *WD* ones, yet inferior to those of the reference. From the LM analysis, it is possible to observe how the addition of superplasticizer was effective in dispersing the individual fibrils; see Table 3-3. This was reflected in the number of visible particles, which decreased from 3581 to 2561 upon the addition of superplasticizer. This indicates that the superplasticizer was still able in this case to act as a water-reducing agent and improve the dispersion of the nanofibrils. The water retention value of the NFC is related to the gel's viscosity as well as its level of dispersion, how well the cell wall was refined. The WRV of the NFC-Control and the NFC-Tempo were 5.59 g/g and 9.24 g/g, respectively. Hence, the higher WRV of the NFC-Tempo indicates a better-dispersed gel with higher level of fiber deconstruction. The presence of more agglomerates in the NFC-Control gel (in this case a network not so refined) could have influenced the paste's lower workability in comparison to the NFC-TEMPO one. Although the TEMPO nanofibrils presented clearly a more viscous gel, maybe other properties of the TEMPO gel (e.g., the carboxyl groups causing electrostatic repulsion between nanofibrils) and how it interacts with the cement particles in the fresh and hardened states are different. In addition, TEMPO-mediated oxidation is known to modify the rheological properties of the material itself (cellulose), so the thixotropy of this suspension is different, with particles more inclined to rearranging themselves to the initial state (inert). It is worth pointing out that for the mixtures with NFC content superior to 0.5%, both gels went through a filtration process with a final concentration of solids of 10%. In those cases, the NFC-Control gel remained saturated, however, the water present in the NFC-TEMPO gel represented 98% of the fibrils' water-retaining capacity. It is important to keep in mind that the distinct WRV could have affected the total w/c of the specimens. However, the retained water by the fibrils was not evaluated regarding its availability to work as mixing water, thus this topic was not brought to discussion on the present paper.

As the specimens containing MCC, the *MecS*, *MagS* and *Surf* did not have a significant impact on the flow behavior of the mixtures with NFC when compared to the *WD* mixtures. Note here that it was not possible to perform ultrasonication on the NFC suspension at the particular fiber content of 0.5%.

3.3.3. Mechanical behavior of NFC composites and the influence of dispersion methods

The results of the compression tests are presented in Table 5. This table contains the averages and standard deviations of the compressive strength, strain capacity, and modulus of elasticity for specimens containing 0.05% of NFC and produced using various dispersion methods under investigation. The reference cement paste with no addition of NFC is designated "0%".

The addition of a small amount of nanocellulose, i.e., 0.05%, changed the mechanical properties of the hardened cement pastes slightly. The addition of 0.05% NFC without any dispersion (*WD*) did not alter the compressive strength of the specimens, while the use of different dispersion methods during the suspension production influenced it differently in every case. The use of specific dispersion methods, namely the addition of superplasticizer and the TEMPO-oxidation process, was necessary to obtain a positive effect of almost 10% on the compressive strength. In this way, the addition of NFC can lead to a reduction in the defects, and this can have an impact on the compression results.

Table 3-5 Compressive mechanical parameters of the reference mixture, 0.00%, and the cement paste with 0.05% by wt. of NFC and MCC subjected to the different dispersion methods.

Type of fiber	Dispersion method	Compressive strength (MPa)	Strength ratio (-)	Maximum strain (%)	Modulus of elasticity (GPa)
	Ref (0%)	54.3 ± 1.7	1.00	0.62 ± 0.08	17.0 ± 2.8
NFC	*WD*	52.8 ± 1.4	0.97	0.56 ± 0.14	16.0 ± 4.5
	MecS	51.6 ± 1.8	0.95	0.53 ± 0.05	17.5 ± 1.8
	Super	58.2 ± 0.6	1.07	0.70 ± 0.19	17.2 ± 2.1
	Surf	53.4 ± 2.4	0.98	0.53 ± 0.09	17.6 ± 0.5
	US	42.7 ± 2.8	0.79	0.38 ± 0.07	17.1 ± 3.0
	MagS	50.3 ± 2.2	0.93	0.47 ± 0.01	20.9 ± 3.4
	TEMPO	58.5 ± 2.7	1.08	0.53 ± 0.06	14.8 ± 0.9
MCC	*WD*	58.4 ± 1.4	1.07	0.58 ± 0.03	19.6 ± 0.8
	MecS	51.2 ± 5.0	0.94	0.37 ± 0.05	20.9 ± 0.3
	Surf	49.4 ± 6.5	0.91	0.36 ± 0.06	19.4 ± 0.4
	US	61.0 ± 2.7	1.12	0.56 ± 0.08	18.7 ± 1.9
	MagS	48.3 ± 0.3	0.89	0.39 ± 0.05	19.5 ± 0.4

Due to the results obtained for the specimens containing fibers dispersed by means of mechanical stirring (*MecS*), magnetic stirring (*MagS*), and ultrasonication (*US*), these methods were not considered in the subsequent bending tests. Their use also did not influence the workability of the samples, as previously discussed. Thus, the methods *Super* and *TEMPO* were selected as the most promising and were used further in the investigation.

Figure 3-4a presents the response of the specimens containing no fiber (0.0%) as well as 0.5% by wt. and 1.0% by wt. of NFC without dispersion (*WD*) submitted to bending test. Figure 3-4b offers the same results as shown in

Table 3-6 but in the form of the ratios SR, DR, and MR, which represent the increase or decrease in a given flexural parameter when compared to the reference. From Figure 3-4b and

Table 3-6, great improvement in flexural strength and modulus can be observed due to the incorporation of NFC. It is important to highlight that the NFC-reinforced specimens' curves were drawn based on the linear portion of data. The most enhanced mechanical parameter was the flexural elastic modulus: The mixture containing 0.5% NFC yielded values more than 6 times higher than that of the reference (plain cement paste). The addition of 1.0% NFC enhanced this parameter by more than 5 times. Flexural strength increased by more than 2 and 3 times with the addition of 0.5% and 1.0% of NFC, respectively.

(a)

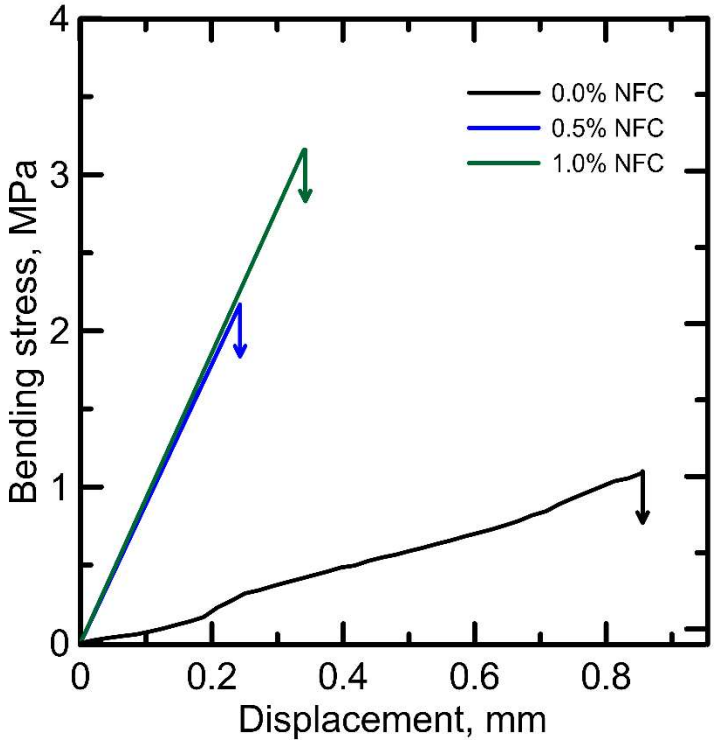

(b)

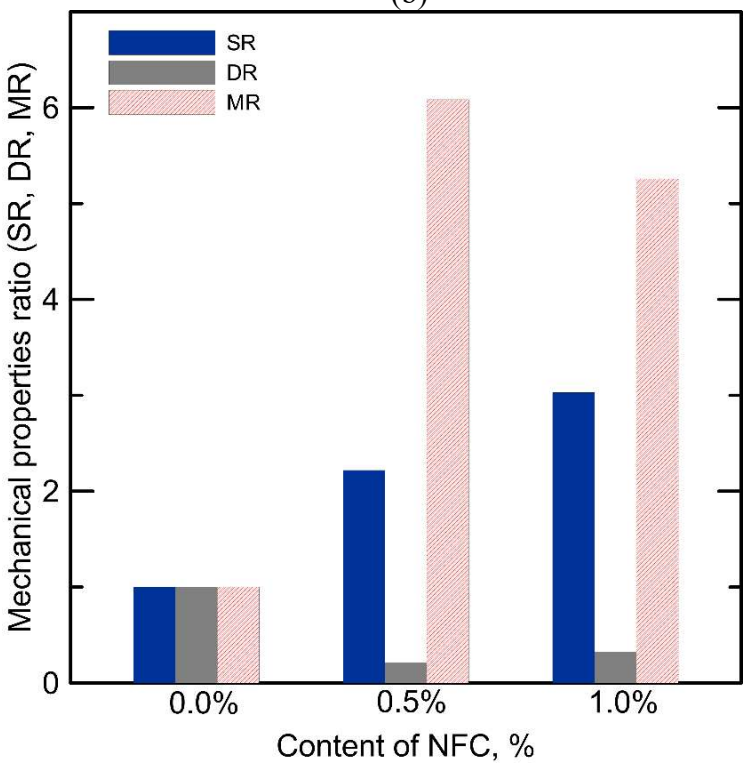

(c)

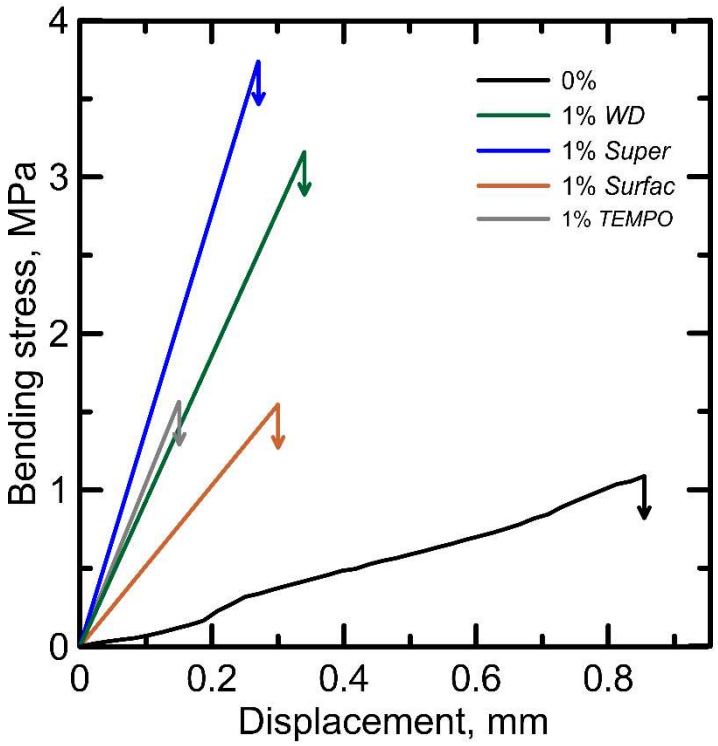

(d)

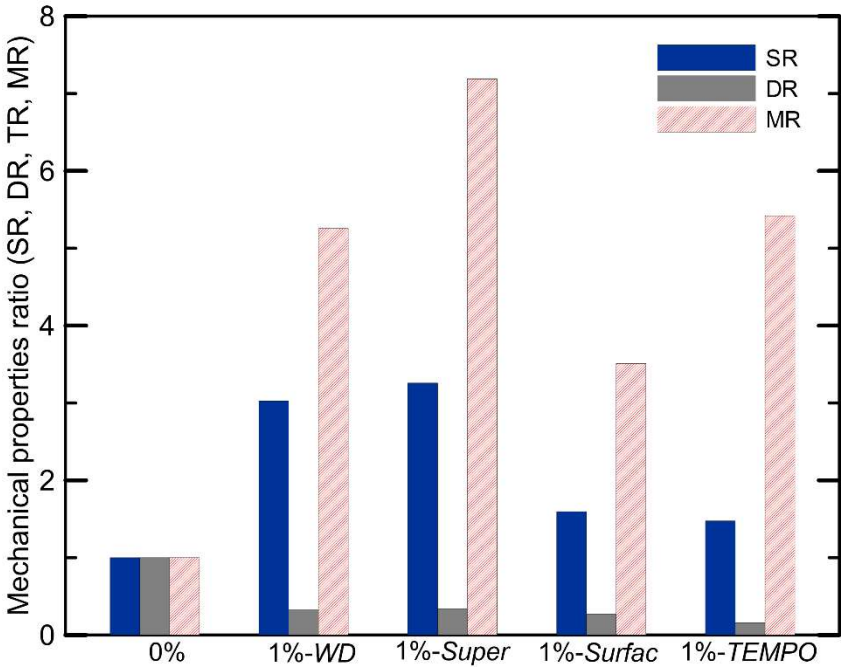

Figure 3-4 Results of four-point bending tests on NFC reinforced cement pastes: (a) Stress-displacement curves of the specimens with NFC without dispersion (*WD*) methods applied; (b) mechanical properties ratio for each

percentage of NFC *WD*; (c) stress-displacement curves of the specimens with 1% of NFC with dispersion methods applied (*Super*, *Surfac* and *TEMPO*). The reference (0%) and the specimens not subject to dispersion (*WD*) are presented for comparison, and (d) mechanical properties ratio for 1% of NFC subject to various dispersion techniques (*Super*, *Surfac* and *TEMPO*).

The possible reason for the excellent material performance with respect to the flexural elastic modulus and flexural strength due to the addition of fiber may be attributed to the NFC's intrinsic properties such as high strength, stiffness, large surface area, and the presence of hydroxyl groups as well [10,11]. The combination of the high specific surface area with the hydroxyl groups may promote a strong interface between the nanocellulose and the cement hydration products. This strong interaction, however, can lead to more brittle rupture of the composites reinforced with NFC. Indeed, a lower strain capacity was measured in both the compression and bending tests as also reported elsewhere [10,53] .

Table 3-6 Flexural mechanical parameters calculated based on four-point bending tests of the cement pastes' plates. Specimens with 0.50% by wt. and 1.00% by wt. of NFC subjected and not subjected (*WD*) to dispersion methods. Specimens with 0.50% by wt., 0.75% by wt., and 1.00% by wt. of MCC subjected and not subjected (*WD*) to dispersion methods. Results of the reference (0%) are shown for comparison.

Type of fiber	Fiber content (%)	Dispersion method	Flexural strength (MPa)	Maximum deflection (mm)	Flexural modulus (GPa)
-	0.00	-	1.08 ± 0.3	1.15 ± 0.34	1.57 ± 0.58
NFC	0.50	*WD*	2.40 ± 0.45	0.24 ± 0.03	9.55 ± 1.07
	1.00	*WD*	3.27 ± 0.29	0.37 ± 0.03	8.25 ± 0.53
	1.00	*Super*	3.53 ± 0.24	0.39 ± 0.10	11.29 ± 1.87
	1.00	*Surf*	1.72 ± 0.05	0.31 ± 0.03	5.51 ± 0.83
	1.00	*TEMPO*	1.59 ± 0.19	0.18 ± 0.04	8.51 ± 1.82
MCC	0.50	*WD*	4.34 ± 1.54	0.42 ± 0.01	11.36 ± 2.71
	0.75	*WD*	5.68 ± 1.18	0.39 ± 0.08	13.71 ± 3.83
	0.75	*US*	3.72 ± 0.25	0.30 ± 0.04	12.24 ± 1.39
	1.00	*WD*	4.02 ± 0.67	0.34 ± 0.11	11.57 ± 2.56

The optimal content of NFC without applying dispersion methods (*WD*) was based on the equivalent bending stress values. Therefore, in the range of NFC percentage evaluated, the specimens containing 1.0% NFC presented the best results with respect to this parameter. Accordingly, the dispersion techniques that showed positive effects on the compression and flow table tests were applied to the suspension of nano-fibrillated cellulose at 1% in mass and included into the cement paste plates. The attempt was to better disperse the NFC in the cement paste, resulting in advancements in flexural behavior.

Figure 3-4c shows the stress-displacement curves of the cement pastes containing 1% NFC with superplasticizer and TEMPO oxidation treatment. The values of mechanical properties are presented in Table 6 as well as in Figure 3-4d, where these values are presented in the form of ratios (SR, DR an MR).

In comparison to the reference, the dispersion methods resulted in an increase in both flexural strength and elastic modulus. This behavior was observed also for the specimens with NFC addition without dispersion, as previously discussed. Comparing the results of the *WD* and *Super* specimens, the use of superplasticizer could promote advances in the elastic modulus: The modulus ratio (MR) increased from 5.3 to 7.2, representing an improvement of more than 130%. The LM was also carried for NFC-*Super* and the results are presented in Table 3-3. As mentioned in Section 3.3.2, the number of visible particles decreased from 3581 to 2561 upon the addition of superplasticizer. This indicates that the superplasticizer interacted with the nanofibrils in a way to avoid them to agglomerate (bind together), promoting a better dispersion. From the results of the flow table test, flexural parameters and the LM analysis, it is reasonable to associate the use of superplasticizer with a better dispersion of the fibrils yet maintaining the water reducing capacity of superplasticizer. In fact, the use of superplasticizers is frequent in systems with reduced workability, and in the case of NFC-reinforced cementitious matrices, their use may be necessary [25,26,54,55].

The use of the NFC produced with TEMPO-mediated oxidation led to flexural modulus values comparable to that of the *WD* specimens, although the equivalent bending stress did not achieve the same improvement. Regarding the mechanical parameters from the compression tests, only the strength value had a positive increase with the use of TEMPO-treated NFC. One possible explanation may be the fact of the chemical surface's modification having converted part of the

hydroxyl groups into carboxylates. This led to less hydrogen bonding between the NFC and the matrix. Moreover, as discussed in the Section 3.3.2, the SEM and WRV analysis indicated that the TEMPO-mediated oxidation resulted in better dispersed yet more viscous gel. The fact that the NFC TEMPO did not improve the flexural parameters as much as the NFC control did can be related to its higher viscosity that could have hampered its dispersion on the paste. Thus, the paste mixing procedure may not have been enough to disperse the NFC TEMPO uniformly during the preparation of the specimens.

Based on the mechanical test results and the discussions above, the addition of superplasticizer with further mechanical stirring (*Super*) may be considered the most promising method for the dispersion of NFC for later use in cement pastes. It is possible to correlate the results from the flow table and the LM with the enhancement in the mechanical properties as a result of a better dispersion promoted by the superplasticizer.

3.3.3.1. Microstructure of cement paste containing NFC

The MIP results are presented in Figure 3-5, including total porosity and pore size distribution according to the size classification as proposed by Mindess *et al*. [56]. Small nanopores are specified as those of up to 5 nm in diameter, medium pores range between 5 nm and 25 nm, and large pores are larger than 25 nm. Compared with the reference, the addition of NFC increased the total pore volume from 95 to 110 mm^3/g while increasing the relative number of small pores by approximately 17%. Since a part of the NFC diameter distribution is in the same range as the small pores, the increase in this range may be due simply to the addition of the nanocellulose. By analyzing the pore size distribution, one can observe that the most significant change occurred in the number of large pores: In the reference mixture their fraction corresponded to 27% while for NFC specimens it reached 34%. The addition of superplasticizer was efficient in decreasing this trend. The total porosity and the quantity of large pores decreased in the presence of the superplasticizer when compared with NFC-*WD* specimens. The more flowable mixture containing superplasticizer, as shown by the flow table results, could also play a role on this feature, since superplasticizer can promote a more homogeneous microstructure.

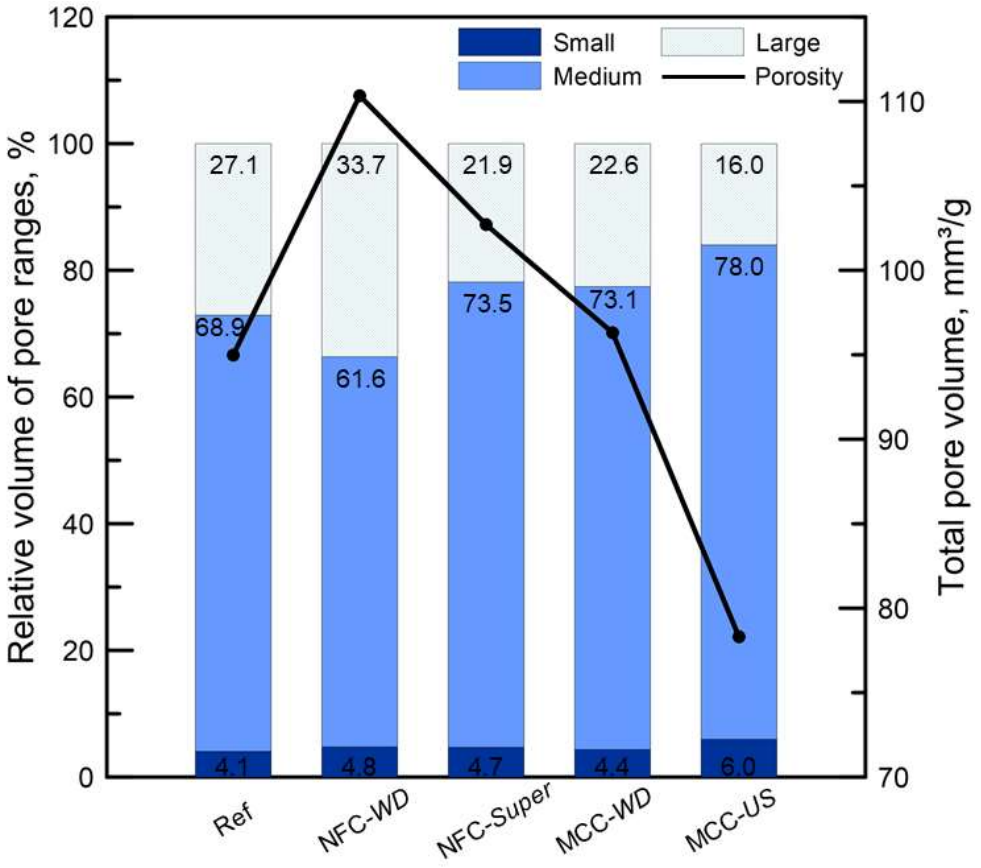

Figure 3-5 Pore size distribution according with the relative volume of pores (left axis) and porosity (continuous line, right axis) for specimens containing 0.5% NFC both with and without superplasticizer and MCC both subjected and not subjected to the ultrasonication process.

The curves from TGA and DTG analysis are presented in Figure 3-6. The peaks usually related to calcium silicate hydrate, calcium hydroxide, and calcium carbonate are shown as well. It is not possible to see any significant change in those peaks with the presence of NFC, with or without superplasticizer, besides the one corresponding to calcium carbonate. The peak of $CaCO_3$ is more pronounced in the sample with NFC *WD*, due probably to its more porous microstructure, which allows the ingress of CO_2. There is also a slight difference at around 280 ºC that may be associated with the formation of aluminates.

No clear difference was noticed with the addition of NFC regarding the hydration, which could be noticed by the TGA analysis. Although the increase of mechanical behavior of cementitious matrices with nanocellulose is often related to modifications on the hydration, some studies have reported that alteration in hydration does not happen at every NFC dosage and age [57–59]. Even though the

use of superplasticizer had lowered the fraction of the large pores, the matrix was more porous due to the presence of NFC. As the analyzed parameters from the bending test were positively affected by the presence of the NFC, the microstructural results may lead to the assumption of the bridging effect's existence having been facilitated by nanocellulose. Similar to the well-known effect of the macro-fibers, the morphology of the NFC could enable them to bridge nano/micro cracks, leading to an effective force transfer [19]. However, as indicated by the curves presented in Figure 3-4a and c, the addition of NFC was not capable to increase the deflection capacity of the cement paste' specimens, therefore, their failure mode remained brittle. Such a bridging mechanism could be related to the strong bond between the nanocellulose and the hydration products due to their high specific surface area and the presence of hydroxyl groups [10,12]. More of the possible strength mechanisms is discussed in Section 3.3.5.

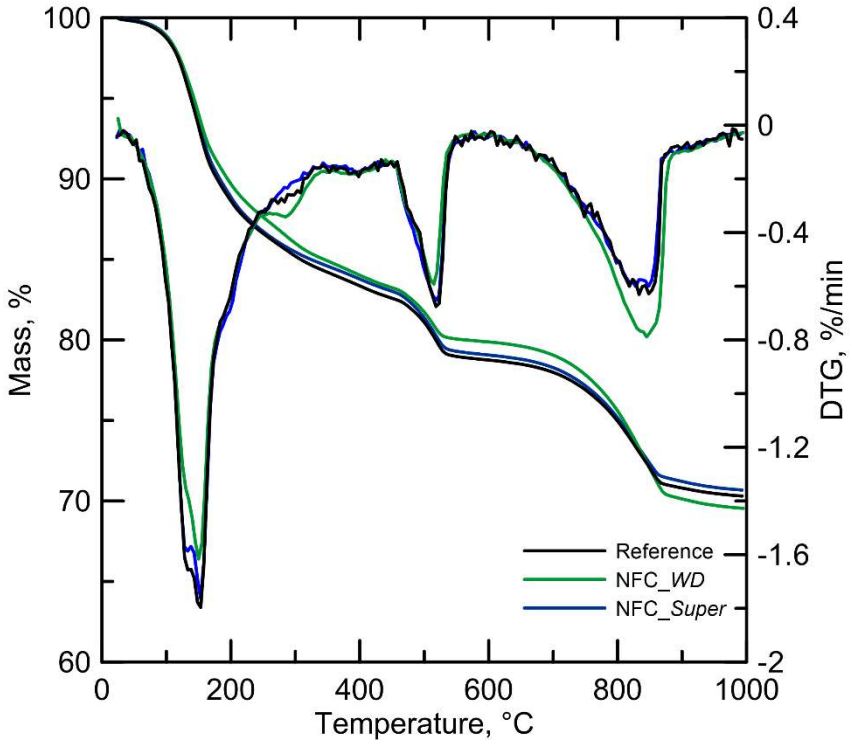

Figure 3-6 TGA and DTG curves of cement paste reinforced with 0.5% of NFC. The most suitable dispersion method was addressed.

3.3.4. Mechanical behavior of MCC composites and the influence of dispersion methods

Table 3-5 contains the averages and the related deviations of the compressive mechanical parameters for each dispersion method applied to the specimens containing 0.05% MCC. The addition of MCC without the use of any dispersion method (*WD*) produced a positive effect regarding compressive strength, with 7% improvement in relation to the reference specimens. The dispersion methods applied did not result in strength enhancement, except for the ultrasonication (*US*), with 12% and 5% improvement if compared to the *WD* and the reference specimens, respectively. The ultrasonication (*US*) method had already been successfully used to disperse cellulose nanocrystals in cement paste [22]. In the present case of microcrystalline cellulose (MCC), the ultrasonication showed itself to be efficient in breaking up the possible agglomerations of MCC, and this was reflected in the compressive strength. The addition of MCC enhanced the elastic modulus, regardless of the dispersion method employed. The small content of 0.05% by wt. of MCC was able to improve the modulus of elasticity by 10% to 23%, depending on the dispersion technique. Previous research with similar results had attributed this behavior to a formation of a denser matrix and to intrinsic properties of MCC, namely high elastic modulus and crystallinity [16,28,30].

Due to compression and flow table preliminary results, the ultrasonication dispersion method was the only one applied to produce specimens for the bending tests and further analysis.

The equivalent bending stress versus displacement curves of the specimens reinforced with MCC are shown in Figure 3-7. It is important to highlight that the MCC-reinforced specimens' curves were drawn based on the linear portion of data. The percentage of MCC was 0%, 0.5%, and 1% without any dispersion method's having been applied. The 0.75% content was additionally included due to the mechanical properties obtained for the mixtures containing 0.5% and 1% fiber, as explained farther on.

Table 3-6 brings the same mechanical properties as discussed for NFC reinforced specimens: flexural strength, maximum deflection, and flexural modulus. Figure 3-7b shows the properties presented in

Table 3-6, but in the form of ratios; see Section 3.2.3.5.

(a)

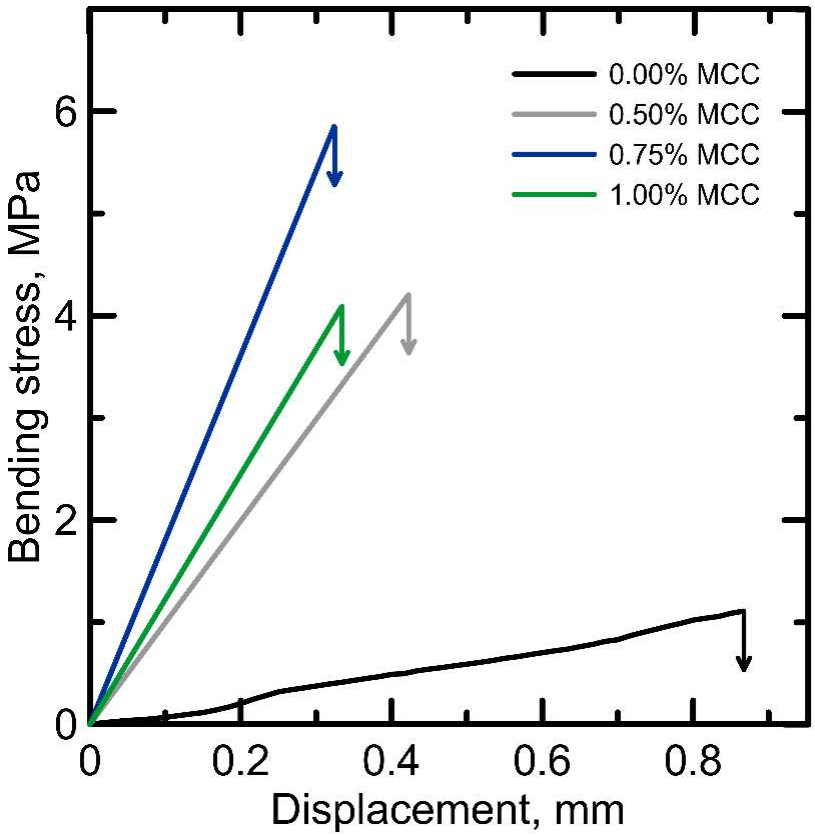

(b)

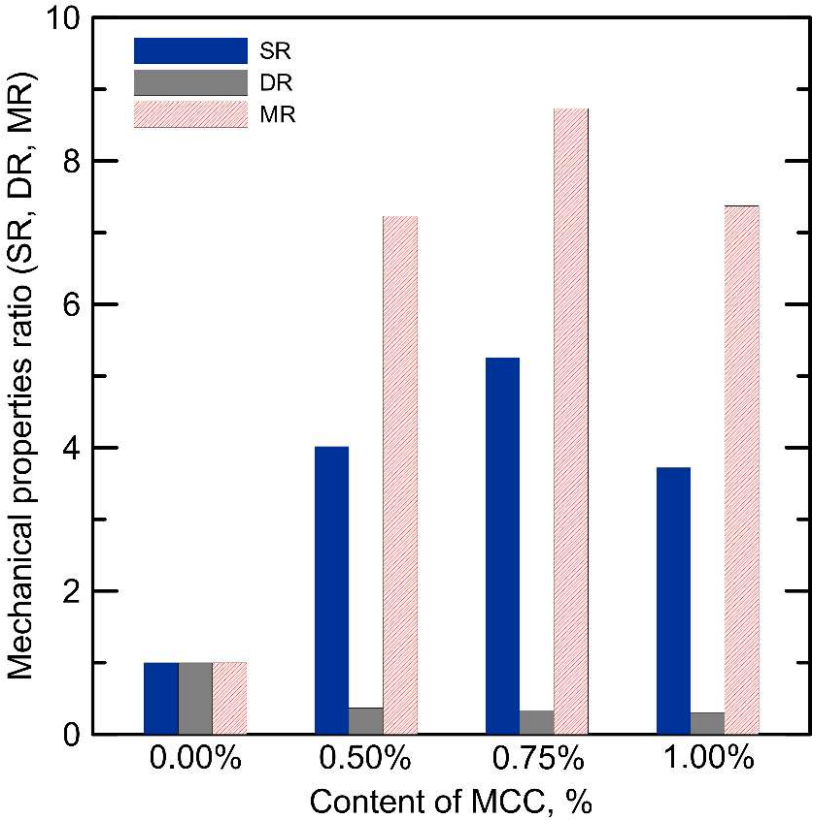

(c)

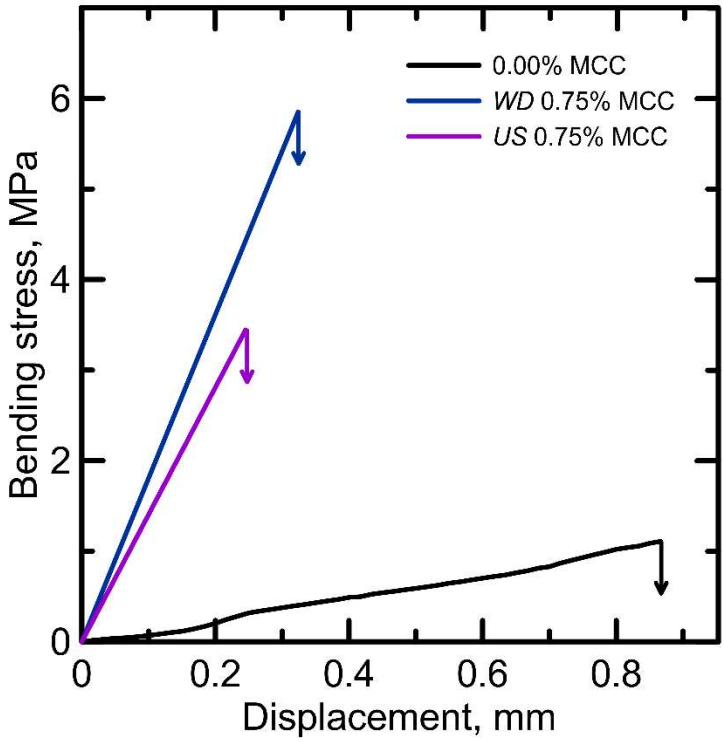

(d)

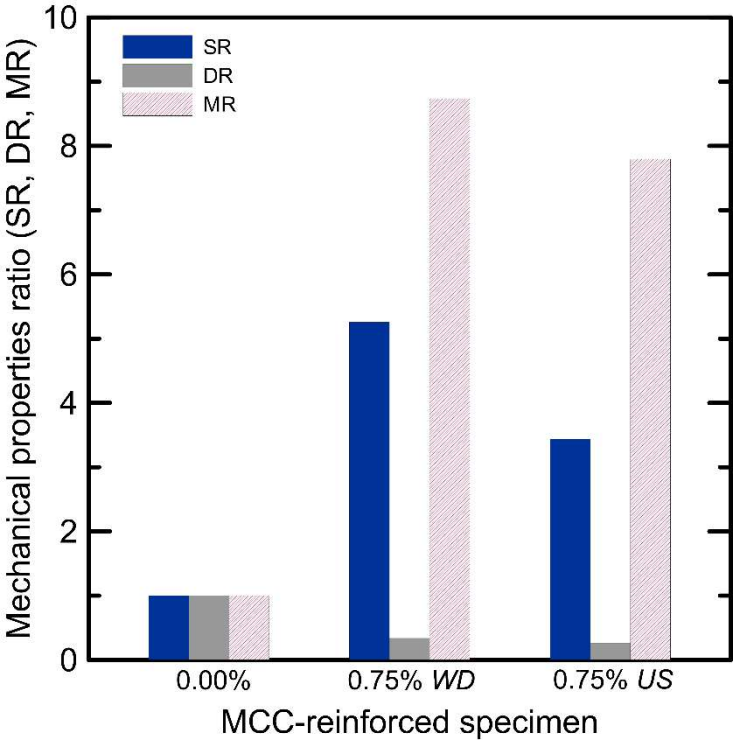

Figure 3-7 (a) Typical stress-displacement curves of specimens containing 0.0%, 0.5%, and 1% MCC without any dispersion methods applied (*WD*). The 0.75% was included to investigate the range between 0.5% and 1% for a possible

optimal content. (b) Stress, deflection, modulus, and toughness ratios from the bending tests, values obtained for the reference having been divided by values corresponding to each MCC content; (c) stress-displacement curves comparing the dispersion method applied (*US*) with the reference (0%) and the specimen not subjected to dispersion (*WD*) with 0.75% of MCC.

From the analysis of both Figure 3-7 and

Table 3-6, it can be noticed that the addition of 0.5% and 1.0% of MCC absent any dispersion method was able to improve the flexural strength and elastic modulus. For instance, 0.5% of MCC promoted an enhancement of these parameters by factors of approximately 4 and 7, respectively. In the present case, this excellent response is attributed to the filling effect of MCC as discussed in the following Section 3.3.4.1.

When evaluating the mean strength values in

Table 3-6, a small decrease in the addition of 1% MCC can be observed in comparison to the mixture containing 0.5% MCC. Thus, the optimal content of MCC could be between these two concentrations. Therefore, 0.75% MCC was included in the investigation to consider this range. The strength values presented in

Table 3-6 show that indeed 0.75% can be seen as the optimal MCC content from among the concentrations tested. The improvement due at the optimal content reached almost 5 times in terms of its equivalent bending stress. The most improved mechanical property was the flexural elastic modulus, showing an enhancement of more than 8 times.

The ultrasonication dispersion method was applied to the specimens reinforced with 0.75% MCC, i.e., the optimal content. In relation to the reference, the use of the ultrasonication method was able to increase the values of flexural strength and flexural modulus. However, in comparison to the 0.75% *WD* specimens, the method did not favor positively the mechanical properties evaluated. This result differs from that obtained from the compressive tests, where the ultrasonication dispersion enabled further enhancement of the mechanical behavior of the

specimens containing MCC. The great difference between those tests is, however, the content of MCC submitted to ultrasonication: 0.05% for the compression tests and 0.75% for the bending tests. This percentage corresponds to an increase in MCC addition by 15 times. Hence, the quantity of MCC corresponding to an addition of 0.75% exceeded the amount of material that can be dispersed by the present methodology. The contrasting behaviors indicate that the ultrasonication is efficient in dispersing MCC in small concentrations, such as that in the 0.05% specimens, but not so for much greater concentrations. The results of the flow table and the microstructure analysis support this assumption; see Section 3.3.2.

3.3.4.1. Microstructure of cement paste with MCC

The pore size distributions and total pore volumes of the cement pastes reinforced with 0.5% MCC without dispersion (*WD*) and subjected to the ultrasonication process (*US*) are shown in Figure 3-5. Comparing the MCC *WD* and the reference mixture, it is obvious that while total pore volume did not change much, the pore size distribution was affected by the addition of MCC. The relative number of large pores decreased, and that of the small ones increased. This trend is intensified when the ultrasonication method is used for fiber dispersion: while the large pores amounted to 23% in the reference mixture, in MCC *US* their content was 16%. For the small pores, however, an increase from 4.4% to 6% was observed. This all resulted in an expressed reduction in the total pore volume, from 95 mm^3/g to 78 mm^3/g. The more compact pore size distribution may evidence an efficient packing effect promoted by the addition of MCC. This effect was enhanced by the ultrasonication process, indicating that efficient dispersion was achieved by distributing the MCC particles more uniformly within the matrix and reducing the agglomeration.

The denser matrix attained upon MCC addition is mostly due to the filler property of MCC rather than deep changes in its hydration products [16,20,30]. In the present investigation, the TGA and DTA curves did not indicate any significant alterations, as shown in Figure 3-8. The exception is peak that corresponds to the C-S-H products, which shifted approximately 23 C° to the right, when compared to the curve of the reference. The ultrasonication process although expressively changed the porosity, also did not alter the thermogravimetric analysis. The analysis of the microstructure suggests that the

great improvement in the mechanical properties of the cement pastes reinforced with MCC comes from a denser matrix, promoted by the filler effect of the MCC.

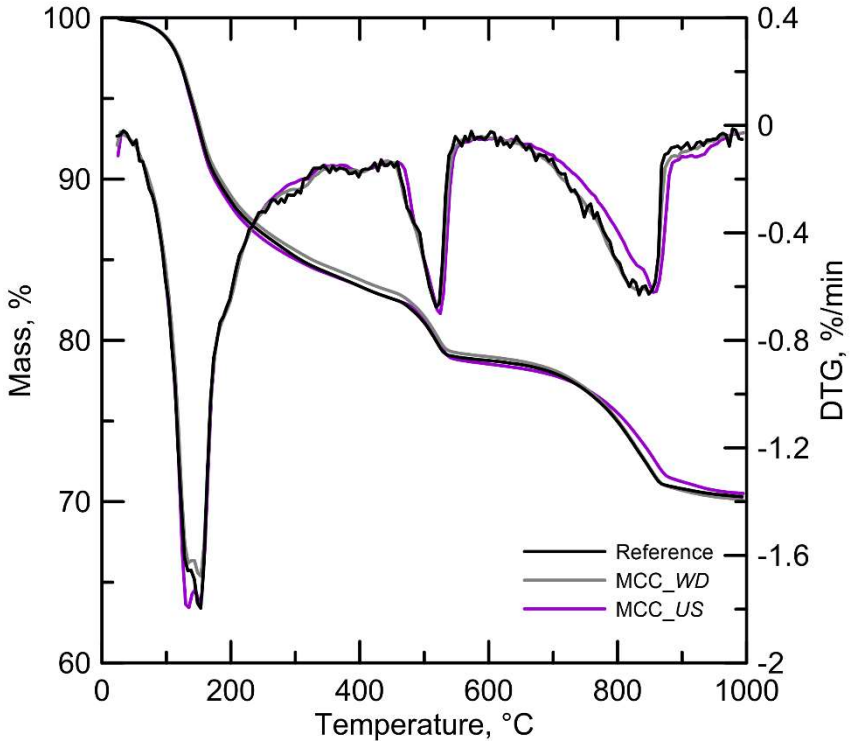

Figure 3-8 TGA and DTG curves of cement paste reinforced with 0.5% of MCC. The most suitable dispersion method was addressed.

3.3.5. Comparison between MCC and NFC cement paste composites

Figure 3-9 presents the equivalent bending stress versus displacement curves of the cement paste reinforced with 0.5% and 1.0% of MCC, represented by the dashed lines, or NFC, represented by the continuous lines. As aforementioned, the NFC and MCC-reinforced specimens' curves were drawn based on the linear portion of data. Also,

Table **3-6** shows the better response of the MCC-reinforced cement pastes in terms of the assessed flexural parameters in comparison to the specimens made with addition of NFC. At a content of 1.0% the differences are however not that evident. Here it is important to point out that 1.0% is beyond the optimal content of MCC (0.75%) as shown in the present study. As for the NFC it seems that the optimal content was not reached since the flexural properties improved when the

NFC dosage increased from 0.5% to 1.0%. However, a further increase in the percentage of NFC would lead to rheological issues.

The fresh state properties varied according to the type of fiber investigated and dispersion method, as shown by the flow table tests. It is important to notice that the objectives related to the dispersion/mixture methods are distinct for each material. The methods applied to the MCC suspensions aimed at the high dispersion of fibers; so, the flow values that may represent a good dispersion of a mixture with MCC should be lower than the reference. This is different for the specimens with NFC since the gel is already dispersed, and the aim in this case is to improve the workability of the specimens since the addition of NFC without dispersion methods led to a great loss in flowability.

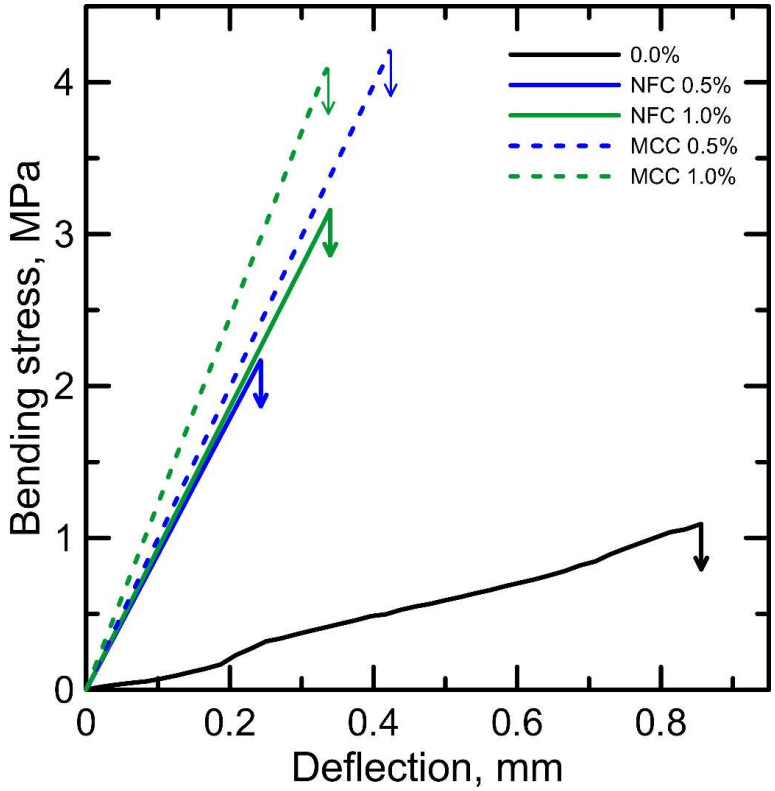

Figure 3-9 Typical stress-displacement curves obtained from the four-point bending tests on cement paste plates containing 0.0%, 0.5% and, 1.0% of either MCC or NFC, without dispersion methods applied (WD).

Three possible reasons for the distinct mechanical behavior can be listed. First, the morphologies of fiber materials show basic differences regarding, as instances, diameter and aspect ratio. While MCC morphology varies from rod-like particles to longer, fiber-like examples, NFC presents a higher aspect ratio and can form entangled networks. Thus, the different morphologies can influence the force

transfer from matrix to fiber and the characteristics of the possible agglomerations. Second, intrinsic properties of NFC and MCC can affect the interface of the fibrils and cement particles. The high specific surface area and the presence of the hydroxyls can lead to interactions through hydrogen bonds promoting a strong fibril-matrix interface. The elastic modulus, tensile strength and crystallinity values also contribute to the strong bond on the interface, as pointed out elsewhere [10,16,17]. The water adsorption capacity may also affect how much water is available in the matrix, interfering with the hydration process. Third, the influences of MCC and NFC on rheology affect the microstructure of the hardened composite, as shown by the flow table and MIP investigations. The porosity and the pore size distribution play an important role on the mechanical properties and the fresh state characteristics which influence them. It can be assumed that the three abovementioned factors act simultaneously and in a distinct way for each cellulose-based material, promoting unique mechanisms of reinforcement.

Assuming that the increase of the total porosity did not result in a denser matrix and there was no visible change in the hydration according to the TGA analysis in the case of the NFC-reinforced specimens, one hypothesis is that the notorious increase in strength and stiffness is due to the existence of load transfer mechanisms promoted by the NFC, as already stated by other researchers [10,52,57,60,61]. The distribution of the NFC, i. e., the fibrils count on a given section of an element also plays a role in the load transfer issue, as well as the fibrils length. Although the high aspect of the NFC is often highlighted, it is important to note that the fibrils are quite short when seen from a macro perspective. It should be observed that their length and quantities may be not enough to prevent microcracks to grow into macro-ones. This is supported by the brittle failure the reinforced cement pastes showed when tested in bending, as seen in Figure 3-4a, Figure **3-7** and Figure 3-9.

As aforementioned, the addition of NFC or MCC was not capable of changing the failure mode of the cement pastes, although the crack-bridging effect can still be considered an acting mechanism. The hypothesis is that the micro and nanofibers could act before the collapse of the material, bridging micro and nano cracks in anticipation of the formation of macro cracks, leading to a certain

limited improvement of mechanical properties but not enough to alter the fracture mode.

It is important to highlight that the study at hand only investigated the hydration of the cement pastes with thermogravimetric analysis (TGA) under an oxygen atmosphere at the age of 28 days. In those analyses, the addition of MCC or NFC did not significantly alter the TGA/DTG curves' aspect. However, these analyses are probably not enough to fully characterize the hydration mechanisms of a cement paste.

3.4. Conclusions

This Chapter presents various approaches to the use of two types of promising cellulose-based materials, MCC and NFC, as reinforcement for cement pastes. These materials differ regarding their scale, according to their diameters, morphological characteristics, and intrinsic properties. Thus, distinct approaches are required for the most efficient dispersion of MCC and mixing of NFC: Ultrasonication was suitable for dispersing MCC while superplasticizer for NFC. Although the active mechanisms may be different in each case, the addition of MCC and NFC enabled considerable improvement in the flexural properties of the composites. More specifically, the following conclusions can be drawn:

- The optimal content of MCC within the investigated range (up to 1%) was 0.75% and facilitated an enhancement of flexural strength and modulus by more than 5 and 8 times, respectively, when compared with the reference mixture without fiber addition.
- The ultrasonication method was found to be the most suitable for MCC among the investigated ones, capable of dispersing small contents of 0.05% to 0.5% of MCC. However, the MCC content corresponding to 0.75% concentration in the cement paste exceed the method capacity, and the benefits of good dispersion could not be observed.
- The simple addition of 0.5% of MCC did not significantly affect the total porosity of the composite although it was efficient in reducing the fraction of large pores (larger than 25 nm) and increasing that of the small pores (smaller than 5 nm). With the ultrasonication process included, the porosity decreased considerably from 95 mm^3/g to 78 mm^3/g.

- The pronounced improvement in flexural performance of the cement paste upon the addition of MCC can be traced back to the less porous microstructure of such composites and good interface interaction between the matrix and reinforcement.
- The optimal content of NFC was 1% and promoted an enhancement of the flexural strength and elastic modulus by more than 3 and 5 times, respectively. In the mixtures under investigation there was no indication of agglomeration by the alteration of the mechanical properties, although the mixture with 1% NFC exhibited low workability.
- The use of superplasticizer was found to be the most suitable for mixtures containing NFC; its addition also promoted enhancement of the flexural properties. The increases in flexural strength and elastic modulus were by 5 and 8 times with the addition of superplasticizer, respectively. Moreover, the MIP results showed that the NFC *Super* specimens had fewer large pores in their microstructure than the NFC *WD*. However, even with this effect of the superplasticizer, the total porosity was higher when compared with the reference mixture.
- The TGA and MIP results suggest that the NFC promotes considerable enhancements of the flexural properties of cement pastes due to the fibers' bridging capacity with respect to nano- and micro-cracks.

3.5. Ji References

[1] CASTOLDI, R. DE S.; SOUZA, L. M. S. DE; ANDRADE SILVA, F. DE. Comparative study on the mechanical behavior and durability of polypropylene and sisal fiber reinforced concretes. **Construction and Building Materials**, v. 211, p. 617–628, 2019.

[2] OLIVEIRA DE SOUZA, L.; SILVA DE SOUZA, L. M.; ANDRADE SILVA, F. DE. Mechanics of Natural Curauá Textile Reinforced Concrete. **Magazine of Concrete Research**, p. 1–31, 2019.

[3] AGOPYAN, V. *et al*. Developments on vegetable fibre–cement based materials in São Paulo, Brazil: an overview. **Cement and Concrete Composites**, v. 27, n. 5, p. 527–536, May 2005.

[4] HISSEINE, O. A. *et al*. Nano-engineered ultra-high performance concrete for

controlled autogenous shrinkage using nanocellulose. **Cement and Concrete Research**, v. 137, n. September, p. 106217, 2020.

[5] FU, C. *et al*. A comparative study on the effects of three nano-materials on the properties of cement-based composites. **Materials**, v. 13, n. 857, 2020.

[6] GUO, H. *et al*. Improvement of stability and mechanical properties of cement asphalt emulsion composites using nano fibrillated celluloses. **Cement and Concrete Composites**, v. 125, n. April 2021, p. 104330, 2022.

[7] ABDUL KHALIL, H. P. S. *et al*. Production and modification of nanofibrillated cellulose using various mechanical processes: A review. **Carbohydrate Polymers**, v. 99, p. 649–665, 2014.

[8] DUFRESNE, A. Nanocellulose: A new ageless bionanomaterial. **Materials Today**, v. 16, n. 6, p. 220–227, 2013.

[9] EICHHORN, S. J. *et al*. Review: Current international research into cellulose nanofibres and nanocomposites. **Journal of Materials Science**, v. 45, n. 1, p. 1–33, 2010.

[10] ARDANUY, M. *et al*. Nanofibrillated Cellulose (Nfc) As A Potential Reinforcement For High Performance Cement Mortar Composites. **BioResources**, v. 7(3), p. 3883–3894, 2012.

[11] ONUAGULUCHI, O.; PANESAR, D. K.; SAIN, M. Properties of nanofibre reinforced cement composites. **Construction and Building Materials**, v. 63, p. 119–124, 2014.

[12] MEJDOUB, R. *et al*. Nanofibrillated cellulose as nanoreinforcement in Portland cement: Thermal, mechanical and microstructural properties. **Journal of Composite Materials**, v. 51, n. 17, p. 2491–2503, 2017.

[13] ANJU, T. R.; RAMAMURTHY, K.; DHAMODHARAN, R. Surface modified microcrystalline cellulose from cotton as a potential mineral admixture in cement mortar composite. **Cement and Concrete Composites**, v. 74, p. 147–153, 2016.

[14] JIAO, L. *et al*. Natural cellulose nanofibers as sustainable enhancers in construction cement. **PLoS ONE**, v. 11, n. 12, p. 1–13, 2016.

[15] SUN, X. *et al*. Cellulose Nanofibers as a Modifier for Rheology, Curing and Mechanical Performance of Oil Well Cement. **Scientific Reports**, v. 6, p. 1–9, 2016.

[16] SILVA, L. *et al*. A facile approach of developing micro crystalline cellulose

reinforced cementitious composites with improved microstructure and mechanical performance. **Powder Technology**, v. 338, p. 654–663, 2018.

[17] CLARAMUNT, J. *et al*. **Mechanical performance of ductile cement mortar composites reinforced with nanofibrillated cellulose**. 2nd International RILEM Conference on Strain Hardening Cementitious Composites. **Anais**...2011

[18] FONSECA, C. S. *et al*. Jute fibers and micro/nanofibrils as reinforcement in extruded fiber-cement composites. **Construction and Building Materials**, v. 211, n. April, p. 517–527, 2019.

[19] COSTA CORREIA, V. DA *et al*. Nanofibrillated cellulose and cellulosic pulp for reinforcement of the extruded cement based materials. **Construction and Building Materials**, v. 160, p. 376–384, 2018.

[20] FILHO, A. *et al*. Mechanical and micro-structural investigation of multi-scale cementitious composites developed using sisal fibres and microcrystalline cellulose. **Industrial Crops and Products**, v. 158, n. April, p. 112912, 2020.

[21] MONDAL, S. Preparation, properties and applications of nanocellulosic materials. **Carbohydrate Polymers**, v. 163, p. 301–316, 2017.

[22] CAO, Y. *et al*. The relationship between cellulose nanocrystal dispersion and strength. **Construction and Building Materials**, v. 119, p. 71–79, 2016.

[23] MOHAMED, M. A. S.; GHORBEL, E.; WARDEH, G. Valorization of micro-cellulose fibers in self-compacting concrete. **Construction and Building Materials**, v. 24, n. 12, p. 2473–2480, 2010.

[24] NILSSON, J.; SARGENIUS, P. Effect of microfibrillar cellulose on concrete equivalent mortar fresh and hardened properties. p. 89, 2011.

[25] PETERS, S. *et al*. Nanocellulose and Microcellulose Fibers for Concrete. **Transportation Research Record: Journal of the Transportation Research Board**, v. 2142, p. 25–28, 2010.

[26] STEPHENSON, K. M. **Characterizing the behavior and properties of nanocellulose reinforced ultra high performance concrete**. 2011. 152 f. Maine. 2011.

[27] CAO, Y. *et al*. The influence of cellulose nanocrystal additions on the performance of cement paste. **Cement and Concrete Composites**, v. 56, p. 73–83, 2015.

[28] PARVEEN, S. *et al*. A novel approach of developing micro crystalline cellulose reinforced cementitious composites with enhanced microstructure and

mechanical performance. **Cement and Concrete Composites**, v. 78, p. 146–161, 2017.

[29] PETERS, S. J. *et al*. Nanocellulose and Microcellulose Fibers for Concrete. **Transportation Research Record: Journal of the Transportation Research Board**, v. 2142, n. 1, p. 25–28, 2010.

[30] PARVEEN, S. *et al*. Ultrasonic dispersion of micro crystalline cellulose for developing cementitious composites with excellent strength and stiffness. **Industrial Crops and Products**, v. 122, n. May, p. 156–165, 2018.

[31] SUPIT, S. W. M.; NISHIWAKI, T. Compressive and flexural strength behavior of ultra-high performance mortar reinforced with cellulose nano-fibers. **International Journal on Advanced Science, Engineering and Information Technology**, v. 9, n. 1, p. 365–372, 2019.

[32] BAKKARI, M. EL *et al*. Preparation of cellulose nanofibers by TEMPO-oxidation of bleached chemi-thermomechanical pulp for cement applications. **Carbohydrate Polymers**, v. 203, n. September 2018, p. 238–245, 2019.

[33] FUKUZUMI, H. *et al*. Transparent and high gas barrier films of cellulose nanofibers prepared by TEMPO-mediated oxidation. **Biomacromolecules**, v. 10, n. 1, p. 162–165, 2009.

[34] HUANG, Y. Y.; TERENTJEV, E. M. Dispersion of carbon nanotubes: Mixing, sonication, stabilization, and composite properties. **Polymers**, v. 4, n. 1, p. 275–295, 2012.

[35] NOLTINGK, B. E.; NEPPIRAS, E. A. Cavitation produced by ultrasonics. **Proceedings of the Physical Society. Section B**, v. 63, n. 9, p. 674–685, 1950.

[36] SESIS, A. *et al*. Influence of acoustic cavitation on the controlled ultrasonic dispersion of carbon nanotubes. **Journal of Physical Chemistry B**, v. 117, n. 48, p. 15141–15150, 2013.

[37] VAISMAN, L.; WAGNER, H. D.; MAROM, G. The role of surfactants in dispersion of carbon nanotubes. **Advances in Colloid and Interface Science**, v. 128–130, n. 2006, p. 37–46, 2006.

[38] FLATT, R.; SCHOBER, I. **Superplasticizers and the rheology of concrete**. [s.l.] Woodhead Publishing Limited, 2012.

[39] SCHINDELIN, J. *et al*. Fiji: An open-source platform for biological-image analysis. **Nature Methods**, v. 9, n. 7, p. 676–682, 2012.

[40] TONOLI, G. H. D. *et al*. Properties of cellulose micro/nanofibers obtained

from eucalyptus pulp fiber treated with anaerobic digestate and high shear mixing. **Cellulose**, v. 23, n. 2, p. 1239–1256, 2016.

[41] REBOUILLAT, S.; PLA, F. State of the Art Manufacturing and Engineering of Nanocellulose: A Review of Available Data and Industrial Applications. **Journal of Biomaterials and Nanobiotechnology**, v. 04, n. 02, p. 165–188, 2013.

[42] ZHANG, M. *et al*. A comparison of ram extrusion by single-holed and multi-holed dies for extrusion-spheronisation of microcrystalline-based pastes. **International Journal of Pharmaceutics**, v. 416, n. 1, p. 210–222, 2011.

[43] ISOGAI, A.; SAITO, T.; FUKUZUMI, H. TEMPO-oxidized cellulose nanofibers. **Nanoscale**, v. 3, n. 1, p. 71–85, 2011.

[44] CABALLERO, B. **Encyclopedia of Food Sciences and Nutrition**. [s.l: s.n.]. v. 1

[45] LUO, X. L. *et al*. Effects of wet-pressing-induced fiber hornification on enzymatic saccharification of lignocelluloses. **Cellulose**, v. 18, n. 4, p. 1055–1062, 2011.

[46] GU, F. *et al*. Water retention value for characterizing fibrillation degree of cellulosic fibers at micro and nanometer scales. **Cellulose**, v. 25, n. 5, p. 2861–2871, 2018.

[47] DIAS, M. C.; MENDONÇA, M. C.; DAMÁSIO, R. A. P. Influence of hemicellulose content of Eucalyptus and Pinus fibers on the grinding process for obtaining cellulose micro / nanofibrils. **Holzforschung**, v. 73, n. 11, p. 1035–1046, 2019.

[48] QIAN, R.; TANG, A.; CHEN, G. TEMPO-Mediated Oxidation of Cellulose and Preparation of Cellulose Nanofibrils. **Journal of Biobased Materials and Bioenergy**, v. 5, n. March, p. 253–257, 2011.

[49] GÓMEZ HOYOS, C.; CRISTIA, E.; VÁZQUEZ, A. Effect of cellulose microcrystalline particles on properties of cement based composites. **Materials and Design**, v. 51, p. 810–818, 2013.

[50] LONG, W. J. *et al*. Rheology and buildability of sustainable cement-based composites containing micro-crystalline cellulose for 3D-printing. **Journal of Cleaner Production**, v. 239, p. 118054, 2019.

[51] MOON, R. J. *et al*. **Cellulose nanomaterials review: Structure, properties and nanocomposites**. [s.l: s.n.]. v. 40

[52] HISSEINE, O. A. *et al*. Feasibility of using cellulose filaments as a viscosity modifying agent in self-consolidating concrete. **Cement and Concrete Composites**, v. 94, n. September, p. 327–340, 2018.

[53] ONUAGULUCHI, O.; PANESAR, D. K.; SAIN, M. Properties of nanofibre reinforced cement composites. **Construction and Building Materials**, v. 63, p. 119–124, 2014.

[54] ONUAGULUCHI, O.; BANTHIA, N. **Plant-based natural fibre reinforced cement composites: A reviewCement and Concrete Composites**, 2016.

[55] SARGENIUS, J. N. AND P. Effect of microfibrillar cellulose on concrete equivalent mortar fresh and hardened properties. p. 89, 2011.

[56] MINDESS, S.; YOUNG, F.; DARWIN, D. **Concrete**. [s.l.] Prentice Hall, Pearson Education, Inc. Upper Saddle River, NJ 07458, U.S.A., 2003.

[57] KOLOUR, H.; ASHRAF, W.; LANDIS, E. N. Hydration and Early Age Properties of Cement Pastes Modified with Cellulose Nanofibrils. **Transportation Research Record: Journal of the Transportation Research Board**, p. 036119812094599, 2020.

[58] HISSEINE, O. A. *et al*. Nanocellulose for improved concrete performance: A macro-to-micro investigation for disclosing the effects of cellulose filaments on strength of cement systems. **Construction and Building Materials**, v. 206, n. February, p. 84–96, 2019.

[59] GONCALVES, J. *et al*. Cellulose nanofibres (CNF) for sulphate resistance in cement based systems. **Cement and Concrete Composites**, v. 99, n. March, p. 100–111, 2019.

[60] CLARAMUNT, J. *et al*. Effect of nanocelluloses on the microstructure and mechanical performance of CAC cementitious matrices. **Cement and Concrete Research**, v. 119, n. October 2018, p. 64–76, 2019.

[61] HISSEINE, O. A.; OMRAN, A. F.; TAGNIT-HAMOU, A. Influence of cellulose filaments on cement paste and concrete. **Journal of Materials in Civil Engineering**, v. 30, n. 6, p. 1–14, 2018.

[62] OLIVEIRA DE SOUZA, L. *et al*. Investigation of dispersion methodologies of microcrystalline and nano-fibrillated cellulose on cement pastes. **Cement and Concrete Composites**, v. 126, n. February 2022, 2022.

4. Effect of microcrystalline and nano-fibrillated cellulose on the mechanical behavior and on the microstructure of cement pastes

4.1. Introduction

Investigations exploring the use of micro and nanocellulose on cementitious matrices are increasing over time. Some studies try to explain the mechanisms through which those inclusions act on the cement environment. Cao *et al*. [1] were the first to propose a theory to describe the action of nanocellulose crystals on cement-based materials. They assembled two mechanisms: steric stabilization and short-circuit diffusion. The former is similar to how the water-reducing agents act by adhering to the cement particles and dispersing them during the mixing process. This can result in a finer and more uniform distribution of cement. The short-circuit diffusion is the mechanism of water molecules diffusing along the nanocellulose networks into the hydration products shell formed around the cement particles.

In 2020, Kolour *et al*. [2] proposed a model of tunnels, reservoirs, and bridges (TR&B) to gather their and others' main findings on the mechanisms behind the effect of cellulose fibrils on cementitious matrices. The "tunnels" part is similar to the short-circuit diffusion aforementioned, which is related to the transportation of water to unhydrated cement particles. The "reservoir" is for the water retention capacity the hydrophilic fibrils present. The retained water could be further used as an internal curing agent. At last, the nanofibrils are seen also as toughening agents due to improvements in fracture energy. This effect can be achieved since they can work as "bridges", preventing crack growth.

Through an extensive investigation of the role of NFC in cementitious matrices, Hisseine *et al*. [3,4] confirm the water-retention-and-release capacity of the fibrils. Furthermore, they also confirmed the internal curing and nanoreinforcing effects NFC presents [5].

The mechanical improvement observed when micro and nanocellulose are added is frequently related to hydration enhancement [2,8–11], although there are

some exceptions [11–14]. The higher degree of hydration is often claimed to be a result of the nucleation (similar to short-circuit diffusion) and of the internal curing effects. Thus, the presence of MCC and NFC also affects the microstructure of the matrices, having even an impact on the calcium silicate hydrate (C-S-H) characteristics [4,6]. In the case of MCC-reinforced composites, the mechanical improvement is related to the denser matrix formed by the presence of the MCC particles [7–10]. The intrinsic properties of MCC and NFC such as a high surface area, high aspect ratio (in the case of NFC), their own tensile strength, and elastic modulus also have consequences on their interaction with cementitious hydrates.

Although the existents theories connected to the behavior usually observed when nanocellulose is integrated into cement-based materials, there is still no agreement on all mechanical and microstructural effects upon its addition. This chapter has the goal of understanding the possible mechanisms responsible for the improvement of the macro mechanical properties detected in Chapter 3. For this, investigations on the mechanical and microstructural levels were made. Characteristics of the hydration evolution were investigated by means of compressive tests, thermogravimetric (TGA), X-ray diffraction (XRD), and porosimetry (MIP) analyses, on samples with 3 and 28 days of curing. In order to complement the MCC and NFC characterization, XRD and TGA analyses were made, so the thermal stability and crystallinity of the inclusions could have been assessed. In addition, 3-point bending and direct tensile tests were performed on specimens with 28 days of age. The papers that performed tensile tests on cementitious matrices reinforced with MCC or NFC used the splitting cylinders approach [3,5,11–13]. Here, a specific apparatus was developed for the direct tensile test to perform this test on specimens with the same geometry as the ones that were submitted to the bending test.

4.2. Experimental program

4.2.1. Materials and production of the specimens

The microcrystalline cellulose MCC (Avicel PH101) was purchased from Sigma Aldrich, as the one characterized in Chapter 3. The nanofibrillated cellulose (NFC) was produced from bleached *Pinus* pulp according to the same

procedure described in 3.2.1. Since the morphology of MCC and NFC are mater of discussion also in this Chapter, their morphology is shown again in Figure 4-1. The cement paste consisted of ordinary Portland cement CEM I 32.5 R, from Schwenk, Germany, and tap water.

(a)

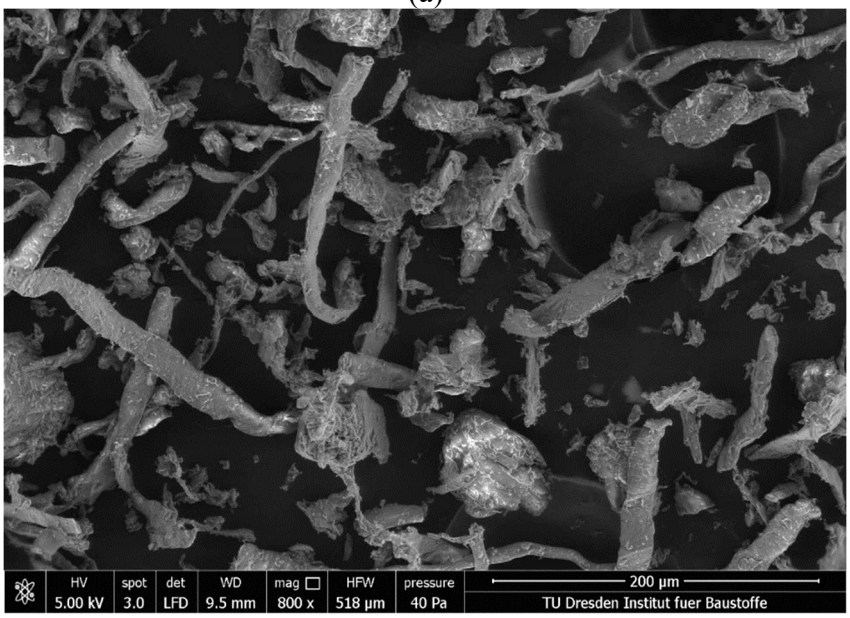

(b)

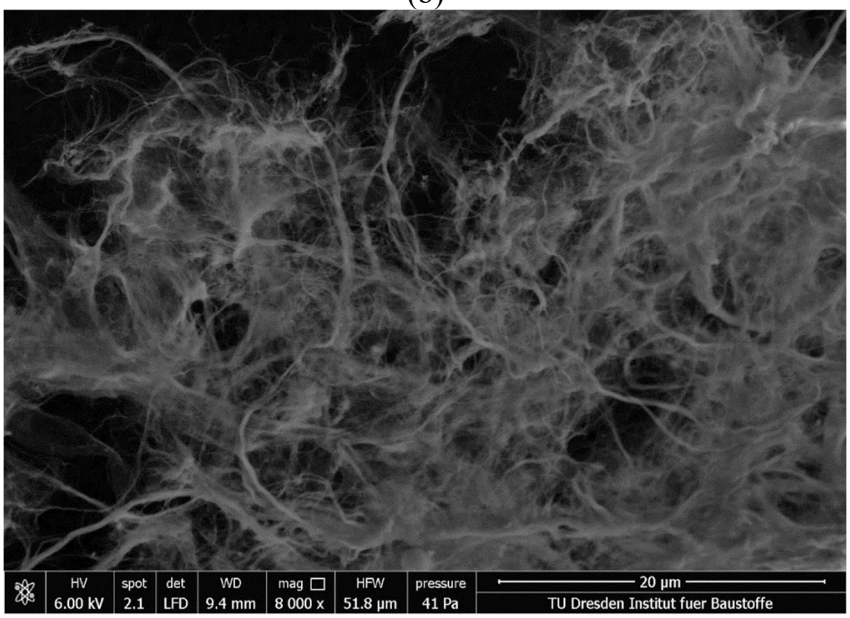

Figure 4-1 SEM images of the cellulose-based inclusions: (a) Microcrystalline cellulose (MCC) and (b) Nanofibrillated cellulose (NFC).

The mixing procedure was carried individually for each inclusion. For the MCC cement composites, the MCC powder was added to the cement and manually mixed for homogenization. Then, water was added and mixed for 5 minutes at 500 rpm. In the case of the NFC specimens, first, the NFC gel and the

mixing water were pre-mixed for 5 minutes at 600 rpm and then the solution was added to the cement and mixed for another 5 minutes at 500 rpm. Note that both mixture procedures are equivalent to the method “without dispersion” in Chapter 3. It is important to emphasize that the water present in the NFC gel was discounted from the mixing water in order to not affect the total w/c. The composition of each specimen is given in Table 4-1.

Table 4-1 Composition of the different variations of the matrices investigated, in weight.

Name	w/c	Inclusion	%	Cement (g)	Water (g)	MCC powder (g)	NFC gel (g)
Ref (0%)	0.35	-	0.000%	100	35.0	0.000	0.00
M0050	0.35	MCC	0.050%	900	35.0	0.050	-
M0075	0.35	MCC	0.075%	900	35.0	0.075	-
M0100	0.35	MCC	0.100%	900	35.0	0.100	-
N0050	0.35	NFC	0.050%	900	32.5	-	2.50
N0075	0.35	NFC	0.075%	900	31.3	-	3.75
N0100	0.35	NFC	0.100%	900	30.1	-	5.00

After the mixing, the fresh paste was poured in prismatic metallic molds of dimensions of 10 x 10 x 60 mm³ and stored in plastic bags until the specific age of testing. In the case of bending and compression tests, one day before each test, the specimens were properly identified and weighed, and their surfaces were measured. In the case of the tensile test, the specifications will be provided in the test methodology section.

The inclusion percentage of the MCC and NFC was of 0.050%, 0.075%, and 0.100%, in relation of the mass of cement. In the case of NFC gel, the percentage considered only the solid part that in this case corresponded to 2% of the gel weight.

4.2.2. Cellulose-based materials’ characterization

This section aims to complement the characterization made in Chapter 3. An Environmental Scanning Electron Microscopy (ESEM, model Quanta 250 FEG, FEI, The Netherlands) was used to investigate the morphology of MCC and NFC shown in Figure 4-1. The crystallinity index for both inclusions was obtained through X-ray diffraction analyses, conducted in an X-ray diffractometer 3003-TT (7000, Germany). The surface area of NFC was evaluated by means of the

Brunauer–Emmett–Teller (BET) method. For the XRD and BET techniques the NFC gel was previously freeze-dried. The thermal deterioration of MCC and NFC was analyzed by thermogravimetric analysis (TGA) with the mass loss and the differential thermal (DTA) curves. The TGA was performed with a NETZSCH Gerätebau GmbH (409C/CD, Germany) equipment.

4.2.3. Mechanical tests

The compression and the three-point bending tests were carried on a Zwick Roell 1445 machine at an actuator displacement rate of 1 mm/min. For the bending test, the prisms of dimensions of 10 x 10 x 60 mm^3 were positioned with a span of 1 mm between the load application points. A load cell of 1 kN was coupled to the system for a more accurate data acquisition. After the bending test, the pieces were collected and five of them with suitable geometry (more than 10 mm^3) were submitted to compression tests, with a configuration in which the applied load surface was 10 mm^2.

For the direct tensile test, the actuator displacement rate was of 0.5 mm/min on prismatic specimens of same dimensions as the ones submitted to the bending test (10 x 10 x 60 mm^3). The difference was the existence of a notch produced on the specimens' production step; see the detail in Figure 4-2a. A load cell of 2.5 kN was added to a Zwick Roell Retroline, on a system with both ends hinged, as shown in Figure 4-1b. The case used for fixing the specimen was composed of two aluminum profiles of 15 x 15 mm^2 (outer) and 11 x 11 mm^2 (inner) and length of 40 mm. A screw type M8 was filled with 1 g of modeling clay and glued to the profiles with ultra-violet glue. Two edges of the screw nut were ground for fitting inside the aluminum profile. The bottom of the case was covered with silicon. The specimen was positioned inside the case, and it was filled with a two-part epoxy glue (each side at a time). The notch was produced with the introduction of a 1 mm staple on each boarder of the mold. Some details of the case producing, and the gluing process are found in Figure 4-2.

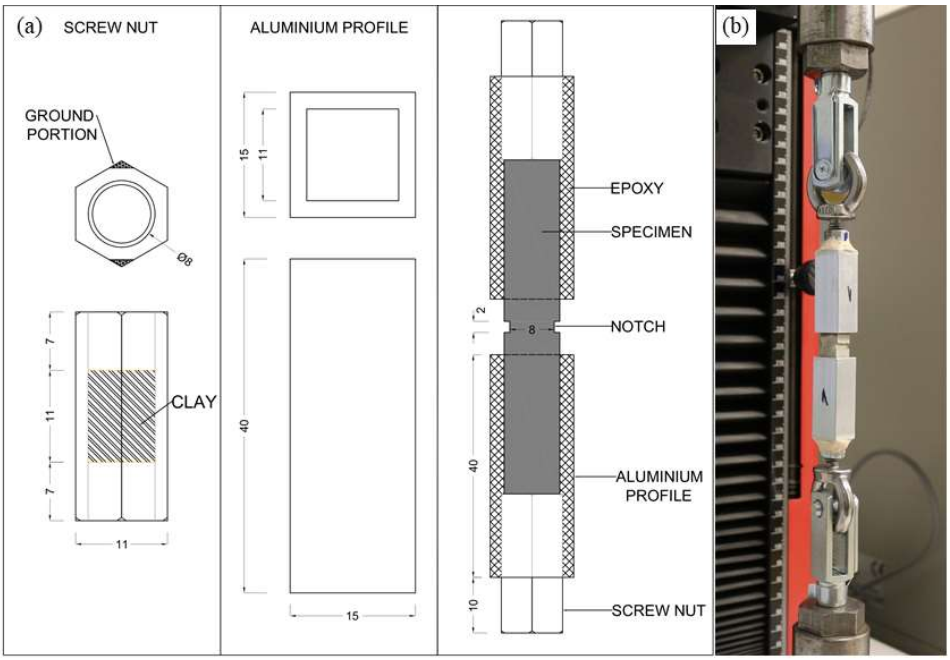

Figure 4-2 –Details of the direct tensile test: (a) Schematic representation of the case elements; (b) Specimen glued in the case and positioned for testing. Measurements in mm.

4.2.4. Microstructure investigation

Thermo-gravimetric analyses were performed on samples of different ages (3 and 28 days) with the same equipment described in Section 4.2.2. The measurements were carried under an oxygen atmosphere with a heating rate of 10 C°/min.

The porous structure of the specimens was evaluated by means of mercury intrusion porosity (MIP) with a Porotec Porosimeter PASCAL 140/440. The samples consisted of cubes of around 10 mm³ and the maximum pressure applied was of 400 MPa at a speed from 6 to 19 MPa/min.

X-ray diffraction (XRD) analyses were conducted to investigate the mineralogical composition of selected specimens. The equipment operated at an angular velocity of 0.02º/s, in intervals between 5º and 70º.

4.3. Results and discussion

4.3.1. Characterization of MCC and NFC

As shown in Figure 4-1, MCC and NFC differ from each other regarding the shape, size, and aspect ratio, as previously discussed in Chapter 3. Those

differences include the surface area of MCC particles and NFC solid fibrils. The surface area for the NFC fibrils, measured by BET, was of 9.72 m²/g. On the other hand, according to current literature, MCC particles present surface area between 1.0 and 1.30 m²/g by N_2 [14]. Thus, NFC provides a greater contact area with particles and molecules present on the cement paste than the MCC particles. This characteristic can interfere on the interfacial bonding between cellulose and hydration products. Besides this, it is reasonable to suppose that the interaction of the NFC fibrils with the water present in the gel itself is strong. With that in mind, the TGA results can cooperate in the investigation on the water role of the NFC gel, apart from its thermal degradation information.

Cellulosic materials are well-known for their rapid thermal degradation at low to moderate temperatures, namely, below 400 °C [15]. The TGA and the differential thermal analysis (DTA) curves of the MCC and NFC are displayed in Figure 4-3. From those curves, it is possible to notice the singularities on the thermal stability of the cellulosic inclusions. While the degradation of NFC took place mainly between 110ºC and 200ºC, this gap was from 275ºC to 350ºC for the MCC. The MCC decomposition occurred mainly in two steps. The first is the loss of 5% in weight until 100 °C was reached, which may represent the removal of physically bound water in the cellulose structure [16]. The second step, the onset point, is at around 280 °C representing the cellulose degradation.

The TGA curve of NFC suggests that the water present in the gel may not be totally free since at 100ºC only 7% of the mass was gone. The DTA curves indicate that different phenomena are related to each cellulosic inclusion: an endothermic event for the NFC, and an exothermic one for the MCC. The degradation of each material itself can also influence the degradation of the composite. In particular the NFC-reinforced specimens, since its degradation takes place close to one characteristic temperature of the composite, 140ºC. It is important to keep in mind that while the solid fibrils content can be considered low, as the maximum of inclusion is 0.1% of the cement mass, the total gel weight is considerable.

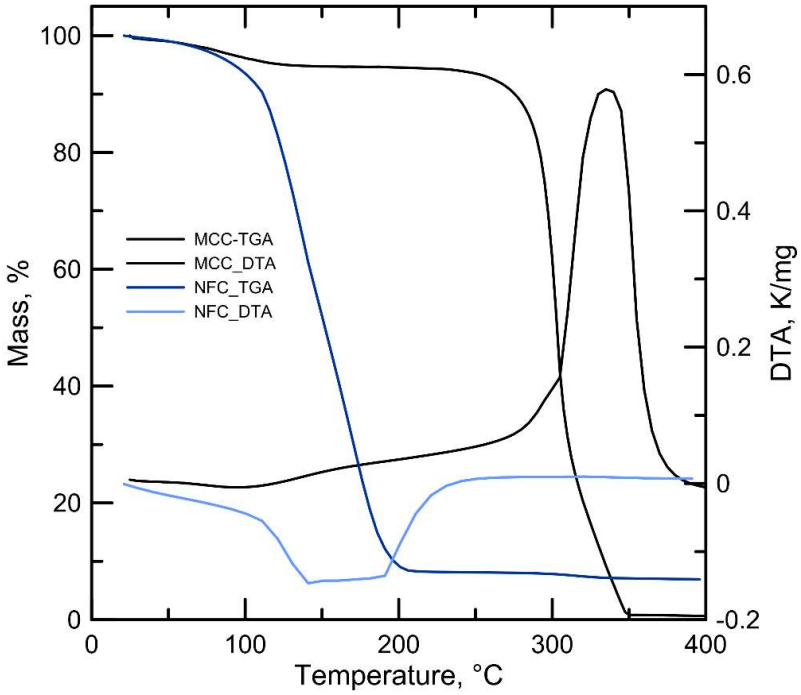

Figure 4-3 Thermogravimetric (TGA, mass) and differential thermal analyses curves of the cellulosic materials, MCC and NFC .

Besides the morphology, the NFC presents a larger amorphous phase, consequently a lower crystallinity, in comparison to the MCC. An estimation of the crystallinity index was calculated by the amorphous subtraction described in [17]. The X-ray diffraction (XRD) pattern of MCC and NFC is found in Figure 4-4. In the case of NFC curve, a sharp peak at 22.4º is observed and was assigned to the (002) plane. For the MCC curve, the sharpest peak occurred at 22.7º. The amorphous plane was designated at the minimum intensity between (002) and (101) planes, at 18.3º [17–19]. The estimated crystallinity of MCC and NFC was found to be around 81.5% and 49.8%, respectively. According to Segal *et al*. [17] this method has an error of around 6.5%. Nevertheless, there is a significant crystallinity difference between the two cellulosic inclusions. The crystallinity index expresses the relation between the crystalline and the amorphous parts. The crystalline parts are arranged in a regular manner, in opposition to the amorphous phases to which they are linked. The MCC particles undergo a hydrolysis process that removes part of their amorphous phases. Thus, the crystalline portions are more frequent in MCC, resulting in a higher crystallinity index compared to NFC. The lower crystallinity index NFC presents is related to its flexibility since the crystal portions constrain the mobility of the amorphous portions. In fact, the

flexibility capacity may interfere on the crack-bridging effect. In addition, it is assumed that a higher degree of crystallinity confers a higher degradation resistance and thermal stability, as indicated by the TGA analysis (Figure 4-3).

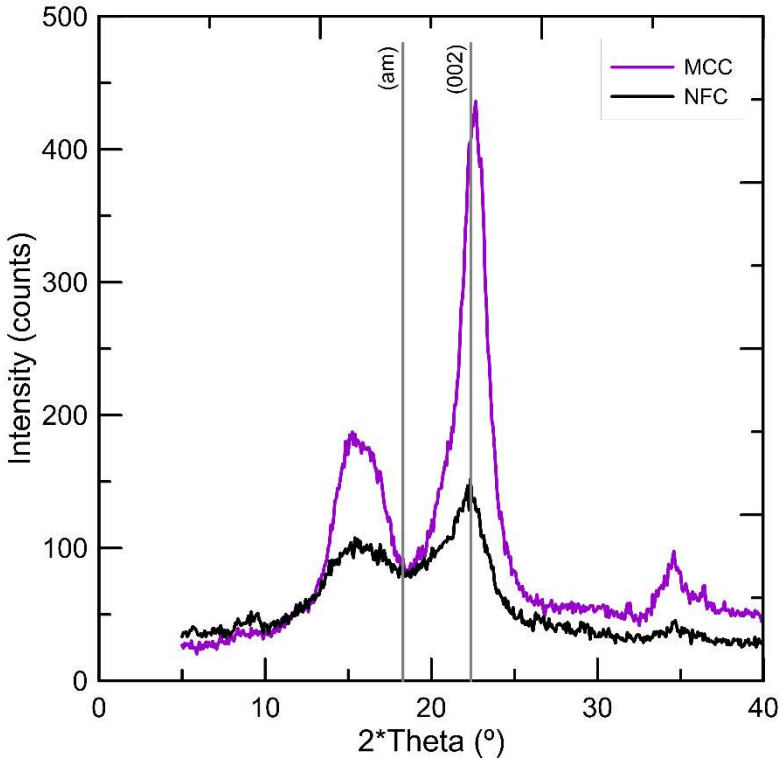

Figure 4-4 - XRD-pattern of the nanofibrillated cellulose (NFC).

4.3.2. Microstructure and hydration aspects

4.3.2.1. Hydration changes

Figure 4-5 presents the evolution of compressive strength between 3 and 28 days of curing, which is a way to follow the possible hydration changes. There was a significant strength increase from the 3-day specimens to the 28-day ones, for all variations. Regarding the influence of the MCC and NFC content, it is possible to note a gradual decrease in the average strength values with the increment of the cellulosic inclusion percentage. However, in comparison to the reference, there was no great difference upon the addition of MCC or NFC as indicated by the error bars.

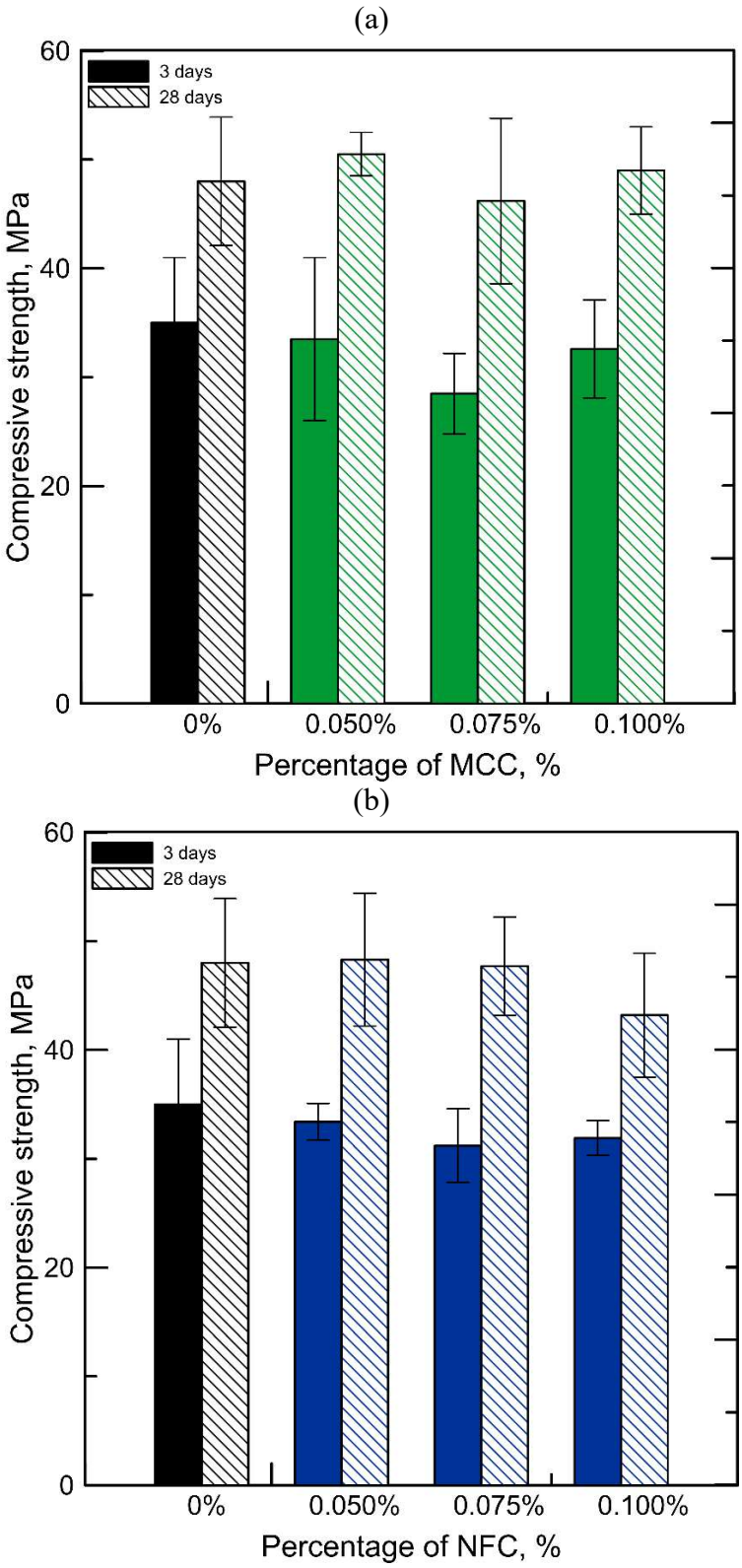

Figure 4-5 Evolution of the compressive strength of specimens with 3 and 28 days of curing. (a) MCC-specimens; (b) NFC-specimens.

The TG and DTG curves of the reference paste is shown in Figure 4-6a, at the ages of 3 and 28 days. On the DTG curves is possible to identify the peaks usually associated to the decomposition of the hydration products. The peak I takes place at around 141ºC and is correlated to the decomposition of calcium silicate hydrate (C-S-H) or ettringite in some cases. Peak II occurred at around 506ºC and can be related to the calcium hydroxide (CH) and Peak III at around 815ºC associated to the decarbonation of calcium carbonate ($CaCO_3$). The reference cement paste of 3 days differs from the one of 28 days presenting shorter peaks I and II, indicating that more of the hydration products, C-S-H and CH were formed until 28 days. The younger sample had a more pronounced peak associated to the calcium carbonate than the sample of 28 days. The presence of calcium carbonate is due to the carbonation reaction of the cement paste or the sample. This mineral is a result from the reaction of CO_2 from the moisture atmosphere with the calcium ions on the cement paste or the calcium silicates hydrates and the calcium aluminate hydrates.

(a)

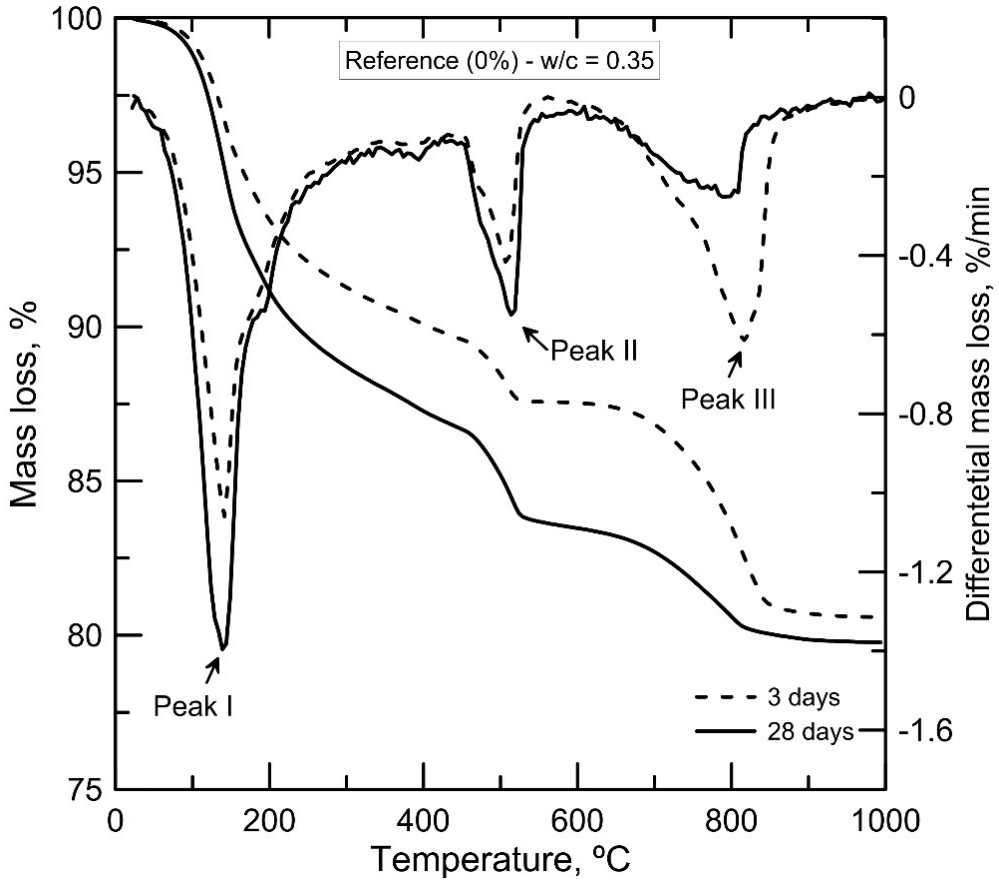

(b)

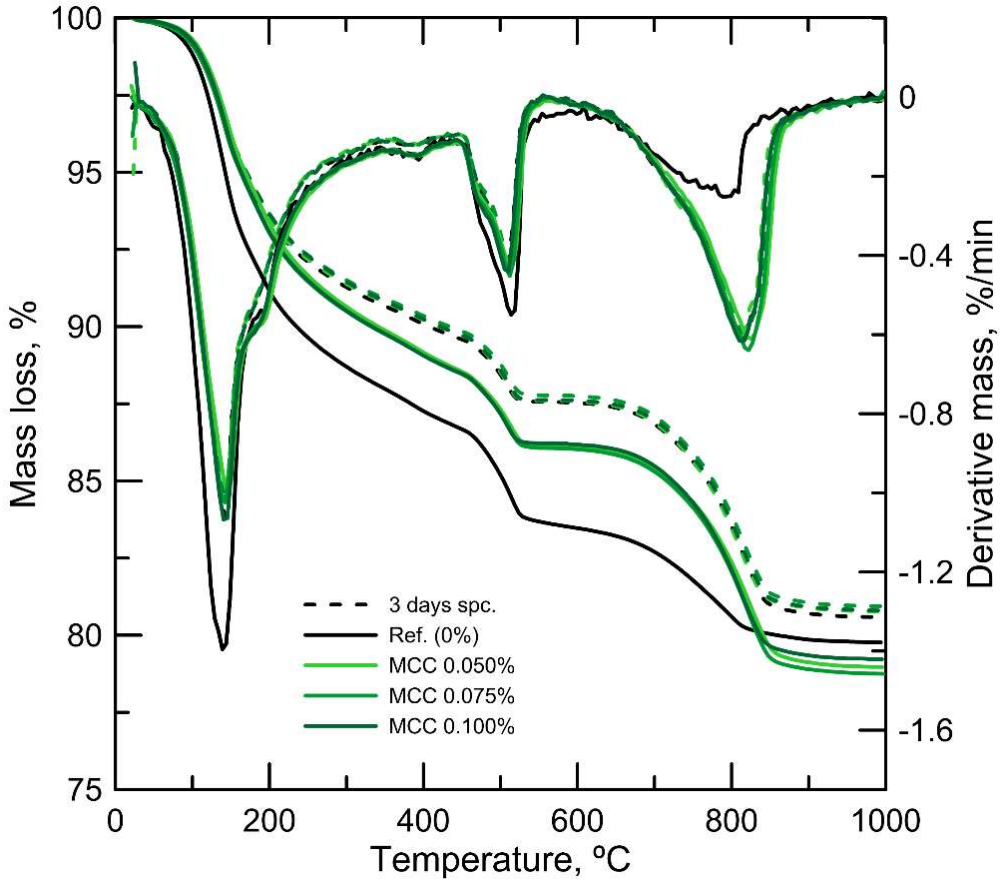

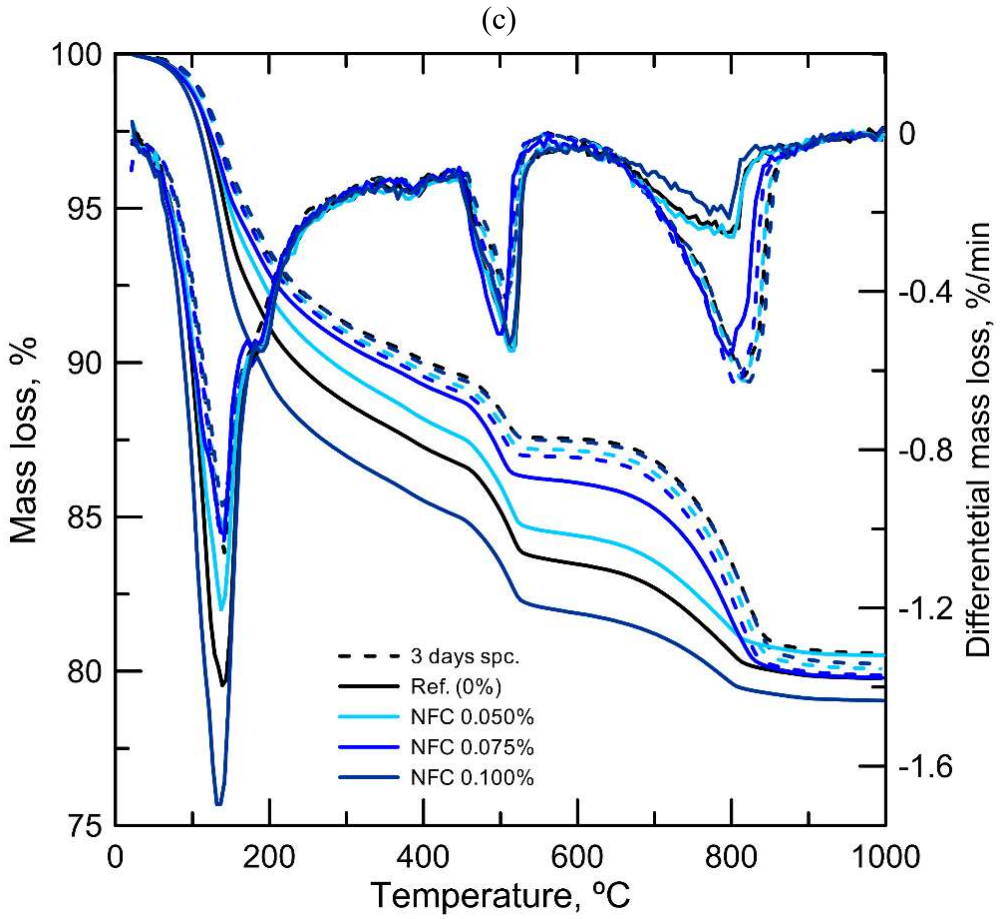

Figure 4-6 - Results from Thermogravimetric Analysis, with the mass loss and its derivative for the specimens: (a) reference (Ref. (0%)), (b) with MCC and; (c) with NFC. Dashed lines represent samples of 3days of curing and continuous lines, 28 days.

When the MCC is added to the cement paste, no significant difference was noticed on 3-day samples (dashed lines in Figure 4-6-b), except a shorter peak I presented by the samples with MCC when comparing to the reference. The DTG curves of the samples with MCC are overlapped. Regarding the 28-day samples, there was a small difference on the total final (at 1000ºC) mass loss when comparing the sample 0.075% of MCC and the reference. From the DTG curves, this variation is attributed to the higher carbonatation rather than the C-S-H and the calcium hydroxide formation. DTG curves show little influence of the MCC content of the pastes, as the curves are fairly similar, expect for peak III, which occurred on slightly different temperatures for each of the MCC contents. Although the specimens with MCC at 28 days presented less amounts of C-S-H and CH than the reference, the compressive strength presented no meaningful change upon the addition of MCC. The results presented in Chapter 3 showed that

when 0.5% of MCC was added, the TG/DTG curves were overlapped, without the carbonation effect here observed. In addition, the MCC inclusion led to a slight compressive strength improvement, considering bigger specimens with lower standard deviation. The results here presented were in disagreement with the usually reported in the literature, where a decrease in carbonation peak is often noticed [7,9,10,20].

Figure 4-6c shows the TGA and DTG curves of the samples with NFC compared to the reference. Considering the 3-day samples, it is worth mentioning that the difference noticed on the samples with MCC regarding the carbonation content was no longer observed on the ones with NFC. That is, the 3-day old samples with NFC had similar $CaCO_3$ content to the reference, although a rather less. On the other hand, the 28-day samples had higher $CaCO_3$ content. There were no great changes related to CH, except a shift on the temperature of the sample with 0.075% of NFC in comparison to the others. It was also the sample with 0.075% of NFC that presented the lowest C-S-H content and highest carbonation content. In contrast, the sample with 0.100% of NFC presented the most pronounced peak I and the lowest related to the decarbonation. This indicates that the sample with 0.100% of NFC at 28 days of curing presented more hydration products than the reference. However, those changes on the hydration were not followed by a significant improvement of the compressive strength (Figure 4-5). Regarding the results presented in Chapter 3, it was not found any difference on the TG/DTG curves of the specimens with NFC. According to the literature, there are few discussions on the influence of NFC on each hydration product and those appoint to higher C-S-H and CH formation with nanocellulose [21,22]. It is important to be aware that not all percentages of inclusion result in an improvement of the hydration [2], even though this seems to be the majority trend [4,21–25].

The common characteristic to all samples and ages was the shorter peak related to the C-S-H degradation upon the addition of NFC and MCC. In spite this had occurred to samples with 3 and 28 days, this effect was intensified on the older samples. The exception as mentioned and discussed was the sample with 0.100% of NFC.

By revisiting the results of the TGA of the NFC gel shown in Section 4.3.1, one can notice that most of its degradation took place close to the temperature

characteristic related to the C-S-H, around 140ºC. This feature may interfere on the TGA curves of the specimens reinforced with NFC (Figure 4-3c) and on its interpretation. Despite this, the sample with 0.100% of NFC was still able to have a more pronounced peak I (C-S-H) than the reference, at 28 days. TG analysis of the sample with 0.100% of NFC was the only one that could indicate an actual increase of the hydration products, if the gel degradation is not considered. It is also important to restate that the specimens with NFC had lower amount of mixing water on their dosages so the water in the gel could replace it. However, from the small free water lost until 100ºC shown on the TGA curve, one can assume that the water present in the gel is not as available as the mixing water for the hydration reactions to take place. This could have influenced the hydration process of the NFC-specimens.

In order to complement TGA results obtained by the samples with 0.075% and 0.100% of NFC, XRD analyses were performed, in order to investigate the mineralogical composition of the pastes, without the possible influence of the similar decomposition temperatures for the NFC fibrils and C-S-H. The spectrogram from 0.075% and 0.100% of NFC variations at 28 days of curing are shown in Figure 4-7, as well as the reference. The peaks related to ettringite, portlandite (calcium hydroxide) and residual clinker were identified. The presence of vaterite was identified on the spectrograms of the samples with NFC. None of the spectrograms indicated the presence of cellulose, with no peak at 22.4º.

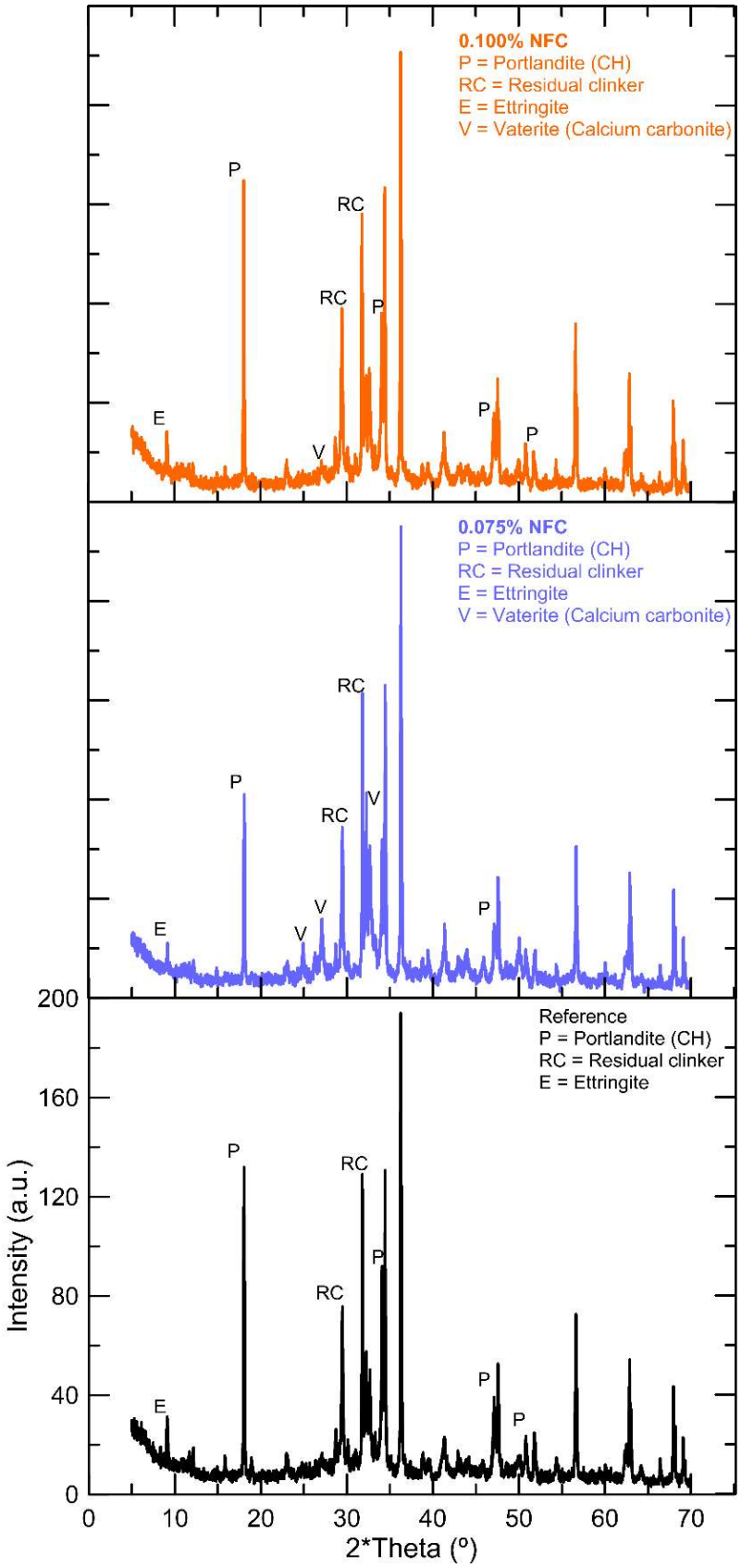

Figure 4-7 - X-ray diffraction patterns of the cement paste of reference, the one reinforced with 0.075% and the one 0.100% of NFC, at 28 days of curing.

To support the analysis, Figure 4-8 gathers the quantitative results of the main components in percentage of each sample. The residual clinker comprehends the alite (C_3S), belite (C_2S) and aluminate (C_4Af) phases. The carbonate includes calcite, dolomite, and monocarbonate. In the case of samples with NFC, there was a significant presence of vaterite, which is also a polymorph of calcium carbonate. The amount of the hydration products, ettringite and portlandite, was higher for the reference sample than for the ones reinforced with NFC. The amount of 'amorphous part' also is probably related to the C-S-H gel. Thus, one can assume that the presence of the nanocellulose reduced the hydration reactions. The amount of residual clinker, higher for the samples with NFC, supports this assumption as well as the compression tests results. The pronounced carbonation could have been induced by the presence of NFC. Nevertheless, this behavior shall be further investigated under a carbon dioxide atmosphere to support this autogenous carbonation theory. Yet, calcium carbonite can be considered an hydration phase of cement and could be partially responsible for the mechanical behavior that will be discussed on the following Section.

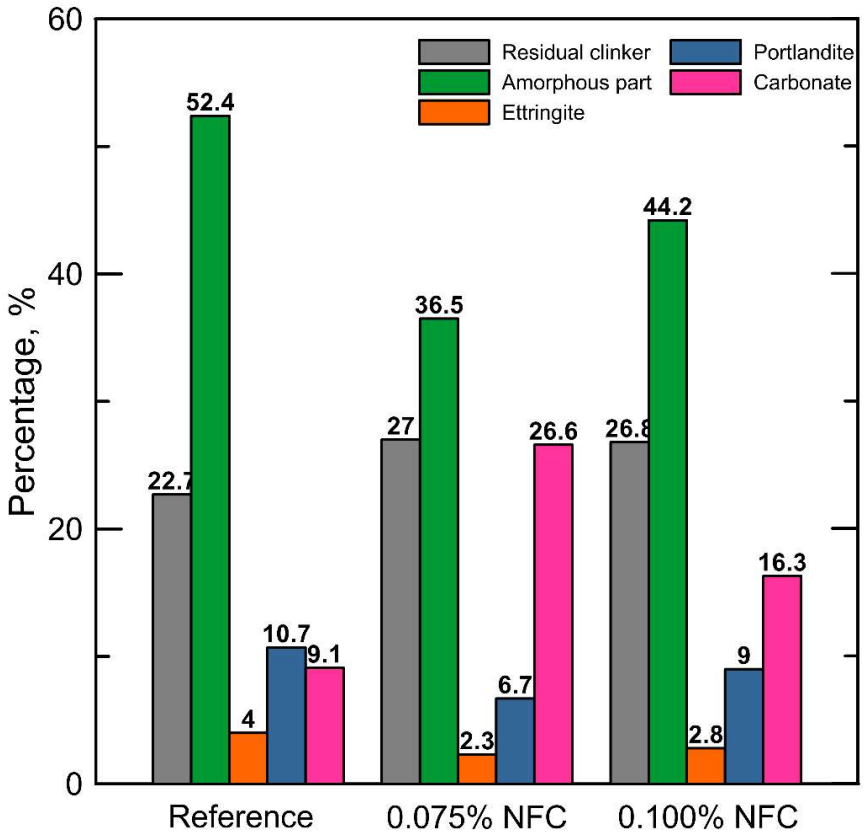

Figure 4-8 - Main components of the cement pastes with 0.075% and 0.100% of NFC, at 28 days of curing.

By comparing the two samples with NFC, the main difference is regarding the amount of the amorphous part, which corresponded to 36.5% for the 0.075%-sample and 44.2% for the 0.100% one. Taking into consideration the ettringite, portlandite and the amorphous phases, it is possible to consider that the sample with 0.100% of NFC presented a more advanced hydration state in comparison to the one with 0.075%. This founding was supported by the TGA analysis even though the compressive average strength values showed the opposite.

Is is noteworthy the difference in calcium carbonate contents: 26.6% for the sample with 0.075% of NFC versus 16.3% to the one with 0.100% of NFC. This was also observed on the TGA analysis. Among the calcium carbonate portion, the vaterite represented 17.9% of the total composition of the 0.075%-sample while it represented 6% of the 0.100%-sample's composition. Vaterite is a product from the carbonation of C-S-H, identified as a sharp peak on TGA curves [26,27]. In fact, the DTG from the 0.075%-sample showed a sharper peak in comparison to the others on the calcite range.

4.3.2.2. Porosity profile

Before describing the changes on the porosity profile of the samples upon the addition of MCC and NFC, the size distribution of those additions should be known. According to Zhang *et al*. [28], the commercially available MCC presents a particle size ranging from 2 to 260 μm with a mean diameter of around 50 μm, even though on previous research (see Chapter 3), the average size of the MCC particles was around 115 μm [29]. As described in Chapter 3, the diameter of the nanofibrils used in the present work was of around 48 nm [29]. The pores were classified according to according to their diameters [30]: nanopores (<10 nm), mesopores (10-50 nm), macropores (50-200 nm), and larger pores (>200 nm). Figure 4-9 presents the pore composition for specimens with 3 and 28 days of curing. Other characteristics of the porosity profile of the specimens can be found in Table 4-2.

After 3 days of curing, there was a relative increase of the macro and larger pores and a decrease of the nano and meso ranges upon the addition of MCC. The average pore size presented in Table 4-2 corroborated this analysis. The impact on the macro and larger pores was more meaningful on the sample with 0.100% of

MCC. From the TGA analysis, it was not possible to distinguish any difference regarding the hydration of samples with MCC at 3 days of curing, except for a shorter peak related to the C-S-H degradation. As the hydration time continued to 28 days (Figure 4-9b), the trend was to increase the relative percentage of nano and meso pores and decrease the macro and larger ones. However, this effect of increasing the relative portion of nanopores was more significant for the reference sample than for the ones with MCC. The nanopore range is usually associated with gel pores, the pores present within the layers of C-S-H [31]. From the TGA curves, the samples with MCC presented indeed shorter peaks related to C-S-H and CH, indicating a delay of the hydration reactions. Despite that, the dominant (modal) pore diameter decreased from around 32 nm to around 20 nm, through the MCC presence.

The increase on the range of macro and larger pores is often reported on the literature [7,9,10] and it is correlated to possible agglomeration sites within the matrix. The filling effect that MCC could have presented is not observed since the relative pore larger volume range supposedly filled by the MCC particles (with average size of around 115 μm) increased.

(a)

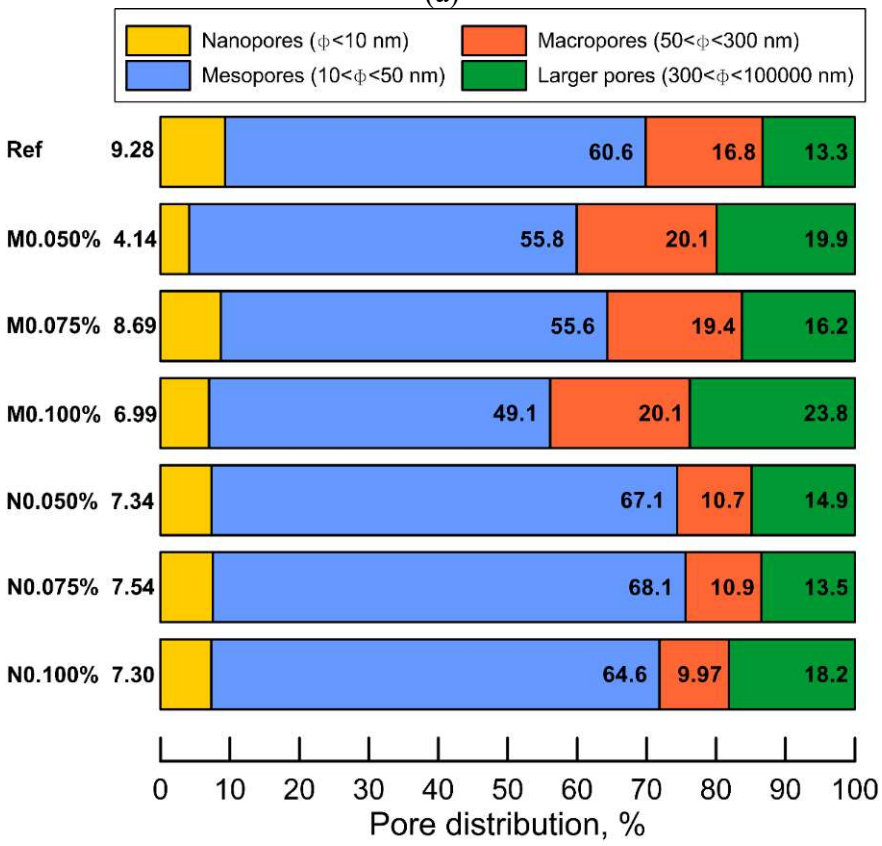

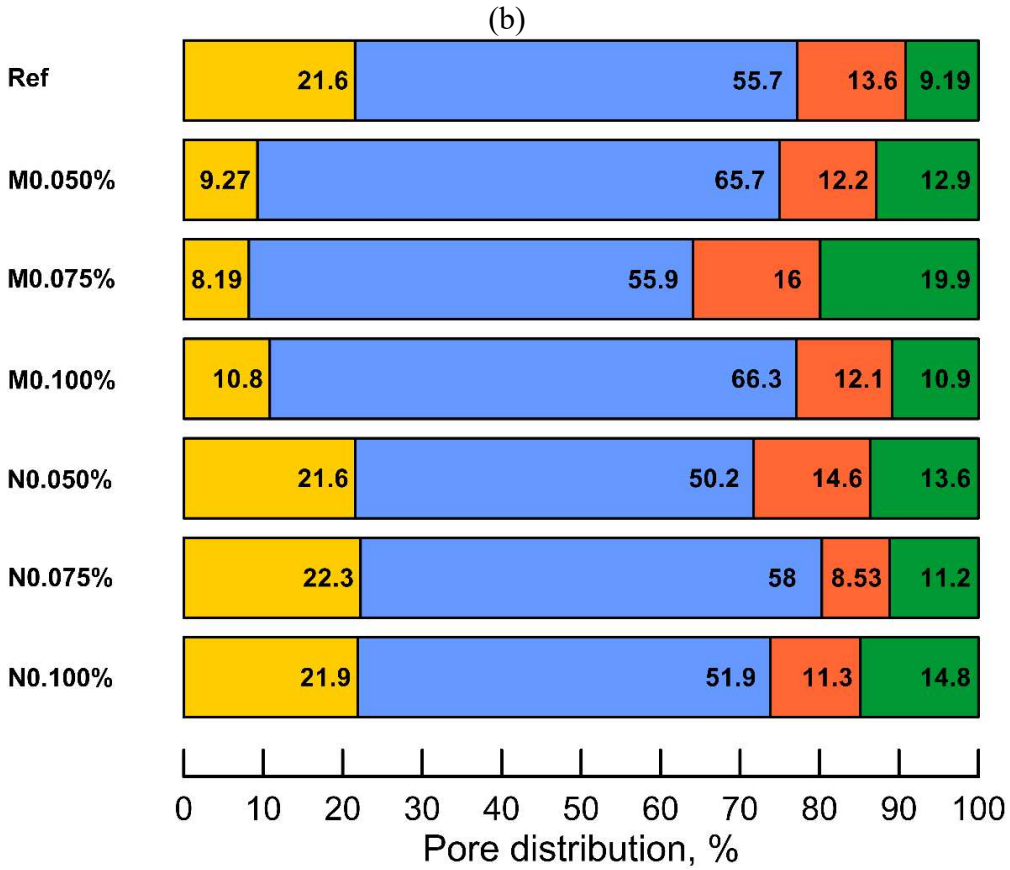

Figure 4-9 Pore size distribution according to MIP investigations for (a) 3-days of curing and; (b) 28-days of curing.

With the addition of NFC, at 3 days, there was an increase of the mesopores and a decrease of the macropores. In the sample with 0.100% of inclusion, there was also an increase on the larger pores range, not observed on the other samples. From the third to the twenty-eighth day of curing, there was a very significative increase of the nanopore relative composition of the microstructure of the samples with NFC, similarly to what was observed on the reference. Comparing the pastes with 0.075% and 0.100% of NFC, there was an increase and a decrease on the mesopores range, respectively. In both cases a decrease of the macropores is noticeable. The average pore diameter did not present any significant change, and the trend of the modal pore size was toward a continuous decrease for the 3-day old samples, as already reported [24,32,33].

According to the size distribution of the NFC fibrils described in Chapter 3, they would be able to fill the nano and mesopores. However, this effect was not observed on the 3-day samples. It is important to stress that the NFC in the gel form brings its porosity and the newly formed interface can have an impact on the

pore distribution of the sample. From the MIP results, this effect could have been attenuated on the older samples. In essence, even though the role of NFC on the microstructure of cementitious materials is rather unclear, all the improvements observed in current literature regarding the pore distribution have been attributed to hydration positive effects [23,24,33–35]. However, the analyses so far did not lead to this conclusion.

Table 4-2 Characteristic of the porosity of cement pastes with several percentages of MCC or NFC.

Sample	Average pore diameter (nm)		Modal pore diameter (nm)	
	3 days	*28 days*	*3 days*	*28 days*
0% - Ref	24.7	16.6	37.8	31.8
N0050	24.4	17.1	30.0	30.4
N0075	23.5	16.1	26.4	29.5
N0100	23.8	16.9	24.5	30.5
M0050	34.3	20.2	38.5	20.0
M0075	26.7	24.1	40.3	20.3
M0100	30.5	19.3	33.1	20.4

4.3.3. General mechanical behavior of the reinforced cement pastes

The results obtained from the mechanical tests, namely compression, three-point bending, and direct tensile tests, performed at 28 days of curing, are presented in Table 4-3. The compression tests were also carried out for the specimens with 3 days of curing to complement the hydration investigation, as seen in Section 4.3.2.1.

Table 4-3 Results from the mechanical tests for the NFC and MCC composites. The results include the average strength (σ) and the standard deviation (SD), in MPa.

Specimen	Compression				Bending		Tensile	
	3 days		28 days		28 days		28 days	
	σ	*SD*	*σ*	*SD*	*σ*	*SD*	*σ*	*SD*
Ref (0%)	35.0	6.0	48.0	5.9	8.1	0.4	3.36	0.30
N0050	33.4	1.7	48.4	6.1	10.6	1.5	3.79	0.32
N0075	31.2	7.5	47.8	2.0	11.6	1.1	5.93	1.45
N0100	31.9	3.4	43.2	4.5	10.6	2.5	5.80	0.70
M0050	33.5	3.7	50.5	7.6	8.4	0.9	4.42	0.54
M0075	28.5	1.6	46.2	5.7	10.2	0.5	5.73	0.59
M0100	32.6	4.5	49.0	4.0	13	1.9	4.60	0.54

Figure 4-10 assembles the results shown in Table 4-3 according to the influence factor (IF). The IF is the ratio of the strength of the reference and the strength of a selected variation. The IF can be interpreted as an improvement factor upon the addition of MCC or NFC, in reference to the plain specimen with no inclusion (0%). The purpose of Figure 4-10 is the straight comparison of the different strengths and the attempt to trace a trend between them.

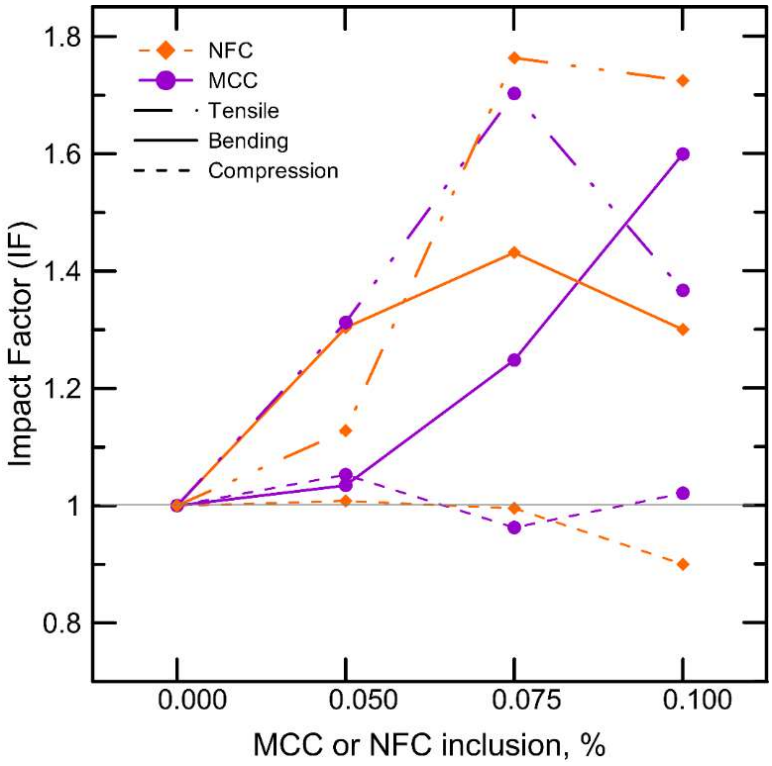

Figure 4-10 Comparison between the mechanical strength IF values of the cellulosic inclusions, MCC and NFC, according to the percentage of addition at the 28 days of curing.

There was a significant flexural and tensile strength improvement for all the percentages of MCC and NFC. The optimal percentage of NFC inclusion was 0.075%, with an IF of 1.43, representing a gain of 43%. However, taking into consideration the error between 0.075% and 0.100%, those averages could be considered in the same range. For the MCC-reinforced specimens the IF of 1.60 was obtained with 0.100% of MCC. The improvement in the flexural strength promoted by the NFC addition is usually attributed to the possible bridging capacity this material may offer [4,5,13,36,37]. The enhanced flexural strength could also be related to a hydration improvement [4,22–25], although this is not a rule [2,4,29,34]. In the case of MCC, the positive effect on the flexural strength is related to the changes on the porosity profile and improvements on the hydration [7,9,10,29].

The NFC addition led to a decrease in the compressive strength of the cement pastes. This effect was intensified as the percentage increased, as shown by the dashed orange line in Figure 4-10. This adverse effect upon the presence of nanofibrillated cellulose had already been reported elsewhere [5,21,29,38,39]. The

main reason for the detriment of the compressive strength of those composites is air entrainment, leading to a more porous structure and agglomeration of the fibrils network.

Considering the MCC-reinforced composites, the effect on the compressive strength varied with the percentage of inclusion. However, it is important to mention that those compressive strength averages could be considered statistically equal if one considers the deviation values presented in Table 4-3. Previous studies have reported divergent results, with some presenting improvement on compressive strength upon the MCC addition [7,9,20,40], while others have observed the opposite effect [10,41,42]. Those divergent results may have the same source: the MCC hydrophilic nature with the consecutive water absorption can either work as a water supply enhancing the hydration degree or represent insufficient water to form C-S-H gel in the first hours of hydration [7,42].

The tensile strength values resulted from the direct tensile tests are depicted in Figure 4-10c. It is worth noting the expressive strength increase, especially beyond 0.050% of inclusion. The greater improvement for both cellulosic inclusions was at the percentage of 0.075% with IF values of 1.70 and 1.76 for the MCC and NFC additions, respectively. When the tensile strength was evaluated on cement-based matrices with the addition of MCC or NFC, all studies showed an improvement of this mechanical parameter [3,5,11–13]. The tensile strength enhancement was attributed to the bridging cracks capacity of the inclusions at the micro and nanoscale. Hisseine *et al*. [3] observed a greater increase in the tensile strength if compared to the flexural one, for equal NFC percentage. This behavior was also observed in the present study.

It is interesting to highlight that, in general, there was either a detriment or no effect on the compressive strength upon the addition of the cellulose-based materials, contrary to the significant improvement observed in the case of flexural and tensile strengths. In that way, the direct tensile test was important to attempt to evaluate the effect of the additions on the tensile strength, as during the flexural tests, tensile and compressive stresses take place. Although most of the mechanical behavior improvement have been correlated to hydration enhancements in the literature [4,21–24], this was not the case on the present study, as previously discussed on Section 4.3.2.1 and shown in Chapter 3 as well.

Even though there was a similarity on the strength values reached by each inclusion, it is important to keep in mind their differences and their possible distinct acting mechanisms. In the present investigation, the differences between the MCC and NFC on the flexural and tensile strengths most probably rely on their distinct morphologies shown in Figure 4-1 and on their physical properties. Each cellulosic inclusion result from different processes involved in their production. The defibrillation process is responsible for the refinement of the fibrils resulting in a higher aspect ratio of the NFC in comparison to the MCC. This characteristic is commonly linked to the reinforcing effect on the matrices, not only the cementitious ones [29,43]. However, the agglomeration and flocculation are also attributed to the high aspect ratio, resulting in some limitation of the NFC application. While the aspect ratio could be one possible reason for the NFC-reinforcement effect, the crystallinity index could be part responsible for the superior mechanical properties displayed by the MCC-specimens. The properties related to the cellulose crystals have been previously used to justify the improvement observed on composites reinforced by two materials with different crystallinity indexes [43,44].

As shown in the literature and in the present study, the specific surface area of MCC and NFC is around 1.30 [45] and 9.72 m^2/g, respectively. The hydroxyl groups present on the cellulose surface can interact with the cement particles and mixing water on the fresh state and with the hydration products on the hardened state. Thus, this difference between MCC and NFC possibly alters the action of those materials into the cementitious system. In addition, the NFC gel presents 98% of water and an amorphous porous part. These two features can interfere on the microstructure of the specimens with NFC as related by Kolour *et al*. in [46]. According to them, the presence of the NFC and the interaction of the fibrils with the water molecules modify the capillary network of the system [46].

4.4. Conclusions

This Chapter was designed to understand how MCC and NFC could act on the hydration evolution of a cement paste, regarding the microstructural aspect. In order to accomplish this, the present investigation was composed of compressive tests, TGA, XRD, and MIP analyses of the composites at 3 and 28 days of curing. In addition, to complement the cellulosic inclusions' characterization, analyses of

BET, XRD, and TGA were performed and confirmed the expected higher surface area NFC presents despite its lower crystallinity and thermal stability, in comparison to MCC.

The mechanical evaluation constituted of 3-point bending and direct tensile tests. For the tensile tests, a new arrangement is proposed to fit small-prismatic-geometry specimens of size 10 x 10 x 60 mm^3. The following specific conclusions can be drawn:

- According to the TG/DTG investigations, the MCC addition led to a decrease of the hydration products, C-S-H and CH, and a decrease in the carbonation. This effect was only observed for the 28-day samples, as the 3-day ones were comparable to the reference.
- The addition of 0.050% and 0.075% of NFC resulted in a similar effect of the addition of MCC, considering the decrease of the peaks related to C-S-H and CH and increase of carbonation. On the other hand, the addition of 0.100% of NFC was followed by an increase of the peak related to C-S-H and comparable-to-reference CH and $CaCO_3$ peaks. Despite this result, the XRD analysis showed that indeed the addition of NFC did not contribute for an enhanced hydration.
- The MIP results showed that at 3 days of curing there was an increase of the macro and larger pores upon the addition of MCC. Although there was a decrease of the nanopores relative proportion at 28 days for the samples with MCC, the modal pore decreased from around 32 to 20 nm.
- Regarding the porosity profile evolution of NFC-specimens, there was an increase of the mesopores and a decrease of the macropores at 3 days of curing, in comparison to the reference. The lower proportion of the macropores remained after 28 days of curing, although in general the samples with NFC showed similar porosity profile regarding average and modal pores, in comparison to the reference.
- In general, the addition of NFC led to a denser microstructure than the addition of MCC.
- The changes in both hydration and porosity analyses did not affect the compressive strength evolution of MCC- and NFC-reinforced specimens.

- The addition of MCC and NFC resulted in great benefits of flexural and tensile strengths. With 0.075% of NFC, the percentage of flexural and tensile increase was 43% and 76%, respectively in comparison to the reference. And with 0.075% of MCC, this increase was 25% and 70%.

The results provided by the investigations collected in this Chapter indicate that the mechanical improvements are more linked to the reinforcement capacities of MCC and NFC than to their capability to positively affect the hydration. Even though the TG/DTG analysis of the sample containing 0.100% of NFC indicated a higher peak related to the C-S-H formation, neither the XRD, the MIP nor the compressive strength confirmed the hydration improvement. This behavior could be perhaps related to the NFC gel degradation.

4.5. References

[1] CAO, Y. *et al*. The influence of cellulose nanocrystal additions on the performance of cement paste. **Cement and Concrete Composites**, v. 56, p. 73–83, 2015.

[2] KOLOUR, H.; ASHRAF, W.; LANDIS, E. N. Hydration and Early Age Properties of Cement Pastes Modified with Cellulose Nanofibrils. **Transportation Research Record: Journal of the Transportation Research Board**, p. 036119812094599, 2020.

[3] HISSEINE, O. A. *et al*. Feasibility of using cellulose filaments as a viscosity modifying agent in self-consolidating concrete. **Cement and Concrete Composites**, v. 94, n. September, p. 327–340, 2018.

[4] HISSEINE, O. A. *et al*. Nanocellulose for improved concrete performance: A macro-to-micro investigation for disclosing the effects of cellulose filaments on strength of cement systems. **Construction and Building Materials**, v. 206, n. February, p. 84–96, 2019.

[5] HISSEINE, O. A.; OMRAN, A. F.; TAGNIT-HAMOU, A. Influence of cellulose filaments on cement paste and concrete. **Journal of Materials in Civil Engineering**, v. 30, n. 6, p. 1–14, 2018.

[6] CAO, Y. *et al*. The influence of cellulose nanocrystals on the microstructure of cement paste. **Cement and Concrete Composites**, v. 74, p. 164–173, 2016.

[7] PARVEEN, S. *et al*. A novel approach of developing micro crystalline cellulose reinforced cementitious composites with enhanced microstructure and mechanical performance. **Cement and Concrete Composites**, v. 78, p. 146–161, 2017.

[8] PARVEEN, S. *et al*. Characterizing dispersion and long term stability of concentrated carbon nanotube aqueous suspensions for fabricating ductile cementitious composites. **Powder Technology**, v. 307, p. 1–9, 2017.

[9] PARVEEN, S. *et al*. Ultrasonic dispersion of micro crystalline cellulose for developing cementitious composites with excellent strength and stiffness. **Industrial Crops and Products**, v. 122, n. May, p. 156–165, 2018.

[10] SILVA, L. *et al*. A facile approach of developing micro crystalline cellulose reinforced cementitious composites with improved microstructure and mechanical performance. **Powder Technology**, v. 338, p. 654–663, 2018.

[11] PETERS, S. *et al*. Nanocellulose and Microcellulose Fibers for Concrete. **Transportation Research Record: Journal of the Transportation Research Board**, v. 2142, p. 25–28, 2010.

[12] EL-FEKY, M. S. *et al*. Effect of nano silica addition on enhancing the performance of cement composites reinforced with nano cellulose fibers. **AIMS Materials Science**, v. 6, n. 6, p. 864–883, 2019.

[13] EL-FEKY, M. S. *et al*. Nano-fibrillated cellulose as a green alternative to carbon nanotubes in nano reinforced cement composites. **International Journal of Innovative Technology and Exploring Engineering**, v. 8, n. 12, p. 484–491, 2019.

[14] ARDIZZONE, S. *et al*. Microcrystalline cellulose powders: Structure, surface features and water sorption capability. **Cellulose**, v. 6, n. 1, p. 57–69, 1999.

[15] JONOOBI, M. *et al*. Characteristics of cellulose nanofibers isolated from rubberwood and empty fruit bunches of oil palm using chemo-mechanical process. **Cellulose**, v. 18, n. 4, p. 1085–1095, 2011.

[16] CHIRAYIL, C. J. *et al*. Isolation and characterization of cellulose nanofibrils from Helicteres isora plant. **Industrial Crops and Products**, v. 59, p. 27–34, 2014.

[17] SEGAL, L. *et al*. An Empirical Method for Estimating the Degree of Crystallinity of Native Cellulose Using the X-Ray Diffractometer. **Textile Research Journal**, v. 29, n. 10, p. 786–794, 1959.

[18] TONOLI, G. H. D. *et al*. Properties of cellulose micro/nanofibers obtained from eucalyptus pulp fiber treated with anaerobic digestate and high shear mixing. **Cellulose**, v. 23, n. 2, p. 1239–1256, 2016.

[19] PARK, S. *et al*. Cellulose crystallinity index: Measurement techniques and their impact on interpreting cellulase performance. **Biotechnology for Biofuels**, v. 3, n. May 2010, 2010.

[20] FILHO, A. *et al*. Mechanical and micro-structural investigation of multi-scale cementitious composites developed using sisal fibres and microcrystalline cellulose. **Industrial Crops and Products**, v. 158, n. April, p. 112912, 2020.

[21] SUN, X. *et al*. Rheology, curing temperature and mechanical performance of oil well cement: Combined effect of cellulose nanofibers and graphene nano-platelets. **Materials and Design**, v. 114, n. August, p. 92–101, 2017.

[22] SUN, X. *et al*. Cellulose Nanofibers as a Modifier for Rheology, Curing and Mechanical Performance of Oil Well Cement. **Scientific Reports**, v. 6, p. 1–9, 2016.

[23] JIAO, L. *et al*. Natural cellulose nanofibers as sustainable enhancers in construction cement. **PLoS ONE**, v. 11, n. 12, p. 1–13, 2016.

[24] MEJDOUB, R. *et al*. Nanofibrillated cellulose as nanoreinforcement in Portland cement: Thermal, mechanical and microstructural properties. **Journal of Composite Materials**, v. 51, n. 17, p. 2491–2503, 2017.

[25] ONUAGULUCHI, O.; PANESAR, D. K.; SAIN, M. Properties of nanofibre reinforced cement composites. **Construction and Building Materials**, v. 63, p. 119–124, 2014.

[26] HEWLETT, P.; LISKA, M. **Lea's Chemistry of Cement and Concrete**. Fourth ed. [s.l.] Elsevier Science & Technilogy Books, 2004. v. 58

[27] RAMACHANDRAN, V.S.; BEAUDOIN, J. J. **Handbook of Analytical Techniques in Concrete Science and Technology**. [s.l: s.n.].

[28] ZHANG, M. *et al*. A comparison of ram extrusion by single-holed and multi-holed dies for extrusion-spheronisation of microcrystalline-based pastes. **International Journal of Pharmaceutics**, v. 416, n. 1, p. 210–222, 2011.

[29] OLIVEIRA DE SOUZA, L. *et al*. Investigation of dispersion methodologies of microcrystalline and nano-fibrillated cellulose on cement pastes. **Cement and Concrete Composites**, v. 126, n. February 2022, 2022.

[30] ROUQUEROL, J. *et al*. **Liquid intrusion and alternative methods for the**

characterization of macroporous materials (IUPAC technical report)Pure and Applied Chemistry. [s.l: s.n.].

[31] BENTUR, A.; MINDESS, S. **Fibre Reinforced Cementitious Composites**. Second ed. [s.l: s.n.].

[32] BARNAT-HUNEK, D. *et al*. Effect of eco-friendly cellulose nanocrystals on physical properties of cement mortars. **Polymers**, v. 11, n. 12, 2019.

[33] ALOULOU, F.; SABRINE, A.; SAMMOUDA, H. Influence and dispersion of nanofiber of wood modified on properties of cement based mortars. **Journal of Renewable Materials**, v. 7, n. 7, p. 631–641, 2019.

[34] GONCALVES, J. *et al*. Cellulose nanofibres (CNF) for sulphate resistance in cement based systems. **Cement and Concrete Composites**, v. 99, n. March, p. 100–111, 2019.

[35] CUENCA, E.; MEZZENA, A.; FERRARA, L. Synergy between crystalline admixtures and nano-constituents in enhancing autogenous healing capacity of cementitious composites under cracking and healing cycles in aggressive waters. **Construction and Building Materials**, v. 266, p. 121447, 2021.

[36] FU, C. *et al*. A comparative study on the effects of three nano-materials on the properties of cement-based composites. **Materials**, v. 13, n. 857, 2020.

[37] SUPIT, S. W. M.; NISHIWAKI, T. Compressive and flexural strength behavior of ultra-high performance mortar reinforced with cellulose nano-fibers. **International Journal on Advanced Science, Engineering and Information Technology**, v. 9, n. 1, p. 365–372, 2019.

[38] EZ-ZAKI, H. *et al*. Influence of cellulose nanofibrils on the rheology, microstructure and strength of alkali activated ground granulated blast-furnace slag: a comparison with ordinary Portland cement. **Materials and Structures**, v. 54, n. 1, p. 1–18, 2021.

[39] GUO, H. *et al*. Improvement of stability and mechanical properties of cement asphalt emulsion composites using nano fibrillated celluloses. **Cement and Concrete Composites**, v. 125, n. April 2021, p. 104330, 2022.

[40] LONG, W. J. *et al*. Rheology and buildability of sustainable cement-based composites containing micro-crystalline cellulose for 3D-printing. **Journal of Cleaner Production**, v. 239, p. 118054, 2019.

[41] GÓMEZ HOYOS, C.; CRISTIA, E.; VÁZQUEZ, A. Effect of cellulose microcrystalline particles on properties of cement based composites. **Materials**

and Design, v. 51, p. 810–818, 2013.

[42] ANJU, T. R.; RAMAMURTHY, K.; DHAMODHARAN, R. Surface modified microcrystalline cellulose from cotton as a potential mineral admixture in cement mortar composite. **Cement and Concrete Composites**, v. 74, p. 147–153, 2016.

[43] XU, X. *et al*. Cellulose Nanocrystals vs. Cellulose Nano fi brils: A Comparative Study on Their Microstructures and E ff ects as Polymer Reinforcing Agents. **ACS applied materials & interfaces**, v. 5, p. 2999–3009, 2013.

[44] BARNAT-HUNEK, D. *et al*. Effect of cellulose nanofibrils and nanocrystals on physical properties of concrete. **Construction and Building Materials**, v. 223, p. 1–11, 2019.

[45] EICHHORN, S. J.; YOUNG, R. J. The young's modulus of a microcrystalline cellulose. **Cellulose**, v. 8, n. 3, p. 197–207, 2001.

[46] KOLOUR, H. H. *et al*. An investigation on the effects of cellulose nanofibrils on the performance of cement paste and concrete. **Advances in Civil Engineering Materials**, v. 7, n. 1, p. 463–478, 2018.

5. Effect of nanofibrillated cellulose on shrinkage of cement pastes

5.1. Introdução

The design of a structure must contemplate its lifetime service, which implies considering cracks as a possible entryway for deleterious agents. Cracks are formed due to several causes, and not all of them involve external forces. For instance, shrinkage is a volumetric deformation due to changes in water content and chemical process that can lead to crack formation even at a very early age [1]. Thus, it is reasonable to adopt actions to prevent and mitigate issues related to excessive shrinkage. Some measures can be applied as suitable in-situ curing practices, although this approach is not always possible. In this way, the development of materials that are tailored to control shrinkage deformation is desirable.

There are several strategies to mitigate shrinkage in cementitious materials, such as controlling hydration reactions, reduction of the surface tension of pore solution, internal water supply and the inclusion of internal restraints such as aggregates and different types of fibers [2–6]. The motivation for using natural fibers-based materials is to combine the benefits of internal curing and restraint effects. The internal curing effect may be theorized from the hierarchical yet porous microstructure those fibers present and their hydrophilic and hygroscopic nature [7]. Those intrinsic characteristics allow water retention and possibly further release, working as an internal water supply. The restraint effect comes from the morphologic and physical properties such as the high aspect ratio some natural fibers-based materials exhibit. As examples of the use of macro natural fibers in controlling the shrinkage, Kawashima and Shah observed a positive effect on autogenous shrinkage of cement pastes and mortar with 2 and 3% of cellulose fibers, and their presence also delayed the crack formation and decreased its width on concrete specimens submitted to restrained drying tests. Similar results were found by Rapport and Shah [8] and Motta *et al*. [9] with lower cellulosic fiber content, and by Buch [10] regarding plastic shrinkage.

Nanocellulose had already been used as auxiliary material to enable the study of the shrinkage of high water-to-cement ratio cement paste specimens due to its high water absorption ability, preventing bleeding [11]. Moreover, nanocellulose can also mitigate the autogenous shrinkage of cementitious materials [12–14], as shown in detail in Chapter 2.

Regarding autogenous shrinkage, there are challenges related to its measurement due to the time it starts and the time its deformations become significant. Shrinkage initiates as soon as the hydration products are formed, changing the cement paste from a liquid and colloidal suspension into a hardened and porous solid [15]. During hydration, different types of pores are formed depending on how the solid skeleton arranges itself. If there is no extra water supply, the pores drain water from capillary networks leading to the drop of the relative humidity. Thus, in a combination of different mechanisms, including self-desiccation, surface tension, disjoining pressure and capillary tension, cement paste shrinks [16]. Here, autogenous shrinkage deformation is related to the bulk deformation of a closed system, not subject to external forces [16]. Given the fact that hydration and self-desiccation are at their highest rate at early ages and so is autogenous shrinkage, the measurement should start as soon as possible. Therefore, it is important to keep in mind that the decision on the starting point will affect the measured deformation [17,18]. In other words, the comparative result between different mixtures is directly affected by the time zero definition as well as the magnitude of the deformations.

Although by definition the autogenous shrinkage starts even before setting, the initial deformation may not correspond to the stress development of interest [19]. The target time zero is when the autogenous shrinkage can effectively generate internal stresses. The most common and utilized method is the penetration resistance test, also known as the Vicat needle test. In fact, the time zero recommended by ASTM C1698-09 for the autogenous shrinkage test is the final setting time obtained with the Vicat test. Nevertheless, this penetration test indicates mechanical development, and not always a microstructural relation can be traced. Moreover, the conditions that the specimens submitted to the Vicat and shrinkage tests can be different [17]. Due to its importance, alternative methods of time zero determination of cementitious materials have already been developed and discussed in several studies. Among the methods used, electrical conductivity,

acoustic emission, temperature evolution and ultrasonic pulse velocity (UPV) can be mentioned as non-destructive ones [19–24]. In addition, indirect methods have been suggested as the comparison between chemical and autogenous shrinkage [20] and the analysis of the autogenous length change measurements [19,20].

The main objective of the present work is to evaluate the influence of nanofibrillated cellulose (NFC) gel on the autogenous shrinkage behavior of cement pastes. Three distinct water-to-cement ratios (w/c) were used to prepare the pastes since NFC can interact differently with the cement particles and the available water depending on the water content of the environment. The percentages of NFC inclusion were 0.000%, 0.025% and 0.050% in relation to cement weight and the specimens had w/c of 0.30, 0.35 and 0.40. In order to better understand the impact of NFC during the hydration evolution, especially on the early age of cement pastes, flow table, bleeding and ultrasonic pulse velocity tests were performed. Two approaches, namely the hardened sealed prism and the corrugated tube methods, were used to assess the autogenous shrinkage behavior. In addition, the total free shrinkage was investigated. The shrinkage measurements were performed for 28 days. The time zero for the corrugated tube specimens was determined through different methods: a destructive test (Vicat needle), a non-destructive one (UPV) and an indirect methodology (rate of autogenous deformation). A comparison between them was made and how each one of them interferes on the magnitude of the shrinkage was discussed. For the investigated mixtures, the inflection point from the rate of deformation curve was considered the most appropriate time zero so the meaningful stresses could be taken into consideration during the shrinkage development.

The choice to carry this Chapter only with NFC as inclusion material was based on the preliminary screening results of MCC-reinforced specimens. Those results can be found in Appendix A.

5.2. Materials and methods

5.2.1. Composition and preparing of cement pastes

The cement pastes were prepared with German Portland cement type I (CEMI 42.5 R) from HeidelbergCement AG, tap water and a nanofibrillated cellulose

(NFC), obtained from bleached *Pinu*s pulp, the same one used in Chapter 4. The derived NFC was in a gel form, containing 2.0% of nanofibers.

To investigate the influence of the NFC on the shrinkage behavior of different cement pastes, the w/c ratios and the content of NFC were varied. The investigated w/c ratios were 0.30, 0.35 and 0.40 and the contents of NFC were 0.000, 0.025 and 0.050 wt.%. The percentage values of NFC are in respect with the mass of cement, and the mass of solid nanofibers presented in the gel. In order to keep the same w/c ratio as in the reference specimens (0.000 % of NFC), the water in the NFC gel was discounted from the mixing tap water amount. The composition of each paste mixture is given in Table 5-1.

Table 5-1 Cement pastes with NFC mixture proportions. Values of cement, water and NFC gel are given in weight (g). The flow table test results are presented with the values before and after the strokes, in mm.

Sample	w/c	NFC %	Cement (g)	Water (g)	NFC gel [1] (g)	Flow table test (mm)
30-N00	0.30	0.000	100	30.00	0.00	104/191
30-N25	0.30	0.025	100	28.78	1.25	107/181
30-N50	0.30	0.050	100	27.55	2.50	102/171
35-N00	0.35	0.000	100	35.00	0.00	142/236
35-N25	0.35	0.025	100	33.78	1.25	117/213
35-N50	0.35	0.050	100	32.55	2.50	106/186
40-N00	0.40	0.000	100	40.00	0.00	214/280
40-N25	0.40	0.025	100	38.78	1.25	171/243
40-N50	0.40	0.050	100	37.55	2.50	140/230

[1] Nanofibrillated gel with 2% of solids (nanofibrils).

All the materials were kept in a temperature-controlled room (temperature of 21 ± 3 °C and RH of 50 ± 5%) prior to the mixing of the specimens. The mixing water and the NFC gel were mixed for 5 min at 600 rpm to homogenize the suspension. The cement was placed in the bowl and the water-and-NFC suspension was added. The moment when the water is in contact with the cement was considered to determine the age of the mixture. The paste was mixed for 1 min at 140 rpm and 4 min at 285 rpm in a bench-mounted planetary mixer of 5 l.

The cement paste used for the corrugated tube autogenous shrinkage, flow table, Vicat needle, UPV and bleeding tests were mixed in one single batch.

5.2.2. Shrinkage tests

5.2.2.1. Total shrinkage

Prisms with dimensions of 160 x 20 x 20 mm³ were cast with steel pins embedded in the middle of the two 20 x 20 mm faces to enable the length measurements. The specimens were kept in an environmentally controlled room (temperature of 21 ± 2 °C and RH of 50%), where they were demolded after around 24 h and where the measurements were carried out. Shortly after demolding, the specimens were placed into a rigid framework vertically mounted and automatic readings were performed continuously for 28 days. The displacement measurements were taken by a dial gauge every 30 min or when it detected a length variation of 0.001 mm. Three prisms of a same composition were produced, and the results here presented are the average of a set of specimens.

5.2.2.2. Autogenous shrinkage

Two different approaches were used to assess the autogenous shrinkage behavior of the cement pastes with NFC: sealed prism and corrugated tube methods [25]. The advantages of the use of sealed prisms include a more direct comparison with the free-drying shrinkage specimens since they can be cast in the same molds and exposed to the same curing conditions. Also, casting cement paste prisms is a well-established procedure in most laboratories and the molds can be reused as much as needed. One of the main downsides of this method is the loss of the very early-age deformation measurements since the specimens need to be stiff enough to be handled. As mentioned, it is reasonable to assume that the very early-age displacement measurement is important to fully understand the phenomenon. Regarding this issue, the use of corrugated tubes is a good alternative as it allows the displacement measurement as soon as the tubes are filled. Due to the singularities, pros and cons of the two methods, a comparison is here performed.

For the prismatic specimens, the same methodology described in 2.2.1 was applied, except for the sealing of the prisms with aluminum foil before their placement into the frame.

One single batch was intended for the autogenous shrinkage using the corrugated tubes, Hägermann flow table, Vicat needle, ultrasound and bleeding tests. Right after mixing, the necessary volume of cement paste for the autogenous shrinkage, around 400 ml, was set apart for filling the tubes while the other tests were carried out. One end of each corrugated tube was closed with a plastic plug, which was covered with Vaseline to prevent leaking, especially for the more flowable mixtures. The tube was then placed vertically in a rigid plastic pipe to enable the filling process. The system tube-plus-pipe was positioned on a vibrating table where it was filled while vibrating. After filling three tubes of a given composition, they were cleaned from any spills, weighted, and placed into metal frameworks horizontally mounted. The length changes were continuously read at every 30 min or when the dial gauge detected a variation of 0.001 mm. The moment from the time that the water was added until the first reading was of around 45 min for the more flowable mixtures and of around 80 min for the stiffer ones.

5.2.3. Flow table

The workability of each composition was estimated by means of the Hägermann flow table test [26]. The spread diameters of the samples were measured before and after the strokes, at the age of 7 min.

5.2.4. Bleeding test

The method here adopted was based on the one proposed by Josserand and de Larrard [27] with modifications. A cylindrical PVC mold with 145.0 mm of height by 36.5 mm of diameter was fixed on a plate base from the same material. The cement paste was poured in at the age of around 15 min until the height of 125 mm. Then, the layer of water that accumulated on the top of the surface was sucked with a pipette at intervals of 30 min. The first measurement was made after 30 min the paste was poured into the cylindrical mold. The mold was not moved during the test and a lid was used to cover the mold to prevent water evaporation. After the test, both the pipette and the beaker used to pour the removed water were dried and weighted so any fine particles that may have been sucked with the bleeding water could be discounted on further calculation. A correlation between

the weight of the removed water and what it represented in terms of the height of the cylindrical mold was made and this value is here determined as equivalent height.

5.2.5. Time-zero determination

Although the use of the corrugated tubes allows the measurements at a very early age, i. e. as soon as the tubes are filled, the strains during the plastic phase may not lead to considerable internal stresses that generate cracks. The choice and definition of the starting point can alter the result, including the magnitude of the strains. Such decision affects comparisons between different mixtures, as further shown. Based on the literature, there are some alternatives for the determination of the time zero. The methods used here for the determination of the time zero include two indirect approaches, namely the final setting time by Vicat needle and the evaluation of the ultrasonic pulse velocity (UPV) curve. In addition, the deformations obtained from the autogenous shrinkage test were analyzed regarding their inflection point and strain rate.

The ASTM C1698-09 [25] advises to take the final setting time defined with the penetration resistance measured by the Vicat needle test (ASTM C191-19) [28] as the time zero for the measurements. According to also ASTM C1698-09, the measurements are made manually. Thus, the tubes should be stiff enough to prevent disturbances that lead to mismeasurement. However, in the present study, the readings are automatically performed, and the possible errors induced by the manual reading are minimized. The Vicat needle test itself may be a source of inaccuracy since the fresh pastes are submitted to different environments despite the shrinkage and penetration resistance tests take place in the same room. For instance, the plate-and-conical ring arrangement used for the Vicat test is not as a closed system as the corrugated tubes so the bleeding water may have influence on the hydration development. Besides, it was reported differences in the temperature experimented by Vicat and autogenous samples tests [17] that may interfere in the hydration. In addition, during the measurements with the needle, the sample surface must be in contact with air, representing another interference in the hydration. Although the limitation of the method, the initial and final setting times defined by the penetration resistance are good start points for evaluation of

the behavior of the mixtures. Thus, the Vicat needle test was carried following ASTM C191-19.

The UPV method can be used to follow the hydration evolution of cementitious materials [23,29,30]. It is known that the velocity is sensible to the hydrate formation and the duration of its sharp slope corresponds to the cement hardening process. Thus, the increase of the velocity is associated with the formation of the solid phase of cement: both the volume fraction of solids and the connected fraction [23]. The ultrasonic pulse velocity of compression waves was automatically read by the software CELplus from Geotron-eletronik (version 1.3) at intervals of 20 seconds. The distance between the transducers was 25 mm and attached to a flexible container which was filled with the total volume of paste 280 ml. The transducers were directly in contact with the fresh paste. The readings started at the age of around 20 minutes and continued until 23 hours.

Unlike the penetration resistance and the UPV tests, the direct analysis of the deformation enables the evaluation of the material itself that is in fact submitted to the shrinkage strains. Thus, with this approach there is no need for extra tests because the measurements of the length change already give the information that can lead to the determination of the time zero. There are some ways of interpreting the curves obtained from those measurements, especially when there are replicates, like the present case. One of the indicators of the time zero is the scatter between replicate samples, as discussed elsewhere [17,31]. The evaluation is performed considering the three samples, and the correspondent average curve. Another approach for the analysis of the autogenous strain deformation is regarding its rate, as it will be discussed in Section 5.3.2.1.

5.3. Results and discussion

5.3.1. Fresh properties

The workability measured by means of the flow table test gives a brief understanding of the rheology of the cement pastes and how it is affected by the inclusion of the NFC. The results are presented in Table 5-1, the spread diameters both before and after the strokes. In general, the inclusion of any percentage of NFC led to a significant loss of workability for all three w/c, as pointed in Chapter 3. The reduction of the diameter was more perceptible before the strokes, with the

decrease reaching 65% of the reference value for the 40-N50 specimen. The specimens with the w/c of 0.40 were the ones more affected by the presence of NFC on the test before and after the strokes. The minimum spread diameter allowed by the apparatus is around 105 mm, so the fact that the spread values before the strokes remained the same for the samples with NFC and w/c of 0.30 did not mean the rheology was not affected by the NFC. It is worth reminding that the amount of water present in the gel was discounted from the mixing water (see Table 5-1). Thus, the presence of NFC may not be the only one responsible for all the changes in the flow behavior of the cement pastes.

Due to their intrinsic characteristics such as hygroscopicity and hydrophilicity, the nanofibrillated filaments can take water out of the fresh cement paste. This capacity can be easily assessed by the bleeding test. The results are presented in Figure 5-1 as the height of accumulated, or bleeding, water versus time, for all the mixtures. The axis corresponding to the accumulated water was adapted for each variation of w/c so it would be possible to observe the differences among the samples. From the reference samples (black lines and symbols), it is possible to notice this difference as the final level of accumulated water value went from 0.3 to 2.0, and 3.4 when the w/c went from 0.30 to 0.35, and 0.40, respectively. It is possible to observe that the addition of NFC decreased the amount of accumulated water, and this response was incremented according to the percentage of nanocellulose. This behavior was noted for the three water-to-cement ratios here analyzed and for all the time intervals that presented changes in the measurement. Although the low height of accumulated water sample 30-N00 presented, 0.3 mm, the presence of NFC was still capable of altering the free water content on the surface of the samples. Such alteration became even more considerable for the samples with w/c of 0.35, with 0.025 and 0.050% of NFC lowering the bleeding water height from 2.0 to 1.5 and 0.9, respectively. When the amount of water is increased on the samples with w/c of 0.40, the effect of 0.025% of NFC was nearly negligible, although this percentage was able to decrease the time interval in which there were measurements changes. The trend suggests that a higher amount of nanocellulose would be necessary to significantly retain water in those samples. This behavior can be understood as the capacity of the NFC fibrils to uptake and “hold” part of the mixing water into the bulk matrix, even at very early

ages. A similar response was found by Hisseine *et al*. [12], where the authors also relate this capacity to the intrinsic properties of the nanocellulose.

The flow table and bleeding tests results indicate that NFC alters meaningful aspects of the cement pastes in the fresh state. This discussion will be better explored in Chapter 6. The rheology and bleeding water can modify other properties, including shrinkage behavior. Even though the mechanisms are not completely clear, the relation between the mixing water and the cement particles is influenced by the presence of the nanocellulose. Such influence can change according to the w/c.

(a)

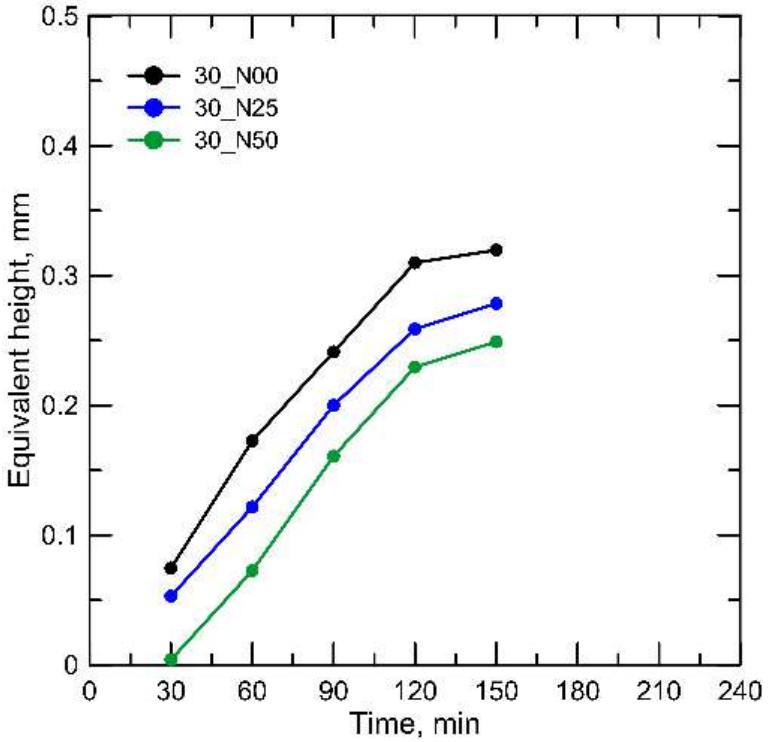

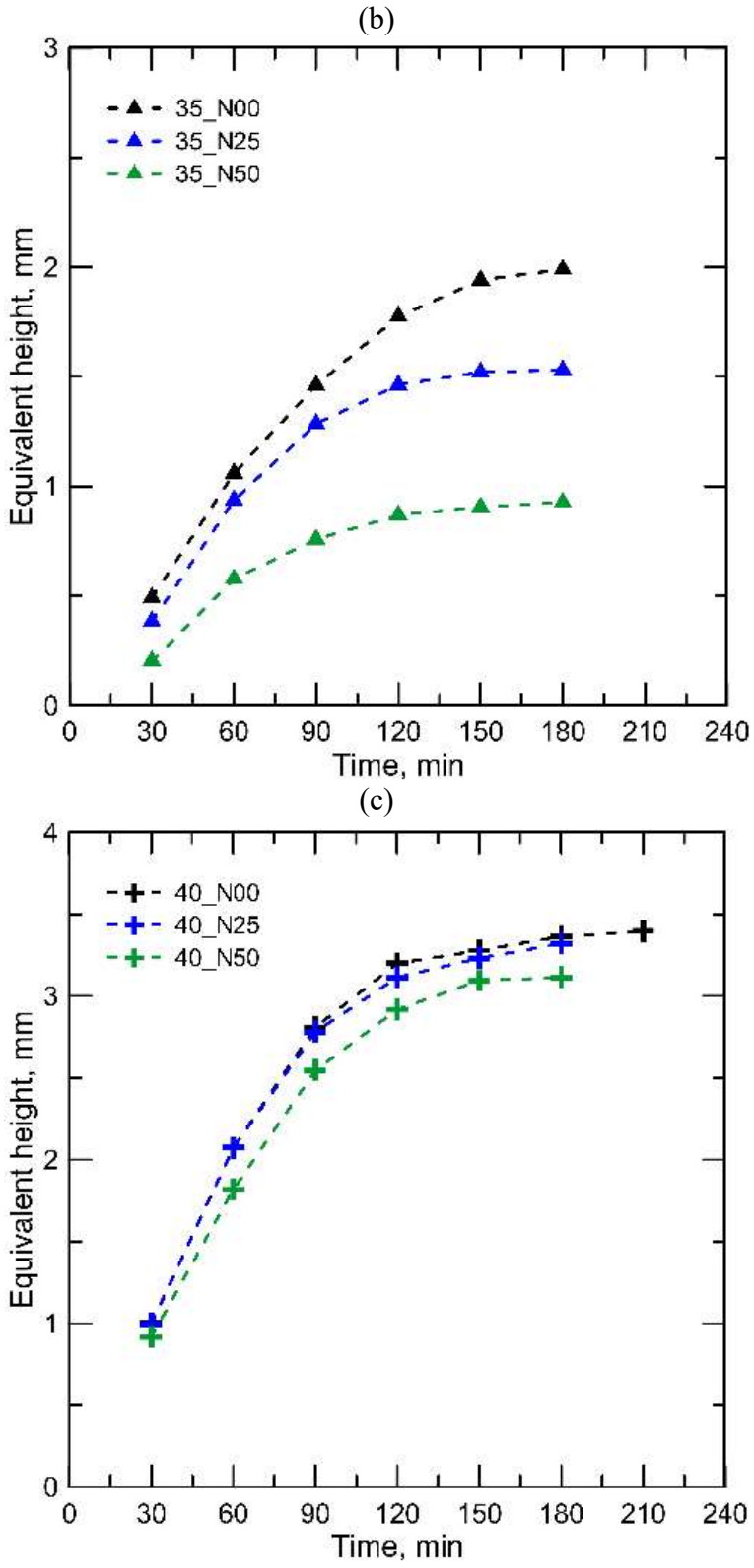

Figure 5-1 Bleeding height versus time for cement pastes with water-to-cement ratio of: (a) 0.30; (b) 0.35; (c) 0.40. The time zero is one when the fresh paste was poured into the molds.

5.3.2. Evolution of the solid skeleton

The initial and final setting times resulted from the Vicat test are presented in Table 5-2 for all mixtures. It is possible to notice that the inclusion of NFC promoted a decrease in the setting time, for all water-to-cement ratios under investigation. The difference was more pronounced when the w/c changed from 0.35 to 0.40, and not too significant for the w/c of 0.35. Although a delay in the setting time of cementitious matrix with macro and nano cellulosic fibers is usually observed [32–34], a similar effect of accelerating the setting time was found by Mejdoub *et al*. [35]. The delay in the setting is often attributed to steric stabilization between nanocellulose and cement particles and to the interactions with the -OH groups [36], while the accelerating effect could be associated with the hydration enhancement upon the addition of nanocellulose [35]. The latter effect can be attributed to alkaline hydrolysis and the possibility of nanocellulose acting as a nucleating agent in a cementitious matrix [37].

Table 5-2 Values of initial setting time (IST) and final setting time (FST) in hours determined by the Vicat needle penetration test for all cement paste variations.

w/c	NFC%	IST (h)	FST (h)
0.30	0.000	4.63	6.17
	0.025	4.56	5.92
	0.050	4.39	5.96
0.35	0.000	5.30	6.13
	0.025	5.34	5.92
	0.050	5.29	5.83
0.40	0.000	7.14	9.13
	0.025	6.95	8.93
	0.050	6.83	8.63

Figure 5-2 shows the UPV (continuous line) and the UPV rate (dashed line) curves of the 30_N00 sample. The first three hours were suppressed from the curve since this period presented many disturbances and scattering points. The UPV rate curve was obtained after the fitting of the UPV curve with a nineth order polynomial curve. The minimum and maximum points of the rate curve are here denominated as Critical Point 1 (CP1) and Critical Point 2 (CP2) and are highlighted in both curves in Figure 5-2. The CP1 has already been used as the

time zero reference point for starting the measurements of autogenous shrinkage tests [38].

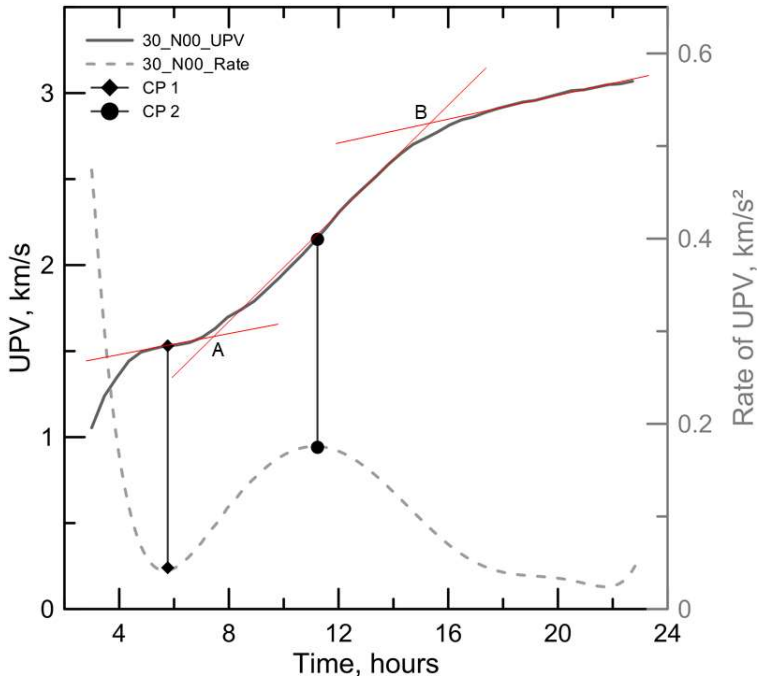

Figure 5-2 Ultrasonic pulse velocity (UPV) and its rate curves of 30_N00 sample.

Many authors [23,29,30,34,39] suggest the division of the UPV curve into three stages in an attempt of detecting the main phases of the hydration development of cement pastes. The process that the fresh cement paste goes through from a viscous suspension to a solid material has an intermediate phase, usually called transition phase. This transition phase is taken as an important yet critical phase since severe changes occurs in the cement microstructure in this period. One of the methods to identify the transition phase from the UPV curves is to trace tangents to the curves (red lines in Figure 5-2) and their intersection (points A and B) divide the curve into the three stages. The transition phase is the second one, where the velocity slope is steeper. It is also when the setting takes place. When the NFC is included, the UPV curve became smoother, as shown in Figure 5-3. In addition to this behavior, the initial (at 3 h of age) and final (at 23 h of age) values of the UPV curves are slightly distinct among the mixtures. For instance, the velocity curve of the 30_N50 started with the lowest value and ended with the higher one, even though its evolution was more gradual, in comparison with the other curves. Two factors that had already been identified as responsible for decreasing the velocity are the water content (w/c) and the presence of pores

[23,29,30]. It is important to emphasize that the amount of water on the gel has been discounted to remain the same w/c among the mixtures, and it can be discussed if this water in the gel acts the same way as the mixing water. The capacity of the nanofibrils to retain water even at early ages was addressed in Section 5.3.1. Besides that, NFC presents a porous structure and the morphology of the gel itself can also interfere on how the waves go through the sample. Those both characteristics may be responsible for the 30_N50 velocity shape.

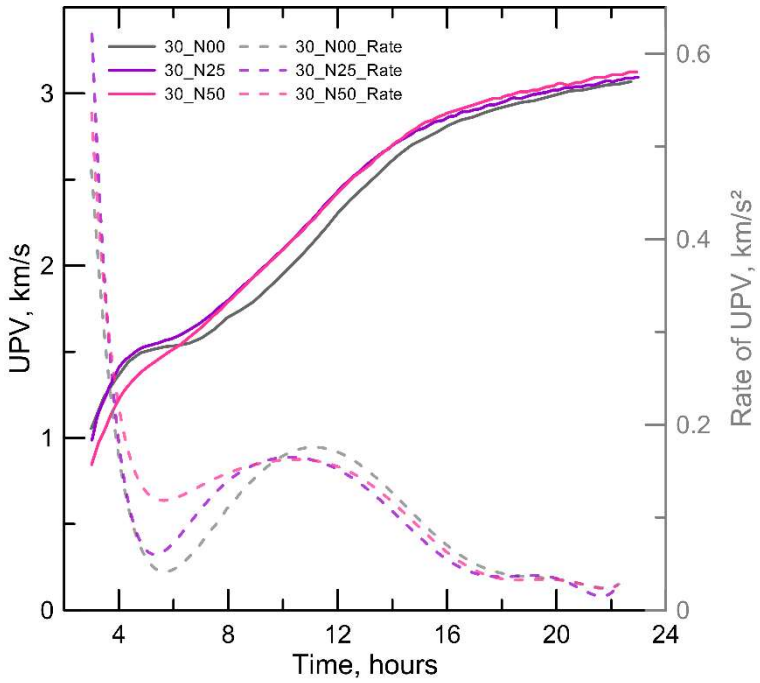

Figure 5-3 Ultrasonic pulse velocity (UPV) of the samples with water-to- ratio equals to 0.30 variations sand their correspondent rate curves for the first 23 hours.

This "smooth effect" resulted from the addition of NFC is more perceptible in the sample with the highest NFC content, of 0.05%. However, it is difficult to detect the baseline to trace the tangents from the UPV curve. Therefore, the rate of the UPV curve helps to understand the evaluation of the velocity development. The time that takes for each sample to reach the minimum (CP1) and the maximum (CP2) values in the rate curve are of interest and they are presented in Table 5-3 with their correspondent values of velocity and velocity rate. From Table 5-3 it is possible to notice the small difference between the UPV rate values of CP1 and CP2 for 30_N50, highlighting the "smooth effect" upon the addition of 0.05% of NFC.

Table 5-3 Values of the time that corresponds to Critical Points 1 and 2, obtained from the rate of UPV curves. CP1 and CP2 correspond to the minimal and maximum values of the UPV differential, respectively.

Sample	CP1			CP2		
	Time (h)	UPV (km/s²)	UPV rate (km/s²)	Time (h)	UPV (km/s²)	UPV rate (km/s²)
30-N00	5.77	1.53	0.041	11.23	2.16	0.176
30-N25	5.42	1.55	0.600	10.33	2.15	0.165
30-N50	5.67	1.49	0.118	10.56	2.18	0.162
35-N00	5.97	1.63	0.005	13.64	2.23	0.102
35-N25	4.05	1.62	-0.081	12.05	1.96	0.114
35-N50	4.02	1.62	-0.030	11.77	1.98	0.124
40-N00	8.09	1.65	0.045	13.80	2.04	0.094
40-N25	6.29	1.51	0.020	14.31	2.08	0.102
40-N50	6.28	1.46	0.035	15.02	2.06	0.101

The hydration begins to develop since the first contact between water and cement particles. Then, only when there is the necessary minimum of hydrates formed, the velocity abruptly increases. This point corresponds the CP1. The hydration reactions proceed with the continuous increasing of hydrates until the rate of velocity reaches its peak, the CP2. After reaching CP2, it is possible to observe the decrease in the velocity rate and its subsequent stabilization. Thus, the acceleration and the following deceleration in the velocity rate curve indicate that the threshold of solidification was achieved, as observed elsewhere [23,29,30]. This threshold of solidification can be understood as the establishment of a solid path between both ends of a sample [29]. In this investigation, the time to reach the CP2 i.e., the time correspondent to the maximum rate of UPV, was considered as a possible alternative for the time zero. It can be noticed from Table 5-3 that, except for the samples with w/c of 0.40, the time correspondent to CP2 had a similar trend as the Vicat test: the presence of NFC shortened the time to achieve the evidenced point. Regarding the CP1, those values are closer to the initial setting time determined by the Vicat test than CP2 values are when compared to the final setting time.

5.3.2.1. Shrinkage strain analysis

The autogenous shrinkage strain curves of 30-N00 variation are presented in Figure 5-4a and zeroed as soon as the measurements started at 0.9 h. One can

observe the high scatter between the replicates during the first hours. The possibilities for this high scatter include the following: (i) the deformation in the plastic phase is driven by the settlement of the corrugated tubes, (ii) the tubes may be better attached to the measuring point after the setting [31] and (iii) the time difference to fill the three tubes. Despite the high dispersion in the first hours, it is possible to notice that the shape of the three curves starts to get closer to each other after 9 h. The deviation between the three samples is plotted in Figure 5-4b as well as its differential over time. From Figure 5-4b it is noticeable that the moment when all the samples begin to shrink in the same way is from 9 h on, as guided by the pink line. This is corroborated by the rate of the scatter (dashed line) that became steady and minimal at 9 h.

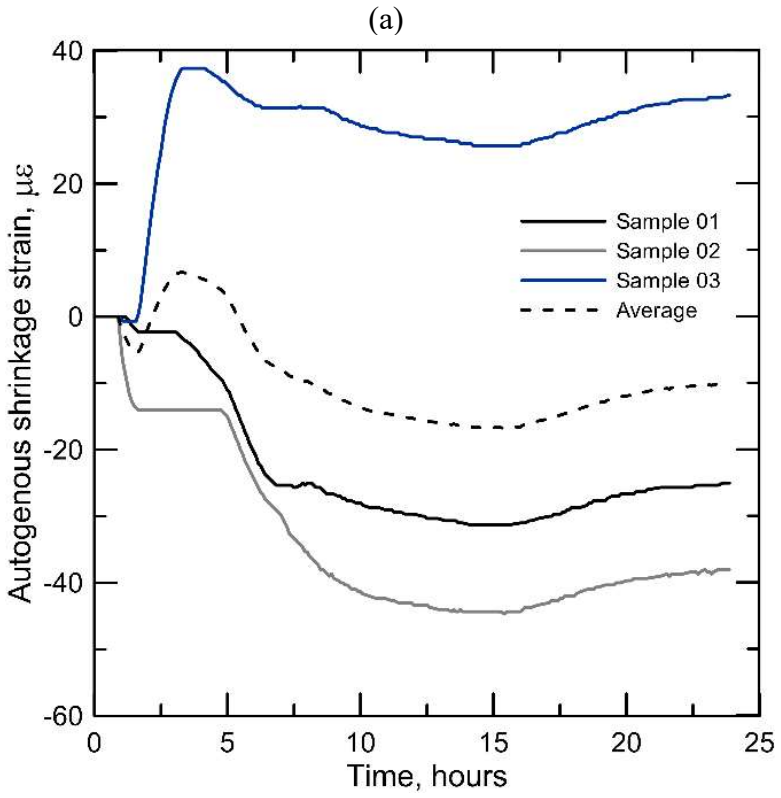

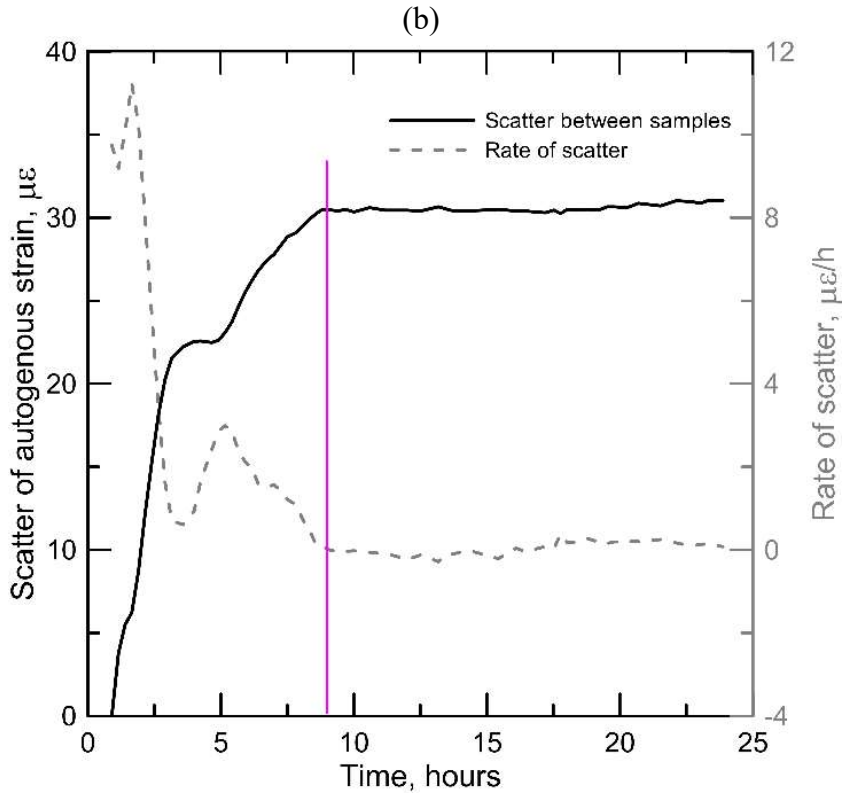

Figure 5-4 Analysis of the deformation of the 30_N00 replicates during the first 24 hours. (a) Autogenous shrinkage deformation zeroed at the first measurement; (b) The scatter between the three samples and the correspondent rate.

Figure 5-5 brings the rate of deformation of all samples 30_N00 with the rate of the average curve highlighted. According to Meddah and Tagnit-Hamou [19], it is possible to identify the three phases that the fresh cementitious materials undergo during the hardening process from the rate of the deformation curve, including the transition phase. With this methodology, the time zero would be the moment when the pattern of the rate of deformation is abruptly changed. This means the reference time is the peak of the rate of deformation, the maximum rate. Although the peak of the rate represents a characteristic time, it should be carefully used as the time zero when the autogenous shrinkage presents expansion, like the present case and as emphasized by Meddah and Tagnit-Hamou [19].

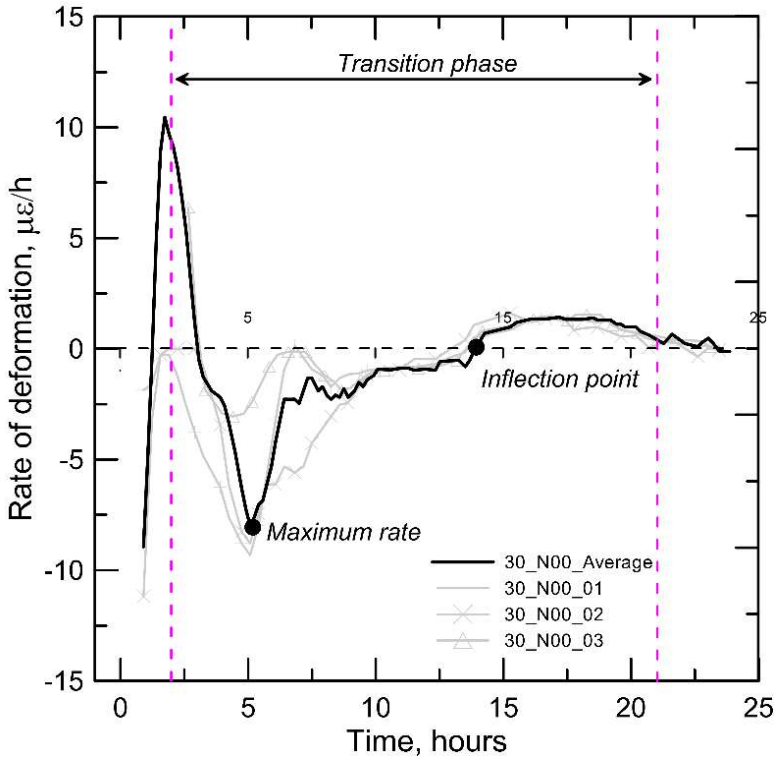

Figure 5-5 Deformation rate of the samples 30_N00.

The dashed lines in Figure 5-5 show the division of the hydration evolution into three phases, namely plastic, transition and solid. The maximum rate is reached at 5.1 h, and it decreases after that at a still considerable sharp slope. The stabilization of the rate occurs at the end of the transition phase, at around 21 h, three hours later than suggested by the UPV analysis (see Figure 5-2). Therefore, the transition phases identified from the UPV and from the deformation rate evaluation differ from each other. The elapsed time until the maximum rate of 5.1 is rather lower than the one expected to be the time zero if one compares the approaches analyzed so far. This value is closer to the initial setting time from the Vicat needle test (see Table 5-2).

The behavior of the curve of the rate of deformation can be explained by the fact that, prior to setting, the increasing slope is related to the chemical shrinkage, as pointed out by Sant *et al*. [20]. As the solidification process progresses, the material gets more resistant to bulk deformations, justifying the decrease of the rate.

The rate of deformation is the first derivate of the deformation curve over time. Since it is a differential curve, the fact that it presents both positive and negative values is an indication of the existence of a local maximum or minimum value. In

this case, it is a local minimal and it is correlated to the inflection. For the 30_N00 mixture, the time when the rate of deformation is zero is 14.3 h. From this time beyond the expansion takes place. As the expansion is also a deformation that should be considered, the time correspondent to the inflection of the rate curve will also be considerable an option as the time zero. The notable points obtained from the rate of deformation analysis for all mixtures are presented in Table 5-4.

Table 5-4 Elapsing time correspondent to the notable points resulted from the rate of deformation analysis, namely minimum scatter (Min. scatter), maximum rate (Max. rate), and inflection. Values in hours.

Sample	Min. scatter (h)	Max. rate (h)	Inflection (h)
30-N00	9.0	5.1	14.3
30-N25	8.6	4.2	13.3
30-N50	9.6	4.5	13.8
35-N00	25.1	10.3	20.1
35-N25	16.2	10.2	19.7
35-N50	10.7	8.2	19.5
40-N00	5.8	13.5	5.0
40-N25	5.8	13.3	9.0
40-N50	8.5	13.6	9.2

5.3.2.2. Comparison between the time zero methods

This topic is devoted to comparing the three approaches used for the determination of the time zero. This time is the reference from which the shrinkage deformations will be zeroed. The time zero can be taken as a critical value since it affects the magnitude of the shrinkage values, leading to a mis comparison between mixtures.

Figure 5-6a assembles the notable times obtained from the Vicat needle and UPV tests, and from the rate of deformation analysis of the nine mixtures. Grouping the results according to the water-to-cement ratio, the times correspondent to the characteristic points follow different patterns. For instance, for the specimens with w/c of 0.30, the maximum rate and the initial setting point (IST, from Vicat) values were close to each other, the same way the CP1 was similar to the final setting time (FST, from Vicat) points. Interestingly, it took the longest time to the inflection point occurs, around 5 h later to the minimum scatter, which marks the error stabilization among the replicates. One noticeable

trend was the same observed on the Vicat test: the addition of the NFC had an effect of decreasing the time of the points. This may indicate an acceleration effect on the hydration reactions upon the presence pf the NFC.

Analyzing the w/c ratio of 0.35, none of the times obtained from different approaches were systematically similar. As shown in Table 5-2, there was a minor distinction between the initial and final setting times, which it is not so frequent with cement pastes. In addition, the scattering among the times was the highest of the water-to-cement ratios, and with the longest time to achieve the minimum scattering of the replicates. Nevertheless, the effect of the NFC in decreasing the time zero options was kept for all approaches, except the inflection one.

Regarding the 0.40 ratio, the IST and the CP1 are proximate, as well as the FST and the inflection times. The first is in agreement to what was observed elsewhere [23,30]. It is worth to highlight that the minimum scatter occurred early in comparison to the other water-to-cement ratios. A relevant aspect is the inflection time of 40-N00 that happened at a significant early time, 5.0 h, even before of the initial setting time. As it will be further discussed, the specimens of this series presented a high value of expansion strain, stablished at the first measurements. The expansion behavior may had overtaken the other mechanisms and hydration processes. Nevertheless, the IST, FST, CP1 and maximum rate presented lower values for the specimens with nanocellulose.

Although all the characteristic points were brought for discussion, the time zero candidates, based on the literature and on the distinct behavior of the cement pastes under investigation, are presented in Figure 5-6. In fact, due to their values, the IST and CP1 seem to be more correlated to the beginning of the setting.

Figure 5-7 shows the autogenous shrinkage deformation evolution over 28 days for the 30_N00 mixture. The different curves correspond to the time zero differently considered for each approach previously discussed. As aforementioned, the use of the corrugated tubes allows very early age measurements although one must keep in mind that the decision of the time zero has great impact on the shrinkage strain result. The line representing the 24 h is also included for a further comparison with the sealed prisms. The average raw data is presented to distinguish which parts of the curve is included or excluded of the analysis. Although all the time zero candidates listed in Figure 5-6b

comprehend the expansion of 30-N00, the maximum rate, FST, minimum scatter and the UPV (CP2) also took a descendent branch that, if considered as part of the resulting curve, increases the total shrinkage strain at the end of the 28 days. This increase obviously depends on the chosen time.

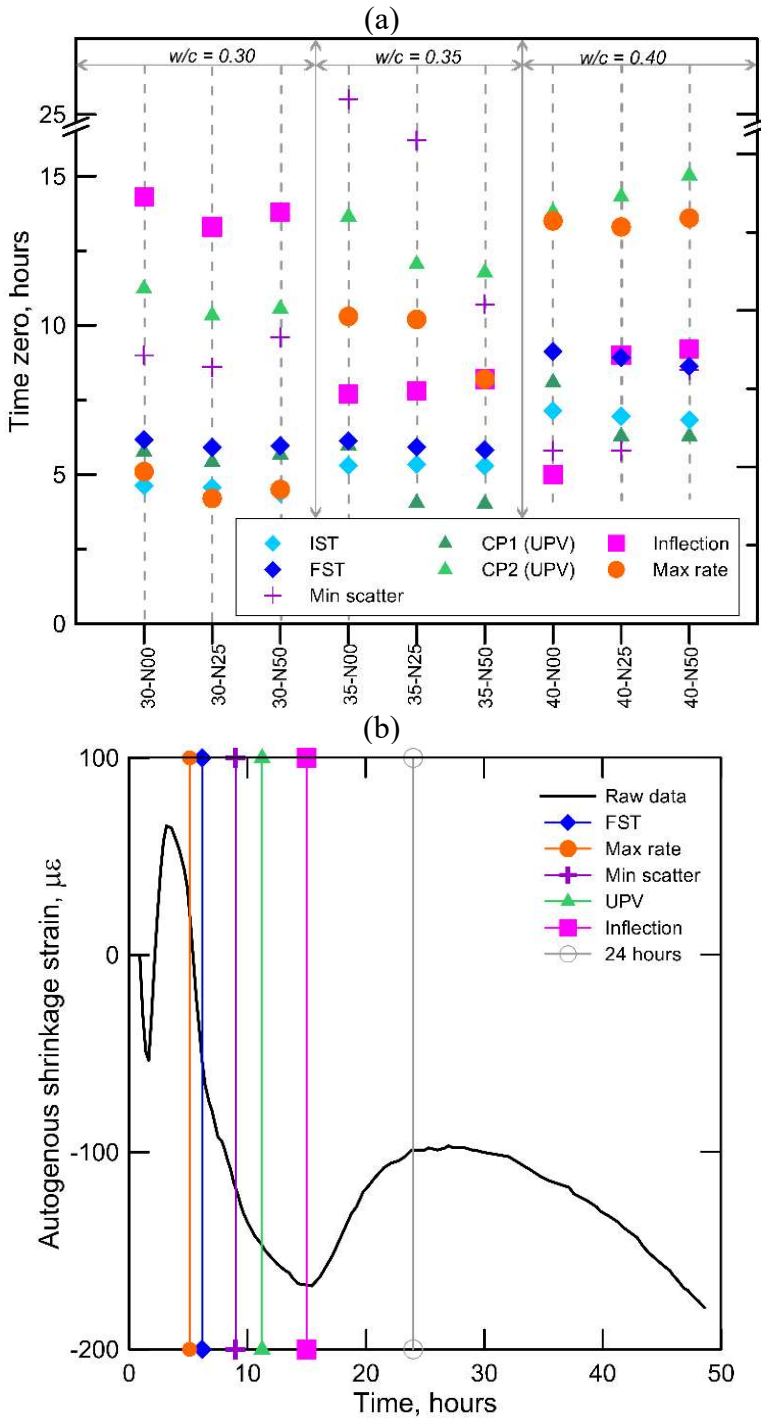

Figure 5-6 Comparison between the notable points obtained from Vicat needle, UPV and rate of deformation. (a) Notable points for all the nine mixtures; (b) Location of each time zero on the raw data shrinkage curve.

The reference time obtained from the inflection point was the one that resulted in the lowest strain value at the end of 28 days. This method considered the expansion developed by the specimen only as positive values of strain, leading to an "up shift" of the curve. The difference between the inflection curve and the others depends on whether each zero time includes or not negative and positive portions. For instance, in the curve obtained with the UPV time zero (Figure 5-7), only a small part of the beginning of the expansion was in the negative portion so the difference between this curve and the inflection one was only of 15 με. The difference between the inflection and other methods was of around 40, 100, 180 and 140 με for minimum scatter, Vicat FST, maximum rate and raw data, respectively.

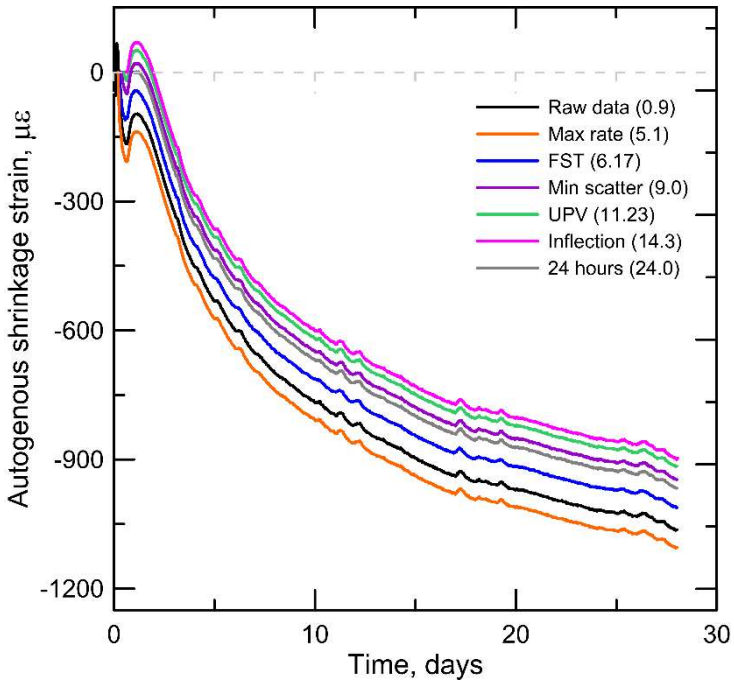

Figure 5-7 Autogenous shrinkage deformation evolution over 28 days for the 30_N00 mixture. The number in parenthesis is the reference time in hours correspondent to each method used to zero the curve.

By analyzing the transition phases identified by the UPV (Figure 5-2) and the rate of deformation curves (Figure 5-5), both CP2 and the inflection point are contained within the correspondent interval. Thus, those points are located before the total solidification of the mixture. The time of 24h is located after the solidification, considering both methods. From Figure 5-7 it is possible to observe that the 24h-curve did not contemplate the expansive deformation entirely. The

expansion took place between 14 and 28 h so the 24h curve only contemplated the last 4 h of the expansion.

The former discussion around the results presented in Figure 5-6a highlights how the different cement pastes affect the time zeros obtained from the methods employed. If one extends this analysis to the nine variations here investigates, the results are the ones presented in Table 5-5. Depending on the choice of the time zero, some variations would not present expansion with positive strain values, or they would be lower than when the inflection is selected. Besides, if the maximum rate or the minimum scatter would have been selected, the benefit of using NFC would not have been noticed in some variations. The opposite scenario is found by the minimum scatter and UPV methods considering the w/c of 0.35.

Table 5-5 Values of maximum swelling (Max. Swell.) and strain at the 28 days of shrinkage test according to the distinct time zero options. Values in in με.

Sample	Inflection		Max. rate		FST		Min. Scatter		UPV	
	Max. Swell.	At 28 days	Max. Swell.	At 28 days	Max. Swell.	At 28 days	Max. Swell.	At 28 days	Max. Swell.	At 28 days
30-N00	70	-897	0	-1089	0	-1010	21	-946	51	-917
30-N25	52	-982	0	-1202	0	-1123	0	-1068	12	-1022
30-N50	22	-575	0	-1192	0	-913	0	-660	0	-628
35-N00	320	-472	246	-547	321	-471	24	-768	126	-667
35-N25	217	-537	173	-567	212	-540	58	-693	130	-622
35-N50	48	-600	48	-601	17	-632	48	-601	58	-591
40-N00	576	-206	422	-359	576	-206	614	-167	402	-379
40-N25	402	-261	300	-363	402	-261	381	-282	254	-409
40-N50	470	-207	372	-304	469	-204	468	-209	313	-363

Based on the discussion along the present topic, the time zero that will be considered for further calculations is the one related to the inflection point of the deformation curve if it is after the IST. The aim of this choice is to dismiss the strains that probably did not produce considerable internal stresses during the plastic phase. Since the series 40-N00's inflexion point was two hours before the IST measured with the Vicat needle, for this specific case, the IST will be taken as the time zero. The authors believe the inflection point better represents the shrinkage behavior, especially having all the expansion represented by positive values of strain.

5.3.3. Autogenous shrinkage

The effect of the NFC inclusion on cement pastes regarding the autogenous shrinkage was investigated by means of two tests: sealed prisms of 24-h aged and corrugated tubes with time zero determined by the inflection point of the deformation curve. The inflection point is calculated from the zero point of the rate of deformation curve. A comparison between the methods is made by the end of the two analyses.

5.3.3.1. Sealed prisms

The autogenous shrinkage strain evolution over 28 days of all mixtures is presented in Figure 5-8a. For better visualization of the strain development on the first days, Figure 5-8b, Figure 5-8c and Figure 5-8d bring the strain development of 4 days, for each water-to-cement ratio. The starting point of measurement of the length change was as soon as the prisms were demolded and sealed, around 24 hours.

The inclusion of NFC affected differently the shrinkage strain of each water-to-cement ratio mix. At the end of the 28th day, 0.025% and 0.050% of NFC increased the autogenous shrinkage in 130 and 320 με, respectively for specimens with w/c of 0.30. This trend was not observed for the specimens with higher water content. For specimens with w/c of 0.35, the inclusion of 0.025% of NFC decreased the autogenous shrinkage by more than 100 με, representing a reduction of 15% of the final strain. Doubling the amount of nanocellulose to 0.050% was enough to increase the strain in 70 με. Although the effect of the nanocellulose in specimens with w/c of 0.40 was not as significant as on the 0.35-specimens, their presence led to a reduction of around 7.0% (60 με).

Besides the positive or negative effect depending on the water and NFC content at 28 days, the inclusion of nanocellulose influenced on the expansion deformation experienced by the pastes. Figure 5-8b shows for instance that 0.025% almost reduced to zero the strain, with a maximum deformation of 9 με facing 35 με of the reference (30-N00). This trend was also observed for the specimens with the w/c of 0.35 and 0.40, as shown in Figure 5-8c and Figure 5-8d. For those w/c ratios, the expansion was reduced to half: 35-N25 and 35-N50 in comparison with 35-N00, and 40-N25 in comparison with 40-N00. In general,

specimens with 0.025% of NFC showed less expansion. Swelling at early ages has already been reported on cement pastes when autogenous shrinkage was investigated [40,41], especially for higher w/c ratios. This behavior is often attributed to the formation of large crystals of Ca(OH)2 and ettringite. The inclusion of NFC into the cement paste may have altered the hydration kinetics and the hydrates in a way that led to the expansion reduction. Although the steady trend of the expansion attenuation promoted by the NFC noticed in all three distinct w/c, Hisseine *et al*. [12] observed the opposite effect with the addition of nanocellulose fibrils. In their study, the nanocellulose probably replenished the absorbed water [12], as well as observed by Kolour *et al*. [13]. Although expressive benefits were reported by the papers [12,13], it is important to highlight that in both papers either there was an extra amount of water [13] or an extra amount of superplasticizer [12] in the specimens with NFC. In the present investigation there is no evidence that the uptaken water, showed by the bleeding tests (Figure 5-1), was released back to the bulk matrix.

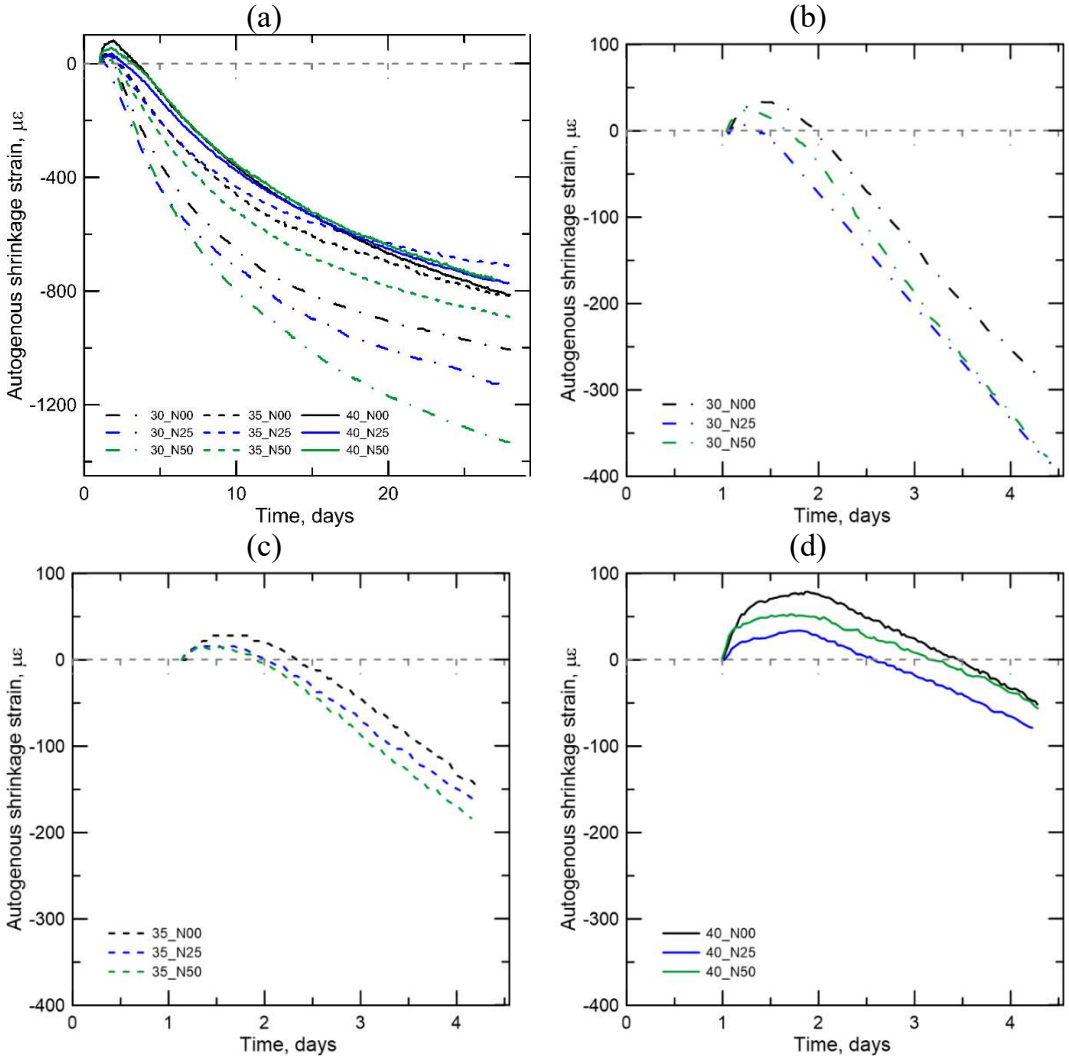

Figure 5-8 (a) Autogenous shrinkage strain development measured by the sealed prisms over 28 days. Zoom at the first four days to highlight the expansion behavior for the specimens with water-to-cement ratio of (b) 0.30; (c) 0.35; (d) 0.40.

5.3.3.2. Corrugated tubes

Figure 5-9 shows the mean autogenous shrinkage deformation curves of all the investigated mixtures along 28 days, after the adjustment according to the time zero discussed in Section 5.3.2. With the intention of facilitating the understanding of the influence of nanocellulose on the shrinkage behavior, the evaluation was divided by w/c ratio. However, one general effect of the addition of NFC for all the w/c ratios was the attenuation of the expansion at the first hours

experienced by the cement pastes. A similar effect was also presented by the specimens tested with the sealed prisms. In the case of the corrugated tubes, this effect was more pronounced on the ratios of 0.35 and 0.40.

Starting with the ratio of 0.30, 0.025% of NFC increased the final strain in 85 με, representing 9% of increase. However, if the percentage of NFC is 0.050%, the shrinkage development is substantially modified, with a reduction of the strain in more than 35% (-320 με). With the smallest values of expansion of this series, and among all the investigated mixtures, the 30-N50 was the first to present negative strains at 1.4 days and remained with the highest strain values until the third day. Beyond, its behavior began to change and at around 4.5 days. At this point, the strain values were lower than its correspondent reference, 30-N00. This trend continued the following days until complete the 28 days of measurement. It is important to highlight that this curve represents the average values of three specimens and all the replicates presented the same behavior and similar shape.

Regarding the 0.35 series, the inclusion of NFC did not lead to any improvement in relation to the final shrinkage strain reduction. One may relate this result to the significant impact of the nanocellulose on the mitigation of the expansion. The difference of the peak expansion value between the reference (30-N00) and the counterpart mixtures 30-N25 and 30-N50 was of 100 and 270, respectively. While the difference of the final shrinkage strain was of 65 and 130, comparing the same pair of values. This means the shrinkage difference between the variations with and without nanocellulose was inferior to their difference in the expansion.

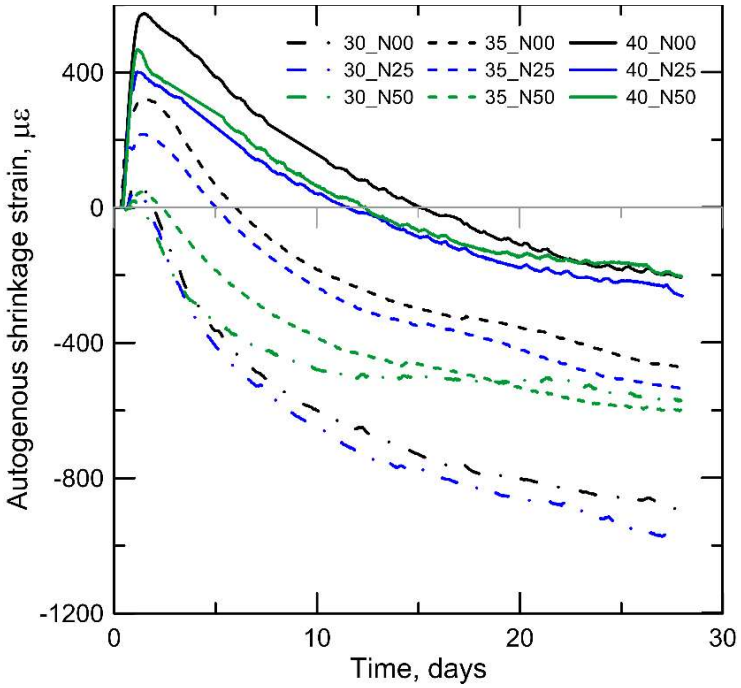

Figure 5-9 Autogenous shrinkage deformation over 28 days after the definition of the time zero.

This expansion/shrinkage relation also occurred to the specimens with w/c of 0.40, as shown in Figure 5-9. The mixtures with nanocellulose reduced more the expansion peak than increased the final shrinkage. In fact, the 40-N50 curve reached the same strain as the reference by the 22nd day on. The discussion in this Section related to the expansion should be considered depending on the boundary conditions given.

When the cement particles undergo the hydration process, pores are created due to the restrictions of the structure of the hydration products. If there is no external water source, the water within the capillary pores is driven to the first pores, leading to menisci formation. The compressive stresses oppose the tensile ones in a way that volumetric changes take place. Thus, the higher strain values reached by some of the mixtures containing NFC can be related to the higher porosity primarily on the first hours. The lower values of velocity of the curves shown in Figure 5-3 from the UPV tests support this theory since this behavior is usually attributed to the presence of voids and pores. In addition, superior values of porosity can be found on systems containing nanocellulose [12,33,42,43].

Results from the flow table and bleeding tests demonstrated the water retention capacity of the NFC in Table 5-1 and Figure 5-1, respectively. However, the

autogenous shrinkage results suggested the NFC does not work as most of internal curing agents, indicating that the water held by the NFC was not available at least during the first minutes. This behavior leads to two possible explanations. Either the water uptaken by the NFC fibrils is not available for further release and replacement of the water that is drained to pores or the pore introduction by NFC suppressed the first effect. The water replenishing capacity of the NFC was already demonstrated by Hisseine *et al*. [12]. Nevertheless, shrinkage is a complex phenomenon that evolves distinct mechanisms and the combination of them.

5.3.3.3. Comparison between the test methods

Figure 5-10 brings the comparison between the methods for autogenous shrinkage investigation, sealed prisms and corrugated tubes. The images were divided according to the w/c ratio for a better visualization. In a general way, the shrinkage values presented by the tubes were lower when compared to the prism curves of a same mixture. The main contributing factor for this behavior was the expansion experimented by the cement pastes at the first hours. Since the prism measurements must start after the solidification, 24 h, the expansion was not completely measured and thus, not considered into the total behavior.

The variation that presented similar behavior among the methods was the ratio 0.40 (**Figure 5-10**c), although the high discrepancy in the values. The expansion measured by the tubes was the responsible for the strain difference of around 600 με between the methods. For the w/c of 0.30, **Figure 5-10**b, the trend of the curves of the tubes showed a progressive increase in shrinkage with increasing amount of nanocellulose. This trend was not followed by the curves of the prisms. The influence of the expansion is also noticed on the w/c of 0.35, which even altered the result of the comparison between specimens with and without nanocellulose, reinforcing the role that expansion took on those results.

(a)

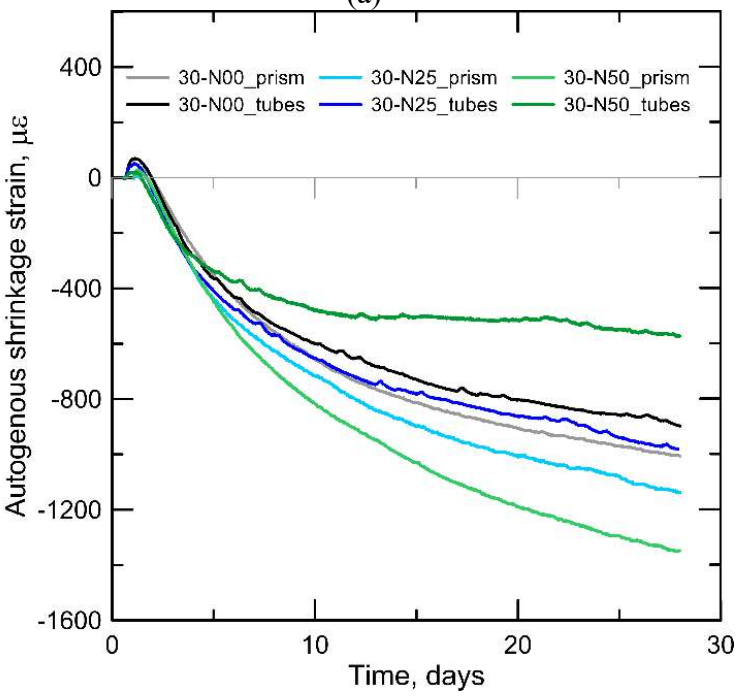

(b)

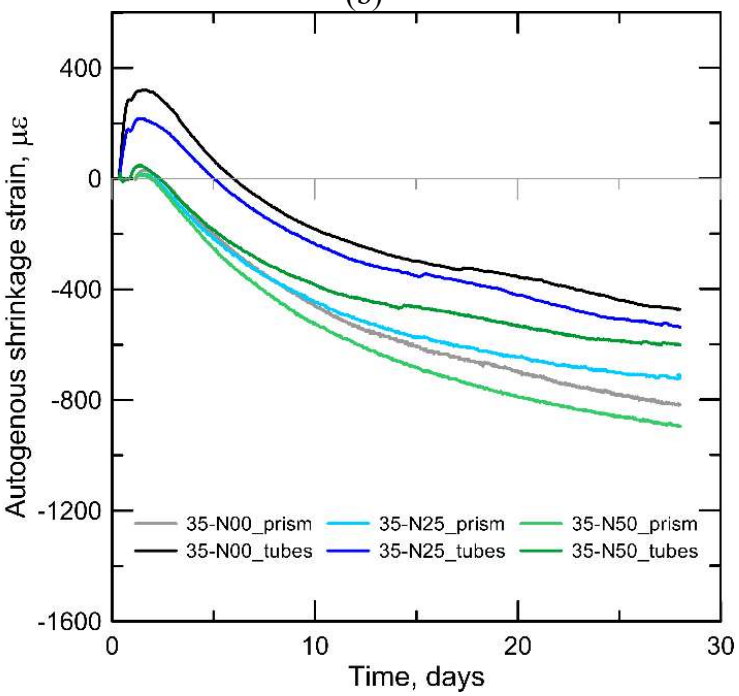

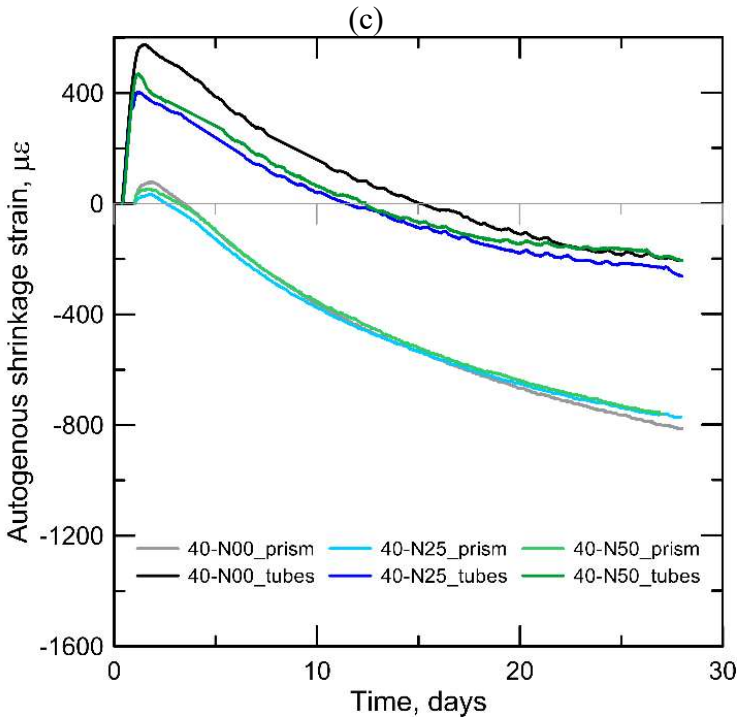

Figure 5-10 Autogenous shrinkage strain using sealed prisms and corrugates tubes with water-to-cement ratio of: (a) 0.30; (b) 0.35; (c) 0.40.

It is interesting to observe the differences concerning the two methods herein analyzed. Besides the significant expansion that can be missed or underestimated with the adoption of the sealed prisms, the initial behavior of the cement pastes within and beyond the transition phase should be understood. The early deformations whether positive or negative can affect the condition of the material either casted in formworks or in-situ situations. In the present comparison, it is clear that not only the order of magnitude but also the conclusion of whether the NFC is able to increase or decrease the deformations is affected by the chosen method.

Besides the results presented by the methods, one should be aware of the possible impact they may have on the process. While the corrugated tubes present as a completely closed system, the metal molds used for the casting of the sealed prisms may not have the same efficiency in keeping a closed and isothermal system. Some possible imperfections on the molds aligned to the time the specimens are handled and exposed to the environment, can contribute to the differences between the results presented. In this matter, the extra 'free' accumulated water may play a crucial role [17,44,45]. Before the complete solidification, the bleeding water could be reabsorbed by the paste, possibly leading to expansion [46]. In fact, the samples that presented a higher bleeding

height were the ones with expansion more pronounced, as shown in Figure 5-1. In addition, the NFC fibrils were effective in holding part of the bleeding water. Thus, it is reasonable to assume, by the shrinkage results, that this water was not reinserted into the cement paste at least during the first hours. Hisseine *et al*. [12] showed that at higher relative humidity, the water rate of release by the NFC is lower.

5.3.4. Total shrinkage

The total shrinkage deformation evolution for 28 days is presented in Figure 5-11. Each line is the average of three specimens of a same composition. The dashed dot, continuous and dashed lines represent the composition with w/c ratio of 0.30, 0.35 and 0.40, respectively. The total shrinkage is a combination of the autogenous and drying shrinkage. The values of total strain for the plain mixtures namely 30_N00, 35_N00 and 40_N00 are in accordance with others found elsewhere [9,47]. A first distinction from the autogenous shrinkage tests with the sealed prisms was the absence of the expansion portion of presented in the first ages.

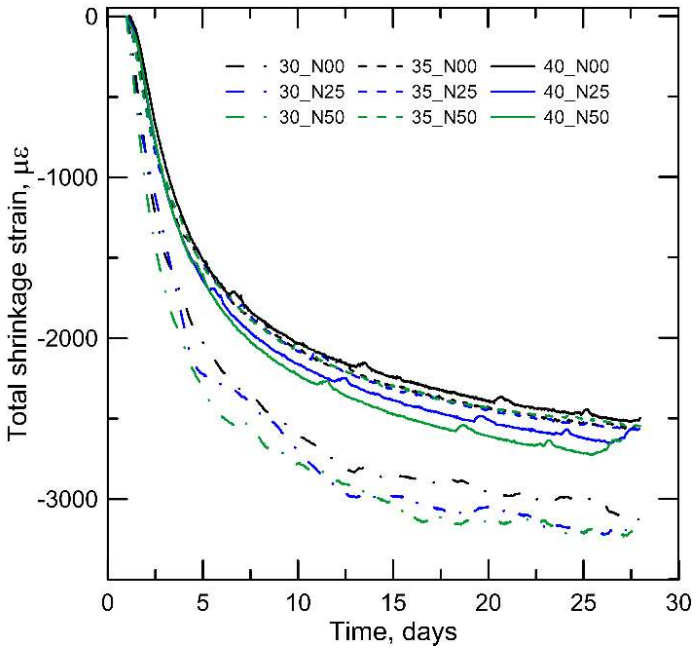

Figure 5-11 Evolution of the total shrinkage deformations in the different cement paste mixtures with (N25 and N50) and without (N00) NFC, for the different water-to-cement ratios.

The overlapping observed by the mixtures with w/c ratio of 0.35 indicates that the inclusion of up to 0.05% of NFC does not affect the total shrinkage, at least for measurements taken after the first 24 h. In fact, the difference between 30-N00 and the ones with NFC (30-N25 and 30-N50), was lower than 1%. Regarding the variation of w/c of 0.30, by the end of 28 days, the inclusion of NFC led to an increase of the shrinkage strain of around 2%. While for the mixtures with w/c of 0.40 the presence of 0.025 and 0.050 % of NFC led to an increase of 2.4% and of 5.5% at 28 days, respectively.

If one compares the total to the autogenous shrinkage measured by the sealed prisms (Figure 5-8), the relation of increase/decrease shrinkage values is not the same. This is a straightforward comparison since the specimens were cast in the same molds, exposed to the same curing conditions and similar handling. The distinct relation of the w/c ratio and the percentage of NFC, and their interaction regarding the free shrinkage behavior has been already observed by Kolour *et al*. [48]. In their research, they reported no benefits in using nanocellulose for decrease shrinkage strain for several w/c, excepted the 0.35, where there was a significant reduction of the deformation upon the addition of a small percentage of NFC (0.05%) [48]. In fact, Ferrara *et al*. [49] also noticed a decrease of the autogenous shrinkage and an increase of the total shrinkage upon the addition of cellulose nanopulp. Both the studies correlated the increase on the total shrinkage to the assumption of the interaction between nanocellulose and mixing water leads to a more porous microstructure working as a facilitator for the loss of moisture [48,49]. Indeed, the results brought by the UPV analysis suggests a more porous matrix even at the first hours of hydration of the specimens with NFC, as shown and discussed in Section 5.3.2.1.

Other two possible reasons, related to the amount of water available into the cement paste, can be responsible for this behavior: the different amount of mixing water among the mixtures with a same w/c, and the water uptake by the nanofibrils. Since the water present in the NFC gel was discounted from the mixing water, in theory the amount of available water was kept the same, regardless the content of NFC on a given mixture. However, the water present in the NFC gel may not behave similarly to the mixing water used. In fact, as discussed in Section 5.3.1 and showed by the flow table and bleeding tests, the presence of NFC immediately changes how the free water behave within the fresh

paste. In addition, the NFC acts as water reservoir since some of the ‘free’ water in the fresh cement paste is uptaken, as shown in Figure 5-1. Moreover, the carbonation effect observed in Chapter 4 could also play a role on the shrinkage deformation increase displayed by the NFC-reinforced specimens.

5.4. Conclusions

The present work raised several discussions related to the shrinkage of cement pastes with distinct water-to-cement ratios with the inclusion of nanofibrillated cellulose (NFC). The percentages of NFC were 0.000%, 0.025% and 0.050% in relation to cement weight and the w/c were equals to 0.30, 0.35 and 0.40. As the autogenous shrinkage starts during the first hours of the hydration and its development can affect other properties, a dense investigation on the fresh properties is necessary. Specific conclusions can be summarized as follows.

- From flow table, ultrasonic pulse velocity (UPV), Vicat needle and the bleeding tests, the nanocellulose significantly altered the fresh structure and the hydration development of all the mixtures analyzed.
- The Vicat needle test and the other characteristic times suggested that the presence of NFC accelerated the hydration reactions, yet with probably a more porous microstructure.
- The rheology is highly affected by the presence of the NFC, modifying the workability and the amount of ‘free’ water on the fresh state. In fact, by means of the bleeding test it was showed the capacity of retaining water the nanocellulose fibrils have.
- The elapsed time for each of the time zero candidates were developed in a different way, depending on the water-to-cement ratio. The inflection of the rate of deformation curve was elected as the one that better represented the autogenous shrinkage evolution. The only restriction is that the inflection must be contained within the transition phase of the liquid/solid phases. It was clear that the chosen time zero plays an extreme important role on the autogenous shrinkage behavior evaluation.
- Regarding the autogenous shrinkage methods, the sealed prisms did not contemplate all the expansion experienced by the specimens as the

corrugated tubes did. The expansion values progressively increased with the amount of bleeding water.

- The expansion peak measured by both autogenous shrinkage methods for all the mixtures was attenuated by the presence of any percentage of NFC, decreasing up to 85% the positive deformation.
- The combination of water-to-cement ratio of 0.30 and 0.050% of NFC resulted in a decrease of 36% of the autogenous shrinkage measured with the corrugated tubes by the end of 28 days.
- The inclusion of NFC into the cement pastes did not significant changed the total shrinkage deformation of the specimens with w/c of 0.30 and 0.35. The presence of 0.050% of NFC increased around 5% the total shrinkage strain.

5.5. References

[1] BAŽANT, Z. P. Theory of Creep and Shrinkage in Concrete Structures: A Précis of Recent Developments. In: **Mechanics Today**. [s.l.] Elsevier, 1975. p. 1–93.

[2] ZHANG, W.; HAMA, Y.; NA, S. H. Drying shrinkage and microstructure characteristics of mortar incorporating ground granulated blast furnace slag and shrinkage reducing admixture. **Construction and Building Materials**, v. 93, p. 267–277, 2015.

[3] GAO, S. *et al*. Effect of shrinkage-reducing admixture and expansive agent on mechanical properties and drying shrinkage of Engineered Cementitious Composite (ECC). **Construction and Building Materials**, v. 179, p. 172–185, 2018.

[4] MECHTCHERINE, V. *et al*. Effect of internal curing by using superabsorbent polymers (SAP) on autogenous shrinkage and other properties of a high-performance fine-grained concrete: Results of a RILEM round-robin test. **Materials and Structures/Materiaux et Constructions**, v. 47, n. 3, p. 541–562, 2014.

[5] KIM, G. M.; YOON, H. N.; LEE, H. K. Autogenous shrinkage and electrical characteristics of cement pastes and mortars with carbon nanotube and carbon fiber. **Construction and Building Materials**, v. 177, p. 428–435, 2018.

[6] LU, T.; LI, Z.; HUANG, H. Restraining effect of aggregates on autogenous shrinkage in cement mortar and concrete. **Construction and Building Materials**, v. 289, p. 1–18, 2021.

[7] ZIMMERMANN, T.; PÖHLER, E.; GEIGER, T. Cellulose Fibrils for Polymer Reinforcement. **Advanced Engineering Materials**, n. 9, p. 754–761, 2004.

[8] RAPOPORT, J. R.; SHAH, S. P. Cast-in-Place Cellulose Fiber-Reinforced Cement Paste , Mortar , and Concrete. **ACI Materials Journal**, v. 102, n. 5, p. 2006, 2006.

[9] SANTOS MOTTA, M. DOS; SOUZA, L. M. S.; ANDRADE SILVA, F. DE. Early-age shrinkage of cement pastes with polypropylene and curaua fibres. **Advances in Cement Research**, v. 33, n. 4, p. 156–167, 2021.

[10] BUCH, N.; REHMAN, O. M.; HILLER, J. E. Impact of processed cellulose fibers on portland cement concrete properties. **Transportation Research Record**, n. 1668, p. 72–80, 1999.

[11] ZHANG, Z.; SCHERER, G. W. Measuring chemical shrinkage of ordinary Portland cement pastes with high water-to-cement ratios by adding cellulose nanofibrils. **Cement and Concrete Composites**, v. 111, n. February, p. 103625, 2020.

[12] HISSEINE, O. A. *et al*. Nano-engineered ultra-high performance concrete for controlled autogenous shrinkage using nanocellulose. **Cement and Concrete Research**, v. 137, n. September, p. 106217, 2020.

[13] KOLOUR, H.; ASHRAF, W.; LANDIS, E. N. Hydration and Early Age Properties of Cement Pastes Modified with Cellulose Nanofibrils. **Transportation Research Record: Journal of the Transportation Research Board**, p. 036119812094599, 2020.

[14] STEPHENSON, K. M. **Characterizing the behavior and properties of nanocellulose reinforced ultra high performance concrete**. 2011. 152 f. Maine. 2011.

[15] HEWLETT, P.; LISKA, M. **Lea's Chemistry of Cement and Concrete**. Fourth ed. [s.l.] Elsevier Science & Technilogy Books, 2004. v. 58

[16] LURA, P. **Autogenous Deformation and Internal Curing of Concrete**. [s.l: s.n.].

[17] WYRZYKOWSKI, M. *et al*. Corrugated tube protocol for autogenous

shrinkage measurements: review and statistical assessment. **Materials and Structures/Materiaux et Constructions**, v. 50, n. 1, p. 1–14, 2017.

[18] CUSSON, D.; HOOGEVEEN, T. An experimental approach for the analysis of early-age behaviour of high-performance concrete structures under restrained shrinkage. **Cement and Concrete Research**, v. 37, n. 2, p. 200–209, 2007.

[19] SEDDIK MEDDAH, M.; TAGNIT-HAMOU, A. Evaluation of Rate of Deformation for Early-Age Concrete Shrinkage Analysis and Time Zero Determination. **Journal of Materials in Civil Engineering**, v. 23, n. 7, p. 1076–1086, 2011.

[20] SANT, G.; LURA, P.; WEISS, J. A discussion of analysis approaches for determining 'Time-Zero' from chemical shrinkage and autogenous strain measurements in cement paste. **International RILEM Conference on Volume Changes of Hardening Concrete: Testing and Mitigation**, p. 375–383, 2006.

[21] TOPU, I. B.; UYGUNOLU, T.; HOCAOLU, I. Electrical conductivity of setting cement paste with different mineral admixtures. **Construction and Building Materials**, v. 28, n. 1, p. 414–420, 2012.

[22] KADI, M. EL *et al*. Use of early acoustic emission to evaluate the structural condition and self-healing performance of textile reinforced cements. **Mechanics Research Communications**, v. 81, n. 2017, p. 26–31, 2017.

[23] TRTNIK, G. *et al*. Possibilities of using the ultrasonic wave transmission method to estimate initial setting time of cement paste. **Cement and Concrete Research**, v. 38, n. 11, p. 1336–1342, 2008.

[24] REINHARDT, H. W.; HERB, A. T. Ultrasonic monitoring of setting and hardening of cement mortar - A new device. **Materials and Structures/Materiaux et Constructions**, v. 33, p. 580–583, 2000.

[25] AMERICAN SOCIETY FOR TESTING & MATER. **C1698: Standard Test Method for Autogenous Strain of Cement Paste and Mortar**ASTM International, , 2014.

[26] GERMAN INSTITUTE FOR STANDARDISATION (DEUTSCHES INSTITUT FÜR NORMUNG). **EN 1015-3: Methods of Test for Mortar for Masonry—Part 3: Determination of Consistence of Fresh Mortar (by Flow Table)**Berlin, Germany, 2007.

[27] JOSSERAND, L.; LARRARD, F. DE. A method for concrete bleeding measurement. **Materials and Structures**, v. 37, n. December, p. 666–670, 2004.

[28] AMERICAN SOCIETY FOR TESTING & MATER. **C191: Standard Test Methods for Time of Setting of Hydraulic Cement by Vicat Needle**, 1987.

[29] LEE, H. K. *et al*. Ultrasonic in-situ monitoring of setting process of high-performance concrete. **Cement and Concrete Research**, v. 34, n. 4, p. 631–640, 2004.

[30] ZHANG, S.; ZHANG, Y.; LI, Z. Ultrasonic monitoring of setting and hardening of slag blended cement under different curing temperatures by using embedded piezoelectric transducers. **Construction and Building Materials**, v. 159, p. 553–560, 2018.

[31] MEJLHEDE JENSEN, O.; FREIESLEBEN HANSEN, P. A dilatometer for measuring autogenous deformation in hardening portland cement paste. **Materials and Structures**, v. 28, n. 7, p. 406–409, 1995.

[32] JIAO, L. *et al*. Natural cellulose nanofibers as sustainable enhancers in construction cement. **PLoS ONE**, v. 11, n. 12, p. 1–13, 2016.

[33] HISSEINE, O. A.; OMRAN, A. F.; TAGNIT-HAMOU, A. Influence of cellulose filaments on cement paste and concrete. **Journal of Materials in Civil Engineering**, v. 30, n. 6, p. 1–14, 2018.

[34] CHOI, H.; CHOI, Y. C. Setting characteristics of natural cellulose fiber reinforced cement composite. **Construction and Building Materials**, v. 271, p. 121910, 2021.

[35] MEJDOUB, R. *et al*. Nanofibrillated cellulose as nanoreinforcement in Portland cement: Thermal, mechanical and microstructural properties. **Journal of Composite Materials**, v. 51, n. 17, p. 2491–2503, 2017.

[36] CAO, Y. *et al*. The influence of cellulose nanocrystal additions on the performance of cement paste. **Cement and Concrete Composites**, v. 56, p. 73–83, 2015.

[37] ONUAGULUCHI, O.; PANESAR, D. K.; SAIN, M. Properties of nanofibre reinforced cement composites. **Construction and Building Materials**, v. 63, p. 119–124, 2014.

[38] LEE, H. K.; LEE, K. M.; KIM, B. G. Autogenous shrinkage of high-performance concrete containing fly ash. **Magazine of Concrete Research**, v. 55, n. 6, p. 507–515, 2003.

[39] ZHANG, Y. *et al*. Ultrasound monitoring of setting and hardening process of ultra-high performance cementitious materials. **NDT and E International**, v. 47,

p. 177–184, 2012.

[40] SCHIESSL, P.; PLANNERER, M.; BRANDES, C. Influence of binders and admixtures on autogenous shrinkage of high performance concrete. **International RILEM Workshop on Shrinkage of Concrete**, p. 179–190, 2000.

[41] TAZAWA, E.; MIYAZAWA, S. Experimental Study On Mechanism Of Autogenous Shrinkage Of Concrete. **Cement and Concrete Research**, v. 25, n. 8, p. 1633–1638, 1995.

[42] HISSEINE, O. A. *et al*. Feasibility of using cellulose filaments as a viscosity modifying agent in self-consolidating concrete. **Cement and Concrete Composites**, v. 94, n. September, p. 327–340, 2018.

[43] GONCALVES, J. *et al*. Cellulose nanofibres (CNF) for sulphate resistance in cement based systems. **Cement and Concrete Composites**, v. 99, n. March, p. 100–111, 2019.

[44] BAROGHEL-BOUNY, V. *et al*. Autogenous deformations of cement pastes : Part II . W / C effects , micro-macro correlations , and threshold values To cite this version : HAL Id : hal-01005282 Autogenous deformations of cement pastes Part II . W / C effects , micro – macro correlations. **Cement and Concrete Research**, v. 36, p. 123–136, 2006.

[45] JENSEN, O. M.; HANSEN, P. F. Autogenous deformation and RH-change in perspective. **Cement and Concrete Research**, v. 31, n. 12, p. 1859–1865, 2001.

[46] BOIVIN, S. *et al*. Experimental Assessment of Chemical Shrinkage of Hydrating Cement Paste. **Autogenous Shrinkage of Concrete: Proceedings of the International Workshop organized by JCI**, p. 81–92, 1999.

[47] MELO NETO, A. A.; CINCOTTO, M. A.; REPETTE, W. Drying and autogenous shrinkage of pastes and mortars with activated slag cement. **Cement and Concrete Research**, v. 38, n. 4, p. 565–574, 2008.

[48] KOLOUR, H. H. *et al*. An investigation on the effects of cellulose nanofibrils on the performance of cement paste and concrete. **Advances in Civil Engineering Materials**, v. 7, n. 1, p. 463–478, 2018.

[49] FERRARA, L. *et al*. **Effect of Cellulose Nanopulp on Autogenous and Drying Shrinkage of Cement Based CompositesNanotechnology in Construction**, 2015.

[50] OLIVEIRA DE SOUZA, L. *et al*. Investigation of dispersion methodologies

of microcrystalline and nano-fibrillated cellulose on cement pastes. **Cement and Concrete Composites**, v. 126, n. February, 2022.

6. Rheological characterization under static and dynamic regimes of cement pastes with microcrystalline and nano-fibrillated cellulose

6.1. Introduction

The study of the rheological properties of cement-based materials is essential for the processes directly linked to the flow performance of the fresh mixture, such as pumping, spreading, casting, compaction, and recently 3D-print requirements [1]. In a simple way, during hydration, the cement paste becomes stiffer until it sets. Thus, the rheological behavior of cementitious materials is highly time-dependent since the hydration continuously develops over time. Although single-point tests, such as slump, give a starting workability value, they do not cover the full rheological understanding of cement pastes. This justifies the use of advanced rheometers for a better understanding of the flow behavior, especially when other materials, such as cellulose, are added to mixture.

Basically, the effects of the cellulosic inclusions on the cementitious materials' rheological properties can be divided into two groups. The first is the one related to cellulose crystals' inclusion, in which the steric stabilization effect is observed [2]. Due to this effect, there is a decrease in the yield stress at a low content of crystal inclusions. After a specific threshold, the crystals' agglomeration effect suppresses the steric stabilization one, and there is an increase in the yield stress and viscosity [2–4].

The second group of expected outcome is the one observed when cellulose fibrils are included, where there is an increase in the yield stress even at low percentage inclusions [4–10]. This effect is normally attributed to the hydrophilicity [8] and morphological aspects of the fibrils [9] that provide volume stability to the fresh material. In fact, the rheological behavior of the suspension itself influences the rheological behavior of the fresh mixtures [11]. In addition, the cellulosic inclusions (crystals and fibrils) intensify the shear-thinning behavior of the fresh material.

The objective of this Chapter is to characterize the effects of increasing percentages of MCC and NFC on rheology of cement pastes. Two distinct regimes, based on a two-point approach were performed. Both static (constant shear rate - CSR) and dynamic regimes were taken into consideration, with the rheological measurements over time. Different ranges of percentages of NFC and MCC were investigated. An additional set of variations of NFC-reinforced specimens were assessed on the CSR test so the role of the water on the NFC gel could be discussed. The rheological behavior of the NFC gel was also investigated, showing a shear thinning behavior. This shear thinning behavior was intensified on the cement pastes with MCC and NFC. In general, NFC inclusion led to a stiffer paste even at low percentages, as 0.010%, while only additions beyond 0.500% of MCC resulted in similar values.

6.2. Experimental program

6.2.1. Materials and mixing process

The mixing process can affect the fresh and hardened properties of cementitious materials, including their microstructure development. The mixing time, speed and the order of each step affect the rheology of fresh cement pastes [12]. Portland cement CEM I 42.5 R produced by HeidelbergCement AG and tap water were used to produce the cement pastes. The microcrystalline cellulose (MCC) and the nanofibrillated cellulose (NFC) were the same as described along the thesis. Their characterizations were developed also along the Chapters 3 and 4.

The mixture compositions and details are given in Table 6-1. The specified mass of each ingredient was used to produce around one liter of cement paste. The cement pastes were reinforced with varied percentages of MCC and NFC, as shown in Table 6-1. The percentage of inclusion is with respect to the cement weight. In the case of NFC, the percentage is related to the fibrils solid content of the gel.

Table 6-1 Composition of the different variations of the matrices investigated, in weight.

Name	w/c	Inclusion	%	Cement (g)	Water (g)	MCC powder (g)	NFC gel (g)
35_Ref	0.35	-	0.000%	900	315.0	0.00	0.00
35M_0050	0.35	MCC	0.050%	900	315.0	0.45	-
35M_0500	0.35	MCC	0.500%	900	315.0	4.50	-
35M_0750	0.35	MCC	0.750%	900	315.0	6.75	-
35M_1000	0.35	MCC	1.000%	900	315.0	9.00	-
35N_0010	0.35	NFC	0.010%	900	310.6	-	4.50
35N_0025	0.35	NFC	0.025%	900	304.0	-	11.25
35N_0025_EW	0.35	NFC	0.025%	900	315.0	-	11.25
35N_0040	0.35	NFC	0.040%	900	297.4	-	18.00
40_Ref	0.40	-	0.000%	900	360.0	0.00	0.00
40N_0025	0.40	NFC	0.025%	900	349.0	-	11.25
40N_0025_EW	0.40	NFC	0.025%	900	360.0	-	11.25

The selection of the percentage of inclusion of MCC (0.05%, 0.50%, 0.75%, and 1.00%) and NFC (0.010%, 0.025%, and 0.040%) was based on the flow value and on the torque limitation of the rheometer. The concept was to compare mixtures with comparable flow values. Since the workability of the cement pastes was more affected by the NFC inclusion than by the MCC's, the percentage of the former was considerably lower than the latter. For those mixtures, a water-to-cement ratio of 0.35 was used. Besides the variations with w/c of 0.35, another set of tests was conducted in order to investigate the water contribution to the rheological behavior of the samples with NFC. Thus, samples with w/c of 0.40 were included to this investigation and their specifications are found in Table 6-1.

All the materials were kept in a controlled room (temperature of 21 ± 3 °C and RH of 50 ± 5%) prior to the mixing of the specimens, for at least 12 hours. Approximately 1 L of cement paste was used in each test. Each type of inclusion needed a pre-step mixing before the contact of the water with the cement particles. This pre-step of mixing is specified as "-00:02:00" (HH:MM:SS) in Table 6-2. Due to their different forms, the NFC gel was homogenized with the mixing water (with IKA T50 digital ULTRA TURAXX), while the MCC powder was mixed with the dry cement (manually with a spoon). For the cement paste mixing, a bench-mounted planetary mixer of 5 L was used. This approach was used in the experiments presented in the previous Chapters. The mixing process details are described in Table 6-2, as well as the chronological order of the tests. The 'time

zero' was taken as the moment when the water (or suspension, in the case of NFC samples) got in contact with the cement particles.

Table 6-2 - Mixing protocol for the fresh cement pastes' rheological tests, dynamic and static.

Time (HH:MM:SS)	Speed (rpm)	Action
-00:02:00 - 00:00:00	600; -	Homogenization of: NFC gel and mixing water; MCC and the cement
00:00:00 - 00:00:30	-	Addition of water/suspension to the cement and manually integration
00:00:30 - 00:01:30	140	Mixing
00:01:30 - 00:02:00	-	Scrapping the material from the wall and bottom of the bowl
00:02:00 - 00:05:00	285	Mixing
00:05:00 - 00:07:00	-	Haegermann flow table test and photos
00:07:00 - 00:10:00	-	Filling the unit cell and shifting it to the rheometer room
00:10:00 - 00:12:00	-	Allocation of the unit cell and setting of program
Static		
00:12:00 - 00:14:00	-	Resting
00:14:00 - 00:15:40	0<γ<50	Pre-shear (see Figure XX)
00:15:40 - 00:20:00	-	Resting
00:20:00	γ<0.15	CSR test
00:25:00	-γ<0.15	Repeat the test at each 5 minutes
Dynamic		
00:12:00 - 00:15:00	-	Resting
00:15:00	0<γ<50	Hysteresis loop (dynamic test; see Figure 1)
00:30:00	0<γ<50	Repeat the test at each 15 minutes

6.2.2. Rheological test

6.2.2.1. Haegermann flow table test

The Haegermann flow table test was performed for every batch before the rheological tests, following the procedure described in EN 1015-3 [13]. The moment when it was performed is detailed on Table 6-2. The measurements were taken before and after 15 strokes. For a visual observation, photos were also taken for each measurement.

6.2.2.2. Two-point tests

For both static and dynamic tests, a HAAKE MARS II Rheometer was used. The equipment had a building material's cell and a vane configuration. Figure 6-1 shows the apparatus, with the detail of the cell unit that receives the fresh paste in Figure 6-1b. A temperature control module was coupled for maintaining the sample at the temperature of 20 ±1 ºC. The paste was carefully filled into the unit cell with a spoon. The time selection of each test was also based on the torque limitation of the equipment.

(a)

(b)

Figure 6-1 (a) The rheometer used coupled with a temperature control module. (b) The cell unit.

The single-batch approach was employed on the rheological tests due to its time efficiency and material saving benefits. Regardless the time duration and the time when each test was performed, the cement paste was permanently kept covered into the unit cell.

6.2.2.2.1. Dynamic test

The dynamic test was performed through the employment of a hysteresis loop of shear rate ramp as shown in Figure 6-2. The tests were performed at every 15 minutes on a same batch, following the single-batch approach.

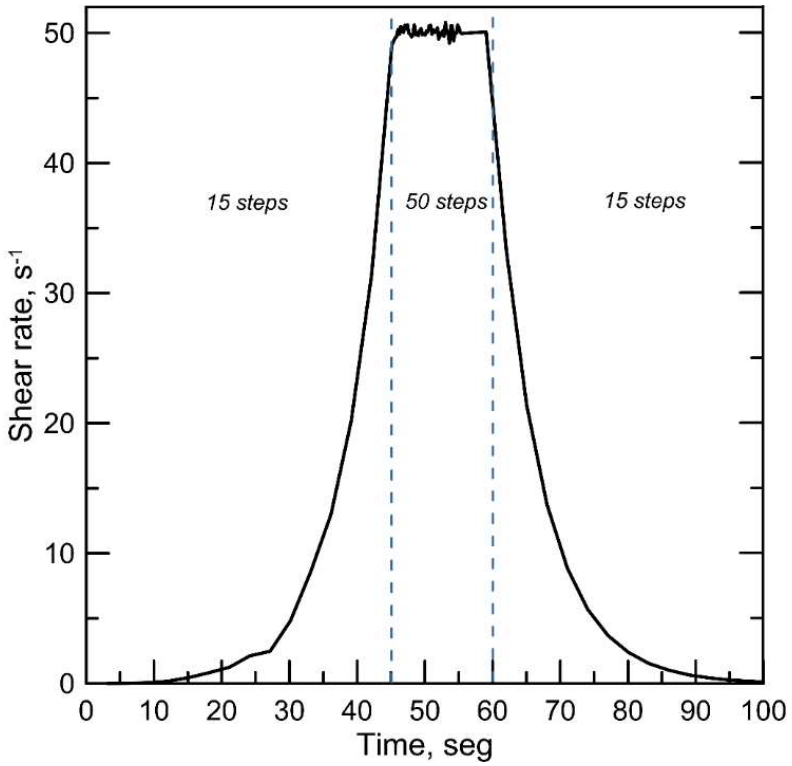

Figure 6-2 Shear rate ramp and the specification of the steps of the hysteresis loop applied on the tests.

As it will be further presented, the cement pastes rheological behavior was not classified as "perfect" Bingham liquids yet endowed with shear-thinning behavior. However, the Bingham rheological parameters are extensively and commonly used as starting values, so they were calculated according to the following equation (Eq 6.1).

$$\tau = \tau_0 + \mu\dot{\gamma} \qquad \text{(Eq 6.1)}$$

Where τ is the shear stress, τ_0 the yield stress, μ is the plastic viscosity, and γ the shear rate. The parameters were calculated after the deflocculation with the

paste at the called equilibrium. That means that the yield stress and plastic viscosity were taken from the descending curve, the final 15 steps in Figure 6-3b. As mentioned above, the shape of the descending curve was far from a straight line. Thus, the yield stress was calculated considering the five last steps and the plastic viscosity, the first three steps from the descending curve. Those steps are highlighted in Figure 6-3b, where one can see the shear stress versus shear rate resulted from the application of the unloading part of the hysteresis loop, for the reference sample at 15 min. Additionally, the thixotropy was calculated as the area of the shear stress versus shear rate loading curve subtracted from the area correspondent to the unloading curve. This parameter is usually related to the energy stored within the particles of the fresh sample.

(a)

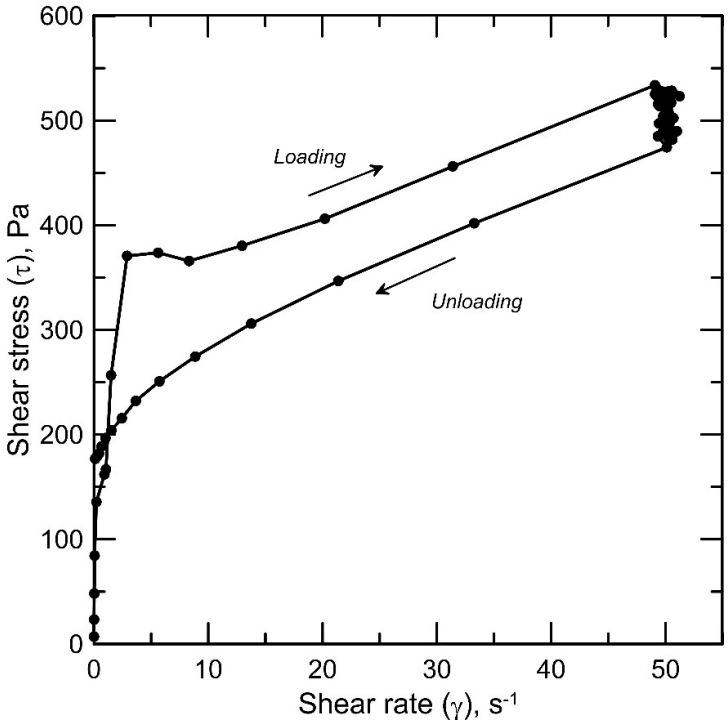

(b)

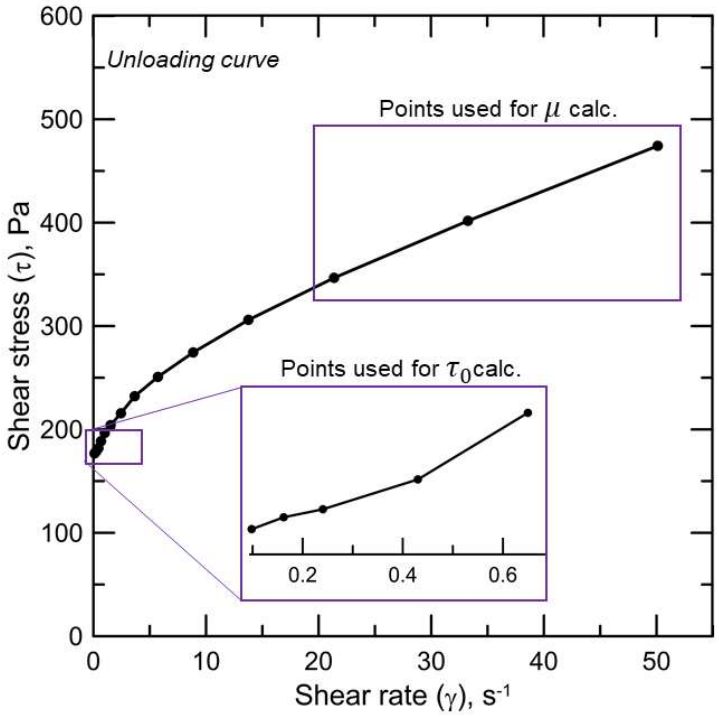

Figure 6-3 – (a) Shear stress versus shear rate of the hysteresis loop. (b) Points considered to calculate the Bingham parameters.

6.2.2.2.2. Static test

One of the strategies to measure the static yield stress of materials is the constant shear rate (CSR) method. With this technique, a considerably low shear rate is applied until a peak value or a plateau is reached. This value is attributed to the flow start and is considered the static yield stress (SYS) of the material at a specific age. Multiple measurements are performed along the time to assess the SYS value at different ages of the fresh cement paste. With the SYS versus time curve, it is possible to calculate the structural build-up ratio. The parameters chosen for the in-hand experiments were based according to the recommendations found in [14].

The mixing was carried out according to Table 6-2. In order to guarantee the deflocculation and corrected positioning of the vane, a pre-shear was performed at 14 minutes of age, in the form of a hysteresis loop. This pre-shear was the same applied to the dynamic tests, showed in Figure 6-2. After the pre-shear, the CSR was applied, at a chosen rate of 0.15 s^{-1}. The static yield stress (SYS)

measurements were conducted at 20, 25, 30, 35 and 40 minutes for the pastes. For each variation, the test was carried for at least two replicates. If the results differed from each replicate more than 8%, another sample was run.

The early age structural build-up evolution of cement pastes over time is characterized by linear evolution as it will be discussed on Section 6.3.2. Each static yield stress is plot according to the time of resting and the angular coefficient is understood as the structuration parameter (A_{thix}). This approach is known as the Roussel's model [15] and it was used due to the shape of the SYS versus rest time curve.

6.3. Results and discussion

To analyze all the results obtained, first, an overall screening regarding the flow behavior is made. Then, the results from the dynamic regime are presented, followed by a discussion about the possible acting mechanisms on Section 6.3.1.3.

6.3.1. Flow table test

Figure 6-4 presents the results obtained from the Haegermann flow table test. The spread diameters were normalized according to the reference (35_Ref). As a baseline, the average spread diameter of the reference sample was of 134.5 and 224.0 mm, before and after the strokes, respectively. The values of the percentage of inclusion can be divided into "low addition", including the 0.010, 0.025, 0.050, and 0.100%, and "high addition", with percentages of 0.50, 0.75, and 1.00%. From Figure 6-4, it is possible to notice the difference between the impacts of the two types of cellulose on the rheology of the cement pastes. The inclusion of the NFC led to a decrease in the cement paste flowability. The impact of the NFC was so meaningful that for matters of workability and equipment restriction, the NFC-samples was limited to the "low addition" range, up to 0.100%. However, under 0.100% of addition, the MCC presence led to an increase of workability, in comparison with the reference. It was only with values beyond 0.500% that the MCC particles worked against flowability.

The switch of behaviors between the samples with low and high additions can be clearly noted on the green curves in Figure 6-4. For instance, the addition of 0.01% of MCC resulted in an 11% wider diameter while 1.00% of MCC resulted

in 85% narrower diameter compared to the reference, before the strokes. This increase of flow face low additions, followed by a decrease of this parameter at higher percentages has been already observed with cellulose nanocrystals [2,3], and it will be carefully discussed ahead in Section 3.1.3.

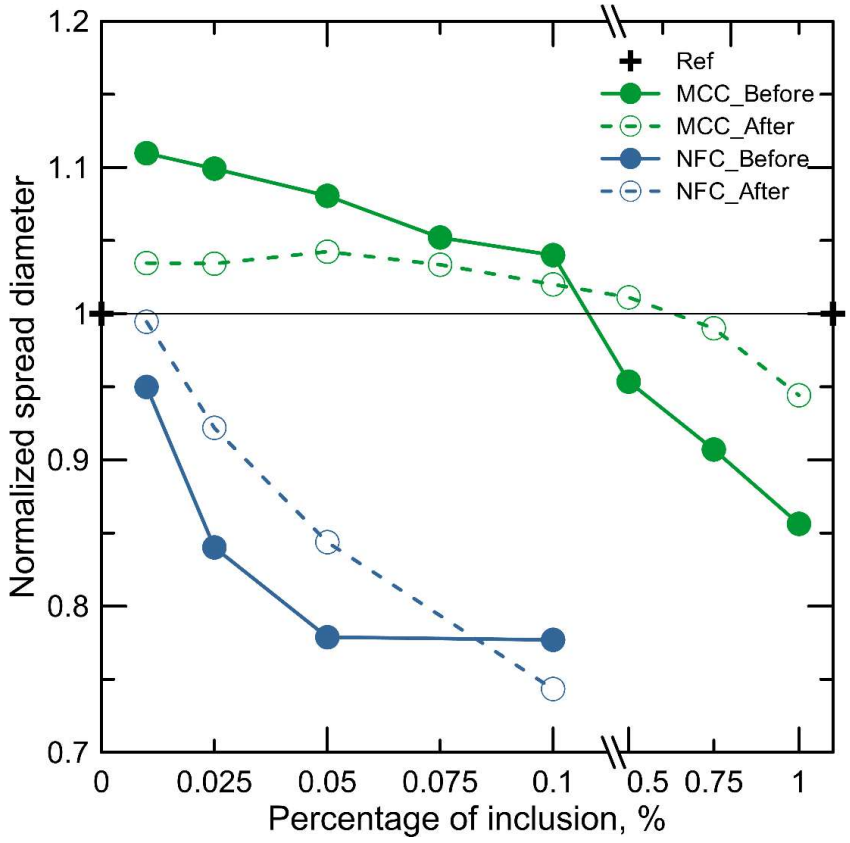

Figure 6-4 Average workability estimated by means of Haegermann flow table test, according to the percentage of each inclusion.

The NFC inclusion promoted, at all additions contents, a severe impact on the workability of the cement pastes. It is important to highlight that the influence on the values before the strokes is limited by the size of the apparatus used. That is the reason of the stabilized value of 0.78 reached for the inclusions beyond 0.050% of NFC. However, the spread diameter after the strokes was continuously narrower than the reference, represented by the values lower than 1.00. The addition of 0.100% of NFC lead to a decrease of 74% of the spread diameter. The same percentage of MCC addition had no significant impact, compared to the reference.

The "static condition" on the flow test, where there were no strokes or other acting movement, was more affected in both observed behaviors promoted by the

low and high additions of MCC. This effect was replicated to the NFC reinforced samples, except of course for those samples where the apparatus limitation was detected.

6.3.2. Dynamic

For the dynamic tests, the addition of 0.050% of MCC was selected as an exemplary of low addition percentage. Furthermore, samples with high addition percentages of 0.500%, 0.750% and 1.000% were investigated. The low addition range was used for the NFC-reinforced samples with the modification of 0.050% to 0.040% due to torque limitations of the rheometer used.

First, the results regarding the reference sample are exhibited and commented. The shear stress versus shear rate curve and the apparent viscosity versus shear rate of the reference sample at the age of 15 min are presented in Figure 6-5 and in Figure 6-6, respectively. Multiple comparisons between its behavior and the others' samples are made along the following topics. The calculated parameters at 15 minutes of age are presented in Table 6-3.

Table 6-3 Parameters calculated from the curves obtained from the dynamic tests. The units are displayed for each parameter. The samples were 15 min aged.

Mixture	Bingham parameters		Energy,
	Yield stress, Pa	*Plastic viscosity, Pa*s*	
35_Ref	173.6	4.53	3.60
35M_0050	189.9	5.20	4.68
35M_0500	253.1	6.18	6.22
35M_0750	314.5	6.98	5.85
35M_1000	338.6	7.07	6.41
35N_0010	237.4	5.28	5.14
35N_0025	309.2	5.69	6.43
35N_0040	410.4	5.42	6.45

The evolution of the yield stress and the plastic viscosity over time, until 120 minutes of the reference is showed in Figure 6-7-a and b, respectively. After 60 minutes, the yield stress was significantly and continuously increased as the hydration reactions contributed to the formation and strengthening of the mineral skeleton of the paste. From 15 minutes of hydration to 120 min, the yield stress

went from 173.6 to 225.7 Pa. The applied hysteresis loop and the strain rate level have influence on the rheological behavior of cement fresh materials [16]. The maximum viscosity value achieved was of 4.53 Pa.s at 15 min. After this age, the viscosity continually decreased until the age of 60 min. Then, the viscosity values tended to rise until the end of the test, 120 min.

6.3.2.1. MCC

Figure 6-5 shows the shear stress versus shear rate curves of the samples with MCC, at 15 minutes of age. In comparison to the reference's curve, the MCC addition led to a stress increase in all rates and at all percentages investigated. The low addition of 0.0500% resulted in a non-significant increase of the stress, which was expected according to the flow table test results shown in Figure 6-4. It is possible to notice the "gap" between the low and the higher additions on the shear-strain curves. Besides the shear stress, the Bingham parameters, namely yield stress and plastic viscosity, also increased, as shown in Table 6-3. At 15 minutes, the addition of 0.05%, 0.50%, 0.75%, and 1.00% of MCC resulted in yield stress increase of 9%, 46%, 81%, and 95%, respectively.

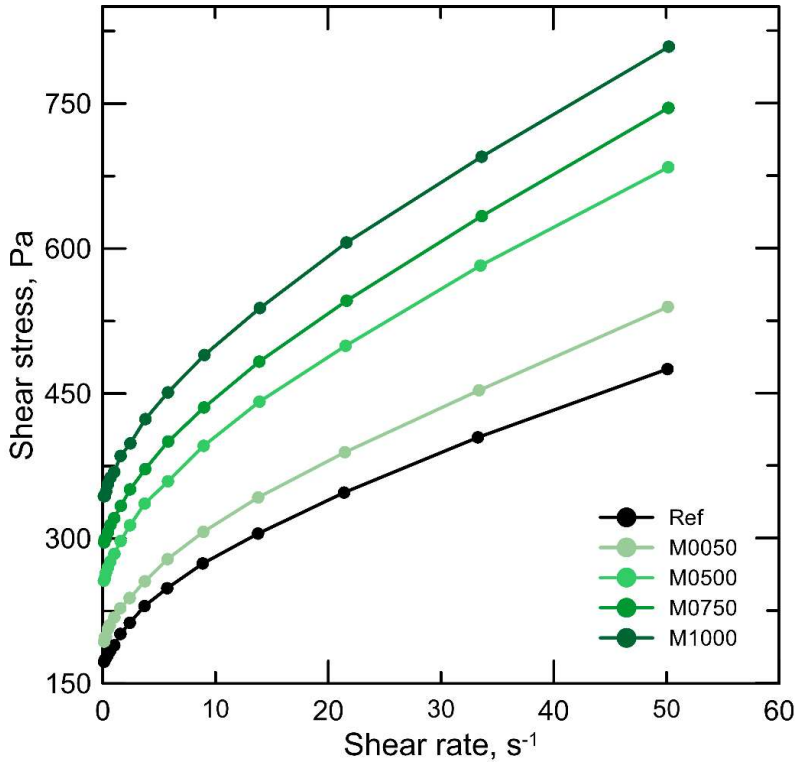

Figure 6-5 Shear stress *versus* shear rate curves of the samples with and without MCC inclusion, at the age of 15 minutes.

The apparent viscosity was also recorded by the rheometer system and Figure 6-6 shows the results. The decrease of the viscosity with the increase of the shear rate is a typical behavior found on materials known as “shear-thinning”. The addition of MCC headed to a strengthening of this shear-thinning behavior. As more MCC was present on the mixture, the higher the initial apparent viscosity was, and more abrupt the drop of this value. The difference between the reference and the samples with MCC was more perceptive at the initial rate, until 3 s^{-1}. After that, the values came closer although the ones presented by the samples with MCC were always higher.

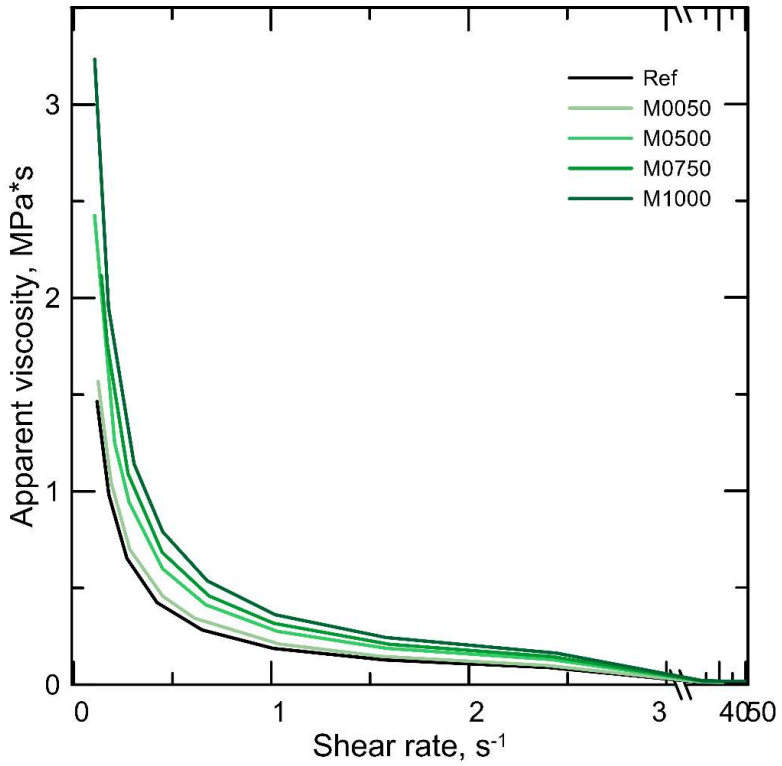

Figure 6-6 Apparent viscosity of the samples with different percentages of MCC of the samples at 15 minutes. The x-axis is interrupted from the shear rate 3 s^{-1} until 40 s^{-1} for highlighting where the difference was more perceptible.

Figure 6-7 presents the evolution of the yield stress and the plastic viscosity over time, until 120 minutes of the samples with MCC. Those parameters were calculated as described in 2.2. The first highlight is regarding the test duration. The inclusion of 0.05% and 0.50% led to a decrease of the test duration in 15 min and the inclusion of 0.75% and 1.00%, in 30 min. This was due to the torque limitation at the beginning of the hysteresis loop. The effect of the MCC on the development of the yield stress was given by an up-shift of the curve, in relation

to the reference, to higher values but essentially a similar shape. This shift reached higher values for higher percentages of MCC. If comparing the difference between the ages of 15 and 90 minutes, the increase of the yield stress was in the order of 10%. At 90 minutes, the inclusion of 0.05%, 0.50%, 0.75%, and 1.00% of MCC resulted in yield stress increases of 8%, 38%, 69%, and 94%, respectively. This increase of around 94% in the yield stress was approximately the same for all ages, when comparing the 35_Ref and 35M_1000 average results.

(a)

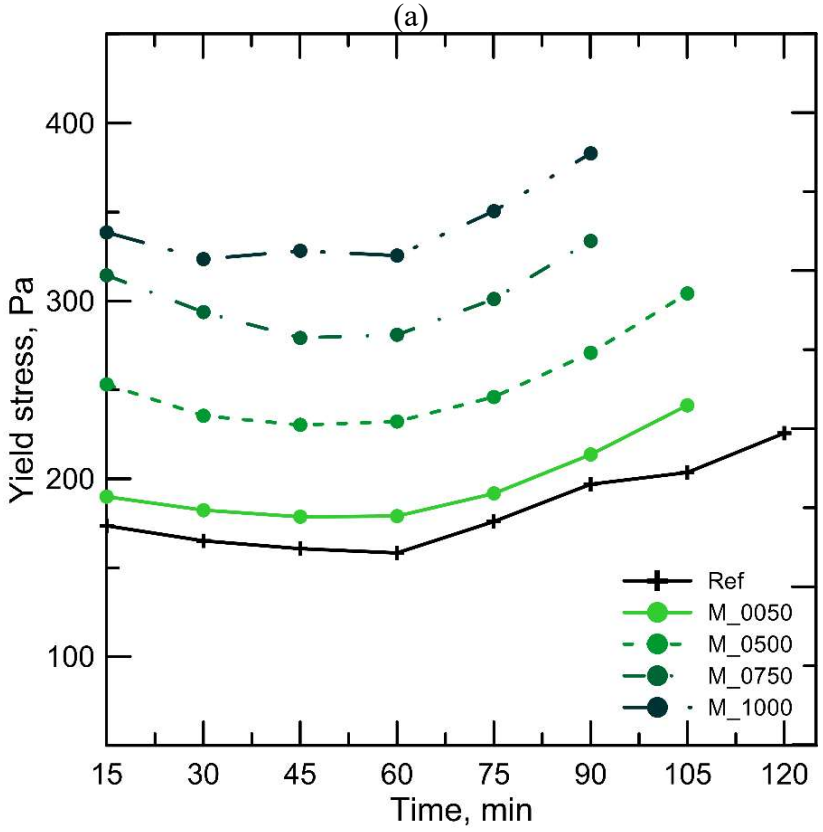

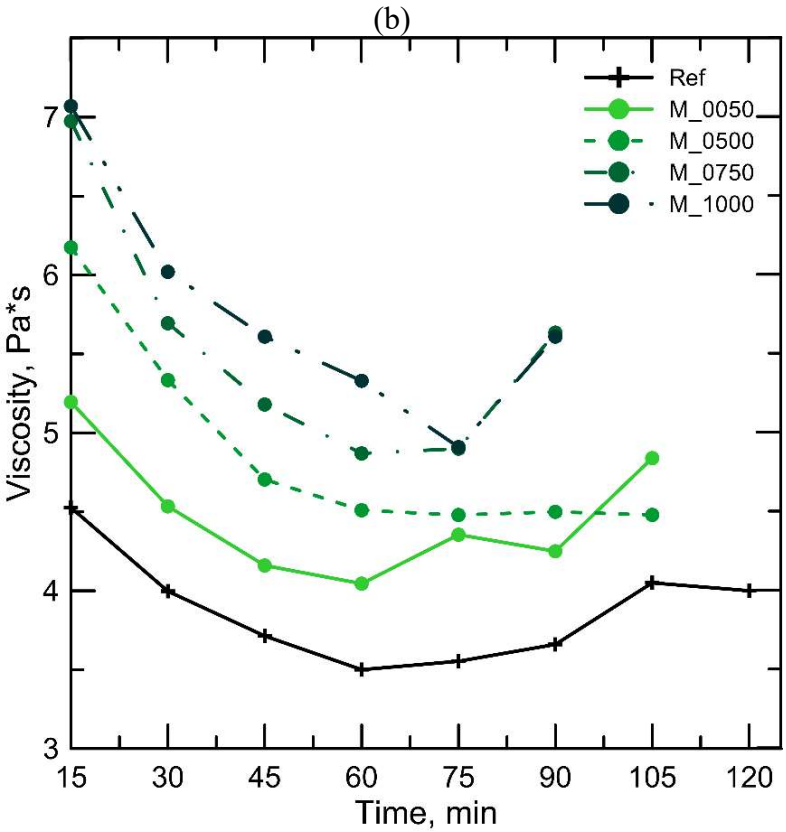

Figure 6-7 – (a) Yield stress and (b) plastic viscosity obtained for the dynamic test of the samples without (reference) and with different amounts of MCC, over time.

When analyzing the viscosity behavior upon the addition of MCC in Figure 6-7b, one can notice that again, the trend was nearly the same, with higher values though. The maximum viscosity value took place at the first measurement at 15 minutes, for all the MCC-samples, followed by a considerable decrease until around 60 minutes. Beyond this age, there was a recovery of the viscosity values, which was sharper for the samples with MCC, specially at the age before the end of the test. The initial increase in viscosity when the MCC was added was of 15%, 36%, 54%, and 56%, in relation to the reference.

The more intensive influence on the yield stress than on the plastic viscosity promoted by the MCC has already been observed [17]. The possible cause for this behavior is brought in section 3.1.3. Usually, when MCC is added to cementitious materials with inclusions percentages of more than 0.2%, a reduction of the flowability of the fresh material is observed [17–19]. Those observations were made at inclusions percentages of more than 0.2%. However, as observed in

Chapter 3, the MCC addition not always lead to a decrease in workability [20,21]. A similar behavior is found in mixtures containing cellulose nano crystals [2,4].

The effect of the MCC on cementitious materials' rheology is usually attributed to the increase of interactions when the MCC is added: besides the cement particles-water molecules interactions, there are now the MCC-cement particles and MCC-water molecules interactions. Those interactions may be driving by the -OH presence and the water retention capacity that decreases the free water on the fresh cement pastes.

6.3.2.2. NFC

The shear stress versus shear rate curves resulted from the first application (15 minutes) of the hysteresis loop on the samples with different percentages of NFC is found in Figure 6-8. As expected, the inclusion of NFC led to an increase of the shear stress at every shear rate tested. This effect was similar to the observed on MCC-reinforced samples although once again at considerably lower percentage of inclusion. The addition of 0.010% of NFC led to more pronounced changes in the stress-strain curve, and consequently on the Bingham's parameters, then the ones observed for the 0.050% of MCC, as shown on Table 6-3.

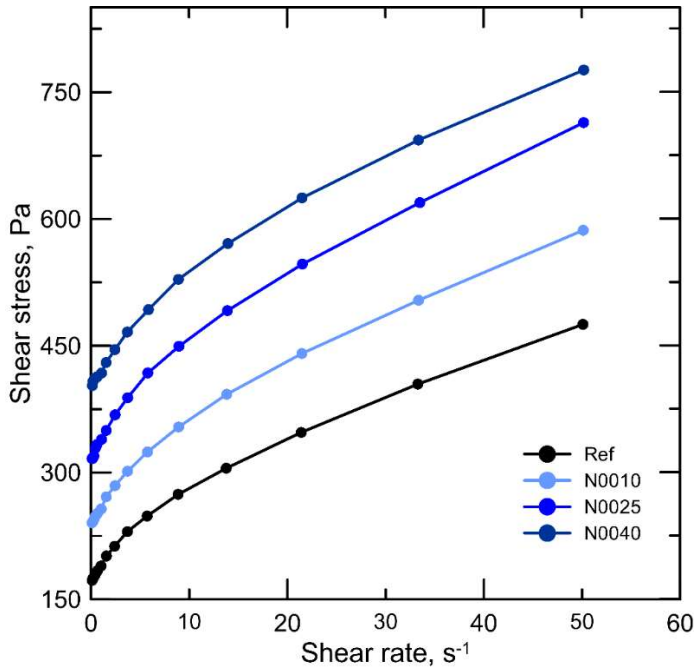

Figure 6-8 Shear stress *versus* shear rate curves of the samples with NFC inclusion and the counterpart reference, at the age of 15 minutes.

Figure 6-9 Apparent viscosity of the samples with different percentages of NFC, at 15 minutes. The x-axis is interrupted from the shear rate 3 s-1 until 40 s-1 for highlighting where the difference was more perceptible.shows that the initial (at 15 min) apparent viscosity values increased with the increase of NFC's presence on the cement paste. Some characteristics of the viscosity curves may be mentioned as the fact that all values presented by the mixtures with NFC were higher than the reference. However, the difference between the maximum and minimum values was more significant for the samples with NFC, emphasizing the steeper trend of decreasing the viscosity values after the initial measurement.

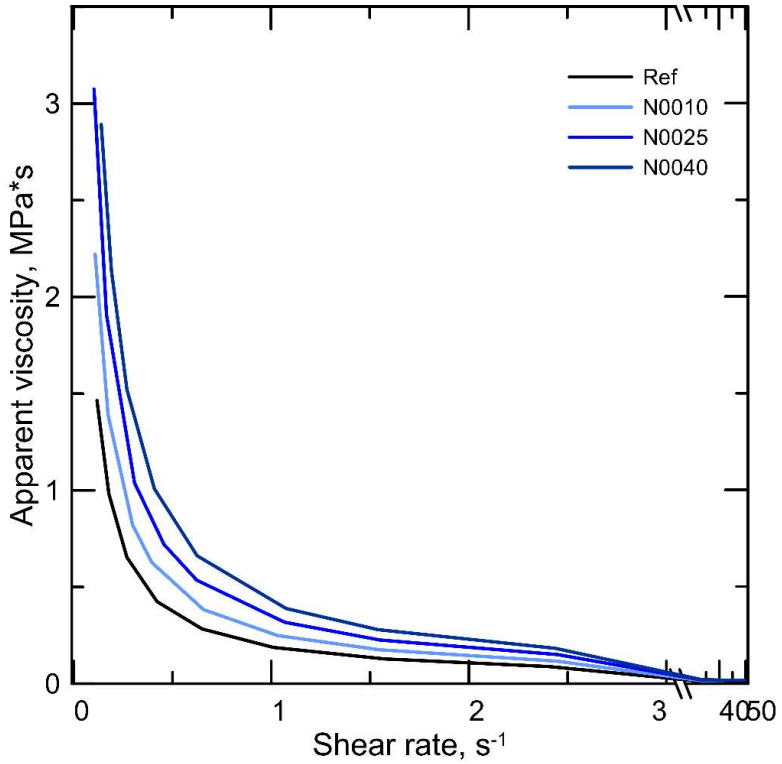

Figure 6-9 Apparent viscosity of the samples with different percentages of NFC, at 15 minutes. The x-axis is interrupted from the shear rate 3 s^{-1} until 40 s^{-1} for highlighting where the difference was more perceptible.

Figure 6-10a and b show the yield stress and plastic viscosity of the samples with NFC, respectively, over time. The initial (at 15 minutes) yield stress of the samples with 0.000%, 0.010%, 0.025%, and 0.040% of NFC was 173.6, 237.4, 309.2, and 410.2 Pa, respectively. This represents an increase of the yield stress value in 37%, 78% and 136% in comparison to the reference. Interestingly, the test time decreased in 15 min as each increase of NFC percentage, representing

the progressively growing stiff of the paste. Similar to the reference, the yield stress of each sample began to significantly increase after the first 60 minutes of age, although at a higher rate than the reference.

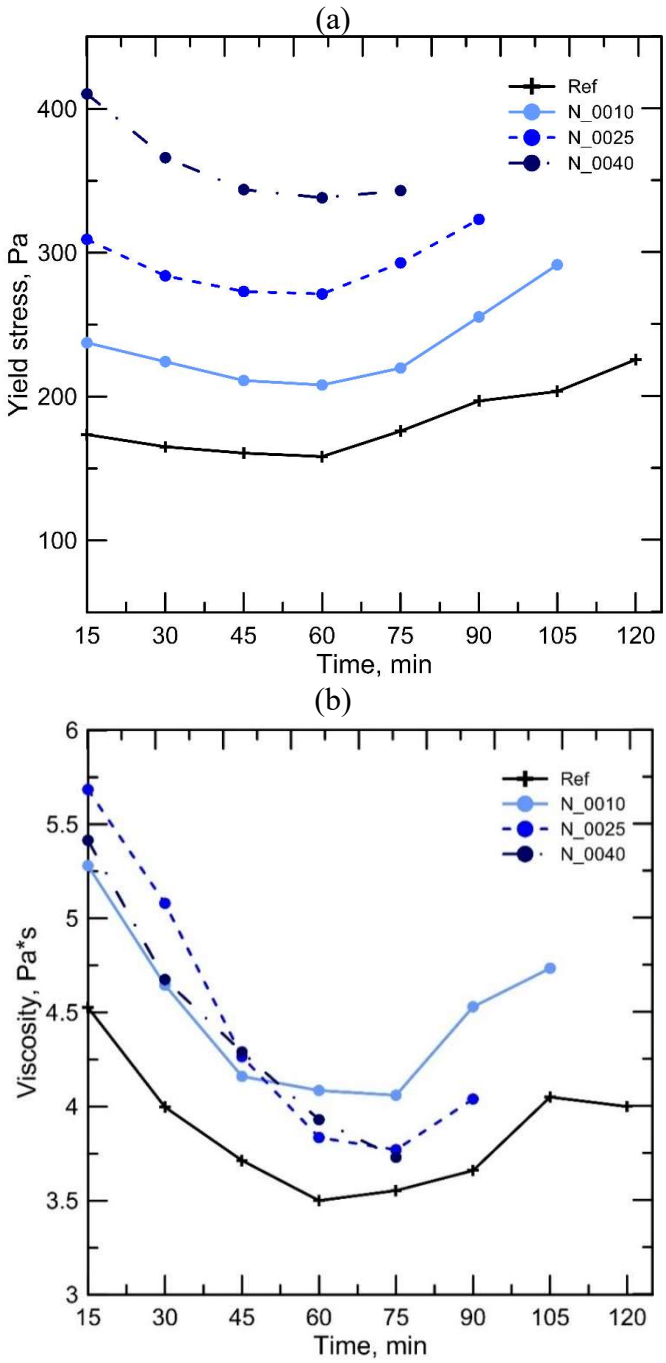

Figure 6-10 - (a) Yield stress and (b) plastic viscosity obtained from the dynamic test. Samples without (reference) and with different amounts of NFC, over time.

The plastic viscosity development of the samples with NFC presented different behavior between the variations of NFC. The N_0025 and N_0040 samples reached their minimum viscosity value 15 minutes later than the reference. However, the sample N_0010 presented a "viscosity plateau" between 45 min and 75 min, with a further significant increase of this parameter. The N_0040 did not show the "recovery" of the viscosity value since the test duration was limited for this variation.

It seems to be a consensus of the Literature on this topic that the cellulose fibrils' presence decreases the flowability of cementitious materials [4–10]. The possible reasons for this behavior are discussed in the following sections.

6.3.2.3. Comparison between MCC and NFC effects

Figure 6-11 gathers the values of the Bingham's parameters, namely yield stress and plastic viscosity, of all variations here investigated. In this way, the comparation between MCC and NFC effect is more straightforward. The results include the first and final measurements common to all mixtures. Both cellulosic materials increased the yield stress and plastic viscosity values. However, it is perceptible that the NFC had a greater impact on the yield stress, resulting in higher values of this parameter. The higher values obtained from the NFC-reinforced mixtures mean that the paste became stiffer from a macroscopic point of view. On the other hand, the MCC affected more the plastic viscosity, promoting an even more expressive shear-thinning behavior than the NFC did.

Although the outcomes present similarity, namely higher yield stress and viscosity, the mechanisms microscopically acting can be distinct for each inclusion. As addressed in Chapter 2 (Section 2.2.1), the interaction forces responsible for the rheological behavior of cementitious materials are affected by the solid particles' characteristics [16]. In addition, the hydration reactions gradually change the flocculation configuration. When other solid components are added to the system, they change the interparticle dynamic, besides integrating their own characteristics. Thus, the morphological aspects of each cellulosic material influence the resulting behavior. The interparticle interactions are usually intensified when the particle size decreases [22,23], so the fact that NFC size distribution is considerably smaller then MCC, see Chapter 3, should be already taken into account on the assessment. Moreover, the shape and the surface area

characteristics are related to how available the hydroxyls are for the hydrogen bonds.

Obviously, one thing in common between NFC and MCC it is main chemical constituent – cellulose – and the presence of the hydroxyl groups. The OH- interactions with cement particles are usually claimed to be one of the possible reasons for the increase of the shear stress. However, NFC and MCC present distinct production processes (Chapter 2, Section 2.1), resulting in differences on the functional groups [3]. Thus, although present in both materials, the OH- interactions can unequally act on each system.

The hydrophilicity of the NFC plays an important role in the flow development of flow behavior of the fresh cement mixtures. The flow behavior is highly dependent on the w/c ratio since the suspension characteristics are related also to the liquid part [16]. As more water the paste presents, more disconnected the particles are, changing the flocculation degree. When NFC is added to the system, the fibrils capture part of the mixing water, as demonstrated by the bleeding tests in Chapter 4. Once there is less water available into the system, the solid proportion increases, resulting in a closer cement-cement and fibrils-cement linkages. The MCC is also hydrophilic, although their water retention capacity is significantly lower than NFC's.

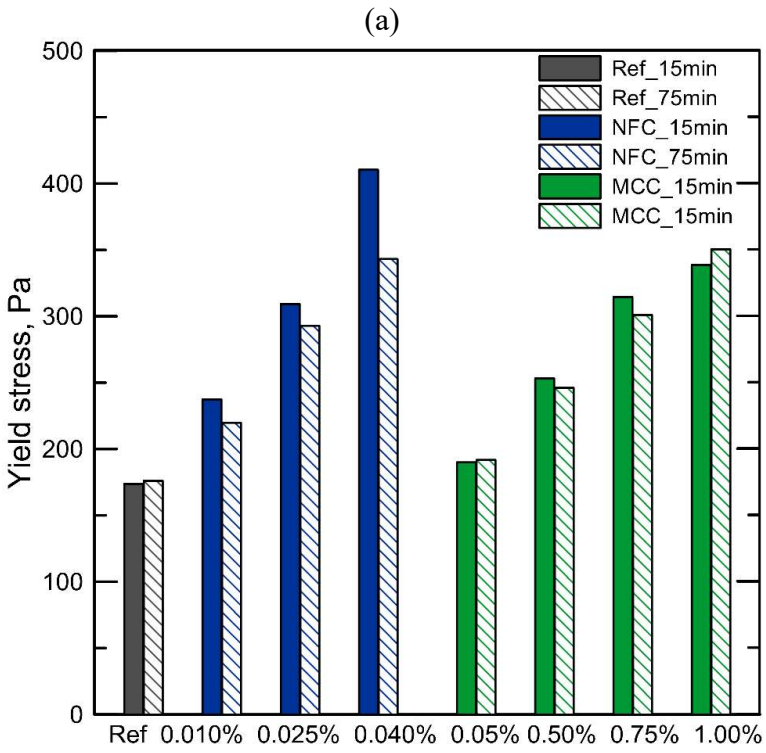

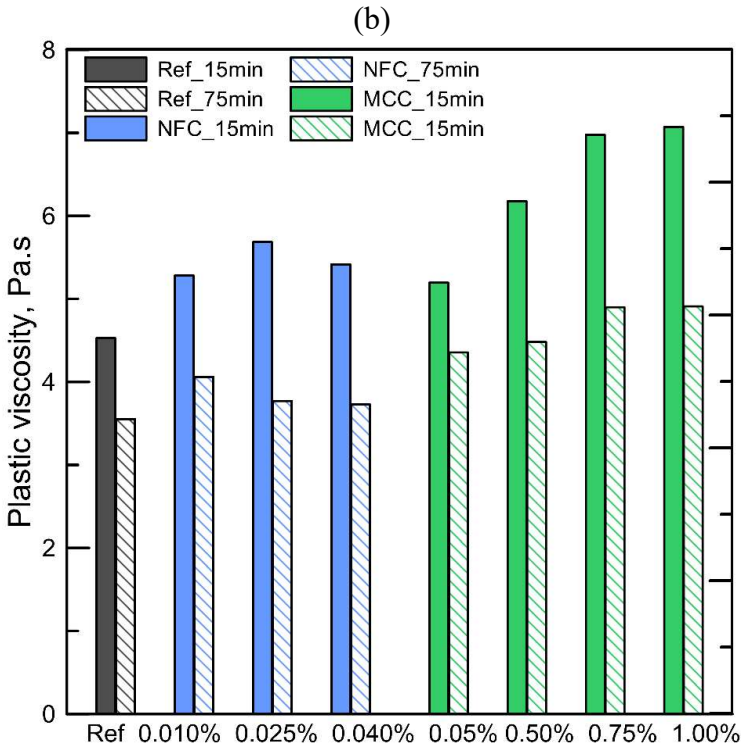

Figure 6-11 Comparison of the effect of both inclusions, NFC in blue and MCC in green, on the rheological parameters: (a) yield stress and (b) plastic viscosity, at 15 min and 75 min.

Although the morphological differences lead to unique water retention capacities, one key difference between the dynamic behavior may rely on the rheological properties of the gel itself. Figure 6-12 brings the shear stress versus strain curve of the NFC gel. From the curve, the yield stress of the gel is 7.5 Pa. It is possible to observe that the gel itself presents a shear-thinning behavior, as constated elsewhere [10]. When added to the fresh mixture, the gel can bring part of its stress resistance contribution. However, if first the fibrils mutually act with the cement particles, this scenario evolutes with the development of the hydration products.

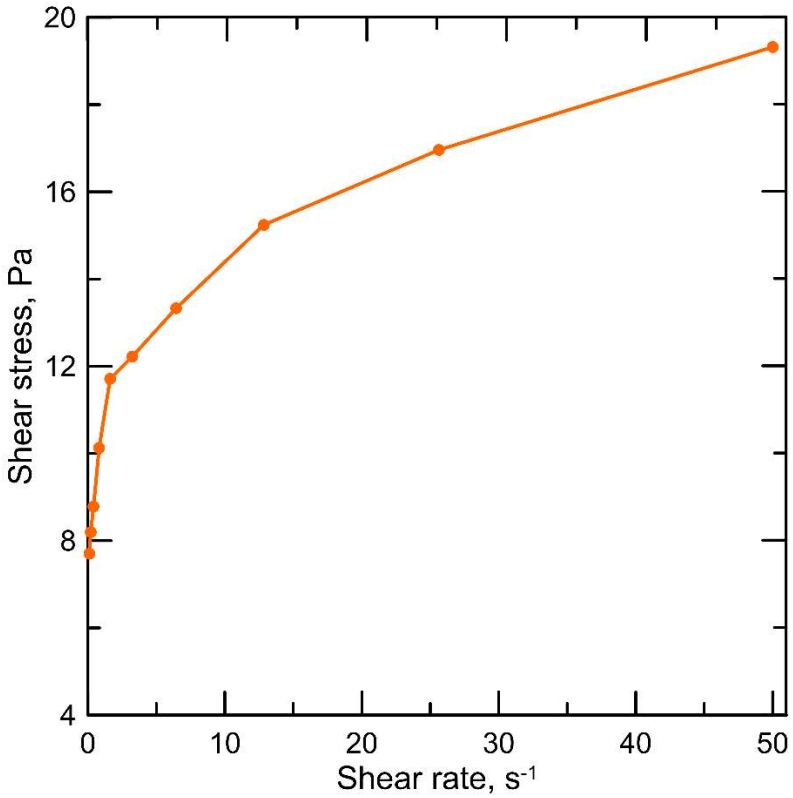

Figure 6-12 Shear stress versus shear rate curve of the NFC gel.

The yield stress can be taken as the minimum shear stress required so the material start to flow. As mentioned, both MCC and NFC presence into the mixture increased this parameter, but with even higher values presented by NFC-reinforced ones. The basic mechanisms behind this behavior are based on the cellulosic morphology. The NFC presents a significantly higher value of water retention capacity, affecting mostly the local w/c ratio. This feature makes that the cement particles and the solids fibrils are closer to each other, intensifying their interactions. In addition, the NFC's long fibrils can be easily entangled, and the formed network can be more effective on the increasing of the energy required to start the flow than the clusters probably formed by the MCC.

How difficult it is to break the colloidal system is represented by the plastic viscosity. Since the cellulosic inclusions increased the shear stress at all shear strain values, it is acceptable to relate part of the viscosity increase to the higher shear stress. Although both MCC and NFC inclusions led to an increase of this parameter, the plastic viscosity reached higher initial and final values on the mixtures with MCC. The entangled mesh promoted by the NFC long fibrils that

represented an obstacle to initiate the flow, at high values of shear rate they could have been dissolved. The fibrils are flexible, and they could also be oriented to the flow direction, instead of opposing to it. Moreover, it is possible that with the shear rate history given, the NFC could have started to release some of the retained water.

Another possible reason for the viscosity attenuation is the entrapped air [8]. The higher porosity profiles showed in Chapters 3 and 4, especially for the specimens reinforced with NFC, can mitigate the viscosity gain by releasing the air present in the fresh mixtures. The air does not represent a barrier to the applied shear.

6.3.3. Static

The percentage variations of MCC and NFC considered on the static regime were the same as the ones presented in the dynamic tests. The results presented in this section are the average of at least two replicates, and they did not show a deviation value of more than 6%. One extra section to discuss the role of the water present in the NFC gel is addressed.

6.3.3.1. MCC

The evolution of the static yield stress (SYS) over time is showed in Figure 6-13. It is possible to observe that there is a gain in the SYS with time, as expected since the evolution of the hydration reactions promotes a stiffer matrix. In comparison with the reference, the MCC promoted a stiffer matrix on the mixtures with high addition of MCC. Taking the reference as a baseline, there is a significant difference between the low and high MCC addition ranges. The low addition of 0.050% of MCC led to inferior SYS values at every age of the paste. While the addition of 0.500%, 0.750% and 0.100% cause a progressive increase of the same parameter. This result was closer to the one observed in the flow table tests, where there also was a distinction on the behavior between the low and high additions of MCC. The flow table test and the static test (CSR) are obviously more similar to each other than when the dynamic is considered due to the shear movement. At this stage, it is possible to perceive the steric stabilization effect manifestation, which is commonly used to explain the behavior of dispersing the

cement particles [10,24,25]. Above the addition of 0.500% of MCC, the increase of the SYS value is visible, and one can attribute this effect to the interactions promoted by the MCC particles to the cement-water-MCC system.

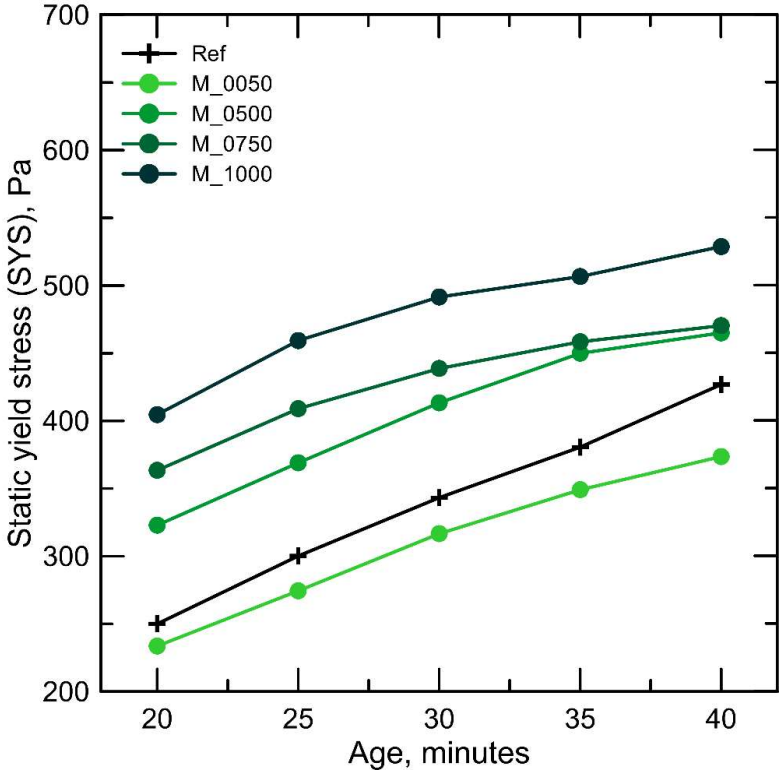

Figure 6-13 The evolution of the static yield stress (SYS) over time for the mixtures with MCC (in green), and the reference (in black) for comparison.

Comparing to the nanocrystals effect, the MCC addition presented a non-monotonic behavior on the static regime, showing some discrepancy between the low and high addition ranges. When this behavior is observed, it usually indicates that there are two competing forces. In this case, the electrostatic repulsion known as steric stabilization effect, and the MCC agglomerates forming clusters. At a low percentage, the dominant effect is the steric stabilization; at high percentages, the interactions promoted by the -OH groups and the formation of MCC clusters prevails. By the results obtained from the table test analysis in Figure 6-4, the threshold percentage between the two effects' predominance is 0.100%. Figure 6-14 shows a scheme of the scenario.

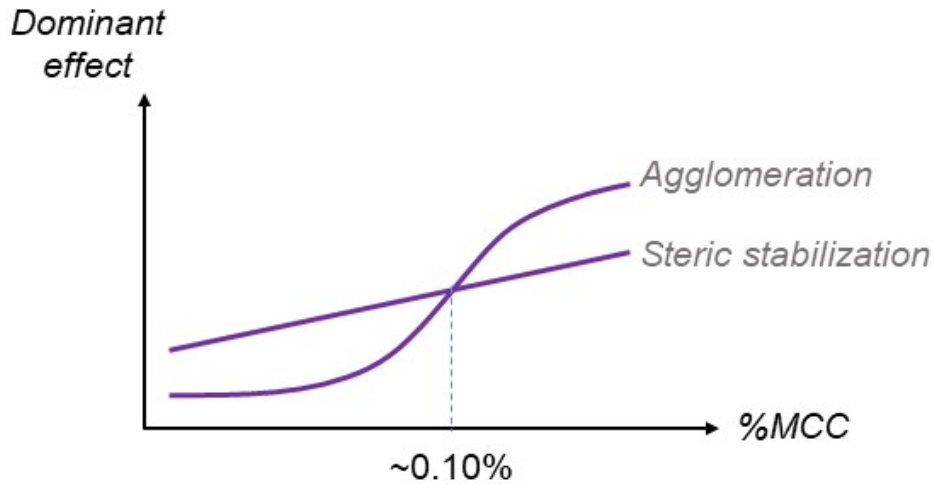

Figure 6-14 - Scheme of the non-monotonic effect of MCC inclusion on static rheological behavior of cement pastes.

Despite the superior SYS values reached by the MCC-reinforced samples, after 35 min there is a decrease on the stress rate gain. This trend was followed for all mixtures with high addition of MCC, as indicated also by the Athix index value showed in Table 6-4.

6.3.3.2. NFC

The static yield stress (SYS) values reached by the samples with NFC at different ages are shown in Figure 6-15. Different from the MCC's results (Figure 6-13), every inclusion percentage of NFC led to an increase of the SYS at all ages analyzed. The inclusion of 0.010%, 0.025% and 0.040% of fibrils increased the initial, at 20 min, SYS in 28%, 64% and 103%, respectively.

Similar to the MCC-reinforced mixtures, there was a reduction of the SYS rate gain at 35 min on the samples with 0.010% and 0.025% of NFC. The N_0040 trend was more distant from a straight line. There was no improvement of the parameter Athix calculated from the Russel's model, as displayed by the Table 6-4. From the initial stress values also showed in Table 6-4, the acting mechanism that were responsible for the improvement of the dynamic parameters discussed in section 3.1.3 are still active on the static state. However, the inferior values of the Athix parameter can indicate that further in time, the water retained by the NFC hydrophilic and nanofibrillated structure could be released again in the system. This can result in the lower SYS gain rate. The Athix values were only inferior

due to the measurement taken after 30 minutes. In addition, the effect of the NFC on the mineral skeleton development investigated by means of ultrasonic pulse velocity (Chapter 5), showed that the fibrils alter the hydration evolution.

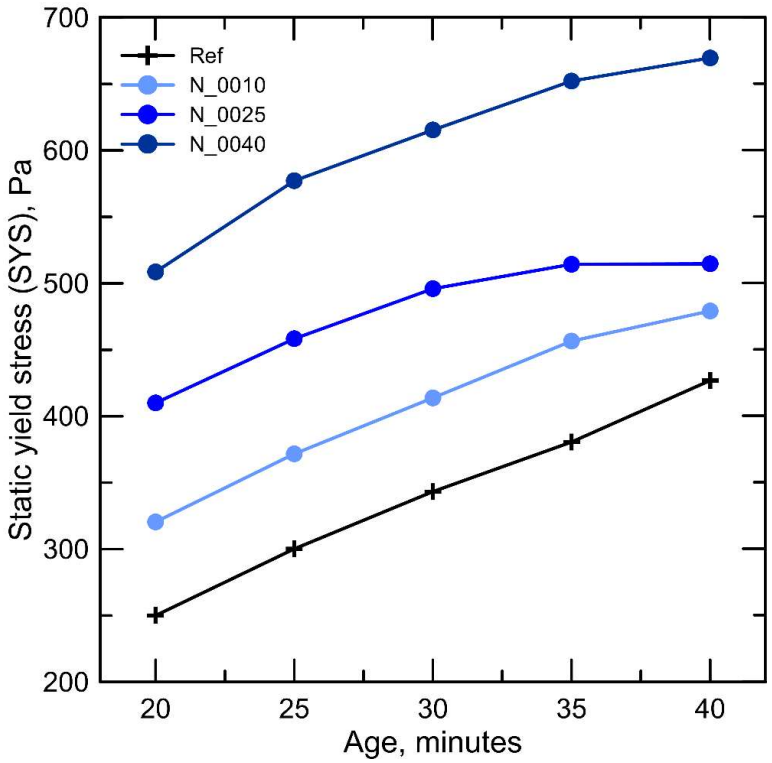

Figure 6-15 The evolution of the static yield stress (SYS) overtime for the specimens with NFC (in blue), and the reference (in black) for comparison.

If one compares the ability of enhancing the structural build-up based on the SYS values, it is clear that the use of NFC was more efficient in comparison to the MCC's one. Furthermore, the initial stress values were significantly higher on the NFC-reinforced samples, indicating the stiffer condition.

Table 6-4 Structural build-up parameters calculated based on Roussel's model [15].

Mixture	Roussel's model	
	Athix, Pa/min	*Initial stress, Pa*
35_Ref	8.7	79.6
35M_0050	7.1	96.6
35M_0500	7.3	184.9
35M_0750	5.3	270.0
35M_1000	5.9	300.8
35N_0010	8.0	166.9
35N_0025	5.3	319.4
35N_0040	7.9	366.3

6.3.3.2.1. The water in the NFC gel

Through the development of each Chapter of the present work, the amount of water that was effectively available as mixing water on the mixtures with NFC was a matter of discussion. A brief investigation on the effect of the water present on the NFC gel is presented, based on two different water-to-cement ratios, 0.35 and 0.40. For this purpose, only the percentage of 0.025% of NFC was considered. The two additional mixtures used for this objective were designed as follows:

- Ref_LW: when the water present in the gel is subtracted from the composition, there is an assumption that the rheological changes are only due to the water retention.
- N_0025_EW: the presumption is that the water present in the gel does not contribute to the mixing water of the original mixture.

The composition of each mixture can be found in Table 6-1. Figure 6-16a brings the results of the variations with w/c equals to 0.35. At this w/c level, when the amount of water present in the gel was suppressed from the total water, sample 35_Ref_LW, the SYS development was comparable yet lower to the effect of adding 0.025% of NFC (sample 35N_0025). For 35N_0025_EW variation, there was an increase in SYS values compared to the reference. Those results indicate that the retained water is a possible prevailing factor of the rheological behavior of the mixtures with NFC. Nevertheless, the SYS values presented by

35N_0025_EW suggest that there is another effect besides the water present in the gel that contributes to the rheological effect of the NFC. Based on the Literature, one can attribute it to the fibrils' interactions with the cement particles and also to the fibrils entanglement [4,8,26].

It has been already observed that the water retention ability of the cellulose fibrils depends on the w/c ratios, as shown by the bleeding results on Chapter 5. With that in mind, the w/c equals to 0.40 was included in the investigation. The results are shown in Figure 6-16b and it shows a significant difference on the values obtained in comparison to the 0.35 ratio. When the water in the system is increased, it seems that the effect promoted by the water present in the gel loses its intensity. This is shown by the values distance between 40N_0025 and 40_Ref_LW samples. In this case, the results suggest that the effect of the fibrils is overriding the water retention's one.

The objective of this section was to shed light on whether the water present in the gel is fully available as the mixing water. The results brought throughout the present work has shown that it depends mainly on the w/c employed. When combining the proper w/c, as discussed in Chapter 2, to a specific NFC percentage, one can achieve promising results regarding the rheological stability.

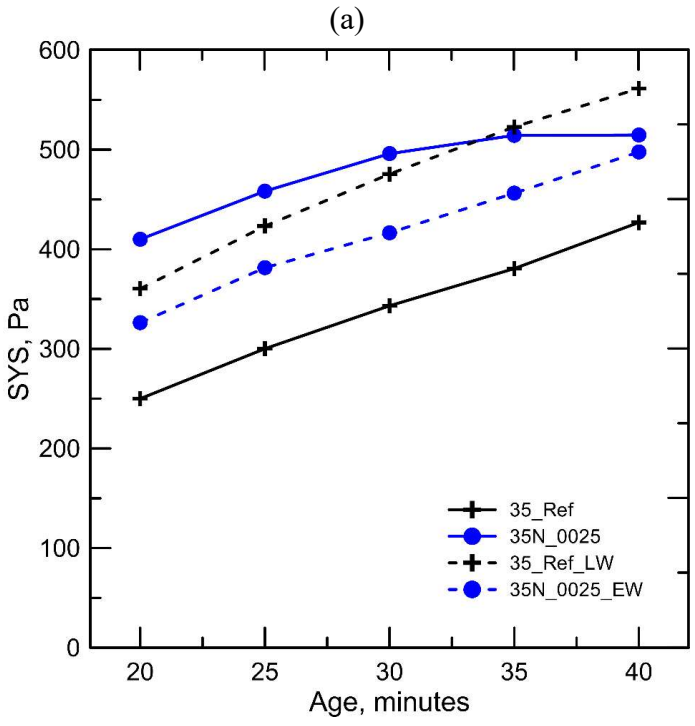

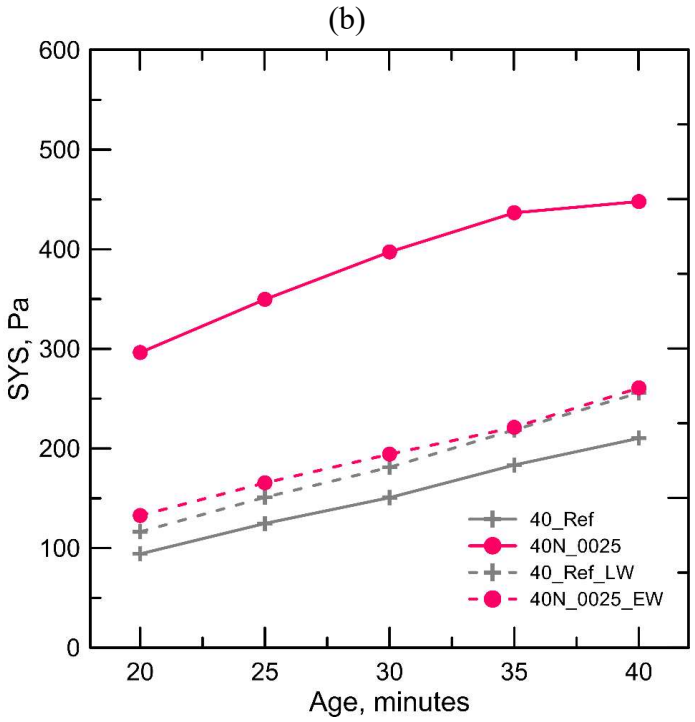

Figure 6-16 The static yield stress (SYS) evolution for samples with 0.025% of NFC, considering the changes on the water amount. Samples with w/c ratio of (a) 0.35 and (b) 0.40.

For a matter of illustration, Figure 6-17 brings a comparison of how the inclusion of only 0.025% of NFC gel impacts the cement pastes of different water-to-cement ratios.

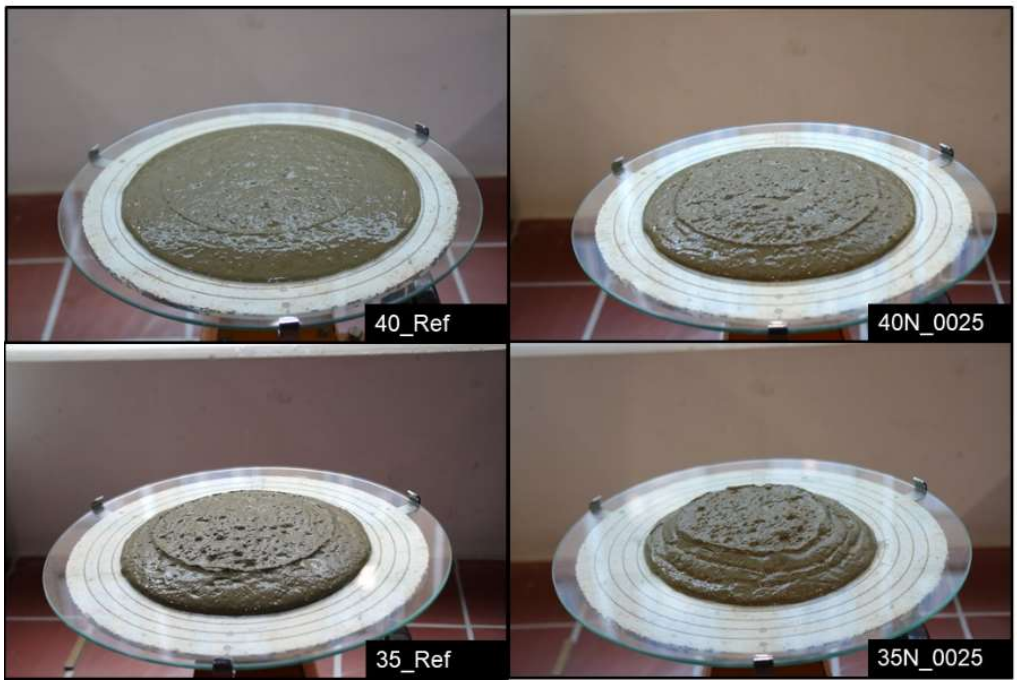

Figure 6-17 Cement pastes of different w/c, namely 0.35 and 0.40, submitted to the flow tablet test after the strokes..

6.4. Conclusions

Regarding the findings about the use of MCC and NFC on the dynamic and static rheological behaviors of cement pastes it is possible to draw the following conclusions.

- The inclusion of both MCC and NFC led to an enhance of the shear stress at every level of strain rate from the hysteresis loops applied. For the MCC-reinforced specimens, this effect was more pronounced on additions higher than 0.500%.
- The two cellulosic inclusions resulted in strengthening of the shear thinning behavior, where both apparent and plastic viscosity values were higher as more cellulose micro and nanofibers were into the paste.
- The values of the Bingham's parameters, namely yield stress and viscosity, were also increased in the presence of MCC and NFC. The main difference was that the NFC inclusion had a more significant effect on the yield stress whereas the addition of MCC on the viscosity.
- The steric stabilization effect was observed on the static and on the flow table tests for additions under 0.500% of MCC.

- The initial, at 20 min, SYS value increased from 250 Pa to 405 and 509 Pa upon the addition of 1.00% of MCC and 0.04% of NFC, respectively. Nevertheless, the MCC and NFC presence led to a slight decrease in the Athix parameter value.
- There were indications that the water present in the gel is only partially available as mixing water, being one of the factors that affects the rheological behavior of the NFC-reinforced pastes. Besides that, the fibrils entanglement and agglomeration also influence the dynamic and static rheological response. Those effects depend on the w/c analyzed.

It is important to remember that all investigations conducted considered very different amounts of MCC and NFC. The MCC range was from 0.050% to 1.000%, while NFC comprehended 0.010% to 0.040%. On top of the possible factors that affect the rheological behavior of the pastes, the NFC gel itself presents a shear thinning behavior, with yield stress of around 7.5 Pa.

6.5. References

[1] ZHANG, C. *et al*. Mix design concepts for 3D printable concrete: A review. **Cement and Concrete Composites**, v. 122, n. February, p. 104155, 2021.

[2] CAO, Y. *et al*. The influence of cellulose nanocrystal additions on the performance of cement paste. **Cement and Concrete Composites**, v. 56, p. 73–83, 2015.

[3] MONTES, F. *et al*. Rheological impact of using cellulose nanocrystals (CNC) in cement pastes. **Construction and Building Materials**, v. 235, p. 117497, 2020.

[4] TANG, Z. *et al*. Influence of cellulose nanoparticles on rheological behavior of oilwell cement-water slurries. **Materials**, v. 12, n. 2, p. 1–14, 2019.

[5] SUN, X. *et al*. Rheology, curing temperature and mechanical performance of oil well cement: Combined effect of cellulose nanofibers and graphene nano-platelets. **Materials and Design**, v. 114, n. August, p. 92–101, 2017.

[6] SUN, X. *et al*. Cellulose Nanofibers as a Modifier for Rheology, Curing and Mechanical Performance of Oil Well Cement. **Scientific Reports**, v. 6, p. 1–9, 2016.

[7] KOLOUR, H. H. *et al*. An investigation on the effects of cellulose nanofibrils on the performance of cement paste and concrete. **Advances in Civil**

Engineering Materials, v. 7, n. 1, p. 463–478, 2018.

[8] HISSEINE, O. A.; OMRAN, A. F.; TAGNIT-HAMOU, A. Influence of cellulose filaments on cement paste and concrete. **Journal of Materials in Civil Engineering**, v. 30, n. 6, p. 1–14, 2018.

[9] HISSEINE, O. A. *et al*. Feasibility of using cellulose filaments as a viscosity modifying agent in self-consolidating concrete. **Cement and Concrete Composites**, v. 94, n. September, p. 327–340, 2018.

[10] BAKKARI, M. EL *et al*. Preparation of cellulose nanofibers by TEMPO-oxidation of bleached chemi-thermomechanical pulp for cement applications. **Carbohydrate Polymers**, v. 203, n. September 2018, p. 238–245, 2019.

[11] EZ-ZAKI, H. *et al*. Influence of cellulose nanofibrils on the rheology, microstructure and strength of alkali activated ground granulated blast-furnace slag: a comparison with ordinary Portland cement. **Materials and Structures**, v. 54, n. 1, p. 1–18, 2021.

[12] DILS, J.; SCHUTTER, G. DE; BOEL, V. Influence of mixing procedure and mixer type on fresh and hardened properties of concrete: A review. **Materials and Structures/Materiaux et Constructions**, v. 45, n. 11, p. 1673–1683, 2012.

[13] GERMAN INSTITUTE FOR STANDARDISATION (DEUTSCHES INSTITUT FÜR NORMUNG). **EN 1015-3: Methods of Test for Mortar for Masonry—Part 3: Determination of Consistence of Fresh Mortar (by Flow Table)**Berlin, Germany, 2007.

[14] IVANOVA, I.; MECHTCHERINE, V. **Evaluation of structural build-up rate of cementitious materials by means of constant shear rate test: parameter study**. (V. Mechtcherine, K. Khayat, E. Secrieru, Eds.)Rheology and Processing of Construction Materials. **Anais**...Dresden: RILEM Bookseries, 2020

[15] ROUSSEL, N. A thixotropy model for fresh fluid concretes: Theory, validation and applications. **Cement and Concrete Research**, v. 36, n. 10, p. 1797–1806, 2006.

[16] BANFILL, P. Rheology of Fresh Cement and Concrete. **Rheology Reviews**, p. 61–130, 2006.

[17] LONG, W. J. *et al*. Rheology and buildability of sustainable cement-based composites containing micro-crystalline cellulose for 3D-printing. **Journal of Cleaner Production**, v. 239, p. 118054, 2019.

[18] SILVA, L. *et al*. A facile approach of developing micro crystalline cellulose

reinforced cementitious composites with improved microstructure and mechanical performance. **Powder Technology**, v. 338, p. 654–663, 2018.

[19] GÓMEZ HOYOS, C.; CRISTIA, E.; VÁZQUEZ, A. Effect of cellulose microcrystalline particles on properties of cement based composites. **Materials and Design**, v. 51, p. 810–818, 2013.

[20] FILHO, A. *et al*. Mechanical and micro-structural investigation of multi-scale cementitious composites developed using sisal fibres and microcrystalline cellulose. **Industrial Crops and Products**, v. 158, n. April, p. 112912, 2020.

[21] OLIVEIRA DE SOUZA, L. *et al*. Investigation of dispersion methodologies of microcrystalline and nano-fibrillated cellulose on cement pastes. **Cement and Concrete Composites**, v. 126, n. February 2022, 2022.

[22] EICHHORN, S. J. *et al*. Review: Current international research into cellulose nanofibres and nanocomposites. **Journal of Materials Science**, v. 45, n. 1, p. 1–33, 2010.

[23] DUFRESNE, A. Nanocellulose: A new ageless bionanomaterial. **Materials Today**, v. 16, n. 6, p. 220–227, 2013.

[24] GONCALVES, J. *et al*. Cellulose nanofibres (CNF) for sulphate resistance in cement based systems. **Cement and Concrete Composites**, v. 99, n. March, p. 100–111, 2019.

[25] CAO, Y. *et al*. The influence of cellulose nanocrystals on the microstructure of cement paste. **Cement and Concrete Composites**, v. 74, p. 164–173, 2016.

[26] KOLOUR, H.; ASHRAF, W.; LANDIS, E. N. Hydration and Early Age Properties of Cement Pastes Modified with Cellulose Nanofibrils. **Transportation Research Record: Journal of the Transportation Research Board**, p. 036119812094599, 2020

7. Conclusions and suggestions

7.1. Conclusions

The present thesis was designed with the purpose to contribute to some of the gaps found in the Literature regarding the effect of micro and nanocellulose fibers on several properties of cement pastes. The following conclusions were drawn.

Although MCC and NFC are cellulose-based materials provided from the same source i.e., natural fibers, their morphologies and properties are quite distinct. Thus, based on a mechanical approach and considering workability issues, a specific mixing protocol was developed for each type of inclusion. It was selected the sonication as the most suitable dispersion method for MCC and the use of superplasticizer as a way of facilitating the mixture of NFC. The optimal percentage of MCC inclusion of 0.75% wt. led to an increase in flexural strength by five times. The optimal percentage of inclusion of NFC was 1.00% wt. and resulted in an increase of three times the flexural strength. The use of superplasticizer on the NFC-reinforced specimens allowed to enhance the increase of the flexural parameters to the same level of the improvements promoted by the MCC. The first microstructural and chemical analysis suggested that MCC changes the microstructure of the cement pastes while the nanofibrils may act by reinforcing their microstructure.

At the microstructural level, neither the MCC nor the NFC had a significant influence on the hydration aspect, at least not as expected. On the other hand, the inclusion of both micro and nanocellulose modified the size pore distribution of the cement pastes, but not necessarily decreased the porosity. However, the improvements observed regarding the mechanical properties, namely flexural and tensile stresses, were indeed meaningful. The reinforcement capacity was better explored by means of a newly developed direct tensile test that allowed the comparison of specimens of similar geometry. The inclusion of 0.075% of MCC and NFC increased the tensile strength in 70% and 76%, respectively. Those results were superior to the ones regarding the flexural strength. Taking into

consideration the results generated by Chapters 3 and 4, it is more probable that MCC and NFC act by reinforcing the cement pastes than improving their hydration.

The investigations brought in Chapter 5 showed that a combination of a proper w/c and a specific NFC content shall lead to a positive effect regarding the mitigation of autogenous shrinkage deformation. The inclusion of 0.050% of NFC into specimens of w/c equals to 0.30 decreased in 36% de shrinkage at the end of 28 days. The total shrinkage was not significantly affected by the presence of NFC. However, the addition of nanofibrils did result in an attenuation of the autogenous expansion in the first hours. The bleeding test results showed how the NFC's water retention capacity measured in Chapter 3 actually work in the fresh cement paste environment.

The study and discussion about the water retained by the nanofibrils initiated in Chapter 5 proceeded in Chapter 6, with the static rheological tests. Those tests indicated that the water present in the gel was only partially available as mixing water. Thus, part of some behaviors observed throughout the thesis development could be, in a low extent, a result of the lower actual water-to-cement ratio. Nevertheless, the NFC fibrils do have an impact on the rheological behavior of cement pastes, as well as MCC particles did. Both cellulosic inclusions increased: the shear stress at every applied shear rate, the shear thinning behavior and the Bingham parameters, namely yield stress and plastic viscosity. The NFC had more influence on the yield stress, while MCC on the plastic viscosity. The effect of steric stabilization of the MCC was verified for inclusions under 0.50% if considering the static conditions. The shear thinning characteristic was also verified on the NFC gel itself. The effect promoted by the NFC on the rheological properties of cement pastes is much more pronounced than the one promoted by MCC if one considers the percentage of inclusion. Generally, it took 1.000% of MCC to reach similar modifications promoted by 0.040% of NFC.

7.2. Suggestions for future works

Although the findings presented in this thesis are relevant and are believed to contribute to the Literature, there is still room for further investigations regarding

the use of MCC and NFC in cementitious matrices. The following suggestions for future works are made.

- The investigation of how the MCC and NFC work under a carbon dioxide atmosphere is essential for the entire comprehension of the role of those materials as inclusions in cementitious materials.
- In order to support the hydration analysis carried out in Chapter 4, a test that considers the hydration kinetics i.e., calorimetry investigations, should improve the knowledge in this matter.
- The potential of TEMPO-oxidated NFC fibrils as reinforcement shall be investigated with the addition of superplasticizer.
- The role of NFC in shrinkage deformations should be further investigated ignoring the water present in the gel as mixing water.
- The investigation of the total and autogenous shrinkage behavior upon the addition of MCC at high percentages, such as higher than 0.50%.
- The mechanical reinforcement at microstructure level can be better investigated by means of fracture mechanics tests. A starting point regarding proper percentages of inclusions of MCC and NFC was giving in Chapter 3.
- Durability issues are often raised when dealing with materials derived from natural sources. Although micro and nanocellulose are expected to be more stable towards alkaline environments than macro fibers, this should be investigated.
- A composite with multi-scale reinforcement based on natural fibers, with either MCC or NFC associated to a macro fiber, has a great potential to exhibit excellent mechanical properties.

Appendix A

Chapter 5 brought an intense investigation into the effect of NFC fibrils on autogenous and total shrinkage behavior of cement pastes. As mentioned in Section 5.1, there were preliminary tests performed on MCC-reinforced specimens that led to the exclusion of them in the continuity of the tests. Those results are presented in Figure A.1. They are from sealed prisms specimens, so they represent autogenous shrinkage tests. The water-to-cement ratio was 0.35. The MCC percentages of inclusion investigated were: 0.025%, 0.050%, 0.075%, and 0.100%, in weight. The rage of evaluated percentage was wider than the one used on the NFC-reinforced tests so a proper screening of the potential of MCC as shrinkage reducing agent could be evaluated. From the results presented in Figure A-1 it was possible to observe that the inclusion of MCC did not promote any reduction in the autogenous shrinkage deformation, at any age nor any trend that indicated this possibility.

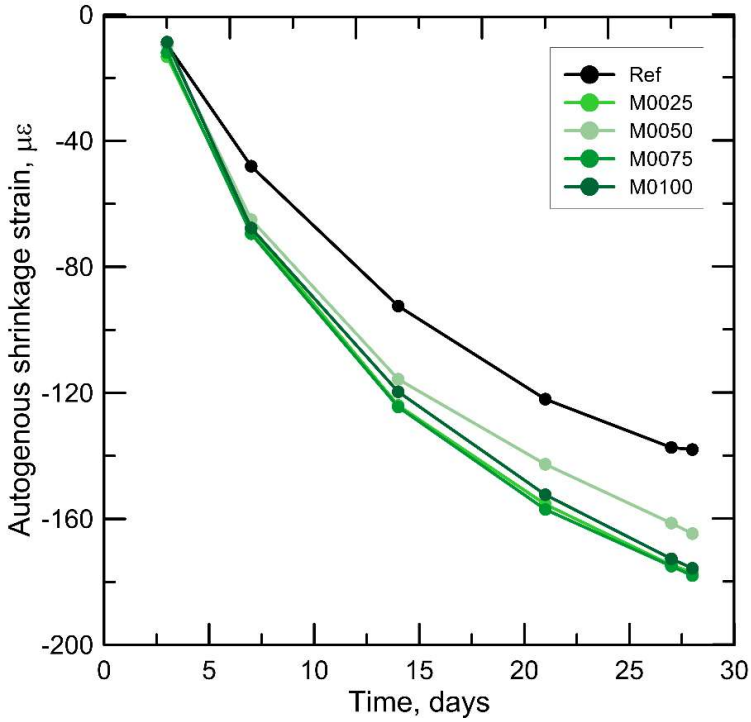

Figure A.1 – Autogenous shrinkage deformation evolution for 28 days of cement pastes with w/c equals to 0.35 and MCC inclusion.